Verisk Inland Flood Model for the United States

Publication Date: July 2020

Revision History

Revision Date	Description
July 30, 2020	Initial publication
April 19, 2022	Updated the Custom Flood Zone topic in the Secondary Risk Characteristics section.
December 15, 2022	Corrected a typo in the Analysis Settings appendix (changed demand surge from off to on).

Table of Contents

List of Figures

List of Tables

1 Facts at a Glance

1.1 Model Abstract

The Verisk Inland Flood Model for the United States captures the effects of precipitation-induced flooding on insured properties in the contiguous United States. It is a fully probabilistic, event-based inland flood model that covers flooding to properties located on and off of floodplains. It captures both large-scale and highly localized floods, including flash floods that result from short-lived but extreme precipitation. The model is built to meet the wide spectrum of flood risk management needs in the insurance industry and accounts for policy conditions specific to the United States.

The model captures all the complexities inherent in a flood generation process to determine the amount of water that accumulates over land as excess runoff and drains into rivers. The contributing factors include the space-time patterns of rainfall, the effects of a highly variable climate, snowmelt, topography, local geology, soil type, antecedent conditions, land use and land cover, and other local factors. The modeling process accounts for the effects of man-made flood defenses and flood regulation, and/or reservoir diversions. The precipitation data was obtained using a coupled Global Circulation Model (GCM) and a Numerical Weather Prediction (NWP) model.

The Verisk model identifies separate flood events through the use of a clustering algorithm that divides flood occurrences spatially and temporally, representing the physical realities of flood. To accommodate widely-used methods of event identification for insurance purposes, the model incorporates the 168 hours clause by dividing on-floodplain events. As a result, the majority of these events are less than 168 hours in duration. Through the use of this algorithm, a total of 442,816 separate flood events are included in the model's 10,000-year catalog.

For local intensity, damage, and loss estimation, the model features a physically-based hydraulic model that incorporates the 18 hydrological regions covering the contiguous United States as well as contributing areas in Canada and Mexico. This hydrological domain covers a total area of approximately 8.2 million km^2 (3.2 million mi^2) and includes detailed river networks extending over 2.2 million km (1.4 million mi), with approximately 335,000 distinct unit catchments. It includes every stream with a drainage area of at least 10 km^2 (3.9 mi^2). To accurately assess flood risk along streams and creeks with drainage areas smaller than a 10-km^2, the model uses physically-based pluvial flood modeling at a 10-m resolution throughout the model domain.

Benefits for insurers include a more robust view of individual risk pricing sensitivity as well as new opportunities for flood insurance product innovation. Risk managers can also identify the assets that are driving their overall risk and develop and design cost-effective risk transfer strategies to manage this risk.

1.2 Model Facts

Model name	Verisk Inland Flood Model for the United States
Release date	July 2020
Software systems	• Touchstone 8.0 • Touchstone Re 8.0
Model domain	Contiguous United States
Modeled perils	Non-hurricane precipitation flooding, including both fluvial (on-floodplain) and pluvial (off-floodplain) hazard
Non-modeled perils	Damage due to the force of moving water, debris collision, sedimentation, or contamination by toxic substances is not explicitly modeled.[1]
Intensity parameter	Inundation depth
Secondary risk characteristics	• Base flood elevation • Basement finish • Builders Risk (project completion, project phase code) • Contents vulnerability • Custom elevation • Custom flood zone • Custom standard of protection • FIRM Compliance • First floor height • Floor of interest • Foundation type • Number of basement levels • Service equipment protection • Wet floodproofing

[1] Because modeled losses have been calibrated to and validated against actual reported losses, the impact of these additional perils on modeled losses is captured implicitly.

Model Domain

The model uses a series of domains beginning with a **Global** Circulation Model (GCM), which is coupled with a **regional** Numerical Weather Prediction (NWP) model. The GCM used by Verisk for its coupled model is the Community Atmospheric Model (CAM), a well-established global atmosphere model developed at the National Center for Atmospheric Research (NCAR). For the NWP model, Verisk used the Weather Research and Forecasting (WRF) model, a next-generation mesoscale numerical weather prediction system designed for both operational forecasting and atmospheric research. The precipitation obtained from this coupled model is then downscaled to be used within the hydrological model. The hydrological domain comprises 18 separate hydrological regions that cover all areas that contribute to flooding within the contiguous United States. It covers an area of approximately 8.2 million km^2 (3.2 million mi^2), which includes the entire contiguous United States (excluding the Great Lakes) as well as some streams and catchments outside the country's borders that drain to rivers in the United States. Of this larger hydrological domain, the area within the United States is about 7.8 million km^2 (3.0 million mi^2). Within this country model domain, losses are estimated for both on-floodplain and off-floodplain locations in the United States.

1.3 Data Sources

The model relies on various government and private entities as data sources for the digital terrain model (DTM), precipitation, waterbody, discharge and water level, soils, land cover, dam and levee, and tide data, among others. Details regarding these data sources are provided in the chapters devoted to Event Generation and Local Intensity Calculation discussions.

See Also

Event Generation Data Sources
Local Intensity Data Sources

1.4 Industry Exposure Database

Verisk recommends using the industry exposure database listed below when running the Verisk Inland Flood Model for the United States in Touchstone Re.

Verisk Industry Exposure Database for the United States

Resolution	90 m
Release date	2020
Vintage	End of 2019

For details, refer to the document *The Verisk Industry Exposure Database for the United States*, available with login through the [Client Portal].

1.5 Stochastic Catalog

A stochastic catalog of events supports the Verisk Inland Flood Model for the United States, as detailed below:

Available catalog(s)	10,000-year
Total number of events	442,816

Each stochastic event considers flooding on- and off-floodplain, as defined below.

On-floodplain	Flooding due to a river overtopping its banks.
Off-floodplain	Flooding due to intense precipitation and runoff

If both on- and off-floodplain flooding impact a property, the model considers the higher of the two flood components and designates it as on-floodplain in the loss calculation. The model omits the lesser component to avoid double-counting and overestimating property losses.

This section provides annual and seasonal frequency distributions for the contiguous United States, and for the nine census divisions shown in Figure 1.

Figure 1. U.S. Census Divisions used for annual and monthly frequency distributions

Annual Frequency Distributions

Figure 2 through Figure 11 compare the annual frequency distribution of simulated flood events in the model's 10,000-year stochastic catalog for the entire model domain and for the nine census divisions.

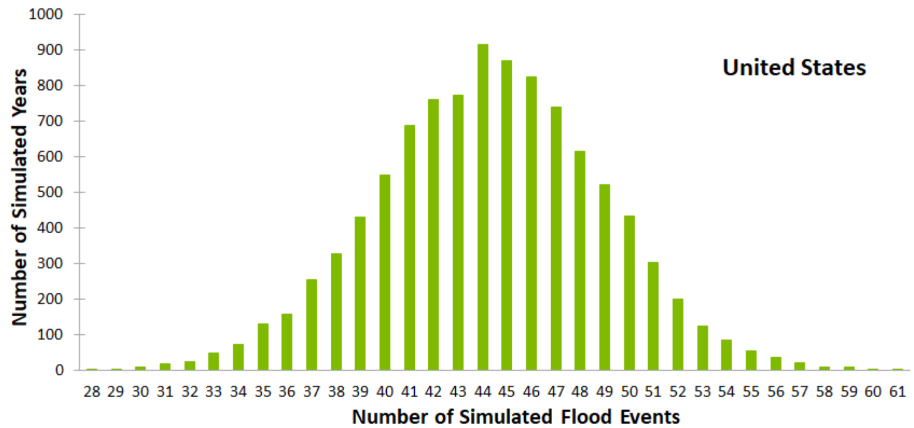

Figure 2. Annual frequency distribution of simulated flood events, United States

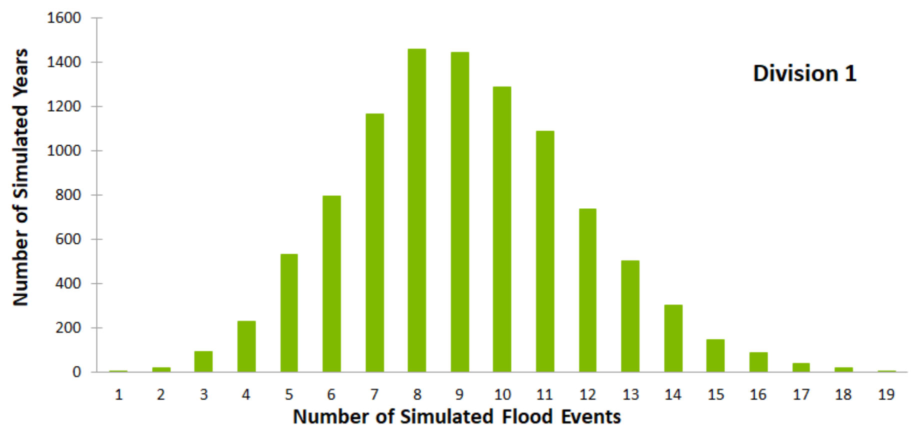

Figure 3. Annual frequency distribution of simulated flood events, Division 1 (CT, MA, ME, RI, NH, VT)

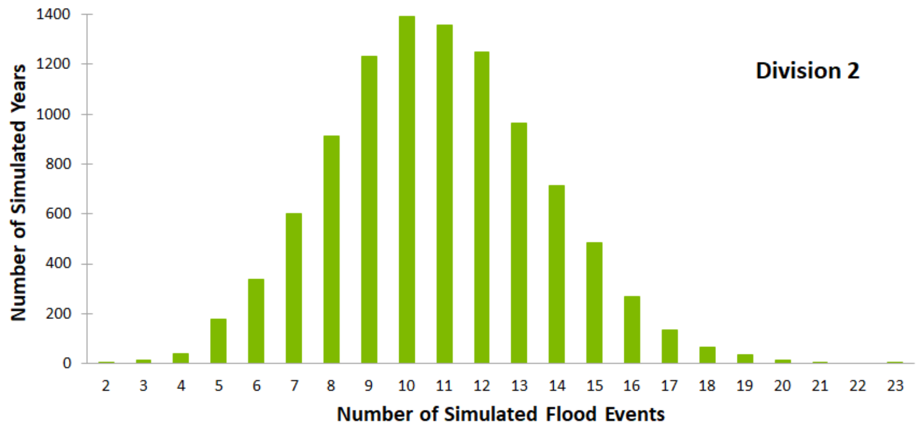

Figure 4. Annual frequency distribution of simulated flood events, Division 2 (NJ, NY, PA)

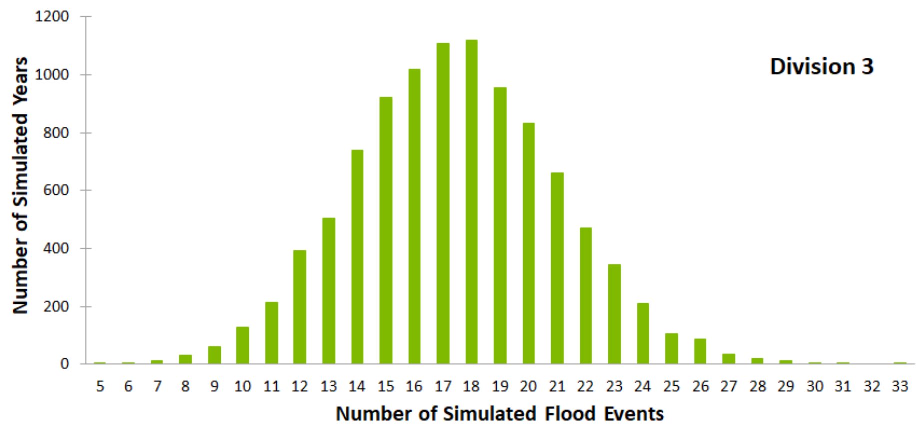

Figure 5. Annual frequency distribution of simulated flood events, Division 3 (IL, IN, MI, OH, WI)

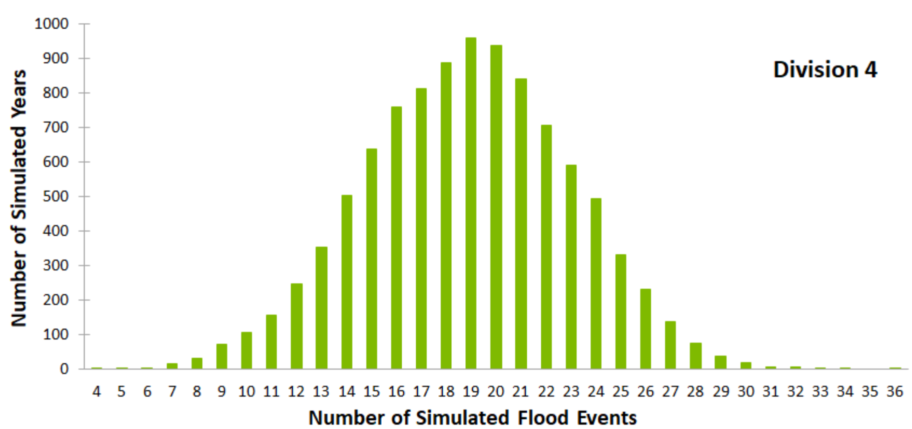

Figure 6. Annual frequency distribution of simulated flood events, Division 4 (IA, KS, MN, MO, ND, NE, SD)

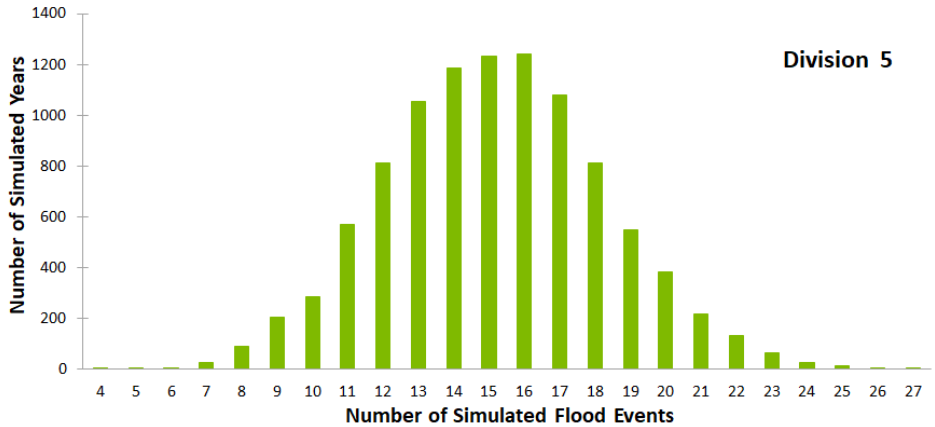

Figure 7. Annual frequency distribution of simulated flood events, Division 5 (DC, DE, FL, GA, MD, NC, SC, VA, WV)

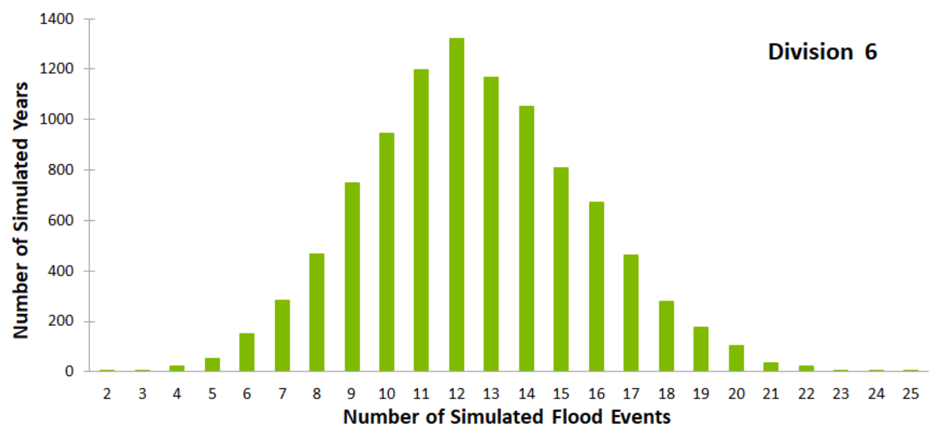

Figure 8. Annual frequency distribution of simulated flood events, Division 6 (AL, KY, MS, TN)

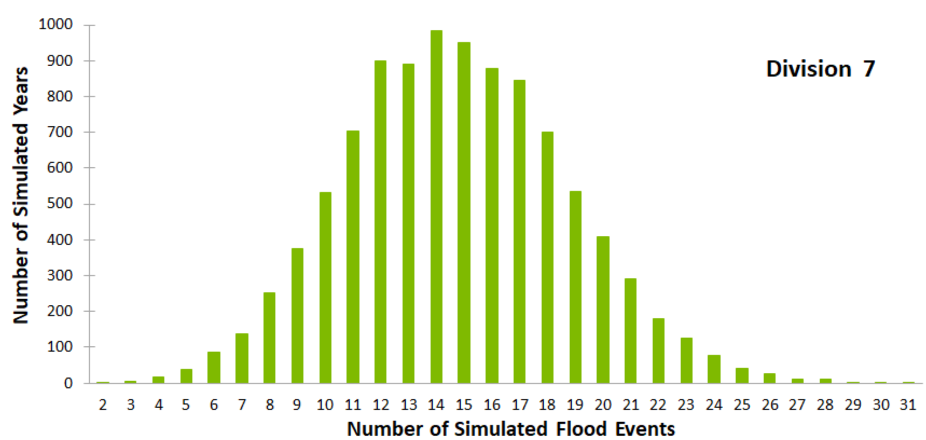

Figure 9. Annual frequency distribution of simulated flood events, Division 7 (AR, LA, OK, TX)

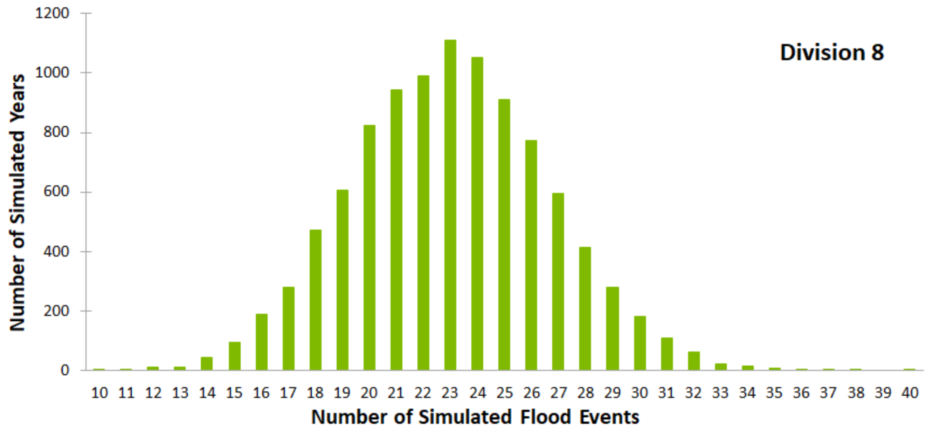

Figure 10. Annual frequency distribution of simulated flood events, Division 8 (AZ, CO, ID, MT, NM, NV, UT, WY)

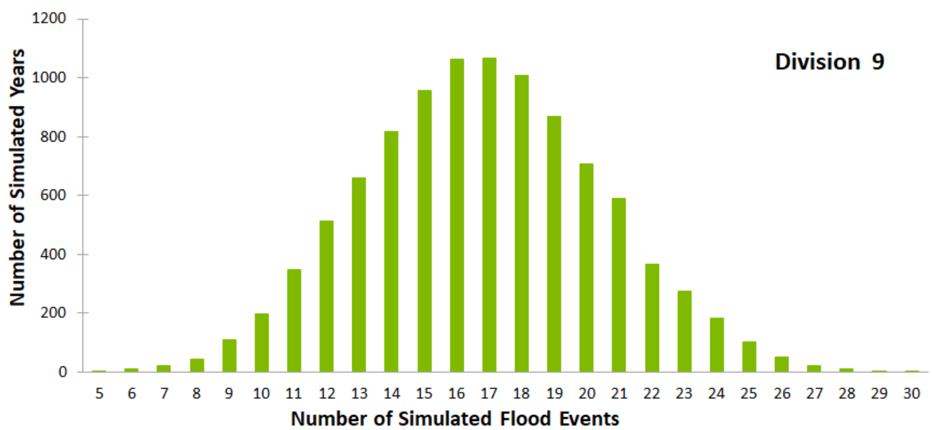

Figure 11. Annual frequency distribution of simulated flood events, Division 9 (CA, OR, WA)

Seasonal Frequency Distributions

Figure 12 through Figure 21 compare the seasonal distribution of simulated flood events in the model's 10,000-year stochastic catalog, for the entire model domain and the nine census divisions.

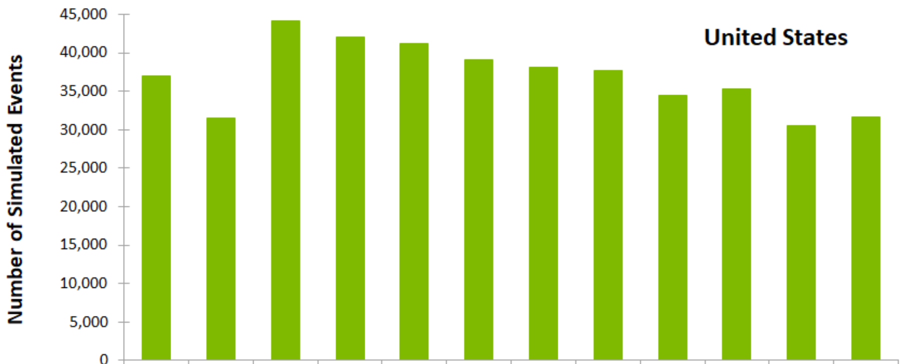

	Jan	Feb	Mar	Apr	May	Jun	Jul	Aug	Sep	Oct	Nov	Dec
Number of Events	36,925	31,509	44,096	42,110	41,173	39,040	38,152	37,738	34,532	35,311	30,579	31,651
Percentage	8.3%	7.1%	10.0%	9.5%	9.3%	8.8%	8.6%	8.5%	7.8%	8.0%	6.9%	7.1%

Figure 12. Seasonal frequency distribution of simulated flood events, United States

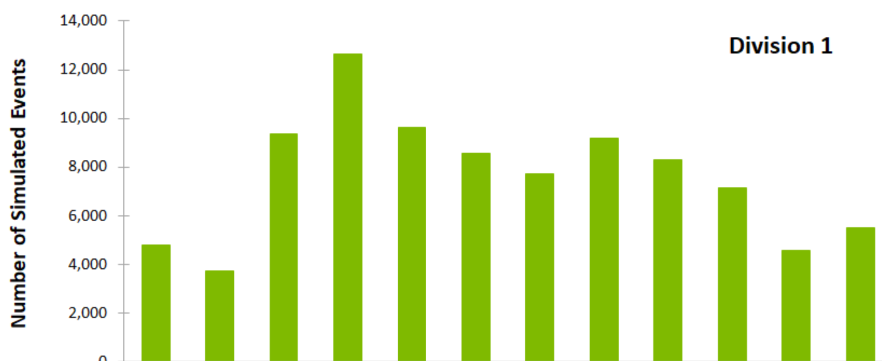

	Jan	Feb	Mar	Apr	May	Jun	Jul	Aug	Sep	Oct	Nov	Dec
Number of Events	4,784	3,709	9,354	12,665	9,623	8,564	7,722	9,176	8,284	7,129	4,583	5,497
Percentage	5.3%	4.1%	10.3%	13.9%	10.6%	9.4%	8.5%	10.1%	9.1%	7.8%	5.0%	6.0%

Figure 13. Seasonal frequency distribution of simulated flood events, Division 1 (CT, MA, ME, RI, NH, VT)

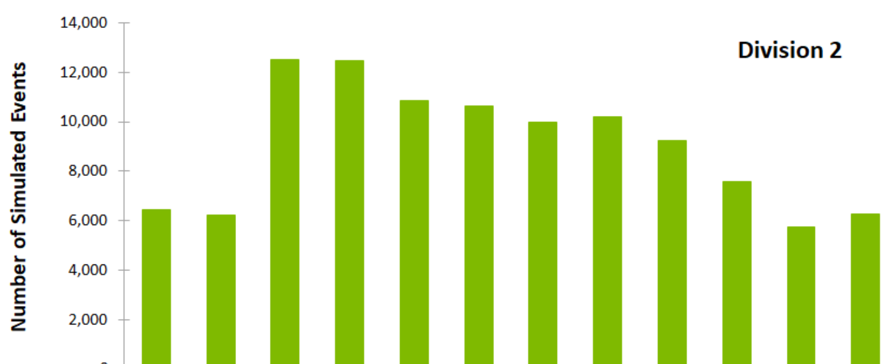

	Jan	Feb	Mar	Apr	May	Jun	Jul	Aug	Sep	Oct	Nov	Dec
Number of Events	6,456	6,235	12,494	12,454	10,846	10,623	9,961	10,206	9,254	7,599	5,741	6,278
Percentage	6.0%	5.8%	11.6%	11.5%	10.0%	9.8%	9.2%	9.4%	8.6%	7.0%	5.3%	5.8%

Figure 14. Seasonal frequency distribution of simulated flood events, Division 2 (NJ, NY, PA)

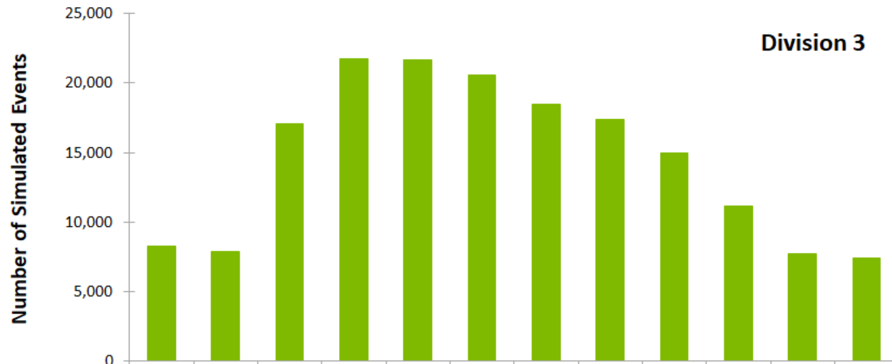

	Jan	Feb	Mar	Apr	May	Jun	Jul	Aug	Sep	Oct	Nov	Dec
Number of Events	8,244	7,852	17,051	21,732	21,679	20,621	18,505	17,364	14,972	11,173	7,747	7,435
Percentage	4.7%	4.5%	9.8%	12.5%	12.4%	11.8%	10.6%	10.0%	8.6%	6.4%	4.4%	4.3%

Figure 15. Seasonal frequency distribution of simulated flood events, Division 3 (IL, IN, MI, OH, WI)

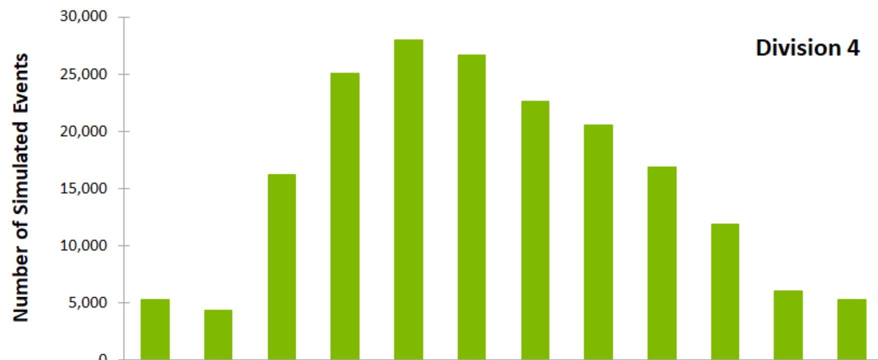

	Jan	Feb	Mar	Apr	May	Jun	Jul	Aug	Sep	Oct	Nov	Dec
Number of Events	5,285	4,305	16,239	25,014	27,934	26,667	22,595	20,529	16,818	11,881	6,003	5,271
Percentage	2.8%	2.3%	8.6%	13.3%	14.8%	14.1%	12.0%	10.9%	8.9%	6.3%	3.2%	2.8%

Figure 16. Seasonal frequency distribution of simulated flood events, Division 4 (IA, KS, MN, MO, ND, NE, SD)

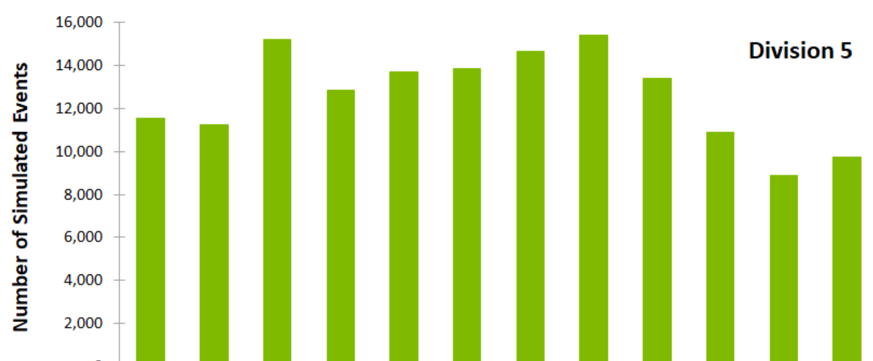

	Jan	Feb	Mar	Apr	May	Jun	Jul	Aug	Sep	Oct	Nov	Dec
Number of Events	11,553	11,266	15,243	12,867	13,728	13,881	14,650	15,419	13,413	10,889	8,870	9,727
Percentage	7.6%	7.4%	10.1%	8.5%	9.1%	9.2%	9.7%	10.2%	8.9%	7.2%	5.9%	6.4%

Figure 17. Seasonal frequency distribution of simulated flood events, Division 5 (DC, DE, FL, GA, MD, NC, SC, VA, WV)

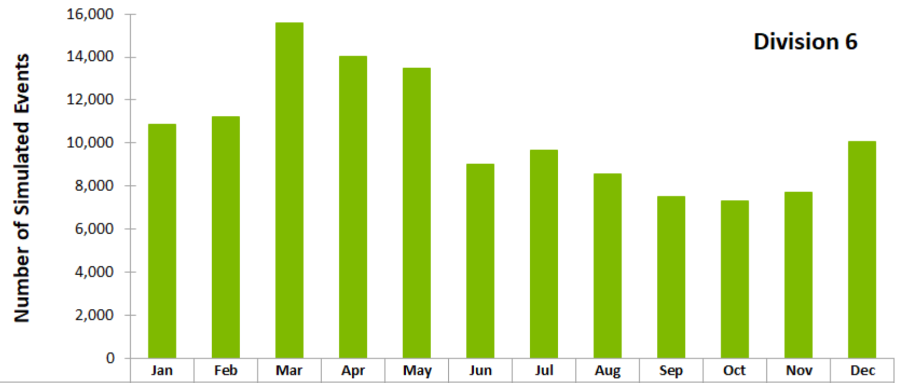

	Jan	Feb	Mar	Apr	May	Jun	Jul	Aug	Sep	Oct	Nov	Dec
Number of Events	10,853	11,209	15,580	14,029	13,495	8,991	9,644	8,556	7,516	7,331	7,709	10,069
Percentage	8.7%	9.0%	12.5%	11.2%	10.8%	7.2%	7.7%	6.8%	6.0%	5.9%	6.2%	8.1%

Figure 18. Seasonal frequency distribution of simulated flood events, Division 6 (AL, KY, MS, TN)

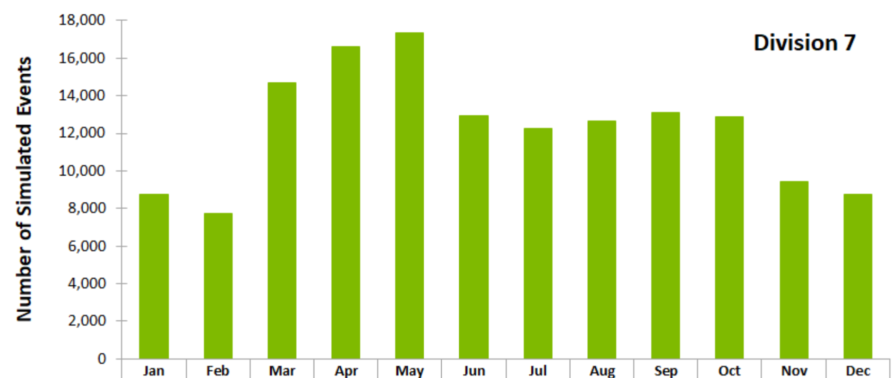

	Jan	Feb	Mar	Apr	May	Jun	Jul	Aug	Sep	Oct	Nov	Dec
Number of Events	8,779	7,753	14,698	16,593	17,363	12,915	12,252	12,650	13,101	12,902	9,411	8,733
Percentage	6.0%	5.3%	10.0%	11.3%	11.8%	8.8%	8.3%	8.6%	8.9%	8.8%	6.4%	5.9%

Figure 19. Seasonal frequency distribution of simulated flood events, Division 7 (AR, LA, OK, TX)

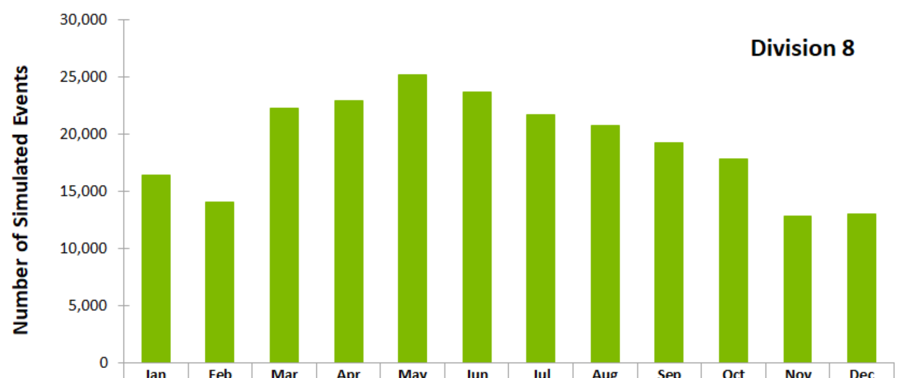

	Jan	Feb	Mar	Apr	May	Jun	Jul	Aug	Sep	Oct	Nov	Dec
Number of Events	16,420	14,022	22,239	22,957	25,222	23,740	21,673	20,730	19,225	17,868	12,869	12,990
Percentage	7.1%	6.1%	9.7%	10.0%	11.0%	10.3%	9.4%	9.0%	8.4%	7.8%	5.6%	5.6%

Figure 20. Seasonal frequency distribution of simulated flood events, Division 8 (AZ, CO, ID, MT, NM, NV, UT, WY)

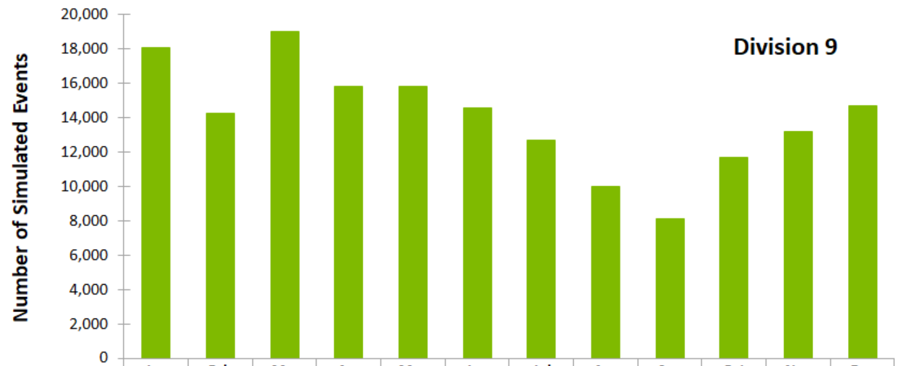

	Jan	Feb	Mar	Apr	May	Jun	Jul	Aug	Sep	Oct	Nov	Dec
Number of Events	18,064	14,264	18,982	15,802	15,804	14,584	12,685	9,992	8,140	11,696	13,160	14,659
Percentage	10.8%	8.5%	11.3%	9.4%	9.4%	8.7%	7.6%	6.0%	4.9%	7.0%	7.8%	8.7%

Figure 21. Seasonal frequency distribution of simulated flood events, Division 9 (CA, OR, WA)

1.6 Historical Event Set

The Verisk Inland Flood Model for the United States includes a historical event set consisting of 20 events, listed below.

Table 1. Historical events available in the Verisk Inland Flood Model for the United States

Event ID	Year	Event Name
1	1993	Great Flood (Mississippi River)
2	1995	California Flood
3	1995	Gulf Coast Flood
4	1996-1997	Pacific Northwest Flood
5	1997	Red River Flood
6	1998	Texas Flood
7	2001	Tropical Storm Allison
8	2006	Northeast Flood
9	2008	Midwest Flood
10	2008	Tropical Storm Fay
11	2009	East Florida Storm
12	2010	Rhode Island Flood
13	2010	Tennessee Flood
14	2011	Mississippi Flood
15	2011	Tropical Storm Lee
16	2013	Florida Panhandle Storm

Event ID	Year	Event Name
17	2013	Colorado Flood
18	2015	South Carolina Flood
19	2016	Louisiana Flood
20	2017	California Flood

1.7 Model Resolution

The Verisk Inland Flood Model for the United States resolution is provided below, along with supported resolutions in Touchstone and Touchstone Re.

General

Model resolution	• On-floodplain - 10 m • Off-floodplain - 10 m

Touchstone

Supported geographic resolutions	• County • Zip code • Address (city and state) • Complete address (street, city, and state) • User-specified latitude/longitude

Touchstone Re

Supported geographic resolutions	• State • County

1.8 Modeled Lines of Business

Touchstone Re supports the following lines of business for reporting modeled losses (the components of each line of business are also indicated below):

Residential	Building, Contents, and Time Element
Manufactured Home	Building, Contents, and Time Element
Commercial/Industrial	Building, Contents, and Business Interruption (Time Element)
Automobile	

1.9 Construction and Occupancy Classes

The model supports a variety of construction and occupancy codes. The number of supported classes in each category is listed below.

Construction classes	81 (including unknown)
Occupancy classes	111 (including unknown)
400-series occupancy	Included (62 classes)

For complete lists of construction classes, occupancy classes, and supported combinations, see theVerisk Inland Flood Model for the United States available on the Client Portal

See Also

Construction and Occupancy Classes, Year Built and Height Bands, and Relative Vulnerabilities

1.10 Modeled Industry Losses

It is important to distinguish between insurable and insured losses when modeling the industry exposure.

Insurable exposure	Total replacement value and number of properties (risk counts) that are eligible for insurance.
Insured exposure	Although eligible for insurance, “take-up” or purchase of insurance coverage for eligible properties varies by peril and region. For example, coverage for some natural perils may be mandatory in a region, and consequently the insurance take-up rate would be 100%. For other natural perils, insurance may be voluntary, and take-up may be in single-digit percentage values. Based on available information, Verisk provides estimates of take-up rates for each modeled region and simulated peril. Insured exposure is calculated by multiplying the take-up rate by the insurable risk count and replacement values.

Insurable losses	Estimated losses to insurable exposure.
Insured losses	Estimated losses to insured exposures.

In this document, modeled **insured losses** have been calculated using private market take-up rates, and **Insurable losses** are estimated gross losses to insurable exposures with the application of the private market deductibles and limits, and automobile deductibles. Take-up rates have not been applied to gross losses.

The losses presented in this document include demand surge.[2]

See Also

Supported Take-Up Rates and Policy Conditions

Insured Occurrence Losses

Modeled insured occurrence loss estimates for selected exceedance probabilities (EP) are provided below:

1% EP (100-year)	USD 8.20 Billion
0.4% EP (250-year)	USD 10.47 Billion

To obtain these modeled losses, Verisk ran the model in Touchstone Re.

See Also

Analysis Settings

Insurable Occurrence Losses

Modeled gross private market insurable occurrence loss estimates for selected exceedance probabilities (EP) are provided below:

1% EP (100-year)	USD 54.87 Billion
0.4% EP (250-year)	USD 72.62 Billion

To obtain these modeled losses, Verisk ran the model in Touchstone Re.

See Also

Analysis Settings

Insured Aggregate Average Annual Losses

Figure 22 shows the modeled insured aggregate average annual loss (AAL) by census division and for the 10 states with the highest losses.

To obtain these modeled losses, Verisk ran the model in Touchstone Re.

[2] With the exception of the loss cost map

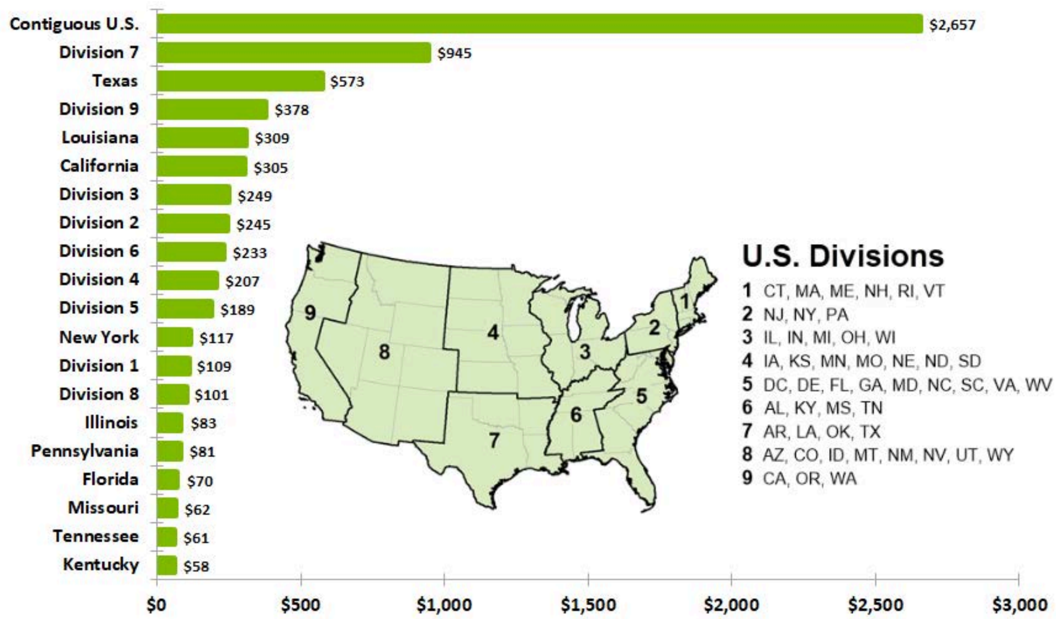

Figure 22. Modeled insured aggregate average annual losses (in USD millions) for the model domain, census divisions, and 10 states with the highest AAL

Table 2 lists, for each state, the percentage of the total insured aggregate AAL that is attributed to on-floodplain and off-floodplain events. These figures are based on the Verisk Industry Exposure Database for the United States. In the Verisk model, 36% of the insured aggregate AAL is attributed to off-floodplain events.

Table 2. Percentage of total insured aggregate average annual loss from on-floodplain and off-floodplain events, by state

State	Contribution to Total Loss		State	Contribution to Total Loss	
	On Floodplain Loss	Off Floodplain Loss		On Floodplain Loss	Off Floodplain Loss
U.S.	64%	36%	MT	88%	12%
AL	85%	15%	NC	72%	28%
AR	92%	8%	ND	81%	19%
AZ	67%	33%	NE	79%	21%
CA	40%	60%	NH	74%	26%
CO	59%	41%	NJ	39%	61%
CT	42%	58%	NM	74%	26%
DC	30%	70%	NV	56%	44%
DE	31%	69%	NY	32%	68%
FL	17%	83%	OH	75%	25%
GA	79%	21%	OK	79%	21%

State	Contribution to Total Loss		State	Contribution to Total Loss	
	On Floodplain Loss	Off Floodplain Loss		On Floodplain Loss	Off Floodplain Loss
IA	79%	21%	OR	85%	15%
ID	86%	14%	PA	70%	30%
IL	75%	25%	RI	10%	90%
IN	70%	30%	SC	62%	38%
KS	75%	25%	SD	83%	17%
KY	85%	15%	TN	87%	13%
LA	94%	6%	TX	55%	45%
MA	20%	80%	UT	41%	59%
MD	42%	58%	VA	70%	30%
ME	64%	36%	VT	89%	11%
MI	54%	46%	WA	90%	10%
MN	45%	55%	WI	77%	23%
MO	84%	16%	WV	90%	10%
MS	82%	18%	WY	92%	8%

See Also

Analysis Settings

Insurable Aggregate Average Annual Losses

Figure 23 shows the modeled gross insurable aggregate average annual loss (AAL) by census division and for the 10 states with the highest losses.

To obtain these modeled losses, Verisk ran the model in Touchstone Re.

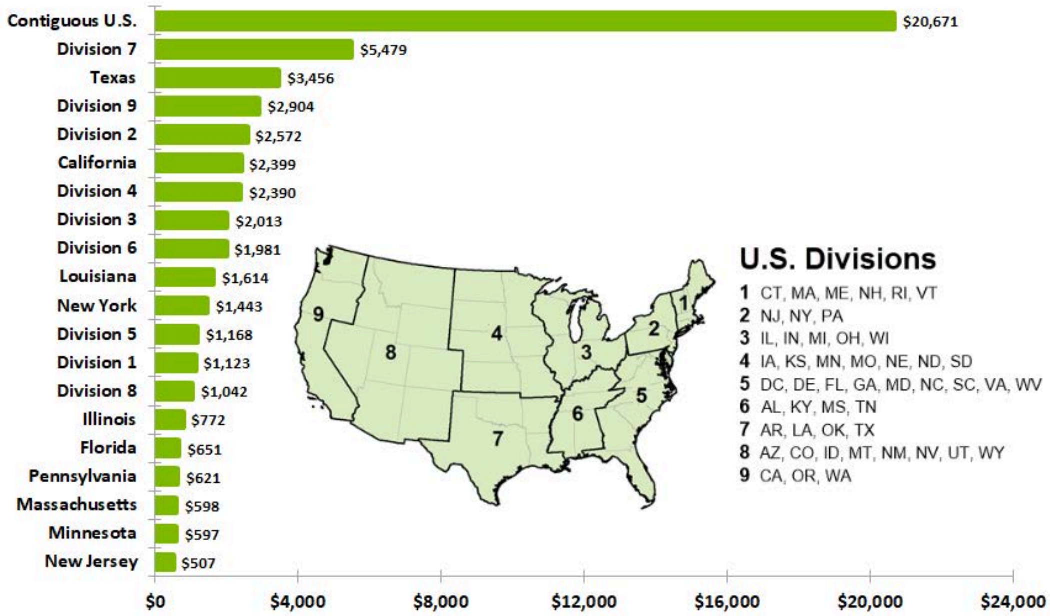

Figure 23. Modeled gross insurable aggregate average annual losses (in USD millions) for the model domain, census divisions, and 10 states with the highest AAL

Table 3 lists, for each state, the percentage of the total insurable aggregate AAL that is attributed to on-floodplain and off-floodplain events. These figures are based on the Verisk Industry Exposure Database for the United States. In the Verisk model, 51% of the insurable aggregate AAL is attributed to off-floodplain events.

Table 3. Percentage of total insurable aggregate average annual loss from on-floodplain and off-floodplain events, by state

State	Contribution to Total Loss		State	Contribution to Total Loss	
	On Floodplain Loss	Off Floodplain Loss		On Floodplain Loss	Off Floodplain Loss
U.S.	49%	51%	MT	77%	23%
AL	80%	20%	NC	66%	34%
AR	85%	15%	ND	66%	34%
AZ	54%	46%	NE	58%	42%
CA	37%	63%	NH	61%	39%
CO	44%	56%	NJ	17%	83%
CT	21%	79%	NM	71%	29%
DC	11%	89%	NV	43%	57%
DE	9%	91%	NY	19%	81%
FL	17%	83%	OH	39%	61%
GA	69%	31%	OK	62%	38%

State	Contribution to Total Loss		State	Contribution to Total Loss	
	On Floodplain Loss	Off Floodplain Loss		On Floodplain Loss	Off Floodplain Loss
IA	56%	44%	OR	74%	26%
ID	69%	31%	PA	51%	49%
IL	50%	50%	RI	6%	94%
IN	35%	65%	SC	57%	43%
KS	47%	53%	SD	65%	35%
KY	74%	26%	TN	71%	29%
LA	93%	7%	TX	52%	48%
MA	9%	91%	UT	39%	61%
MD	15%	85%	VA	35%	65%
ME	61%	39%	VT	76%	24%
MI	27%	73%	WA	85%	15%
MN	19%	81%	WI	56%	44%
MO	69%	31%	WV	82%	18%
MS	76%	24%	WY	79%	21%

See Also

Analysis Settings

Loss Cost

Figure 24 shows the combined loss cost (risk) for flooding both on- and off-floodplain in the contiguous United States. The map shows the average annual loss (AAL), Coverage A (buildings), of a uniform exposure type (construction class 101, occupancy class 301, unknown height and age) with a uniform exposure value, calculated on a 1-km grid.

The loss cost map does not include demand surge. To obtain data for the loss cost map, Verisk ran a detailed loss analysis on the gridded exposure in Touchstone.

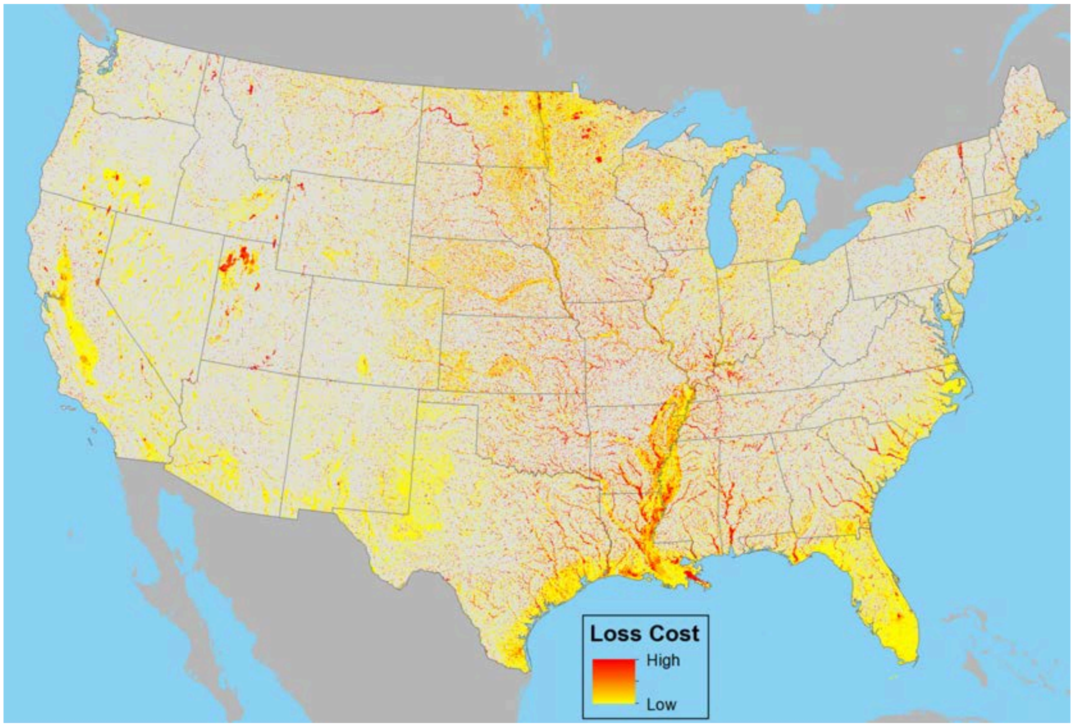

Figure 24. Combined on- and off-floodplain inland flood risk (loss cost) in the contiguous United States

Note: A flood loss cost map can be misleading, due to the coarser gridded exposure. Some exposures are placed in rivers or lakes, where they are always flooded. In addition, the grid does not allow continuous mapping of flood risk along rivers.

See Also

Analysis Settings

1.11 Modeled Losses for Historical Flood Events

Table 4 and Table 5 show modeled insured and insurable loss estimates, respectively, for 20 historical events, based on the *Verisk Industry Exposure Database for the United States* , which is available through the Client Portal.

To obtain these modeled losses, Verisk ran the model in Touchstone Re.

Table 4. Modeled insured losses for historical events (USD, millions)

Event ID	Year	Event Name	Res	Com/Ind	Auto	Total
1	1993	The Great Flood	35.85	1,700.23	620.64	2,356.71
2	1995	California Flood	52.72	691.77	446.63	1,191.12
3	1995	Gulf Coast Flood	139.73	652.52	306.88	1,099.14

Event ID	Year	Event Name	Res	Com/Ind	Auto	Total
4	1996	Pacific Northwest Flood	77.65	1,791.01	786.96	2,655.62
5	1997	Red River Flood	5.00	144.89	85.51	235.40
6	1998	Texas Flood	28.88	433.14	295.84	757.86
7	2001	Tropical Storm Allison	225.91	2,016.15	1,015.39	3,257.46
8	2006	Northeast Flood	22.98	361.08	177.33	561.39
9	2008	Midwest Flood	16.90	566.69	253.18	836.77
10	2008	Tropical Storm Fay	5.35	45.02	25.23	75.61
11	2009	East Florida Storm	2.44	16.25	4.44	23.13
12	2010	Rhode Island Flood	10.26	166.98	39.01	216.26
13	2010	Tennessee Flood	38.66	658.62	215.67	912.95
14	2011	Mississippi Flood	13.52	256.66	143.64	413.82
15	2011	Tropical Storm Lee	30.62	449.09	215.72	695.43
16	2013	Florida Panhandle Storm	0.60	11.72	1.45	13.77
17	2013	Colorado Flood	6.93	191.33	57.02	255.27
18	2015	South Carolina Flood	14.82	77.43	56.65	148.89
19	2016	Louisiana Flood	145.51	943.30	771.19	1,860.00
20	2017	California Flood	3.65	62.74	25.82	92.21

Table 5. Modeled gross insurable losses for historical events (USD, millions)

Event ID	Year	Event Name	Res	Com/Ind	Auto	Total
1	1993	The Great Flood	4,758.36	6,218.30	620.64	11,748.35
2	1995	California Flood	6,567.29	2,581.69	446.63	9,775.63
3	1995	Gulf Coast Flood	3,555.69	2,145.68	306.88	6,053.93
4	1996	Pacific Northwest Flood	7,576.32	5,669.11	786.96	14,301.37
5	1997	Red River Flood	729.43	573.64	85.51	1,404.64
6	1998	Texas Flood	2,269.75	1,571.90	295.84	4,249.16
7	2001	Tropical Storm Allison	10,598.63	8,114.01	1,015.39	20,306.89
8	2006	Northeast Flood	2,479.99	1,425.70	177.33	4,127.94
9	2008	Midwest Flood	2,578.81	2,104.34	253.18	4,975.84
10	2008	Tropical Storm Fay	415.78	200.87	25.23	665.51
11	2009	East Florida Storm	129.67	84.54	4.44	229.34
12	2010	Rhode Island Flood	1,207.78	609.70	39.01	1,875.03
13	2010	Tennessee Flood	2,239.86	2,055.41	215.67	4,584.08
14	2011	Mississippi Flood	1,537.66	934.32	143.64	2,695.64
15	2011	Tropical Storm Lee	3,499.37	1,849.81	215.72	5,664.96

Event ID	Year	Event Name	Res	Com/Ind	Auto	Total
16	2013	Florida Panhandle Storm	29.18	45.17	1.45	79.65
17	2013	Colorado Flood	1,252.42	835.43	57.02	2,156.31
18	2015	South Carolina Flood	581.16	380.85	56.65	1,115.24
19	2016	Louisiana Flood	5,604.01	3,323.24	771.19	10,234.36
20	2017	California Flood	508.01	258.35	25.82	807.26

See Also
Major Historical Floods in the United States
Analysis Settings

1.12 Navigating the Document

Figure 25 illustrates the components of the Verisk Inland Flood Model for the United States. These components are detailed in the sections that follow.

Figure 25. Components of the Verisk Inland Flood Model for the United States

2 Flood Peril in the United States

2.1 Floods: An Overview

A flood is a temporary high-water condition on normally dry land caused by rivers overflowing their natural banks or levees, and/or intense local precipitation or rapid snowmelt. Floods can be caused by natural processes, such as heavy precipitation or snowmelt, or the failure of man-made structures such as levees, dams, and drainage systems in urban areas. Floods are generally parameterized in terms of peak river discharge, precipitation amount, inundated area, and depth of flooding.

The size and scale of floods vary, ranging from minor waterlogged fields or briefly blocked roads to widespread inundation, resulting in the destruction of homes and other structures, sometimes accompanied by the loss of life (people and livestock). Floods are frequent events. Once every few years, a significant precipitation event may occur, or a river or stream may overflow; however, over longer periods of time, catastrophic flood events occur with some regularity (e.g., once in 50 or 100 years, on average).

In evaluating inland river floods, the basic hydrological unit in river systems is the drainage area, or **catchment**—the land area that contributes water to a given cross-section along a river network. Following a dry period, rain falling on a catchment infiltrates the upper layers of soil and rock, with only a small portion flowing over land. Continual rain, however, can saturate surface soils. When the volume of water falling exceeds the available pore space, **surface runoff** begins. The proportion of total rainfall that transforms to surface runoff over a catchment is called the **runoff coefficient**.

Surface runoff usually begins as **sheet flow**— water moves as a thin, continuous film (no channels) over relatively smooth soil or rock surfaces. As the volume of water increases, it forms tiny rills, then gullies, eventually forming small creeks and tributary streams.

Multiple factors determine whether or not a flood occurs:

- Antecedent conditions — the amount of prior rainfall or snowmelt, which determines the degree of soil saturation
- Topography
- Vegetation — type, abundance, and location
- Rainfall intensity, total volume, and duration

Extended wet periods during any season can create saturated soil conditions, after which any additional rain will run off into streams and rivers until the river holding capacities are exceeded — causing flooding.

In some cases, rainfall can be so heavy that even very dry, highly pervious soils cannot absorb the volume of falling water. Such bursts of extreme rainfall (the world record is more than 300 mm/hr) can produce **flash floods**— severe flooding that is highly localized, spatially and temporally.

The rigorous study of floods begins by recording hydrographs for a river within a given drainage basin when a storm is expected. A hydrograph measures the discharge, velocity, stage (height) or other parameters of a body of water over time. Hydrographs are generated from data obtained at one or more stream gauging stations. Figure 26 provides an example of a river discharge hydrograph resulting from over an inch of rainfall in a short period of time.

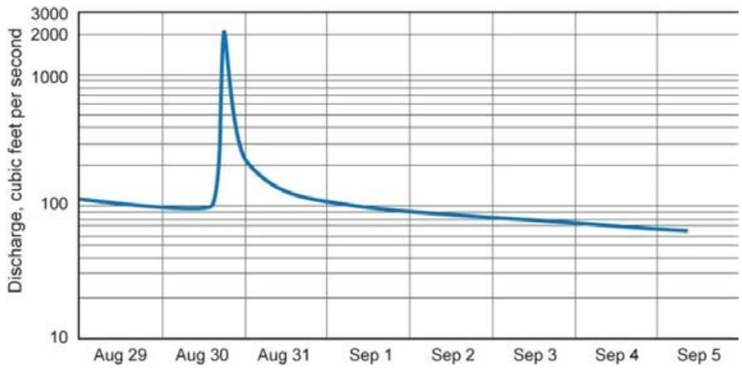

Figure 26. Sample discharge hydrograph

Over time, natural waterways adjust their shape and **conveyance** — a measure of a channel's flow or discharge carrying capacity, in m^3/s — to the precipitation regime over the river basin upstream. For example, a river reach with a 1,000 km^2 upstream drainage area that receives 1,400 mm average annual rainfall will have twice the conveyance (and therefore cross-sectional dimensions) of a reach with the same contributing area and slope, but that receives only 700 mm average annual rainfall.[3]

The best characteristic measure for a given river reach is **bankfull discharge** — the discharge at which a river is flowing full up to its banks, independent of the prevailing precipitation regime, soil type or vegetation. The bankfull discharge typically has a return period of approximately 2 years.

If, at a given location, the ratio of peak flow to its bankfull discharge during a flood is greater than one, the vicinity of that river reach is likely to be flooded under natural conditions.

Rivers

Following a precipitation event or snowmelt, excess runoff drains into streams, with the smaller streams reaching flood stage[4] first, due to their smaller water capacity. Flood waves drain into larger rivers and can propagate through a large region, often affected by additional storms or other conditions that can increase (or mitigate) the water level.

The Verisk model covers all areas that contribute to flooding within the contiguous U.S. —an area of approximately 8.2 million km^2 (3.2 million mi^2). The analysis of flood events

[3] This is only a rough approximation. The relationship between the channel conveyance and the precipitation regime can be more complex due to soil type and underlying geology.

[4] Flood stage occurs when the level of a river reaches a point where it can flood the adjacent areas and potentially cause damage.

occurs along a total river length of 2.2 million km (1.4 million mi) with over 335,000 drainage catchments. It includes every stream with a drainage area of at least 10 km^2 (3.9 mi^2).

Figure 27. The hydrological model domain (left) and a portion of the Mississippi River network (right)

Lakes and Reservoirs

Lakes and reservoirs designed for flood attenuation can significantly affect flow variability and decrease the magnitude of flood peaks. The Verisk model includes data from the USGS National Hydrography Dataset on over 21,000 lakes and reservoirs.

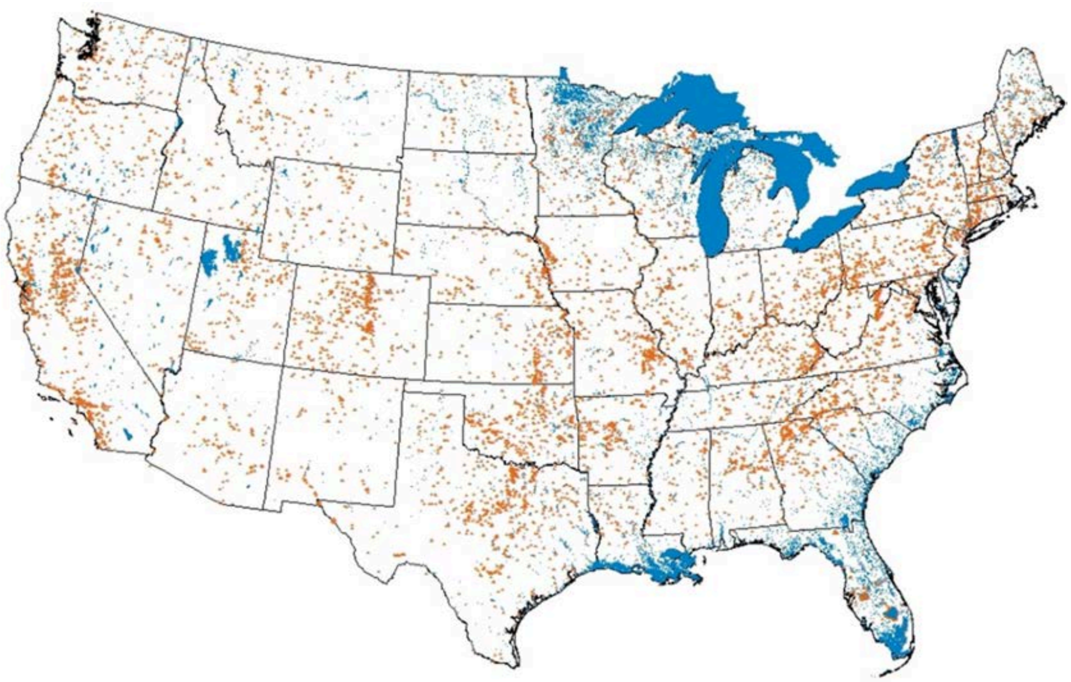

Figure 28. Modeled lakes and reservoirs (orange); Larger water bodies and wetlands are shown in the background (blue)

Levees

The levee system in the United States is expansive and includes state and private levees as well as those managed by the U.S. Army Corps of Engineers (USACE). Levees have a great impact on flood risk, particularly along the lower Mississippi River. According to the USACE, there are an estimated 161,000 km (100,000 mi) of levees in the United States. However, only a limited amount of information on their presence and design level is available through the National Levee Database (NLD).

The NLD includes levee information within the USACE program, FEMA, and other states and federal agencies. Verisk researchers have leveraged the recently updated (June 2018) NLD, which now contains significantly more levee information. In addition, Verisk has supplemented this information with the protected areas depicted in FEMA flood hazard maps.

From these data sources, Verisk has obtained a total of 40,224 km (25,000 mi) of levee information has been obtained from these available data sources as compared to only 23,330 km (14,500 mi) that was previously available. Additionally, Verisk researchers were able to derive an extra 6,436 km (4,000 mi) of levees through the high-resolution Digital Terrain Model (DTM) data available from the United States Geological Survey (USGS).

Figure 29. Levees and levee-protected areas included in the model

Thus, Verisk utilized a total of over 46,660 km (29,000 mi) length of levee presence information in its direct assignment of flood protection along river segments. For the river segments that lack sufficient data on presence of levees, the Verisk model employs an indirect estimation method based on exposure density and total replacement value from

Verisk's Industrial Exposure Database (IED), and protected area demarcation from FEMA flood hazard maps.

Climate

Climate has a major impact on flood risk as it affects the amount of precipitation an area receives, the amount of snow on the ground when spring rains begin, or temperatures rise. The climate also affects soil conditions, which determine the land's ability to absorb water from precipitation. The climate in the contiguous U.S. is highly variable. A tropical climate is found in Florida, while bitter cold winters occur in the Midwest and Northeast. The Great Plains west of the Mississippi River are semiarid, while east of the river the regions can become quite humid. The Southwest and Great Basin regions are arid, becoming desert-like in many areas.

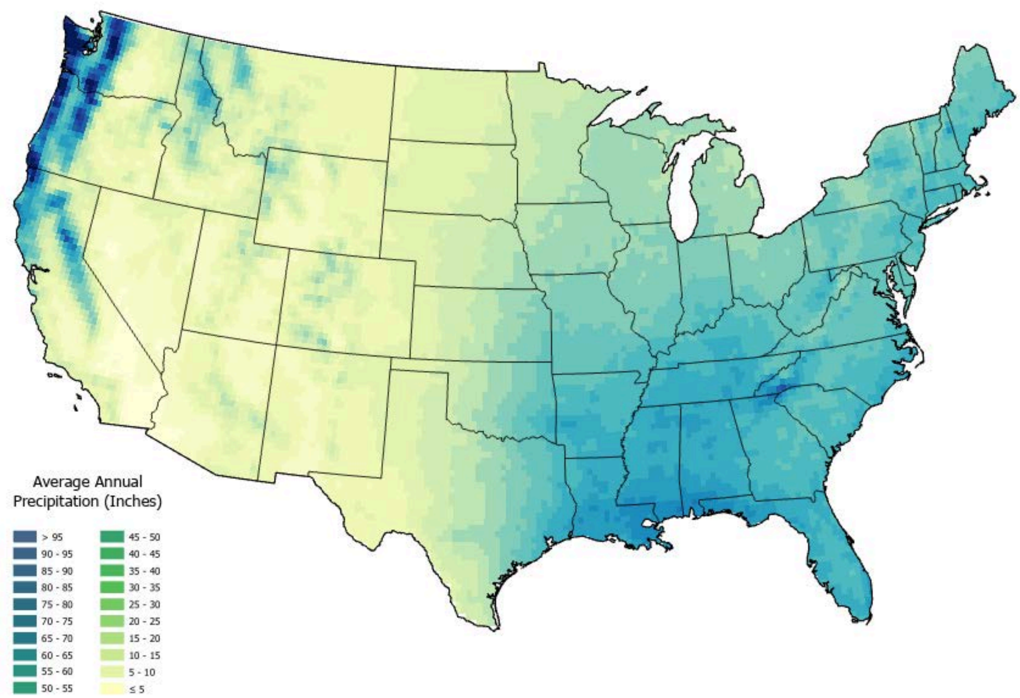

Figure 30. Average annual precipitation across the contiguous United States

Many areas are exposed to the heavy precipitation that accompanies severe storms. Hurricanes pose a risk along the Gulf Coast and East Coast, and hurricane-induced precipitation occurs inland from these areas as far as Missouri.[5] Severe thunderstorms plague the Midwest areas and travel eastward, often threatening eastern states. Heavy snow can occur across the Northeast and Midwest, while the mountainous west often experiences heavy precipitation as well, from storms that originate in the Pacific Ocean or move down from Canada. The west coast has a relatively mild climate although it is susceptible to the

[5] The Verisk Inland Flood Model for the United States does not include hurricane-induced precipitation, or flooding due to storm surge. These perils are included in the Verisk Hurricane Model for the United States.

"Pineapple Express" or other storms that originate in the Pacific Ocean and bring heavy rainfall.

See Also

Climate

Topography

Topography plays a major role in how precipitation and excess runoff flows over land. When snow in higher elevations melts, the runoff, which may be intensified by additional rainfall, can flow downslope and swell rivers downstream. Floods accumulate in low-lying areas and the relatively flat land in the floodplains that surround large rivers can be highly flood-prone.

Figure 31. Topography and some major rivers of the contiguous United States

The contiguous U.S. has a widely varied topography. Eastern regions are hilly and mountainous, although the mountains are comparatively low. The highest point, Mt. Mitchell, North Carolina, is 2,037m (6,683 ft) above sea level. The country's interior is marked by river valleys and the Great Plains, which lead to the high and rugged mountains of the West. West of the Rocky Mountains are areas of desert, fertile valleys, and additional mountain ranges. The highest point in the western contiguous U.S. is California's Mt. Whitney at 4,418 m (14,495 ft). Mt. Whitney is located less than 160 km (100 mi) from the lowest point in the U.S., in Death Valley, which is 86 m (282 ft) below sea level.

Geology and Soil Type

Once precipitation hits the ground, a catchment's, topography, predominant soil type, and geology are important factors in determining how much water will infiltrate into the ground surface and how much will flow over land. Infiltration capacity depends on the unique combination of soil type (specifically its grain size distribution and porosity) and the thickness and porosity of the underlying water-bearing rock formation, or **aquifer**. Aquifers serve as large reservoirs, storing groundwater and releasing it over long periods of time after a storm, thus reducing the variability of river flow and preventing rivers from flooding.

Igneous rocks (e.g., basalt and granite) have a very low infiltration capacity due to their crystalline structure, unless heavily fractured. In contrast, marine sedimentary rocks (e.g., limestone) have a high infiltration capacity, as they are often rich in calcium carbonate, a mineral conducive to dissolution. Acidic precipitation, moving through cracks, dissolves the surrounding rock, and can lead to the formation of **karst**—a network of caverns, and subterranean streams. Karst regions can have tremendous infiltration capacities. Rivers may spring from, or disappear into the rock formation. Other sedimentary rocks (e.g., sandstone and shale) consist of lithified sand and clay. The infiltration capacity of sandstone or shale is usually low unless heavily fractured.

Land Cover and Urbanization

Land cover may significantly affect the runoff coefficient and the catchment hydrograph. In forested areas, tree roots create channels deep into the soil, down to groundwater, increasing infiltration and reducing surface runoff. This effect is less pronounced in pastures or areas covered by shrubs, as grasses and shrubs have shallow root systems.

In urbanized areas, and particularly in large cities, the high percentage of paved areas may increase the runoff coefficient significantly. Additionally, smooth surfaces like asphalt and concrete have a much lower resistance to overland flow. Hydrographs of heavily urbanized catchments have a shorter response time and higher magnitude of peak flows.

Urbanization can also impact a river's path and shape. In the past, marshes and floodplains stretched along river banks, limiting flooding. Now, these natural features have been replaced by man-made embankments and property development, which have increased the flooding problem. Furthermore, to accommodate large volumes of traffic, major shipping rivers have been deepened and straightened — resulting in a considerably shorter length of river that no longer meanders. Heavy rain or a great deal of snowmelt can cause the velocity of the river to increase significantly so that water rushes through, increasing the intensity of floods and the speed at which the water levels rise.

Heavy industrialization characterizes numerous American rivers, many of which have been deepened and straightened to accommodate a large volume of shipping traffic. Both the Mississippi and Missouri rivers are dredged to a depth of at least 2.7 m (8.9 ft) in areas where navigability must be maintained. Dams and locks have affected the flow and shape in order to serve the population with ample water supply and hydroelectric power.

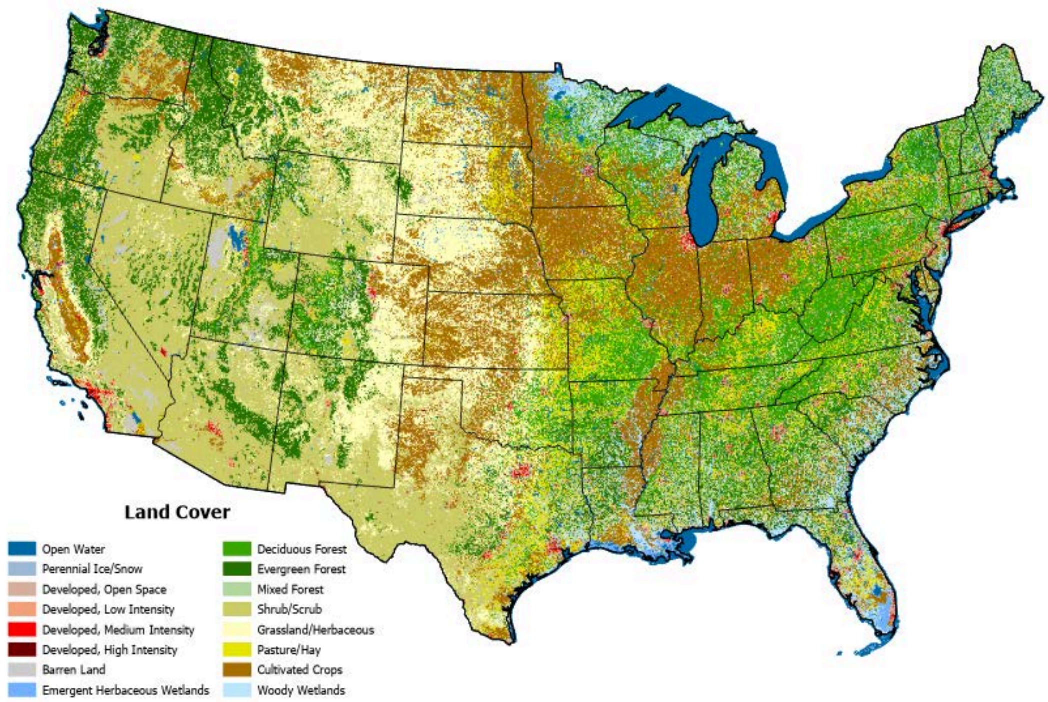

Figure 32. Major land cover types across the contiguous United States

The overall effect of varying soil type, land use and land cover, and hydrologic drainage conditions on the resulting surface runoff is well represented by an empirical parameter known as the **runoff curve number**. The Natural Resources Conservation Service (US Department of Agriculture) has developed a method for obtaining the runoff curve number where, for a given rainfall storm event, the surface runoff is proportional to the runoff curve number. The Verisk Inland Flood Model for the United States does not directly use the runoff curve number to estimate surface flows, but instead uses it as a measure while obtaining regional estimates of other model parameters that affect flooding. Figure 33 shows a map of the runoff curve number in the model's hydrological domain.

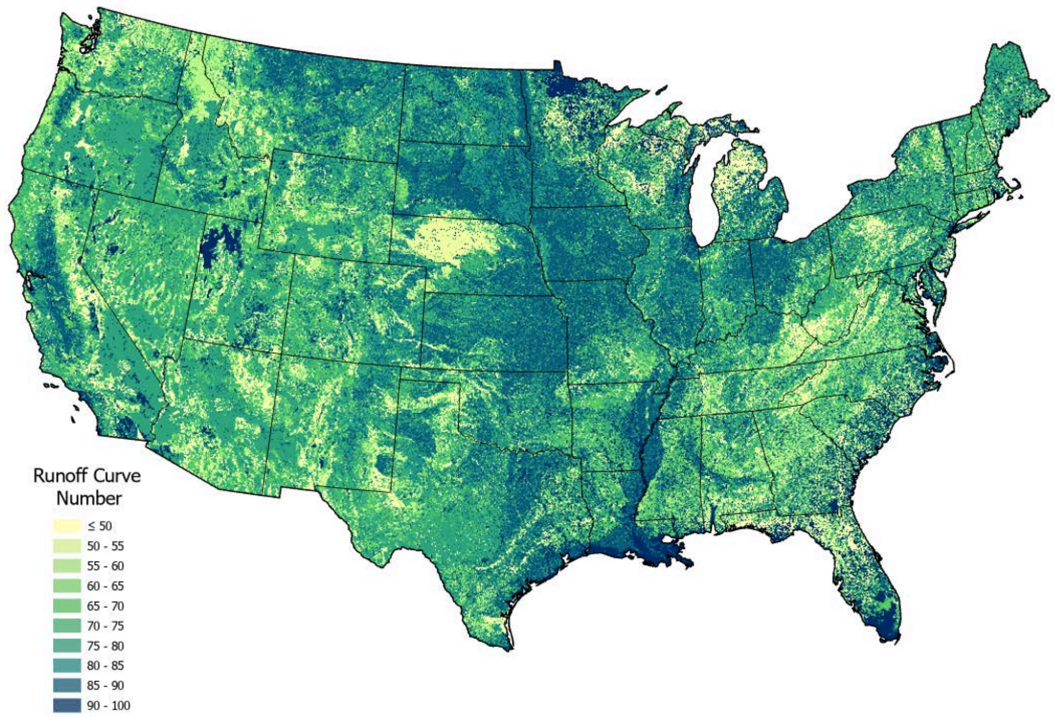

Figure 33. Runoff curve number across the contiguous United States

2.2 Flood Risk in the Contiguous United States

Approximately 3,800 towns and cities in the U.S. are located on floodplains and many areas off of floodplains are still prone to flood damage and loss. Significant risk can exist even in areas with a high level of flood mitigation, particularly in the event of a flood defense failure. Flood disaster declarations are not uncommon, even in regions well equipped to mitigate risk and manage recovery. Figure 34 shows the U.S. counties where flood disasters have been declared between 1959 and 2019.

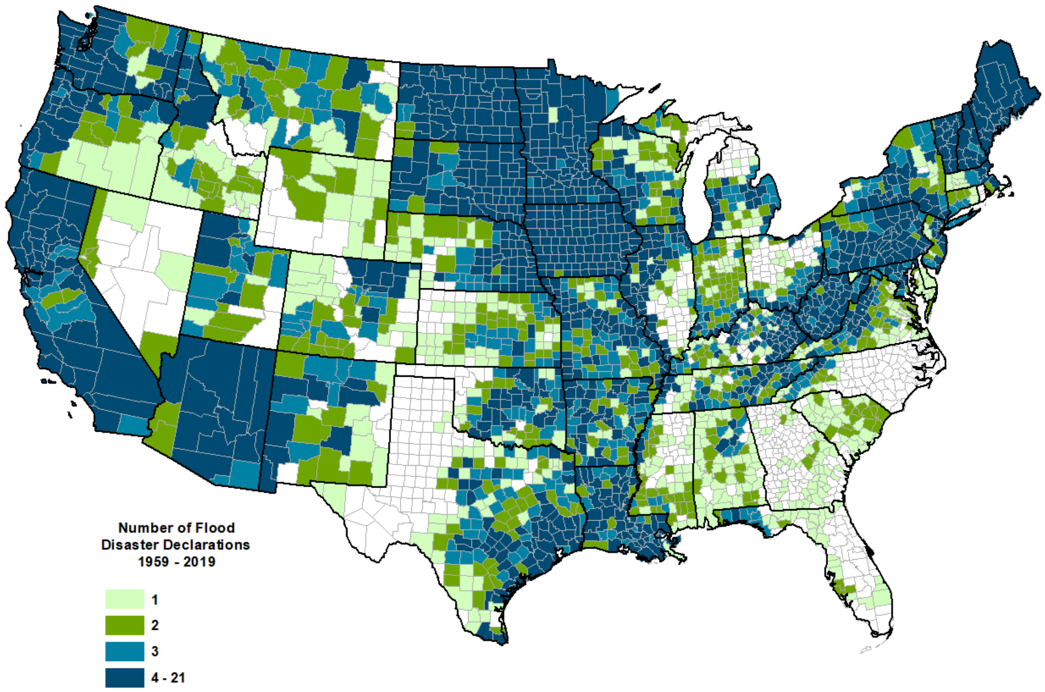

Figure 34. U.S. counties with flood disaster declarations, 1959 – 2019

Inland floods are caused by myriad circumstances that contribute to excess runoff into rivers. These include rain storms, snowmelt, topography, soil type, antecedent soil conditions, drainage conditions, land use and land cover, and flood defenses. This section provides a high-level perspective on how the main contributors of inland flood are modeled, with further details provided in the rest of the document.

The Hazard

The United States possesses multiple characteristics that affect the region's propensity for flooding, including climate, weather patterns, topography, and land cover, among others. Damaging floods due to rainfall occur along many of the major rivers. In mountainous regions, flash floods are common and carry water to the lowlands through numerous medium and major rivers such as Missouri, Ohio, and the Mississippi rivers.

The Exposure

Many areas of high exposure in the U.S. lie along major rivers; about 3,800 towns and cities are located on floodplains and even those outside of floodplains are at risk due to off-floodplain, or pluvial, flooding. This section describes the major rivers and risk of flooding in each of the major regions in the contiguous United States. An overview of the relative population density for the region is provided in Figure 35.

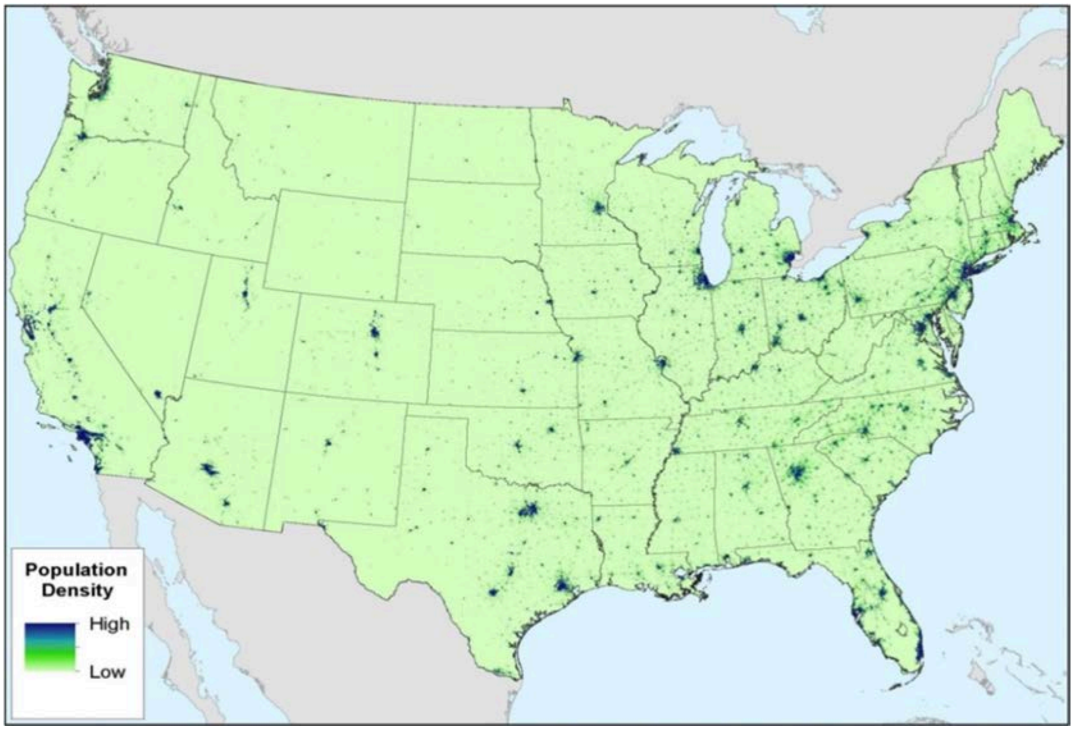

Figure 35. Population density in the contiguous United States

Northeast and Mid-Atlantic

Some of the most densely populated areas in the U.S. are along the northeastern and mid-Atlantic seaboard, with heavy industrial development along many of the region's major rivers. The area is subject to heavy rainfall, while snowfall during the winter contributes significantly to groundwater during the spring rains.

The longest river in the region is the 747 km (464 mi) Susquehanna River, which runs from Otsego Lake, New York, to the Chesapeake Bay, servicing cities in New York and Pennsylvania. New England's longest river is the 655 km (407 mi) Connecticut River, which flows from Quebec, Canada, through Vermont, New Hampshire, Massachusetts, and Connecticut. Upstate New York and Pennsylvania are serviced by the heavily industrialized and urbanized Hudson and Mohawk rivers, which have been the sites of many damaging floods. The Hudson flows through eastern New York, becoming a tidal estuary at the tri-cities area (Albany, Troy, and Schenectady) and then through Manhattan and New Jersey, before reaching the Atlantic Ocean.

Also affecting New York and Pennsylvania, as well as New Jersey, Maryland, and Delaware, is the 484 km (301 mi) Delaware River, which services about 17 million people. The 486 km (302 mi) Potomac River serves about five million people in Virginia, West Virginia, Maryland, and Washington, D.C. Floods along the Potomac have affected government offices and monuments in Washington D.C., interrupting federal offices as well as causing significant damage.

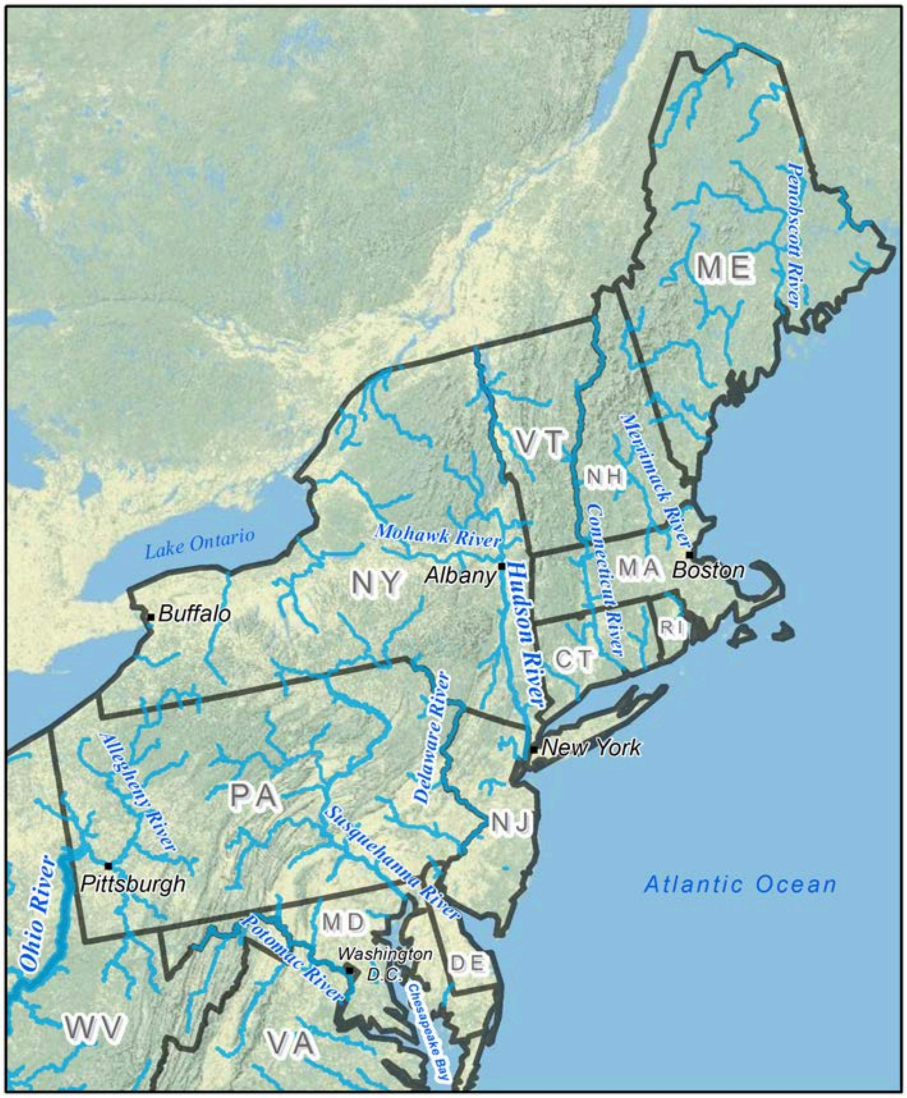

Figure 36. Major rivers of the Northeast and Mid-Atlantic

Southeast

One of the major river networks serving the southeastern states is the Apalachicola-Chattahoochee, which flows 843 km (524 mi) from Towns County, Georgia, into northern Florida, and then into the Gulf of Mexico. The Chattahoochee River, which services Georgia's two largest cities, Atlanta and Columbus, is the site of several industrial plants including Kellogg's production plants and several major wastewater treatment plants.

Running from the confluence of the Holston and French Broad rivers in Tennessee to the Ohio River in Kentucky is the 1,579 km (981 mi) Tennessee River, which is the largest tributary of the Ohio River. This river serves many major urban areas including Chattanooga and Knoxville, Tennessee; Huntsville, Alabama; and Paducah, Kentucky. It serves many important industrial power centers and is heavily used as a major waterway and as an agricultural water source. Also feeding the Ohio River is the 1,107 km (688 mi) Cumberland River, which flows through Nashville, and was the site of devastating floods in 2010.

Figure 37. Major rivers of the Southeast

The Mississippi River

The 3,730 km (2,320 mi) Mississippi River, the second longest river in North America, has a drainage basin of 2.98 million km^2 (1.15 million mi^2), covering just over 40% of the contiguous U.S., and reaches into 31 states. The "upper basin" originates at Lake Itasca, Minnesota, and flows over 2,000 km (1,250 mi) to Cairo, Illinois, where it meets the Ohio River. Due to the Ohio River's huge water volume, the Mississippi nearly doubles in size at this point. The "lower basin" flows nearly 1,600 km (1,000 mi) from Cairo, Illinois to the Gulf of Mexico.

The upper Mississippi River basin serves a population of approximately 30 million within Minnesota, Wisconsin, Iowa, and Illinois. While about 60% of the exposure is agricultural, there are several major cities located in the upper basin as well as industrial facilities. The upper Mississippi River contains 29 dams and locks, most of which were built in the 1930s. North of Illinois, only about 3% of the floodplain is protected by levees while within Illinois, levees protect 53% of the floodplain. The rivers in the upper Mississippi River basin collectively reach over 49,000 km (30,700 mi) and contain approximately 3,000 reservoirs larger than 50 km^2 (19 mi^2); the water in these reservoirs would take over three months, at average discharges, to flow past St. Louis. To maintain the river's commercial navigability, it is dredged to maintain a channel depth of no less than 2.7 m (8.9 ft).

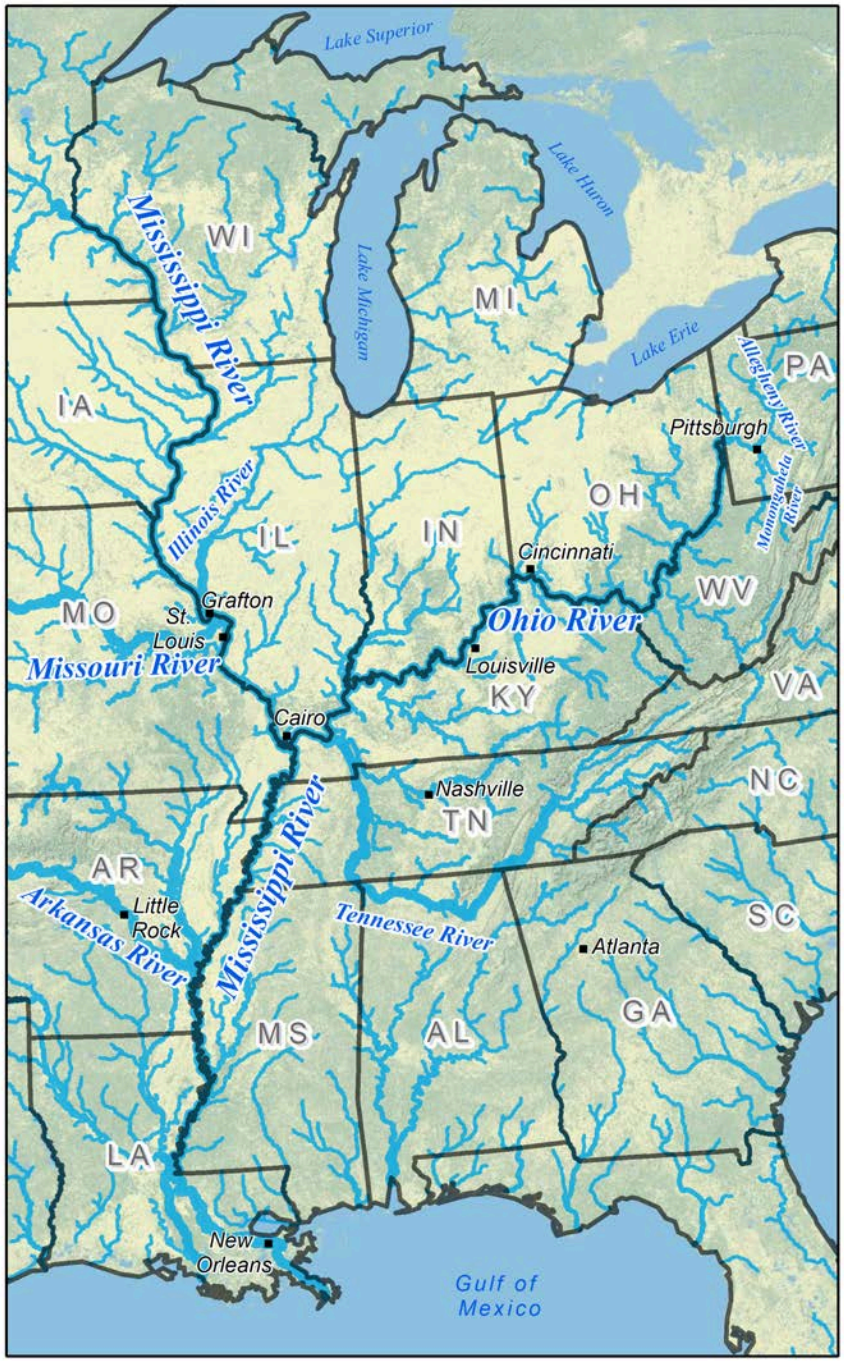

Figure 38. The Mississippi River and its major tributaries

The lower Mississippi feeds an alluvial valley of about 91,000 km2 (35,000 mi^2). The floodplain is flat and its width varies between 40 and 200 km (25 and 124 mi). It contains no locks and has heavier commercial traffic than the upper river. The lower 372 km (230 mi) is a port deep enough to accommodate ocean liners from the Gulf of Mexico and serves many facilities on its way to New Orleans. This section of the river travels through many residential areas, including some containing antebellum mansions, all of which rely on levees for protection; about 83% of the floodplain is protected by levees. The extensive system of levees and floodways in this area, maintained by the U.S. Army Corps of Engineers, has effectively controlled flood waves well in advance of their arrival to this historically flood-prone region.

Main Tributaries of the Mississippi River

The largest tributary to the Mississippi River is the 1,579 km (981 mi) Ohio River, which originates at the junction of the Allegheny and Monongahela Rivers in Pittsburgh, and flows into the Mississippi River at Cairo, Illinois. The Ohio River and its many tributaries affect 15 states across a very large region and serves Pittsburgh, Cincinnati, and Louisville, Kentucky, as well as numerous smaller cities. Some of the deadliest and most destructive floods in the U.S. have occurred along the Ohio River, such as the 1937 floods, which ruined homes located 30 miles from the riverbanks.

Another major tributary of the Mississippi River at Grafton, Illinois is the 439 km (273 mi) Illinois River, which originates in St. Joseph County, Indiana. The river is heavily used for commercial traffic, as well as industrial facilities. In Arkansas, the Mississippi River is fed by the 2,364 km (1,469 mi) Arkansas River, the sixth longest river in the United States, which originates in Lake County, Colorado. The Arkansas River accommodates commercial and passenger traffic and is heavily used for recreation, particularly at Little Rock, Arkansas.

The Missouri River

The Missouri River is the longest river in the United States with a reach of 3,767 km (2,341 mi). Its headwaters are at the confluence of the Jefferson, Madison, and Gallatin rivers at Three Forks, Montana, from where flows across several states to the Mississippi, at a junction north of St. Louis. The Missouri River's drainage area covers approximately 1.37 million km^2 (530,000 mi^2), including over 6,000 km^2 (2,300 mi) in Canada. Its numerous mainstem and tributary dams create the largest combined reservoir storage in the country. The six mainstem dam systems provide an annual energy output of approximately 10 billion kilowatt-hours, or the equivalent of about 1,100 megawatts.

The Missouri river has been greatly altered from its original state with channels and dams, and at 305 m wide (1,000 ft), is now about half its original width. It is heavily used for transporting industrial and agricultural goods, mainly over the 1,181 km (730 mi) stretch between Sioux City, Iowa, to St. Louis. While it is 3.4 m (11.2 ft) deep at Kansas City, a depth of 2.7 m (8.9 ft) and a width of about 90 m (295 ft) are maintained along the commercially navigable stretches. The river is closed to commercial traffic from mid-December through March, and a flow of 850 – 990 m^3/s (approximately 30,000 to 35,000 ft3/s)is maintained during those months at Sioux City and Omaha.

Figure 39. Missouri River and its main tributaries

Upper Midwest

An area of the U.S. that experiences long and damaging floods quite often is in the upper Midwest, within a region bordered by the Missouri River to the south and west, and by the Red River of the North and the Mississippi River to the east.

Minnesota, and North and South Dakota, are often affected by the three main rivers of the international Red River Basin: the Red River of the North and the Rainy and Souris rivers. Due to the local topography, the Red River of the North flows from south to north, traveling through the Fargo-Moorhead area along the Minnesota-North Dakota border. It is 885 km (550 mi) long, with 635 km (395 mi) flowing through the U.S. In 1997, a devastating flood along the Red affected Grand Forks, North Dakota and East Grand Forks, Minnesota.

Mountain Region

The largest river in the intermountain region of the U.S. is the 2,334 km (1,450 mi) Colorado River, which originates in the Rocky Mountains in Colorado. While the Colorado River is heavily managed, many of its tributaries are canyon rivers in the southwestern interior, which have experienced severe and damaging flash floods. In 1997, 12 people were killed from flash floods in Antelope Canyon, Arizona.

In September, 2013, several days of unusually heavy and relentless rain caused highly destructive flash floods in the Boulder, Colorado region. The rivers washed out bridges, homes, trees, and other objects, turning the water flow into a dangerous flow of debris. One of the affected canyons was the Big Thompson Canyon, where other devastating floods have occurred, such as in 1976.

Many rivers that were affected by the 2013 floods feed the 707 km (439 mi) South Platte River, which runs from Park County, Colorado, through Denver on its way to its junction with the Platte River in Nebraska. The flood waves from the 2013 floods carried a great deal of debris from the destruction into Nebraska.

Figure 40. Major rivers of the Mountain region and Southwest

Texas

One of the longest rivers in the United States is the Rio Grande River, which flows 3,051 km (1,896 mi) from the San Juan Mountains in Colorado, to the Gulf of Mexico, along the U.S-Mexico border. Several of the major rivers in Texas run parallel to the Rio Grande in southern Texas and have seen disastrous floods such as the 1998 event that affected the San Antonio and Guadalupe rivers.

The 1,140 km (710 mi) Trinity River flows through some of the most important cities in Texas including Dallas-Fort Worth. The Brazos River runs 1,352 km (840 mi) to the Gulf of Mexico from the junction of two tributaries in Texas, the Salt Fork and Double Mountain Fork. The largest city affected by the Brazos is Waco, Texas, which is protected by floodgates and dams. Nearly 2,500 commercial and recreational vessels travel the Brazos every month.

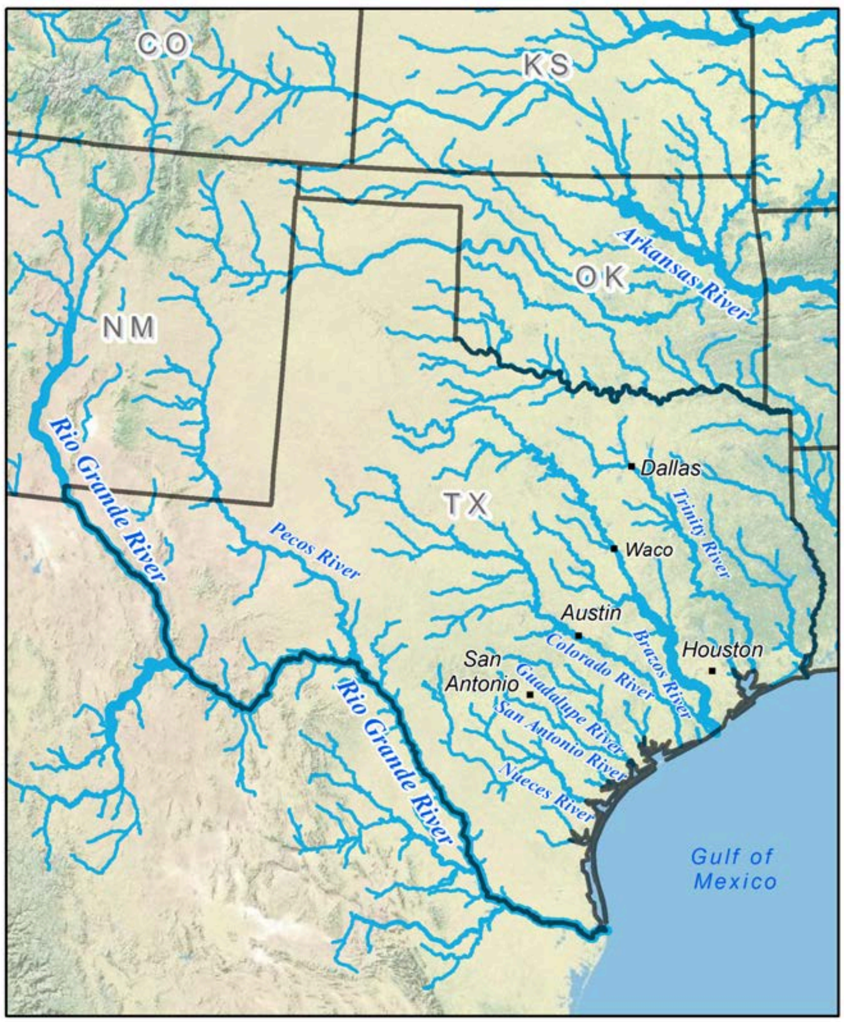

Figure 41. Major rivers in Texas

California

The Sacramento River, the largest and most important river in Northern California, flows over 716 km (445 mi) from Siskiyou County, California, to its confluence with the San Joaquin River at Suisun Bay. The San Joaquin flows nearly 589 km (366 mi) into Suisun Bay from Madera, California. Both the Sacramento and San Joaquin river valleys, which are important resources for fisheries, irrigation, and drinking water in Northern California, were flooded across an area nearly 480 km (300 mi) long and 32 km (20 mi) wide in 1862. Today, flooding has been stemmed dramatically due to several dams along this river network including the Shasta Dam. However, heavy flooding in January 1997 caused levee failures along the Sacramento and San Joaquin rivers, which resulted in extensive damage.

Southern California has been affected by devastating floods along the rivers that service Los Angeles and other major cities. Heavy rains can suddenly transform rivers in arid regions from being nearly dry to flood stage. The Los Angeles River serves Burbank, Glendale, and several other cities as well as Los Angeles. The longest river in Southern California is the Santa Ana, which flows through San Bernardino, Riverside, and Anaheim, before reaching the Pacific Ocean, serving a population of about 4.8 million people. The site of many severe floods, the river has undergone a massive project known as the Santa Ana River Mainstem Project, which includes the Seven Oaks Dam as well as levees and manmade channels.

Figure 42. Major rivers of California

The Pacific Northwest

Along the boundary of Oregon and Washington runs the 2,000 km (1,243 mi) Columbia River. The largest metropolitan area along the Columbia River is Portland, Oregon, although other cities are located along the river including Washington's tri cities: Pasco, Kennewick, and Richland. The river's 400 dams generate over 21 million kilowatts, providing more hydroelectric power than any other river in the world. Many industrial plants rely on the river's power including the now-decommissioned Hanford Engineer Works, near Richland, Washington.

Figure 43. Major rivers of the Pacific Northwest

2.3 Major Historical Floods in the United States

The model supports a historical event set of 20 events (Figure 44). Twelve of these events are described below.

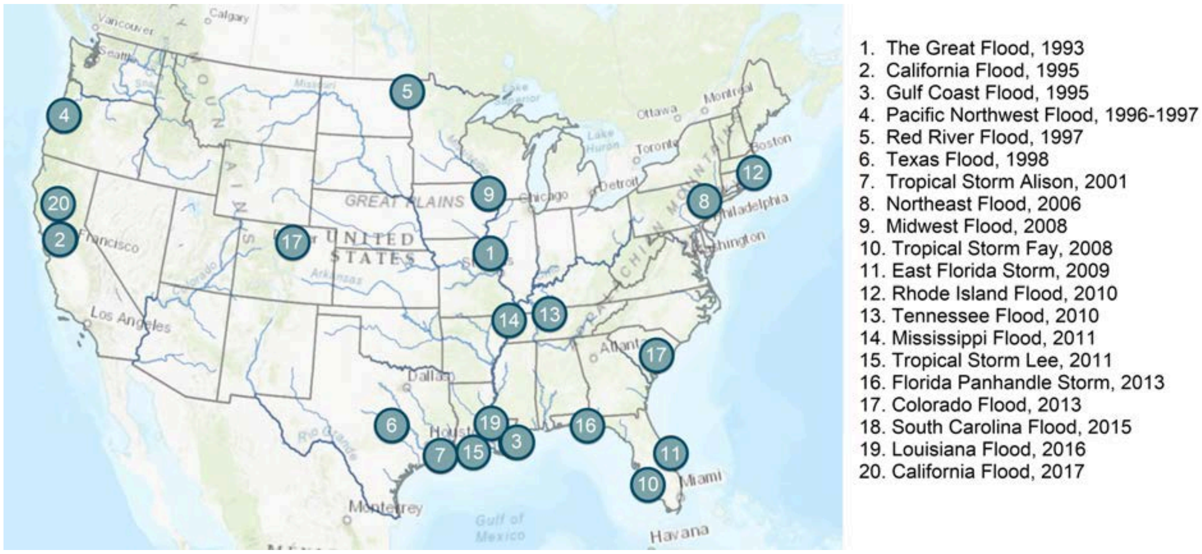

Figure 44. Locations of some major historical floods in the United States

See Also
Historical Event Set
Modeled Losses for Historical Flood Events

1993 The Great Flood (Spring)

One of the greatest natural disasters in U.S. history was its largest and costliest river flood, which took place during the spring of 1993 along the upper Mississippi River and the Missouri River. Water levels in 150 rivers reached or exceeded flood stage affecting North Dakota, South Dakota, Minnesota, Missouri, Iowa, Illinois, Kansas, and Nebraska. Several areas along the Mississippi River had flood levels that surpassed records set in 1973; some areas along the Missouri saw the highest flood levels since 1951.

The floods occurred due to heavy precipitation that followed an unusually wet fall and winter. The weather pattern had formed an "Omega Block"[6] trapping the low pressure system over the area. Between June and August nearly 300 mm of rain fell in many parts of the upper Midwest with some storms lasting more than 20 days. Reports of up to 180 mm in 24 hours were reported in many areas and some areas received 1,219 mm of rain that season. Between April and mid-June, the Mississippi River crested at 2-3 m above flood stage in several areas. Some rivers remained above flood stages for up to 200 days. In Missouri, several towns were flooded for longer than 180 days and persisted for 94 days in parts of St. Louis. Grafton, Illinois was flooded for 195 days.

By the beginning of August, the river levels in St. Louis were 6m (nearly 20 ft) above flood stage, the highest in the city's history, and came just 0.6m short of overtopping the 16m (52 ft) flood wall, built in 1844. The peak flow exceeded 30,580 m^3/s: a rate that would fill Busch

[6] Omega Blocks are very stable weather systems in which a large high pressure system is flanked by two low pressure systems, forming a pattern similar to the Greek letter Omega. The pattern causes storms to follow the same track, producing relentless rain over one area.

Stadium in 69 seconds (NOAA). On August 3, the Mississippi River levees were purposely broken by the U.S. Army Corps of Engineers. Just south of St. Louis, near Columbia, Illinois, 190 km^2 (73 mi^2) of land flooded due to failed levees, submerging several towns and threatening historic sites at Prairie du Rocher and Fort de Chartres. When the floods reached Cairo, where the Mississippi and Ohio rivers meet, it finally diminished due to a drought in the east that had lowered the water level of the Ohio River.

The Great Flood claimed 48 lives and damaged or destroyed over 50,000 homes. Approximately 75 towns were completely submerged as 40 federal levees and over 1,000 private levees were breached or overtopped. Drinking water became scarce due to contamination and failure of septic systems, while wastewater treatment plants were shut down. Chemical spills were transported over large areas and reached alluvial aquifers. Both the Mississippi and the Missouri rivers were closed to water traffic for up to two months, causes severe business interruption losses. Ten airports suffered severe flooding and virtually all railroads in the Midwest were shut down. Bridges along the Mississippi between Davenport, Iowa, and St. Louis were closed.

As a result of this flood, FEMA has lowered the flood risk for more than 12,000 properties through relocation or elevation, or by improving flood defenses.

1995 Northern California Flood (January)

From January 8-14, 1995, several cities in northern California, including Sacramento, experienced the most rainfall the area had seen since 1983. During the second week of January, northern California received 330 mm of rain in many areas, with some receiving up to 610 mm.

The rainfall was attributed to the warm El Niño waters in the Pacific Ocean, which produced storms throughout most of January. The rains had followed a prolonged drought, which had lowered the water level in the rivers, particularly the Russian River. This had allowed plants to grow along the banks, which reduced the absorption capacity of the soil and also slowed the water flow, allowing water levels to build even more quickly when the rainstorms began.

Reservoirs and flood routing prevented the main Central Valley rivers from flooding but smaller streams, basins, and coastal areas quickly exceeded their flood stages. The flooding affected a wide area that extended from Santa Barbara to the California-Oregon border, but the Sacramento area suffered the most.

All but one of northern California's 58 counties was declared a disaster area. Along the Carmel River, the Robles Del Rio area was significantly flooded as were several areas along Highway 1 and Mission Fields. The floods were followed two months later by a second winter storm. The area was still saturated and the storm caused devastating floods throughout Monterey County from March 10-13, 1995.

1998 Texas Flood

During the weekend of October 17-18, 1998, heavy downpours dumped nearly 200 mm (8 in) of precipitation over a vast area covering about 13,000 km^2 (5,000 mi^2), in south-central Texas. The rain storms were due to a low-level flow of moist air from the southeast that met a strong upper level trough in the west.

The resulting floods claimed 31 lives, with at least 17 due to automobiles that were swept away. Record water levels were recorded for many rivers including the San Antonio, Guadalupe, Brazos, Colorado, Sabine, San Jacinto, Medina, and Nueces rivers. Most of the flooding along the Guadalupe River was in the upper reach and spillovers occurred at Canyon Dam, located between San Antonio and Austin. Medina Lake, west of San Antonio, came just 45 cm short of overtopping its 90-year-old dam. Floods exceeded 100-year levels at the lower San Antonio River and also on lower Cibolo Creek.

Several areas between San Antonio and Austin received nearly 750 mm of rain causing flash floods; the National Weather Service issued 163 flash flood warnings, with 60 in the Houston/Galveston area. Austin and San Antonio were under flash flood warnings for four hours. Fortunately the San Antonio River Tunnels, which were completed a few months earlier, successfully protected the downtown areas, but federal disasters were declared in 43 counties. In the city of Gonzales, the Guadalupe River crested at over 16m; its flood stage is around 9m. River levels exceeded 15 m at Cuero, where the flood stage is 6 m. At Victoria, where the flood stage was 6.4 m (21 ft), the river reached nearly 10 m. Over 240 mm of rain fell in San Antonio and Leon Creek, whose flood stage is at 4.6 m, rose to over 8m. The city suffered power outages, downed trees and building damage.

2001 Tropical Storm Allison

Tropical Storm Allison is the costliest Atlantic tropical cyclone that remained below major hurricane strength as well as the first Atlantic storm who's name was retired without ever becoming a hurricane. Allison brought significant flooding and devastation to southeast Texas, Louisiana, and the Southeast and Mid-Atlantic United States as it moved across the region. Areas most impacted by flooding include southeast Texas, particularly Houston, Louisiana, and southeast Pennsylvania. Forty-one fatalities (23 in Texas alone) and USD 8.5 billion (untrended) in damage resulted from this storm.

Allison formed in the Gulf of Mexico from a tropical wave on June 4, 2001, slowly moved north, and made landfall near Freeport, Texas as a tropical storm on June 6. After making landfall, Allison weakened to a tropical depression and stalled out over the region due to an area of high pressure to the north. Allison produced excessive rainfall over the area as it slowly made a clockwise loop over the region during the next few days. During the overnight hours of June 9, Allison reentered the Gulf of Mexico. Over the next couple days, Allison transitioned into a subtropical storm and made landfall on Morgan City, Louisiana on June 11. Alison reintensified as it slowly accelerated while moving east-northeast across Mississippi, Alabama, Georgia, and South Carolina. The storm once again became nearly stationary over North Carolina prior to moving northeast across the Delmarva Peninsula on June 16 and over the western Atlantic by June 17. As Allison continued its northeast movement, it spread heavy rain across southeast New York and Southern New England before dissipating south of Newfoundland on June 20.

Allison produced heavy rainfall along its path, with a maximum storm total of 1,033.27 mm (40.68 in) reported at the Moore Road Detention Pond in northwest Jefferson County, Texas. In Harris County, Texas alone, 73,000 homes and 95,000 automobiles were flooded. In addition, 2,744 homes were destroyed and 30,000 people were left homeless in Texas.

Several hospitals experienced severe flood damage, and almost every major road in Houston was submerged under several feet of water.

Along the rest of Allison's path, reported maximum rainfall amounts include: 758.44 mm (29.86 in) in Thibodaux, Louisiana; over 381 mm (15 in) in southwest Mississippi; up to 406 mm (16 in) in North Carolina; 258.32 mm (10.17 in) in Chaifont, Pennsylvania; 205.74 mm (8.1 in) in Tuckerton, New Jersey; 145.54 mm (5.73 in.) in Granite Springs, New York; 182.88 mm (7.2 in) in Pomfret, Connecticut; and 180.34 mm (7.1 in) in North Smithfield, Rhode Island. These rainfall totals resulted in significant river and flash flooding. In addition, a levee along the Bayou Manchac in Louisiana broke, which exacerbated the flooding. Many businesses and homes experienced flood damage, and numerous roads, bridges, and some rail lines were washed out. In Allison's aftermath, President G.W. Bush designated 75 counties in the storm's path as disaster areas.

2009 East Florida Storm

During the week of May 17 - 23, 2009, a cold frontal passage followed by the development of a strong slow-moving low pressure system produced record-breaking rainfall and flooding across the central Florida Peninsula. Areas hardest hit include Volusia, Seminole, and portions of Orange Counties in northeast central Florida.

Weeklong rainfall amounts between 127 and 381 mm (5 and 15 in) were common across the affected areas. The greatest 7-day observed total of 687.32 mm (27.06 in) was reported by a Community Collaborative Rain, Hail, and Snow Network (CoCoRaHS) observer in Ormond Beach, Florida. Daytona Beach International Airport received 524 mm (20.63 in) between May 17 and 23, which helped set a May monthly rainfall record of 567.18 mm (22.33 in). In addition, many 24-hr rainfall total records were set in Daytona Beach, Orlando, Melbourne, and Vero Beach. The persistent weeklong heavy rainfall resulted in substantial flooding across some neighborhoods in northeast Volusia County, including Daytona Beach and Ormond Beach. Also, rainfall during the previous week contributed to an abnormally wet May, and the resultant flooding continued through the end of the month.

2010 Tennessee Flood (May)

During May 1–2, 2010, a stalled frontal system drew moist, warm air from the Gulf of Mexico over the western half of Tennessee. The area was deluged with a series of heavy rainstorms that produced 1,000-year floods in many areas, including many along the Cumberland River around Nashville and Clarksville.

An average of 355–380 mm fell across most of the region and some areas received over 500 mm. Over a period of 36 hours, Nashville received over 345 mm, far exceeding the previous record of 170 mm for two days of rainfall as well as the record of 280 mm for the month of May. The flood stage of the Cumberland River at Nashville is 12 m, and it crested on May 3 at 16 m. In Clarksville, where the flood state is 14 m, the river crested at 19 m.

The floods claimed the lives of 24 people and displaced over 10,000. Approximately 11,000 properties, over half of which were located outside of the 100-year floodplains, were severely damaged or destroyed. Stretches of several highways were closed and over 2,700 businesses were forced to shut down, some permanently, due to flood damage, putting nearly 15,000 people out of work. The Opry Mills mall closed until 2012 due to severe damage, which had a significant effect on tax revenue for the state as well as business interruption losses.

2011 Lower Mississippi River Flood (Winter-Spring)

Heavy precipitation and snowmelt during the late winter and early spring of 2011 resulted in massive flooding along the lower Mississippi River, particularly in the states of Arkansas, Kentucky, Louisiana, Mississippi, Missouri, and Tennessee. In several places, the river levels surpassed those of the Great Flood of 1993, increasing the destruction in several states that had already endured the "super tornado outbreak" that year.

The flood put to test the system of levees and floodways and by early May, severe flooding predictions led to intentional levee breaches in Arkansas, Mississippi, Missouri, and Tennessee. In Missouri, the levee breach submerged over 500 km^2 (193 mi^2) of farmland, but allowed Cairo, Illinois to be largely spared. Along the lower Mississippi, the discharge reached over 35,000 m^3/s; high enough to threaten New Orleans and Baton Rouge. As a result, three floodways were opened simultaneously for the first time: the Birds-Point New Madrid Floodway in Missouri, and the Morganza Floodway and Bonnet Carré Spillway in Louisiana. The Morganza Floodway alone flooded over 11,900 km^2 (4,500 mi^2) along the Atchafalaya River. The Bonnet Carré Spillway, located 50 km (31 mi) north of New Orleans, allowed much of the excess water to drain into Lake Pontchartrain.

The flood diversion successfully spared parts of several urban areas, saving thousands of homes, and prevented the shutdown of a substantial percentage of domestic oil processing. However, over 21,000 homes were flooded despite the mitigation efforts along with over a million acres of agricultural land; some properties on the land that was intentionally flooded were totally destroyed. Flooded areas were covered with debris, sediment, and were contaminated by chemical spills.

2013 Florida Panhandle Storm

Heavy rain along with river and flash flooding resulted from a continuous influx of deep layer moist tropical air over the southeast United States from July 2 - 6, 2013. While most of the rain fell within a 3-day period from July 2-4, additional bouts of heavy rain continued the following two days. As a result, flash flooding and significant river flooding occurred across Alabama and the Florida Panhandle. This storm also produced flooding rains across portions of North Carolina, Mississippi, South Carolina, Kentucky, and Tennessee.

A large area of at least 254 mm (10 in) of rain fell across southeast Alabama and the Florida Panhandle, with localized amounts of almost 508 mm (20 in) reported in a 3-day period from July 2 - 4. The heaviest rainfall was observed in Washington and Holmes Counties in Florida. Torrential rainfall resulted in severe flash flooding, which flooded homes and washed out roads in Bay and Washington Counties in Florida, and significant river flooding, which inundated homes and businesses and washed out roadways. One river location most notably impacted was the Choctawhatchee River at Bruce-Ebro, Florida, which rose 2.98 m (9.79 ft) and crested 0.39 m (1.29 ft) above its major flood stage of 5.03 m (16.5 ft) on July 8.

2013 Colorado Flood

During September 9 - 16, 2013, a persistent southerly flow of tropical moisture from the Gulf of Mexico and the eastern Pacific Ocean was drawn toward the east-facing Rocky Mountain slopes. This moisture was wrung out by the mountains, which resulted in many consecutive days of unusually widespread heavy rainfall and catastrophic flooding over the Colorado Front Range foothills and neighboring high plains in northeast Colorado and Nebraska. Flooding effects were widespread and lasted days to weeks after the rain ended.

Much of the rain fell within a 36-hr period from September 11 - 13, with reported sustained rainfall rates between 25 and 50 mm/hr (1 and 2 in/hr) near Boulder, CO and northwest toward Estes Park, CO. Rainfall storm totals of over 254 mm (10 in) were common, with the highest totals of greater than 400 mm (16 in) observed in Boulder, CO and in the foothills west and northwest of the city. Boulder set its 1-day, 2-day, 3-day, 7-day, and monthly rainfall records of 230.6 mm (9.08 in), 292.6 mm (11.52 in), 341.8 (13.44 in), 429.3 mm (16.9 in), and 461.2 mm (18.16 in), respectively. In addition, Denver, CO set its September monthly rainfall record of 142.5 mm (5.61 in) from this event. Fort Carson, CO set a daily rainfall extreme for the state of Colorado, with 301 mm (11.85 in) falling from midnight to midnight local time on 12-13 September and 316 mm (12.46 in) from 09 to 09 local time on 12-13 September. Three of the top ten greatest 1-day rainfall totals in Colorado's history occurred as a result of the 2013 Colorado Flood.

Heavy to record-breaking rainfall caused extensive flash and river flooding, 1,138 documented debris flows, and over 1,100 landslide and hillslope failures, which resulted in 8 fatalities. This rainfall devastated towns; over 1,882 structures were destroyed and 780 km (485 mi.) of highways were damaged or destroyed. In addition, more than 3,700 people were evacuated and 18,000 people were forced to leave their homes.

The 2013 Colorado Flood has an estimated streamflow return period of around 500 years on the mainstem and North Forks of the Big Thompson River and parts of the lower St. Vrain River. On Boulder Creek, the estimated return period is only 50 years because the heaviest rain fell in the lower and flatter part of the drainage basin. As a result, the runoff response time was elongated. Rivers in the Colorado Front Range that experienced the greatest flooding include the Poudre, Cache la Poudre, Big Thompson, Little Thompson, and St. Vrain Rivers, as well as Buckhorn, Fourmile, Boulder, Fall, Fish, Lefthand, and James Creeks. Flooding resulting from a combination of heavy local rainfall and runoff from the Front Range devastated many communities in the Colorado high plains. In this area, most of the river flooding occurred along the St. Vrain, Big Thompson, and South Platte Rivers as well as Westerly and Sand Creeks.

Several towns were inundated for many days and it took approximately two weeks for some rivers to recede back below their flood stage after the rain had finally ended. Eighteen counties in northern Colorado were designated as federal disaster areas. Storm total flood damages exceeded USD 2 billion (untrended).

2015 South Carolina Flood

Between October 1 and 5, 2015, the combination of a surface low-pressure system located along a stationary frontal boundary off the U.S. Southeast coast, a slow moving upper low to the west, and a persistent plume of tropical moisture associated with Hurricane Joaquin resulted in record rainfall over portions of South Carolina. Some areas experienced more than 20 in of rainfall over the 5-day period. Many locations recorded rainfall rates of 2 in per hour. This rainfall occurred over urban areas, namely, the tri-county areas (Charleston, Berkeley, Dorchester) and Columbia, where runoff rates are high and on grounds already wet from recent rains.

Widespread, heavy rainfall caused major flooding in areas from the central part of South Carolina to the coast. The historic rainfall resulted in moderate to major river flooding across South Carolina with at least 20 locations exceeding the established flood stages. Flooding from this event resulted in 19 fatalities. Nine of these fatalities occurred in Richland County, which includes the main urban center of Columbia. Thirty-six dam failures across South Caroline were reported. South Carolina State Officials said damage losses were $1.492 billion.

2016 Louisiana Flood

Between August 11 and 13, 2016, a unique warm-core, low-pressure system formed over Louisiana. The storm meandered and strengthened over time, positioning itself with a southeasterly fetch over the Gulf of Mexico, which was experiencing near-record, warm-sea surface temperatures. This positioning provided the storm with a lift and unlimited moisture, resulting in torrential downpours and thunderstorms. The region between Lafayette and Baton Rouge experienced record rainfall totals, exceeding 600 mm (24 in) in some locations. Watson, near Baton Rouge accumulated 797 mm (39.4 in) of rain.

2017 California Flood

California’s longest drought in the state’s history (2011-2017) ended with a series of extreme weather events in the beginning of 2017. These events were so severe, that in turn, they broke the century’s old record of the wettest winter and caused state-wide flooding, especially in the northern and central parts of the state. The back-to-back rain and snowstorms in January and February caused mass local evacuations, excessive overland flows, levee failures, washed out roads, and extreme snow melt in the following months.

The five winter storms that hit California in winter of 2017 were fueled by so-called Pineapple Express, the air and moisture movement between Hawaii and California. Pineapple Express storms can reach 250 by 1,000 miles in size and carry 20 times more moisture than the largest river in the United States, Mississippi, at the river mouth (the Gulf of Mexico).

The most damaged areas were the counties in the Sacramento-San Joaquin Delta, causing more than $1.55 billion in property damages alone.

3 Event Generation

The Verisk model captures the effects of precipitation-induced flooding on any insurable properties in the continental United States. It is a fully probabilistic inland flood model, designed for portfolio risk management, covering flooding to properties located both on- and off-floodplain.

The model captures all the complexities inherent in a flood generation process. These include space-time patterns of rainfall input, and the effects of a highly variable climate, snowfall, snowpack, and snowmelt, topography, local geology, and soil types as well as other local factors and the effects of man-made flood defenses and flood regulation. The model is built to meet the wide spectrum of flood risk management needs of the insurance industry and accounts for policy conditions specific to the United States.

To generate the large set of simulated events that comprise the 10,000-year stochastic catalog, the model employs a precipitation model and large-scale hydrological model. These simulated events are generated by means of a combination of a General Circulation Model (GCM) and Numerical Weather Prediction (NWP) model, which simulates precipitation patterns as they evolve with time over the area of interest. Precipitation output is converted by the hydrological model to overland runoff and flow in rivers, which the model uses to propagate a "flood wave" through the modeled river network. This simulation takes into consideration the amount of time it takes for the flood wave to travel along the rivers, the effects of the river shape, levees, dams, or other structures, and any potential storms that may exacerbate the flood intensity.

The hydrological model computes the discharge at each location along the river network at hourly time intervals, producing a hydrograph that provides the streamflow for each event, along each stream link. Only those hydrograph peak values that exceed the five-year peak discharge constitute the events in the stochastic catalog.

From a modeling perspective, the process of creating the stochastic catalog consists of multiple components, which make up the precipitation and hydrological models:

Precipitation model	Coupled GCM-NWP model
Hydrological model	Runoff generation model[7] Snowmelt model Flow routing model Reservoir regulation model

[7] This module generates runoff as well as flows for small rivers/catchments (unit catchment).

3.1 Event Generation Data Sources

To develop the precipitation and hydrological models, Verisk obtained information from several agencies that gather original climatic and hydrological data. These data sources are listed below.

Historical Precipitation	U.S. National Weather Service (NWS) Climate Prediction Center (CPC) https://www.cpc.ncep.noaa.gov/ Date(s): 1979 to 2018 Resolution: 0.25°
High Resolution Precipitation	Parameter-elevation Regressions on Independent Slopes Model (PRISM) data set[8] https://www.wcc.nrcs.usda.gov/climate/prism.html Date(s): 1979 to 2018 Resolution: 4 km [9]
Sea Surface Temperature / Sea Ice Coverage	National Centers for Environmental Prediction at NOAA for the North American Regional Reanalysis (NARR)[10] https://www.ncdc.noaa.gov/data-access/model-data/model-datasets/north-american-regional-reanalysis-narr Date(s): 1979 to 2018 Data obtained from a reconstruction of the climate over the contiguous United States for the period, by means of a Numerical Weather Prediction model
Land Surface Model	North American Land Data Assimilation System (NLDAS) https://ldas.gsfc.nasa.gov/nldas https://www.emc.ncep.noaa.gov/mmb/nldas/ Resolution: 0.125°
Precipitation Frequency	NOAA Atlas 2, Atlas 14, from NOAA's National Weather Service Hydrometeorological Design Studies Center https://hdsc.nws.noaa.gov/hdsc/pfds/index.html, Resolution: Continuous/Arbitrary

[8] The PRISM data set was developed in partnership by the National Resources Conservation Service (NRCS) National Water and Climate Center (NWCC) and the PRISM Climate Group at Oregon State University.
[9] Verisk aggregated PRISM data to 8 km resolution
[10] Verisk obtained sea surface temperatures from the NARR data set.

	Vintage: 2018
Stream flow	United States Geological Survey (USGS) https://waterdata.usgs.gov/nwis Resolution: Continuous/Arbitrary Dates: from inception of each station to 2017 Annual peak flow data, hourly flow data, concurrent stage-discharge field measurement data, and other data sets
Reservoir storage	United States Bureau of Reclamation (USBR) https://www.usbr.gov/pn/hydromet/select.html Date(s): 1981 to 2017
Dams	International Commission on Large Dams (ICOLD) https://www.icold-cigb.org/ Vintage: 2013 United States Army Corps of Engineers (USACE) National Inventory of Dams datasets https://nid.sec.usace.army.mil/ Vintage: 2013 The Global Water System Project's Global Reservoir and Dam Database (GRanD), v1.01 https://sedac.ciesin.columbia.edu/data/set/grand-v1-dams-rev01 Vintage: 2011
Soils	United States Department of Agriculture (USDA) Digital General Soil Map of the United States (STASTGO2) database https://www.nrcs.usda.gov/wps/portal/nrcs/detail/soils/survey/geo/?cid=nrcs142p2_053629 Resolution: 1:250,000 Vintage: 2014 USDA's Soil Survey Geographic Database (SSURGO) https://www.nrcs.usda.gov/wps/portal/nrcs/detail/soils/survey/geo/?cid=nrcs142p2_053627 Resolution: 1:12,000 to 1:63,360 Vintage: 2018

Land Use / Land Cover (LULC)	USGS, Landsat data from the Multi-resolution Land Characteristics Consortium (MRLC) https://www.mrlc.gov/ Vintage: 2011 (released in 2014) Resolution: 30 m

3.2 Simulating Precipitation

The fundamental process behind stochastic event generation is the simulation of precipitation patterns as they evolve with time over the area of interest. Construction of this simulation is based on original Verisk research, with the intention of generating a precipitation catalog to cover the entire continental United States.

Rainfall simulation for event-driven flood modeling must satisfy the following requirements:

- Simulate realistic storm events over a long period of time (at least 10,000 years) at a high spatial and temporal resolution over the entire model domain
- Preserve both short- and long-term rainfall intensity distributions at each location (e.g., rainfall accumulation for time intervals of 24 hours, 48 hours, and 72 hours)
- Preserve spatial and temporal dependencies in rainfall patterns (e.g., the spatial distribution of areas that receive rain and areas that do not, and realistic storm cells)
- Preserve the dynamics of storm cell movement and the seasonality of storm occurrence

There are numerous stochastic approaches for generating synthetic rainfall patterns. However, these approaches are applicable only for relatively small areas – areas comparable to the size of a typical storm interior [approximately 500 to 1,000 km (300 to 600 mi) in diameter]. Over such small areas, one can assume the statistical properties of the precipitation field to be homogeneous (unchanging with location) and stationary (unchanging over time). Precipitation cell advection (i.e., cell movement above the terrain) can be represented by either a "point process" approach, frequently used in hydrology, or by a space-time anisotropy approach.[11]

Simulating precipitation and runoff over a large-scale domain, such as the continental United States, is challenging for multiple reasons:

- The precipitation field is heterogeneous and non-stationary (frequently with circular advection of the rain cells).
- Precise snowmelt modeling becomes critical as runoff from large mountainous and lowland areas must be simulated simultaneously.
- Expanding the modeling domain to a continental scale means that precipitation is modeled over areas with different climates, therefore requiring local adjustments on

[11] Verisk employs the space-time anisotropy approach in the *Verisk Inland Flood Model for Great Britain*.

both a quantitative and qualitative basis (e.g., with respect to the amount of snow accumulation).

To overcome these challenges, Verisk developed a novel approach. At its heart is a coupling between a general circulation model (GCM) and numerical weather prediction (NWP) model, which generates continuous data on precipitation, snow, temperature, potential evapotranspiration and all other fields necessary for a comprehensive flood model on an hourly basis, at a spatial resolution of 64 km x 64 km (40 mi x 40 mi). The NWP data is then “downscaled” to a resolution of 8 km x 8 km (5 mi x 5 mi) x 1 hr through a process that introduces structured stochastic perturbations that preserve the small-scale variability characteristics of precipitation fields.

Using Coupled GCM and NWP Models to Simulate Precipitation at a Continental Scale

Both the GCM and NWP model mathematically simulate atmospheric circulation by solving the primitive equations for mass and momentum conservation, as well as the thermal energy equation.[12] These models are commonly used in climate change prediction and weather forecasting applications. In the Verisk model, however, the models have been applied for completely different purposes and have been implemented with different modeling frameworks.

General Circulation Models (GCMs)

A GCM is a mathematical model that simulates the general circulation of a planetary atmosphere and ocean over long periods of time, using a specific formulation of the Navier-Stokes (N-S) equations. As illustrated in Figure 45, GCMs utilize a rotating sphere whose key components are atmospheric and oceanic GCMs (AGCMs and OGCMs, respectively), which incorporate sea ice and land-surface components. The sphere's energy sources (radiation, latent heat, etc.) are expressed thermodynamically. With all climate components and driving forces included, these climate models can run on an entirely self-contained basis for hundreds, or even thousands, of years to simulate different climate scenarios.

[12] Navier-Stokes (N-S) equations are widely used as the basis for modeling the behavior of incompressible fluids. They are extensions of the Euler equations and provide the relationship between the velocity, pressure, temperature, and density of a moving fluid, taking into account the effects of viscosity on the flow.

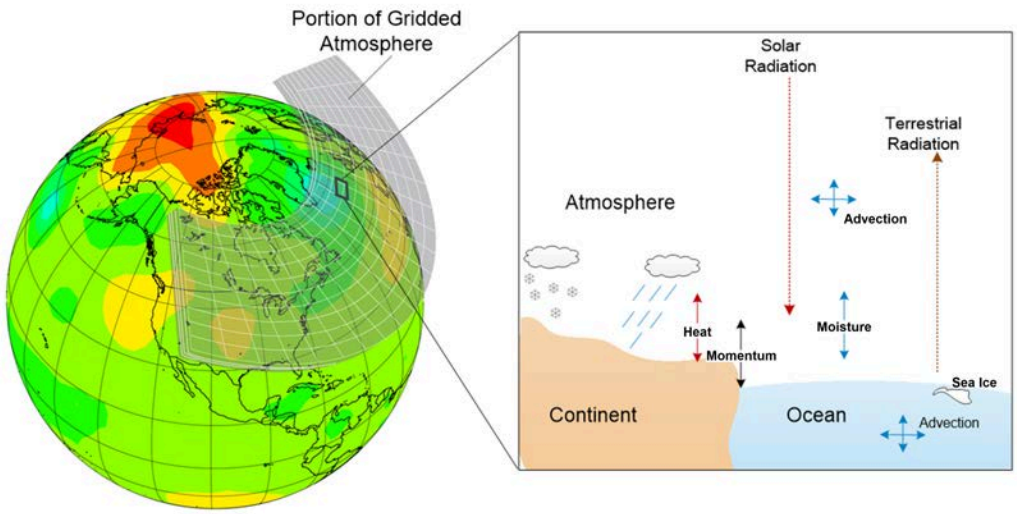

Figure 45. A General Circulation Model (adapted from NOAA)

Ideally, GCMs could be used directly to produce long-term simulations for catastrophe modeling. However, for a realistic simulation of precipitation patterns that represent the vertical structure of the atmosphere and the effects of terrain on atmospheric circulation, a model must have a resolution of at least 100 km (62 mi). This is impractical with a GCM.

There are additional arguments against using GCMs for direct precipitation simulations, including the fact that they rely on simplified microphysics and may not provide a solid representation of precipitation, particularly in mountainous areas. Therefore, Verisk has taken a different approach that couples the GCM with an NWP model at a **mesoscale** (medium-scale) resolution.

Mesoscale Numerical Weather Prediction (NWP) Models

NWP models are widely used for forecasting weather at scales ranging from mesoscale (tens to hundreds of kilometers/miles) to synoptic (a few thousand kilometers/miles or continental scale). While global GCMs are designed to simulate the atmosphere over the entire globe, the higher-resolution mesoscale models can provide more detail when necessary. For example, mesoscale models are useful in situations where local or regional conditions affect weather and climate.

In contrast to GCMs, mesoscale NWP models use more sophisticated microphysics schemes, which provide a better representation of the physics of precipitation particles, or **hydrometeors**. Therefore, they are more appropriate for modeling precipitation, particularly for localized, extreme cases of convective precipitation during the summer months. Additionally, mesoscale models produce superior forecasts for coastal and mountainous regions compared to traditional GCMs, since they use high-resolution topography datasets and detailed sea surface temperatures. These models are most frequently used for short-term predictions over a country-sized region or larger (up to a continent), and are commonly used for local weather forecasting.

NWP models, like GCMs, use a grid (Figure 46), but cover a smaller area. Since they are limited-area models, NWPs require both initial and boundary conditions to simulate the flow of the atmosphere over the region of interest. This design makes them ideal for nesting within a host GCM, from which they can obtain the necessary initial and boundary conditions. NWP models cannot be used for long-term, standalone runs and are therefore not suitable for standalone catastrophe modeling.

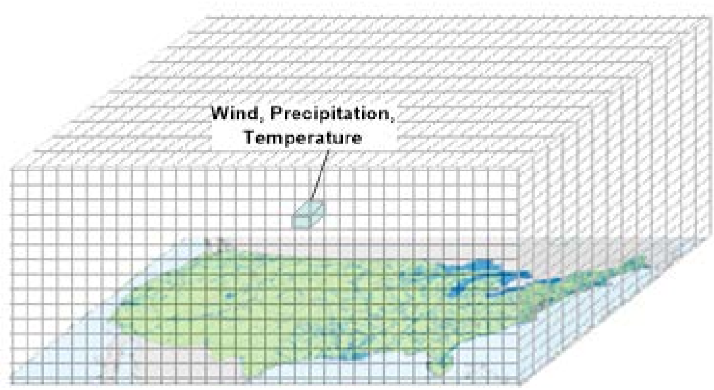

Figure 46. Gridded representation of the atmosphere in an NWP model
Not to scale.

NWP models provide a purely physically-based, large-scale catalog of precipitation at sufficiently high spatial and temporal resolutions. Their physical nature allows them to account for the non-linear interaction between land and the atmosphere, and they incorporate the effects of different types of land cover (water surfaces, vegetation, bare soil, and bedrock). NWP models account for the effects of the widely varying terrain on atmospheric conditions (e.g., storms that move over mountainous regions). They also account for the interaction of multiple storm systems, including stalled systems, which can produce unusually heavy precipitation in an area over a long period of time.

In addition to incorporating the effects of land cover and terrain, NWP models provide a realistic precipitation pattern at the continental scale. By using reanalysis data obtained from historical observations, NWP models can reproduce the frontal and circular precipitation patterns specific to extratropical cyclones passing over the continental United States. There is no purely stochastic model that can reproduce these patterns both spatiotemporally and statistically.

Finally, NWP model output provides components necessary for a robust snowmelt model and the soil water balance (i.e., wind, temperature, and potential evapotranspiration variables).

Coupling the GCM and Mesoscale NWP Models

Verisk's approach to large-scale precipitation simulation benefits from both the GCM and NWP models. The GCM produces long-term, standalone runs, while the mesoscale NWP model provides a better representation of precipitation physics and a higher degree of detail. Verisk employs a GCM running over the entire globe, at a coarse resolution, while a mesoscale NWP model, nested within the GCM, runs over the model domain, at a reasonably high resolution.

The GCM used in the Verisk model is the Community Atmospheric Model (CAM), a well-established global atmosphere model developed at the National Center for Atmospheric Research (NCAR). CAM is capable of running either as a standalone model or as part of the Community Climate System Model (CCSM), for which it provides atmosphere, ocean, land, and sea-ice modeling components to simulate Earth's climate.

In Verisk's implementation, CAM runs together with the Community Land Model (CLM), while sea surface temperatures and sea ice coverage come from an observational dataset from North American Regional Reanalysis (NARR) data (1980–2005). Verisk's 10,000-year catalog, therefore, can be seen as 400 different representations of the climate during this same time period (1980–2005). The grid resolution is 72 cells x 108 cells (cell size 2.5° x 3.33°) with 26 vertical levels.

To provide independence between each of the 26-year runs, Verisk researchers investigated the time required for two parallel runs, starting from the same but slightly perturbed initial conditions, to become uncorrelated. This occurs when the differences between the runs have become equal to the standard deviation of the corresponding fields (temperature, sea level pressure, etc.). This was done based on the analysis of an ensemble of 30 CAM runs. Verisk obtained each member of the ensemble by perturbing the initial conditions and then running CAM for two modeled years. The result from the analysis showed that the time to decorrelate two runs is approximately one month of model time. Verisk obtained the independence between each of the 26-year runs by running CAM for three months while slightly perturbing the initial conditions. The new CAM initial conditions obtained after each one-year CAM run were used for a corresponding coupled 26-year CAM-WRF run, described below.

For the NWP model, Verisk used the Weather Research and Forecasting (WRF) model in order to resolve the climate over the United States. WRF is a next-generation mesoscale NWP system designed for both operational forecasting and atmospheric research. It features an advanced non-hydrostatic representation of the vertical atmospheric structure and its microphysics, a sophisticated observation assimilation system, and a software architecture that accommodates computational parallelism, and system extensibility. The model is very well-established and used for daily weather forecasts.

WRF is suitable for a broad spectrum of applications across scales ranging from meters/feet to thousands of kilometers/miles. The effort to develop WRF has been a collaborative partnership, principally among the National Center for Atmospheric Research (NCAR) and the National Centers for Environmental Prediction (NCEP).

Figure 47 illustrates the coupling of the CAM global model with the WRF-NWP model. The WRF uses a grid centered at latitude 39.47° and longitude -97.3°. The grid resolution is 64 km x 64 km (40 mi x 40 mi) with 24 vertical levels (grid size of 73 cells x 93 cells). Verisk chose this resolution, which is exactly two times coarser than the NARR data, to avoid interpolation in the calibration and validation of the precipitation input. A 10-grid cell boundary condition transition zone around the model domain allows the model to adjust its computational process as it moves from the coarse CAM grid to the finer WRF grid. The transition zone is discarded when the WRF model output is saved, which avoids any possible artifacts due to the transition from the coarser to the finer resolution.

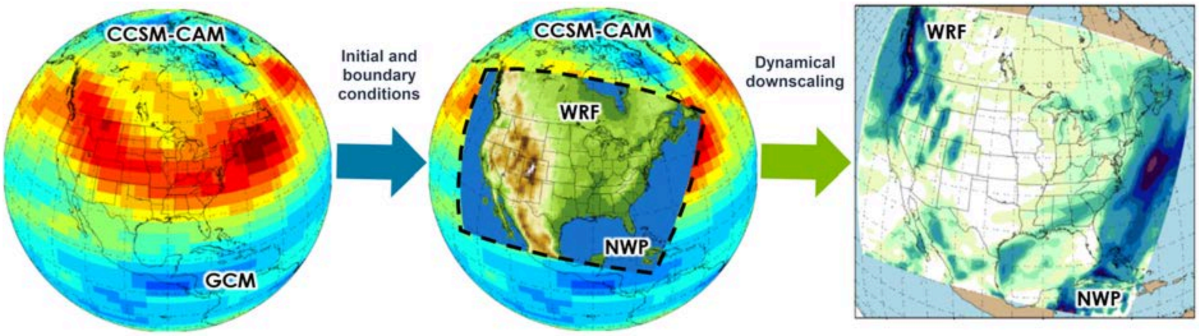

Figure 47. The global GCM (CCSM-CAM) is coupled with the regional mesoscale NWP model, and the output is downscaled to yield precipitation patterns at a high resolution.

To run the coupled CAM-WRF system, Verisk developed a fully automated suite of system and NCAR Command Language (NCL) scripts. The script package provides a sustainable, long-term simulation with checks at regular time-steps. Each day that CAM is run, it produces four six-hour files that provide data on wind, air pressure, air temperature, air humidity, soil saturation, and soil temperature. This data is interpolated to the WRF grid, allowing the WRF model to produce its own output data on total precipitation, total snow, surface temperature, wind, humidity, and potential evapotranspiration.

Spatial and Temporal Downscaling of Coarse-resolution Precipitation

Many characteristics of a flood, including the likelihood of flash flooding, are determined by the intermittent character of the precipitation fields in space and time. Therefore, it is important that these characteristics are addressed once the potentially flood-causing events have been identified and assembled. To do this, Verisk developed a sophisticated downscaling technique that captures the intermittent behavior of precipitation at a resolution fine enough to include all necessary information.

To simulate precipitation fields at a high resolution, an understanding of how hydrometeors[13] form out of turbulent atmospheric conditions is crucial. Atmospheric turbulence can be described using turbulent flow – a law of fluid dynamics that describes the chaotic fluctuations in flow due to continuous changes in velocity and pressure. Most of the kinetic energy released from turbulent motion is contained within large eddies. As this energy "cascades" from large-scale flows to smaller flows, large eddies dissipate into smaller ones.

Turbulent flow is a complex phenomenon; however, this dissipation of energy follows the statistical theory of turbulence, which is relatively straightforward (Kolmogorov, 1941). The theory is based on the energy transfer, or cascade, between eddies and the concept of **self-similarity** – a mathematical property where an object has a shape identical, or very similar, to one or more of its parts. The practical importance of self-similarity is that the

[13] precipitation particles

statistical moments (mean, variance, skew, etc.) follow simple power laws with the degree of aggregation. Thus, one can fix the statistical properties of the rainfall field at a coarse resolution [e.g., the NWP output at a resolution of 64 km (40 mi)] and refine the precipitation field by adding structured perturbations estimated from the coarse-scale observations.

To introduce these structured perturbations requires a geostatistical model that represents the statistical properties of turbulent patterns. Such a model was introduced by Theodore von Kármán (1948) – known also as the Matèrn model in the geostatistical community – to represent the auto-covariance of turbulent fields and capture the pour-law decay of turbulent energy as a function of scale. Following Goff and Jordan (1988) the covariance model for a homogeneous, zero mean field $Z(\vec{x})$ with variance σ^2 is expressed as:

$$C_{zz}(\vec{\tau}) = \sigma^2 \; 2^{(1-v)} / \Gamma(v) \; r(\vec{\tau})^{v} K_v(r(\vec{\tau}))$$

where $C_{zz}(\vec{\tau}) = E\lfloor Z(\vec{x}) Z(\vec{x} + \vec{\tau}) \rfloor$ is the spatial auto-covariance, $r(\vec{\tau})$ is the elliptical norm (i.e., the directionally normalized distance $r(\vec{\tau}) = |\vec{\tau}^{T} Q \vec{\tau}|^{1/2}$, Q is a positive-definite coordinate transformation matrix accounting for anisotropy and K_v is the modified Bessel function of order v). The roughness parameter v describes the behavior of the covariance model near the origin and thus, controls the small-scale variability of the field.

The spectral form of the von Kármán model has an analytical expression:

$$P_{zz}(\vec{k}) = 4\pi v \sigma^2 |Q|^{-1/2} [u(\vec{k}) + 1]^{(-v+1)}$$

where $P_{zz}(\vec{k})$ is the spectral density and $u(\vec{k}) = |\vec{k}^{T} Q^{-1} \vec{k}|$ is the elliptical norm/distance in the frequency plane. The fact that this geostatistical model has an explicit analytical form, its spectral representation, is important because it allows a robust and efficient simulation of the small-scale perturbations of interest.

Figure 48 provides examples of von Kármán models for different values of v and correlation length 10 units. Note that for v= 1/3 the model corresponds to the original proposal of von Kármán, where it follows the Kolmogorov's -5/3 power law for turbulent energy dissipation for wave numbers beyond the correlation length (i.e., in the inertial subrange) and levels off at large scales with a finite variance (i.e., there are no fluctuations at these scales). Therefore, by using a model with variance σ^2 equating the variance of the fluctuations at the resolution of the input field, correlation length corresponding to the grid resolution of this field and roughness parameter v corresponding to Kolmogorov's -5/3 law, one can introduce physically consistent fluctuations at resolutions (i.e., scales) finer than the resolution of the input grid.

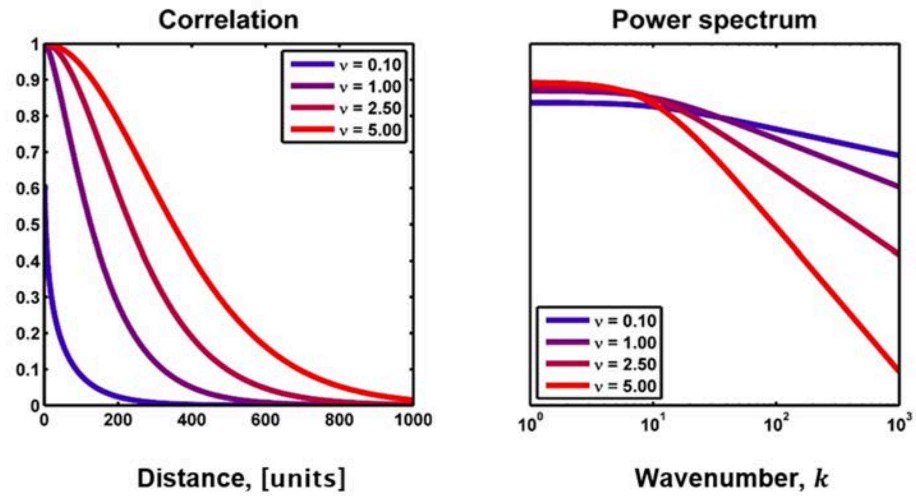

Figure 48. Examples of von Kármán covariance model for different values of the roughness parameter *v*

In addition to their high intermittency, precipitation patterns are characterized by high local anisotropy (i.e., elongation of the fluctuation in a particular direction) introduced by motions in the atmosphere such as fronts, cyclones, and waves. Since the range of the statistical downscaling is significant – from 64 km down to a few kilometers – it is imperative that we capture the anisotropy introduced by these motions in the downscaling process. To do this, Verisk developed a directional multiresolution framework (i.e., a set of functions) for analysis and synthesis of anisotropic fields. Essentially, the approach divides the frequency plane in sectors, which correspond to oscillating directional functions with restricted spatial extent in the physical space (Figure 49).

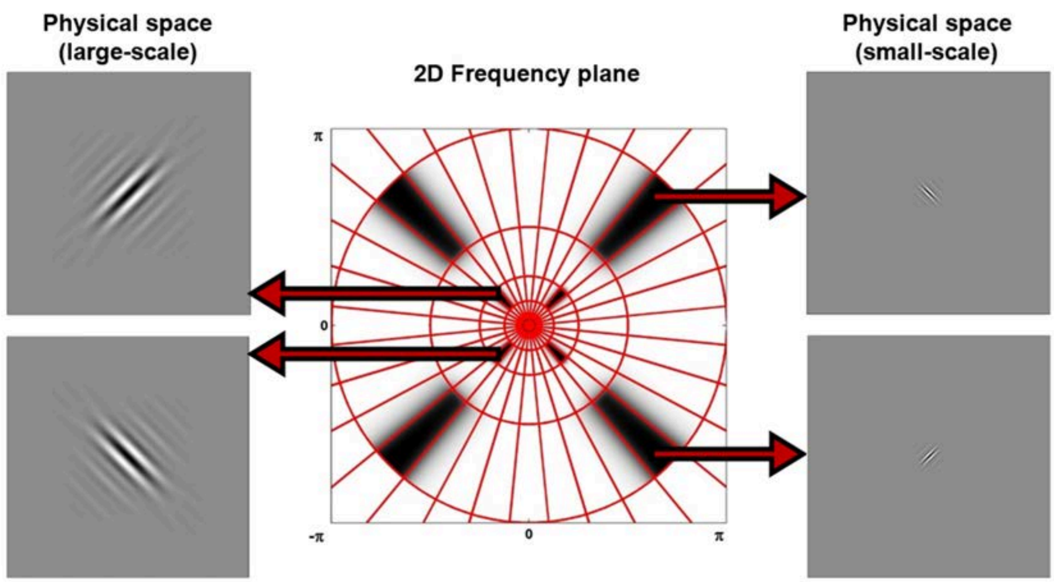

Figure 49. Circular frequency domain partitioning with examples of directional basis functions
Each frequency sector's central angle (0° - 180°) corresponds to a basis function perpendicular to this direction. The total number of functions is the number of directions × the number of frequency bands – i.e., the number of concentric circles on the frequency plane.

By convolving these functions with the input data, the model can analyze the magnitude of the resulting product in multiple directions and obtain the local anisotropy characteristics in terms of a unit ellipse at each grid cell. Figure 50 presents an analysis of local precipitation anisotropy.

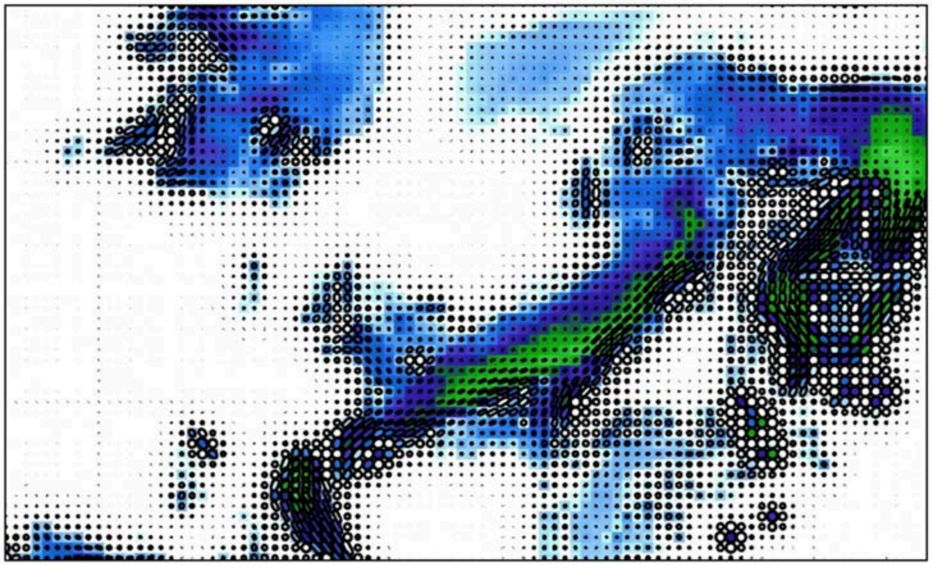

Figure 50. Example of data inferred local anisotropy and variance from coarse (64-km) WRF model precipitation
The ratio between ellipse axes measures the magnitude of local anisotropy. The axes are scaled by the standard deviation of local fluctuations.

Once the local anisotropy model is inferred from data, the fine scale simulation can be performed by first chopping the spectral form of the von Kármán model in pieces by multiplying it with our basis functions on the frequency plane. Finally, we convolve a Gaussian spatially uncorrelated noise with each of the functions and then sum all convolutions in a final product. To account for the local anisotropy, the random number created for each location is scaled for each basis function by the equiangular area of the local ellipse sector corresponding to the direction of this function. Since the area of each ellipse is one, the local variance is preserved and the fluctuations follow the Kolmogorov's law while also obeying the local anisotropy. Figure 51 illustrates a downscaled version of the coarse precipitation in Figure 50.

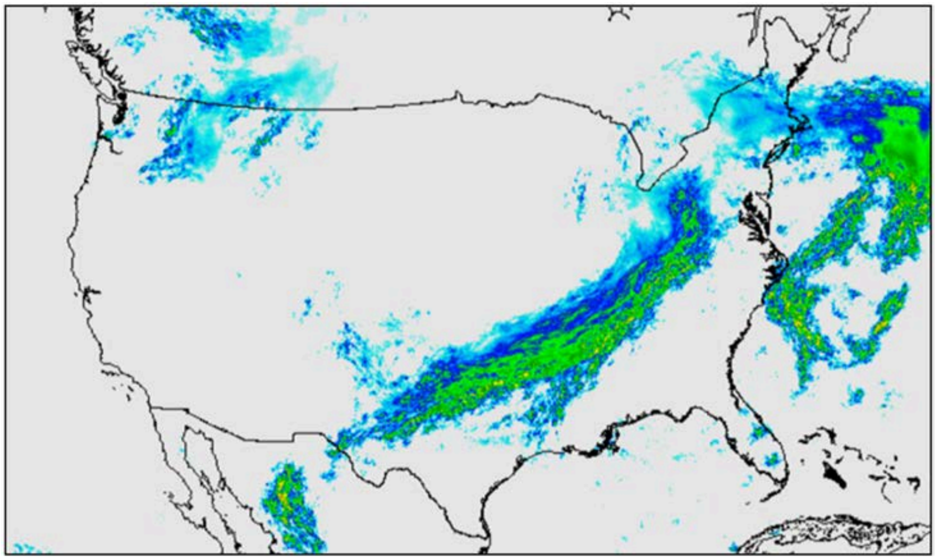

Figure 51. Example of downscaling 64-km WRF model precipitation output to 8-km resolution
Note the realistic radar-like, small-scale detail, elongated in a northeast direction along the cold front in the southern part of the country.

See Also
Coupling the GCM and Mesoscale NWP Models

Precipitation Adjustment

The purpose of Verisk's overall approach to precipitation simulation – from the GCM, through regional the NWP model to statistical downscaling – is to create physically consistent and statistically robust precipitation patterns over the conterminous United States. However, it would be naïve to assume that the numerical model output at 64 km, followed by the statistical downscaling, could reliably represent the true precipitation distribution and, particularly, the local extremes at each 8-km grid cell. Therefore, it was necessary to adjust the output for each grid cell (from the Verisk simulation process) to the local climatology. This adjustment addresses the entire precipitation distribution and its seasonal variation, including the proportion of wet spells, mean precipitation, and extreme accumulations at different recurrence intervals.

The Verisk adjustment process consisted of the following steps:

- Selection of a target dataset, which serves as a good representation of the recent/current climate
- Addressing the bias in the target dataset and building the climatology for each 8-km grid cell
- Quantile mapping to adjust the Verisk precipitation catalog to the target dataset

The first step was the selection of a target dataset, to which the Verisk precipitation catalog would be adjusted. The NWP model output is hourly at 64-km spatial resolution. At this resolution, even after the statistical downscaling, the precipitation values are well correlated at sub-daily time scales, which would result in unrealistically high daily accumulations.

Therefore, Verisk researchers conducted climatological adjustments at a daily time scale. While this left the hourly accumulations relatively high, the correct representation of daily and longer temporal aggregations is much more critical to the Verisk flood model. Verisk selected the PRISM precipitation dataset as a benchmark. This high resolution (4 km) dataset is one of the most reliable daily precipitation datasets. It employs sophisticated algorithms and expert knowledge to account for the local physiography (i.e., terrain, climate, vegetation, etc.) in estimating the daily precipitation amounts.

All interpolation algorithms – even sophisticated algorithms used in PRISM – introduce smoothing. Prominent in intermittent fields like precipitation, smoothing is most evident in extreme precipitation events. Figure 52 presents a comparison of extreme daily precipitation data from over 1,700 gauging stations in United States, with a continuous record from PRISM for the period 1989 to 2018 with corresponding values (i.e., data for the same locations). As indicated, the bias distribution is more negative toward the eastern United States, and PRISM values are 7% to 10% lower than the observed (gauging) data, increasing with recurrence interval.

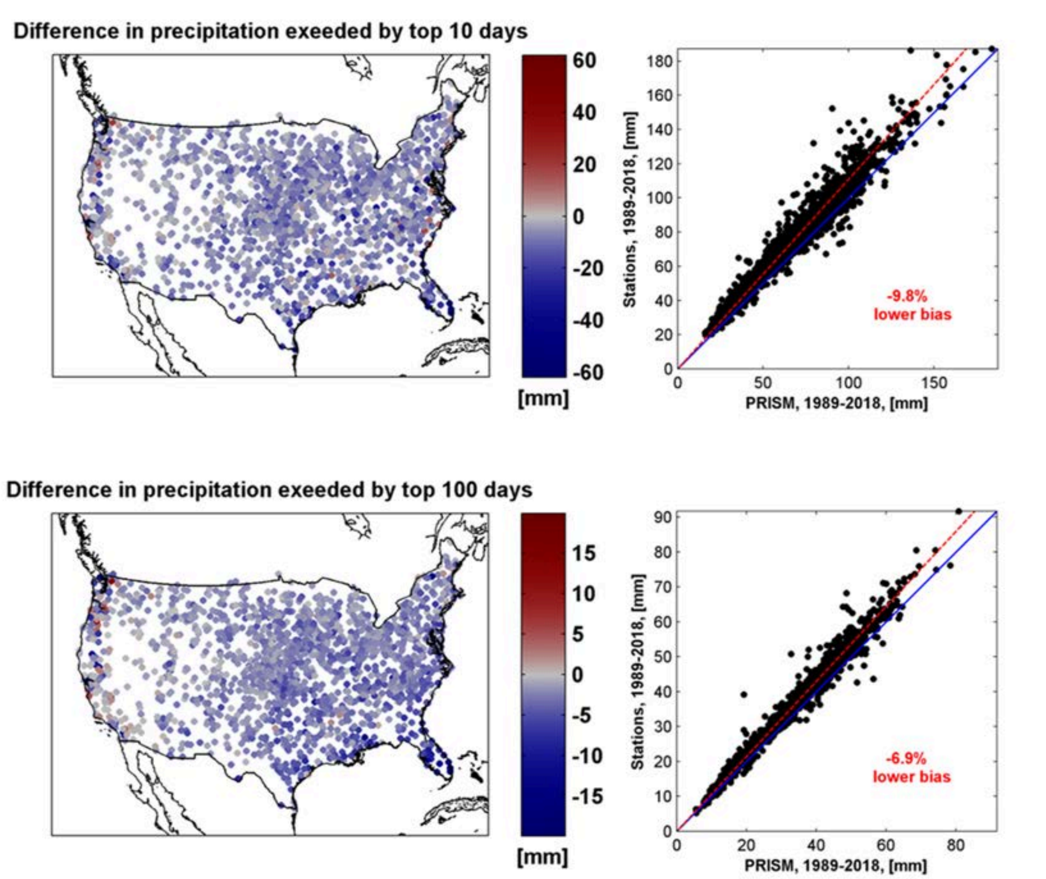

Figure 52. Comparison of PRISM extreme precipitation and gauging station data for the last 30 years.
Precipitation is presented in terms of daily precipitation values exceeded only 10 and 100 days.

To account for the bias, it was necessary to compensate the extremes in the Verisk precipitation climatology. Verisk accomplished this by modifying the tails of the PRISM daily precipitation distributions with those provided by NOAA on their Precipitation Frequency Data Server.[14] The NOAA Atlas[15] provides the precipitation statistics in two forms:

- Annual maximum precipitation
- Partial duration series (i.e., the statistics of ordered series) – hourly, 12 hourly, daily, 3 daily, etc. precipitation accumulation timeseries

For the adjustment, Verisk used the partial duration statistics series because it provides a better representation of intra-annual frequency of extremes and is thus better suited to account for reliable aggregate loss estimates. Figure 53 provides two examples of PRISM daily accumulation data blended with the NOAA Atlas partial duration series for return periods $RP = \{1, 2, 5, 10, 25, 50, 100, 200, 500, 1000\}$ years. This statistic can be considered the value exceeded by $L \times (1 - 1/(365 \times RP))$ days, where L is the length of daily precipitation time series.

Verisk performed this exercise, building the climatology, for each 8-km grid cell.

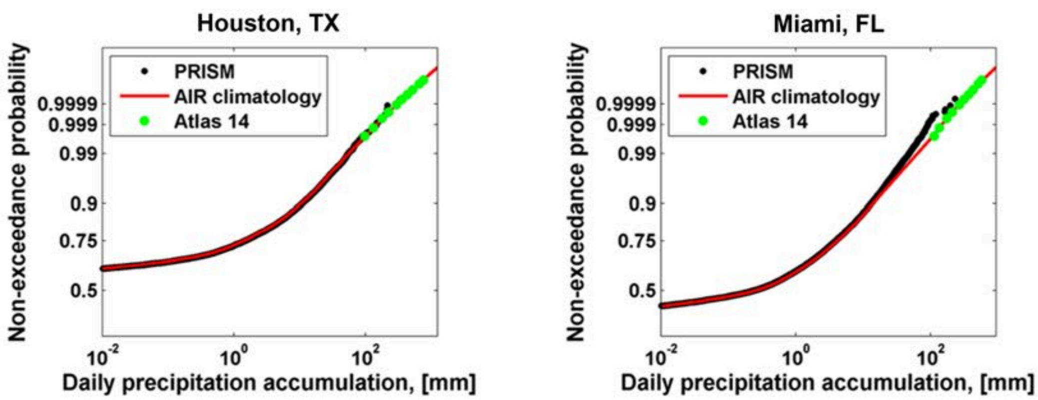

Figure 53. Examples of PRISM time series adjustment with the tails provided by NOAA Atlas 14
While the adjustment for Houston, TX is negligible, for Miami, FL, the adjustment of extreme values is substantial.

For the final step, Verisk employed quantile mapping to adjust the precipitation catalog to the adjusted PRISM climatology. Quantile mapping is a frequently used approach in the natural sciences where a transformation – generally a non-linear one – is made from the distribution of a data source to a desired target distribution. In a general setting, one fits **invertible** marginal models F_X and F_Y to the source and target data, X and Y, and maps the source to destination by using $Y = F_Y^{-1}[F_X(X)]$. Note that F_X and F_Y don't have to necessarily be parametric distribution models, as soon as they are invertible (i.e., map a probability p to itself $p \equiv F[F^{-1}(p)]$, where $0 < p < 1$). Possible solutions include parametric, semi-parametric, and non-parametric approaches. The only requirements are proper treatment of the tails

[14] (https://hdsc.nws.noaa.gov/hdsc/pfds/).
[15] The Verisk model uses NOAA Atlas 14 for the majority of the model domain, and Atlas 2 for the northwestern states. https://www.nws.noaa.gov/oh/hdsc/currentpf.html

of the distributions and resulting quantile functions that are non-decreasing and finite. Specifically, for the variables, AIR used a non-parametric approach to quantile mapping of precipitation, surface temperature, and potential evapotranspiration. The catalog precipitation was mapped to the AIR adjusted PRISM climatology, while the catalog temperature and potential evapotranspiration were mapped to the NLDAS values. For the quantile mapping, AIR used quantile functions derived from the catalog histograms of daily precipitation, surface temperature, and potential evapotranspiration, and mapped each daily value to the climatology target quantile functions derived from PRISM (for precipitation) and NLDAS (for surface temperature and potential evapotranspiration).

Figure 54 presents daily precipitation mapping examples for four locations in the United States. The figure shows the mapping between the initial values (i.e., the output from the downscaling) to the final climatology. In practice, this was completed with an intermediate step, where the tropical cyclone (TC) precipitation (simulated separately) was merged with the non-TC portion of the catalog and adjusted to a TC precipitation climatology.[16] At this intermediate step, the non-TC precipitation was adjusted to monthly quantile functions derived in a way similar to the method described above. Verisk used PRISM data for each month to derive monthly quantile functions where the extrapolated tails of the functions are bounded by the quantiles provided in the NOAA Atlas. In the final step, the TC and the non-TC precipitation were merged,[17] and quantile mapped to the final "total" climatology shown below (Figure 54). Thus, Verisk ensures that the seasonality of precipitation extremes follows the PRISM daily time series.

[16] This process is described in documentation for the Verisk Hurricane Model for the United States.

[17] For the Verisk Inland Flood Model, TC precipitation is not included in the stochastic events.

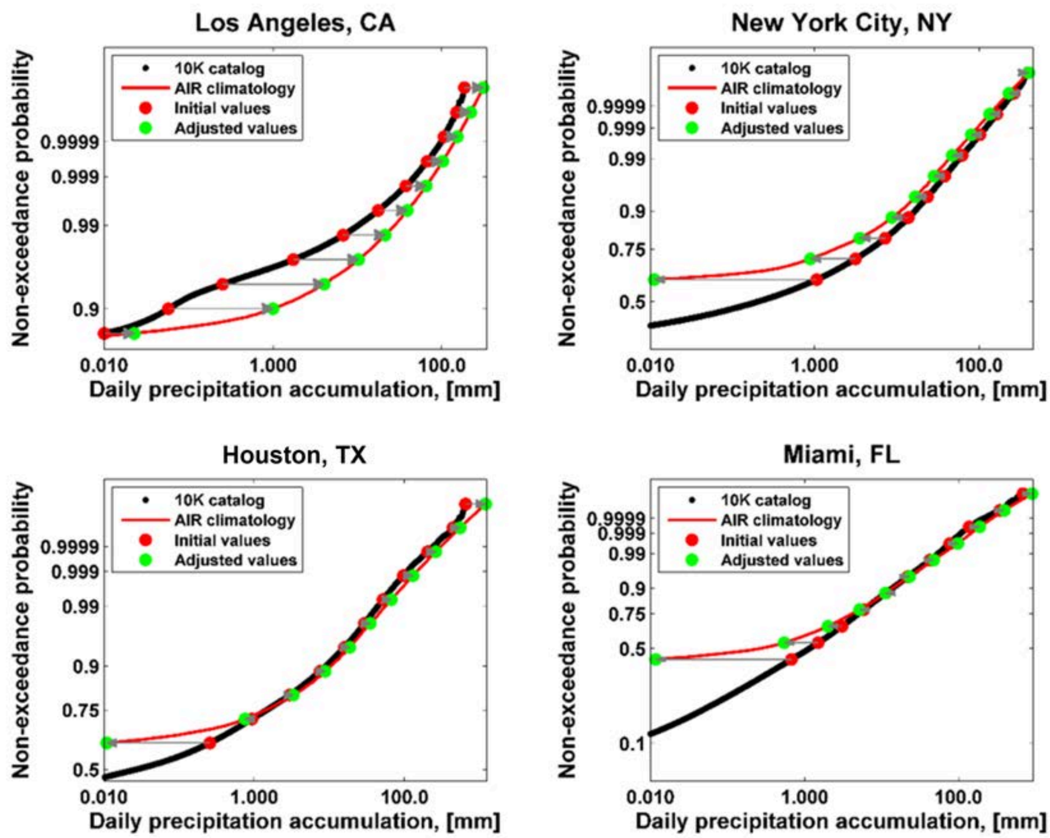

Figure 54. Examples of precipitation catalog quantile adjustment based on Verisk climatology for four locations in the United States

See Also

Defining a Flood Event

Precipitation Validation

To validate the modeled precipitation, Verisk researchers analyzed a suite of different hydrometeorological metrics crucial to accurately simulate flood events. These efforts include the validation of different temporal accumulations at the annual maximum level, basic climatology metrics, seasonality, and historical events' recurrence maps.

Annual Exceedance Probabilities

In the first step of the validation process, Verisk examined the climatologically adjusted model output from an annual maximum perspective, applied to precipitation accumulations of different durations. Researchers looked at how the model performs for precipitation accumulated over 24 hours and 120 hours (i.e., 1- and 5-day accumulation). For each year in the 10,000-year stochastic catalog, Verisk ranked the maximum 1- and 5-day accumulated totals to determine the frequency. This process was also completed for the historical data (the adjusted PRISM dataset), which consists of 37 years of data. Figure 55 presents the results of this analysis for daily precipitation over the 2- and 5-year return periods (50% and 20% exceedance probabilities).

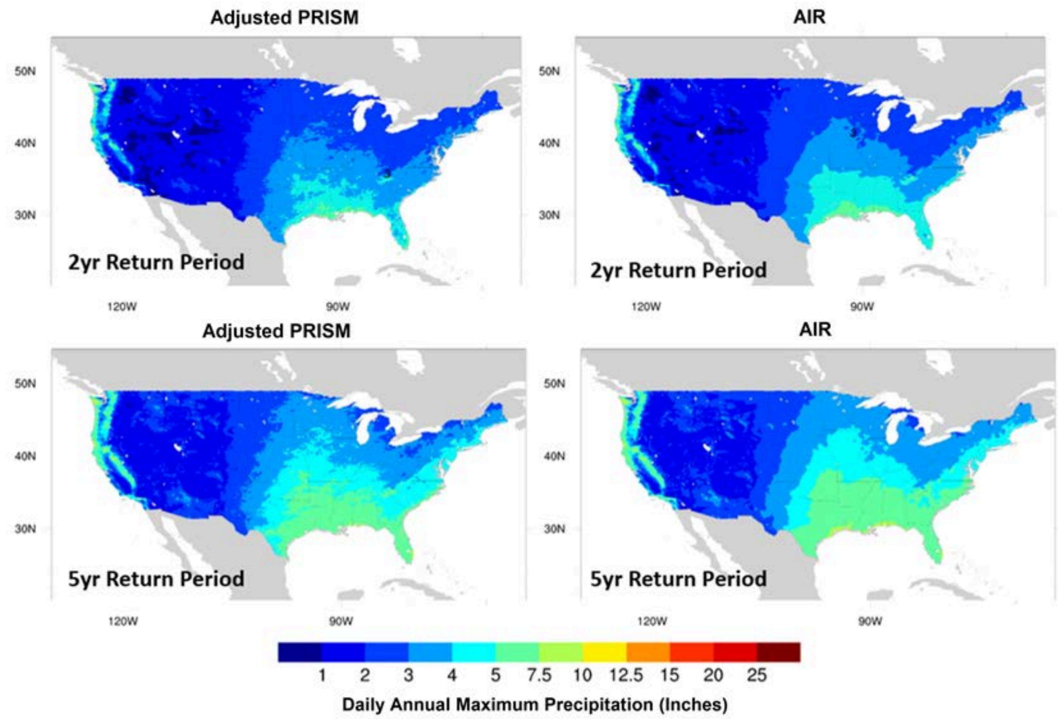

Figure 55. Observed (adjusted PRISM) and modeled (Verisk) 24-hour accumulated precipitation annual maximum values for 2-year and 5-year return periods

As illustrated, Verisk's stochastic catalog for precipitation compares well to the observed data. The spatial signature of maximum values located across the Southeast and Gulf of Mexico, as well as the drying gradient heading west, are well preserved in the model. In addition, the 5-year return period maximums along the East Coast are well captured. The slightly lower adjusted PRISM values compared to the overall model output, shown in all extreme recurrence plots, can be attributed to the overall underestimation of the extremes in the adjusted PRISM dataset. This underestimation is expected to be magnified in the case of annual maximum values.

Figure 56 presents 120-hour (5-day) precipitation accumulation over the 10- and 20-year return periods (10% and 5% exceedance probabilities).

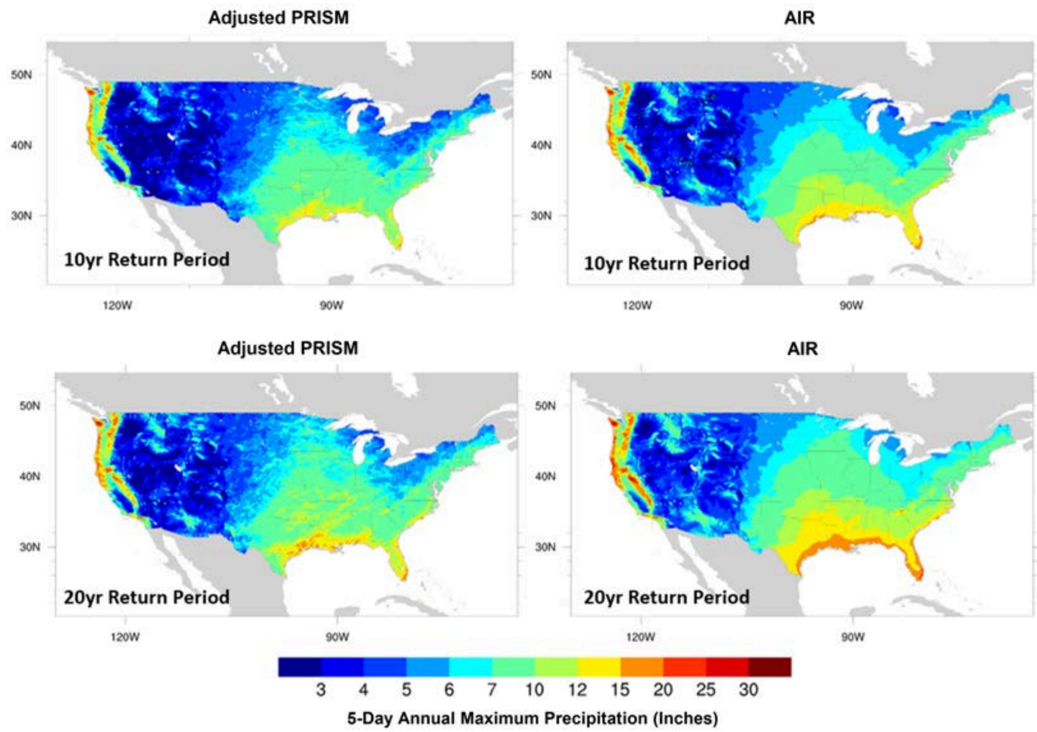

Figure 56. Observed (adjusted PRISM) and modeled (Verisk) 120-hour (five-day) accumulated precipitation annual maximum values for 10-year and 20-year return periods

The Verisk model matched well to the historical record. The model replicates the hydroclimatic signature in the Pacific Northwest – very high precipitation during the 5-day period with some areas receiving 500 to 750 mm (20 to 30 in). In addition, the Verisk catalog reproduces the maximum across the Gulf Coast.

As presented in Figure 56, some modeled maximum values exceed the observed data (adjusted PRISM), particularly for the 20-year return period (5% exceedance probability). This difference is largely due to the limited historical record (37 years), which can be noisy. In contrast, Verisk's 10,000-year catalog produces a smoother signature to the data. Nevertheless, Verisk's catalog successfully captures these varying accumulation durations across return periods.

See Also

Precipitation Adjustment

Climatology

Monthly Rainfall

Antecedent soil moisture conditions are critical for flooding events across the United States, and the model must be able to capture the climatology of rainfall statistics. Verisk researchers analyzed modeled seasonal and monthly accumulated rainfall compared to observed (adjusted PRISM) monthly rainfall data. Figure 57 provides a subset of this analysis, and presents modeled and observed data for a winter and summer month.

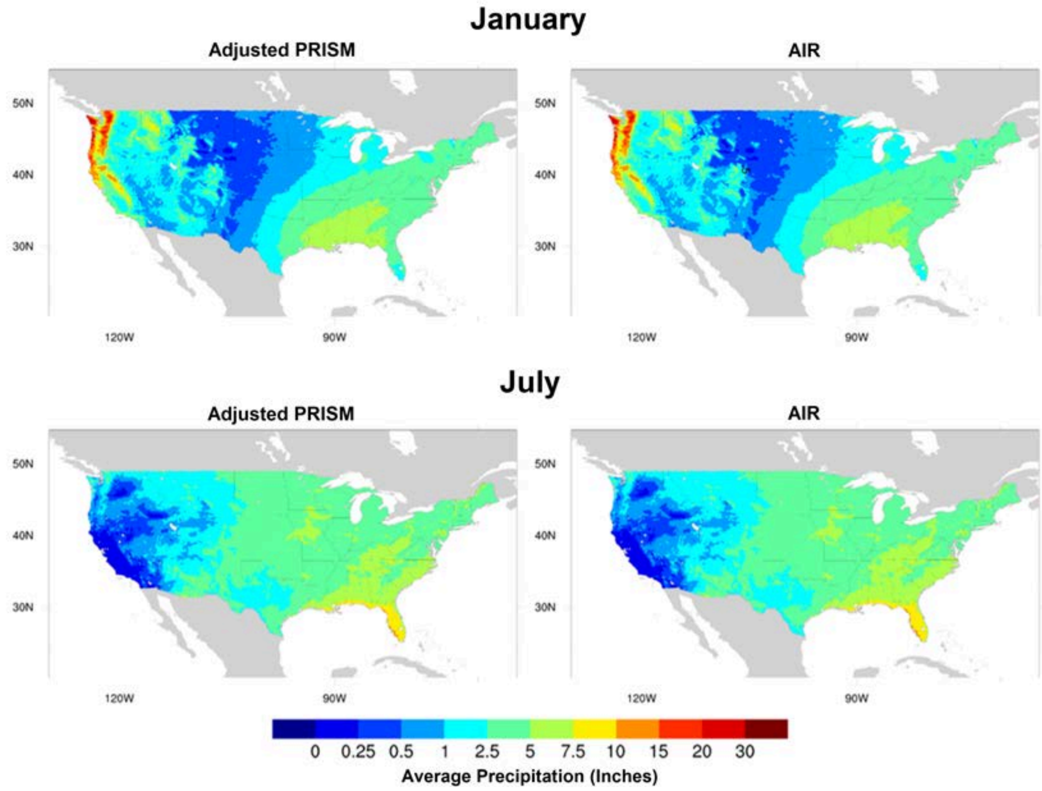

Figure 57. Observed (adjusted PRISM) and modeled (Verisk) monthly average precipitation for January and July

For January, the Verisk model captures climatic spatial signatures of precipitation in terms of the high averages across the Gulf Coast and in the Spokane Mountain region (Pacific Northwest), as well as the relatively dry conditions along the Florida peninsula. As boreal summer reaches its maximum in July, the western portion of the country dries, and the East Coast becomes wetter. As illustrated in Figure 57, Verisk's catalog successfully captures this transition, as well as the monthly precipitation magnitudes.

Wet Day Frequency

In addition to monthly accumulated precipitation, Verisk examined the climatology of wet day frequency – the number of days where total precipitation exceeds a certain value – across the continental United States. This analysis included the following thresholds: 2.5 mm (0.1 in), 25 mm (1 in), 75 mm (3 in), and 125 mm (5 in). Figure 58 compares historically observed (adjusted PRISM) and modeled wet day average annual frequencies for 25 mm (1 in) or more of precipitation.

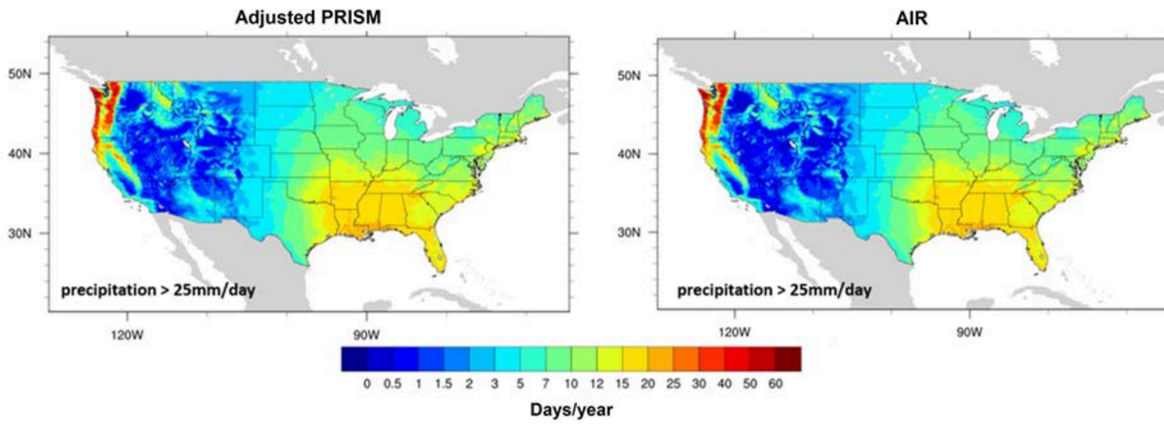

Figure 58. Observed (adjusted PRISM) and modeled (Verisk) average annual wet day frequency
(Number of days per year with precipitation ≥1 in)

As illustrated, Verisk's catalog accurately represents both the spatial signature and the magnitude of wet days across the United States. For both the observed and modeled data (Figure 58), the highest wet day frequencies occur in the mountains of the Pacific Northwest and California, as well as across the Southeast and Gulf of Mexico. The lowest frequencies occur in the western plains, Rocky Mountains, and the desert Southwest.

Return Periods for Historical Events

Verisk completed further precipitation catalog validation by examining recent historical flood events in terms of precipitation extent and magnitude, as well as their recurrence intervals. Selected events are presented below.

South Carolina Flood (2015)

In October 2015, South Carolina experienced a major flood as a result of intense rainfall, and the Charleston area was inundated. Verisk evaluated the modeled return periods for 72-hour precipitation amounts for multiple cities, including Charleston. Figure 59 presents an EP curve for 72-hour precipitation during this event, comparing Verisk-modeled values for one 8 km x 8 km (5 mi x 5 mi) grid cell in the stochastic catalog to the observed data (37 years of adjusted PRISM data). The purpose of this analysis was to properly locate the 2015 flood in the Verisk stochastic catalog, from a frequency perspective.

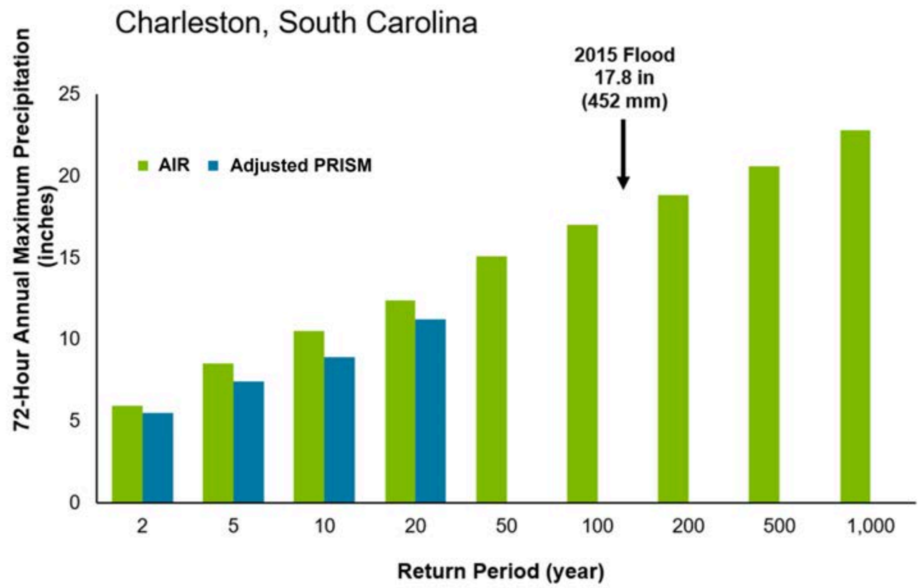

Figure 59. Modeled (Verisk) and observed (adjusted PRISM) return periods for 72-hour precipitation in Charleston, South Carolina.

As illustrated, the model nicely replicates the return period values for Charleston. The 2015 flood would be an approximate 125- to 150-year event, depending on the grid cell/location.

See Also

2015 South Carolina Flood

Louisiana Flood (2016)

In August 2016, torrential downpours and thunderstorms inundated central Louisiana. The region between Lafayette and Baton Rouge experienced record rainfall totals, exceeding 600 mm (24 in), in some locations.

Figure 60 presents the two-day precipitation totals for this storm, as well as the return period for the 48-hour (two-day) maximum, for both NOAA-NWS data and Verisk-modeled data. The NOAA-NWS data are radar-estimated [4-km (2.5 mi) resolution], while the Verisk data are based on observed data from the gridded PRISM dataset [8-km (5 mi) resolution]. For the return periods, Verisk placed the adjusted PRISM maximum 24-hour totals in the model's stochastic precipitation catalog for 24-hour annual maximums. The NOAA-NWS return periods presented are based on their worst-case scenario rainfall totals.

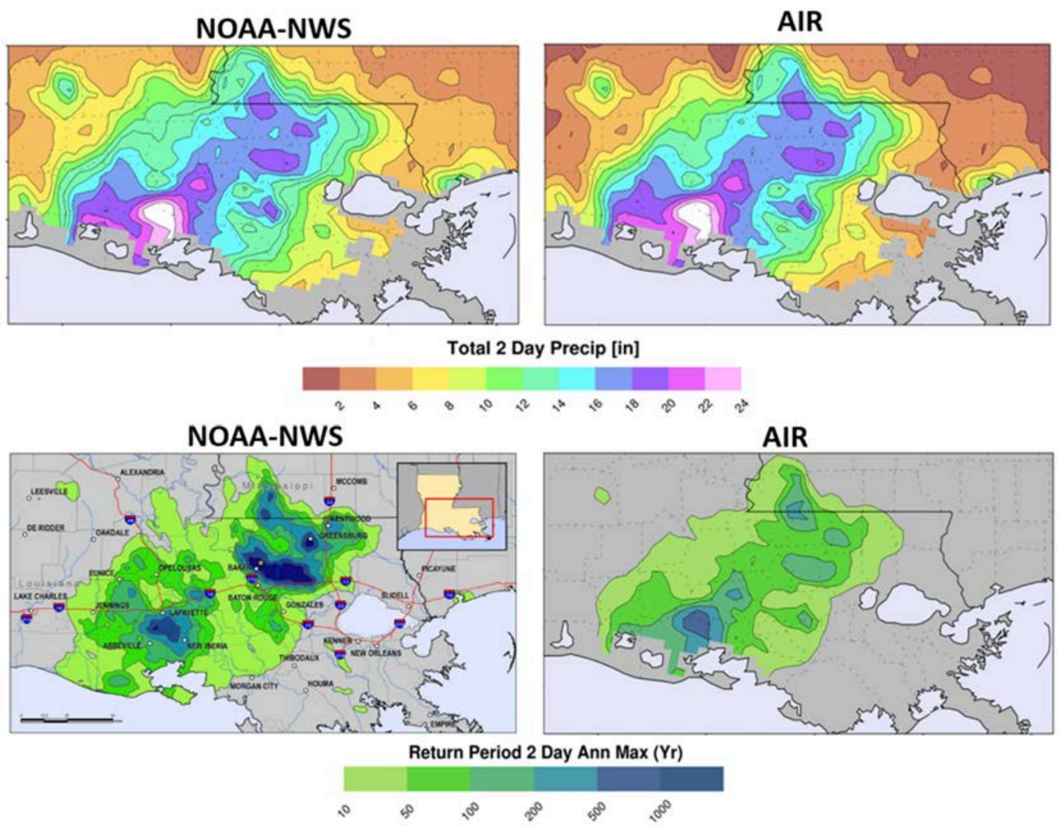

Figure 60. Louisiana flood (2016), observed (NOAA-NWS) and modeled (Verisk) 48-hour totals (top) and recurrence interval or return period in years (bottom)

As Figure 60 presents, the Verisk model estimates the 2016 event as a 100- to 500-year event for a significant portion of central Louisiana. These frequencies compare well to the NOAA-NWS annual EP values, which also generally fall between 100- and 500-year events, with localized 1,000-year events.

Discrepancies between the Verisk and NOAA-NWS frequencies can be attributed to the differences in precipitation inputs. The NOAA-NWS data are mostly radar-based and at a higher resolution. This can result in some higher rainfall totals, leading to isolated regions with larger estimated return periods.

See Also

2016 Louisiana Flood

3.3 The Hydrological Model

The hydrological model transforms precipitation data into runoff (flow over land) and flow in rivers.

The domain for the hydrological model includes an area of approximately 8.2 million km^2 (3.2 million mi^2) and extends beyond the boundaries of the United States, into Canada and Mexico (Figure 61). Eighteen hydrological regions (Figure 62) make up the domain,[18] corresponding to the 18 hydrological regions identified by USGS. [19]

Figure 61. Hydrological model domain

[18] For validation purposes, Verisk combined the Ohio and Tennessee regions.
[19] https://water.usgs.gov/GIS/huc.html

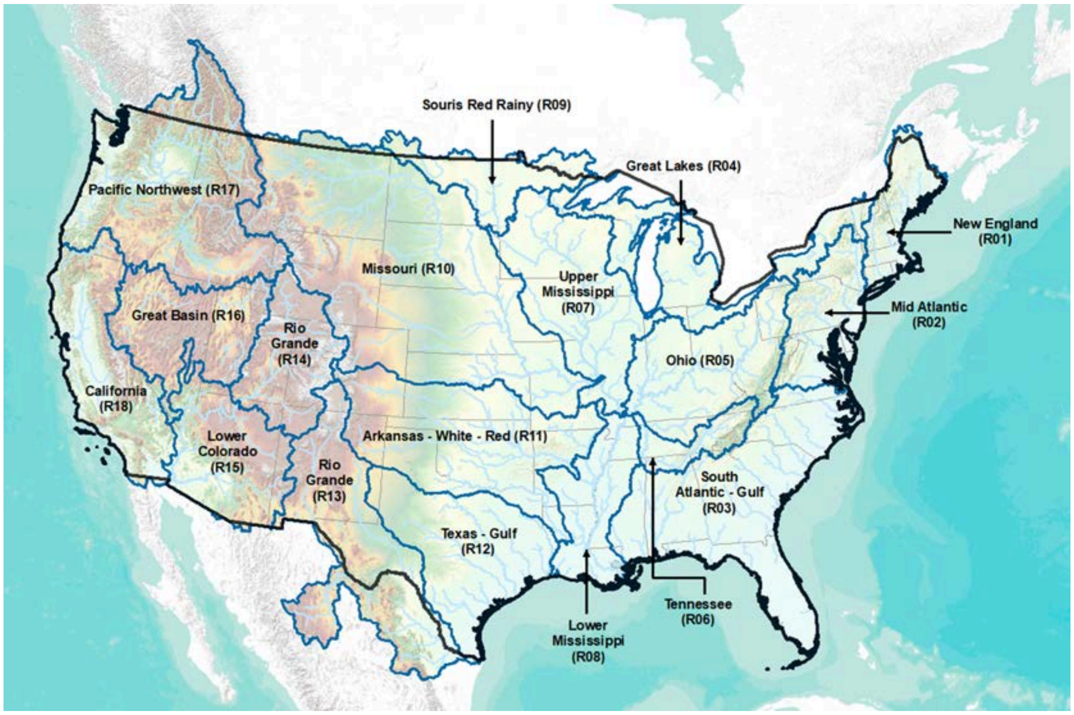

Figure 62. Hydrological regions, based on USGS

The model consists of three major components or modules:

Runoff generation module	Generates both runoff over land and flows in small rivers/unit catchments
Flow routing module	Transfers water through small, medium, and large modeled rivers, and accounts for flow from multiple unit catchments
Snowmelt module	Accounts for the snowpack buildup and for the contribution of melting snow.

Output from the hydrological model (river discharge data in the form of hydrographs) is used to determine inundation depth in the floodplain at 10-m resolution. The pluvial model uses an event's maximum 24-hr precipitation to simulate the overland flows and estimate water depth at 10-m resolution. Once this data has been produced, the pluvial flooding is merged with the fluvial flood extents and the maximal of the two hazards is taken at a given 10-m pixel.

See Also

Simulating Precipitation
Hydraulic Model—Estimating Flood Inundation Depths on the Floodplain
Local Intensity Off the Floodplain

Runoff and Flow Generation

The hydrological model estimates the surface runoff for each **unit catchment** (defined below) and the flow computed at each river reach. Surface runoff is precipitation that does not percolate through the soil, but instead accumulates and travels over the catchment surface – as overland flow, or **runoff** – until it is drained by the nearest stream.

The hydrological response to the precipitation is modeled on a continual basis, at hourly time steps. Floods are modeled over multiple years with an adequate warming period beforehand to minimize uncertainty in estimates of initial soil moisture conditions.

The following definitions will be useful in the discussion that follows:

Stream link	A stream link is the part of a river network that connects two junctions or connects a network initiation and a junction. In the illustration below, there are thirteen individual stream links, indicated by a different color. 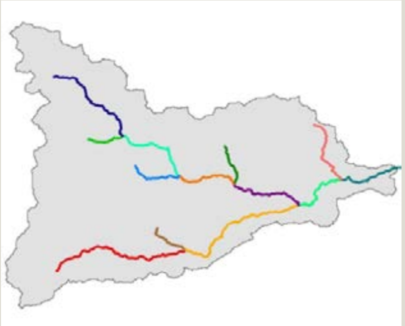
Unit catchment	A unit catchment is the area that drains into a stream link. In the illustration below, there are thirteen unit catchments, each draining into one of the thirteen stream links illustrated above. 
Catchment	A catchment is the area that drains to any defined point along a river network and includes the unit catchments for all upstream stream links. In the illustration below, the dark grey area is the catchment defined for the stream location denoted by the red point. The catchment includes unit catchments draining through all the stream links upstream of the red point. 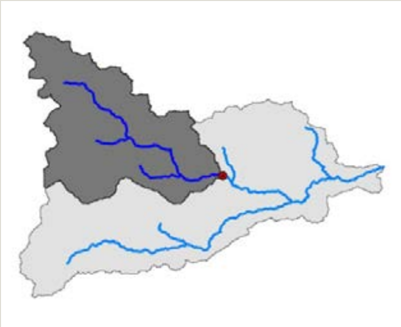

Floodplain	A floodplain is the flat, or nearly flat, land adjacent to a river that experiences periodic flooding under natural conditions. 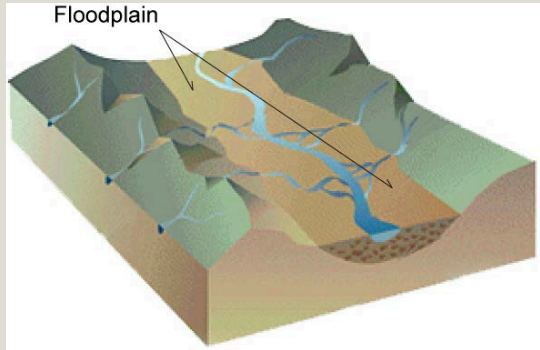

In the model, analysis of fluvial flood events occurs along a river network extending over 2.2 million km (1.4 million mi), with approximately 335,000 distinct unit catchments. Every stream with a drainage area of at least 10 km^2 (3.9 mi^2) is included.

Each unit catchment is modeled individually to represent, as accurately as possible, the spatial variations in precipitation, topography, soil, and land use / land cover characteristics. For each catchment, surface runoff produces flows in that catchment's river. Such flows are then incrementally routed through all downstream river links.

See Also

Hydraulic Model—Estimating Flood Inundation Depths on the Floodplain

Local Intensity Off the Floodplain

Surface and Subsurface Flows

In order to determine when flooding occurs after a storm, the model must accurately assess the surface and subsurface flows occurring in each catchment. Specifically, runoff and baseflow are modeled (Figure 63).

Runoff	Runoff is excess water that runs over the ground surface. It is the catchment's quick response to rainfall, when water cannot infiltrate the soil either because the ground is saturated or the rainfall intensity is higher than the soil's infiltration capacity.[20] Runoff flows relatively swiftly over the surface, eventually into a nearby stream.
Baseflow	Baseflow is the seepage of groundwater that drains from each unit catchment. The water moves relatively slowly through the subsurface before entering a stream. This process is not always storm-dependent, particularly for larger catchments, and may reflect the response from one or more prior storms.

Runoff and baseflow comprise the total flow in rivers, which serves as the basis for the fluvial intensity estimate. The pluvial component, estimated by the pluvial model, is based on the 24-hour maximum cumulative precipitation during an event.

[20] The Verisk model considers runoff in terms of saturation.

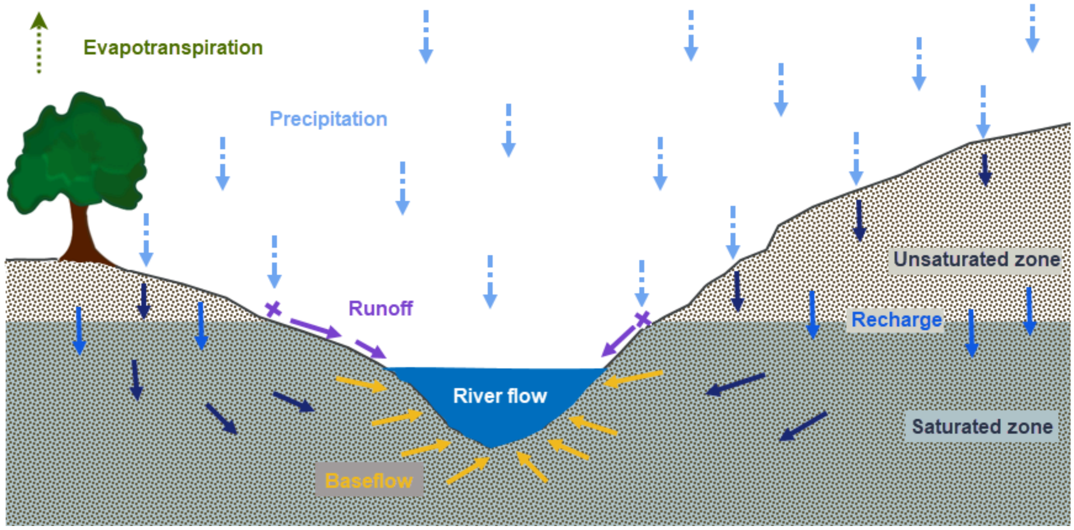

Figure 63. Precipitation may contribute to a river's flow through surface runoff or subsurface flow

The model uses the Probabilistic Distributed Model (PDM), a rainfall-runoff model, to generate surface runoff and baseflow. The PDM assumes that every catchment has a number of storage elements, each with its own soil moisture capacity that follows a particular statistical distribution (Moore, 1985 and 2007). In the Verisk model, this capacity (C) is considered to be uniformly distributed, as implemented in the revitalized flood hydrograph (ReFH) model, between a value of zero (indicating no capacity) and the maximum capacity value denoted as C_{max} (Kjeldsen, 2007).

The PDM transforms the meteorological inputs of rainfall and evapotranspiration into **runoff**, groundwater **recharge**, and **baseflow** (Figure 63). The model then calculates the surface runoff and baseflow contributions to river flow. Additionally, the peak-over-threshold of maximum 24-hour precipitation accumulation is used in the pluvial model.

With the PDM approach, and the soil capacity uniformly distributed between 0 and C_{max}, the precipitation from each hourly time step after accounting for evaporation causes the water depth in each storage element to increase by a specified amount. As a result, at every time step, a proportion of the unit catchment becomes saturated and begins to generate runoff (Figure 64). The hyetograph in Figure 64 indicates the surface runoff that occurs over time as precipitation accumulates during a storm.

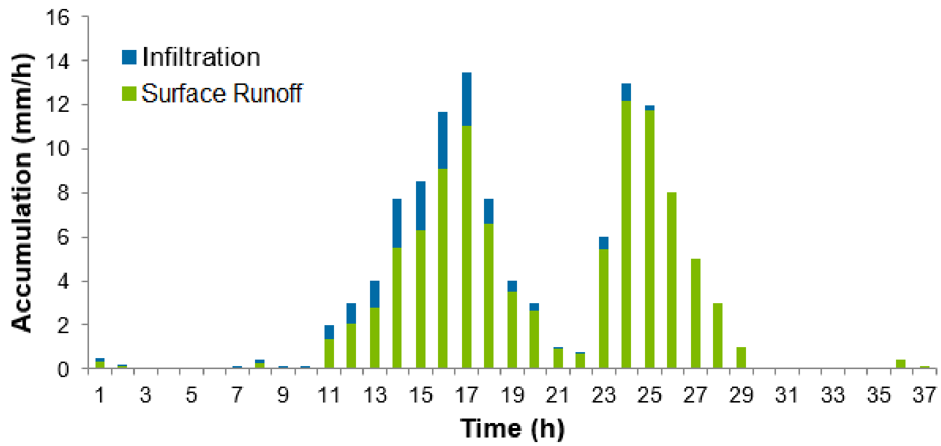

Figure 64. Precipitation accumulation over time for a single storm (hyetograph)

For a given storm, the amount of rainfall generated by the Verisk runoff generation module is dependent on the maximum soil moisture capacity C_{max} and the initial soil moisture, C_{ini} (the moisture at the onset of the storm). Specifically, for a given time step t and the corresponding rainfall amount P_t, the surface runoff q_t can be estimated by solving the following equations:

$$\frac{q_t}{P_t} = \frac{C_t}{C_{max}} + \frac{P_t}{2C_{max}}$$

$$C_{t+1} = C_t + P_t - E_t$$

where C_t is the soil moisture at the beginning of the time step and C_{t+1} is the updated soil moisture after accounting for the precipitation and evapotranspiration, E_t, during the intervening period. Following Moore (2004), the soil moisture loss due to evapotranspiration is estimated based on the following assumption, which relates the soil evaporation to the soil moisture deficit,

$$\frac{E'_t}{EP_t} = \frac{S_t}{S_{max}}$$

where EP_t = Potential evapotranspiration at time t provided by the WRF model, and

E_t = the soil evaporation at time t. The evaporation rate is then applied to the soil moisture to update the soil moisture content. S_{max} is the maximum soil storage over the unit catchment and S_t is the soil moisture content at time t.

Initially, C_t equals C_{ini}, but it increases as rainfall accumulates. Once enough rain has fallen so that C_t equals C_{max}, all of the rainfall is converted into surface runoff.

For each unit catchment, C_{max} is initially determined by relating a unit catchment's C_{max} to the runoff curve number developed by the USDA Natural Resources Conservation Service (Figure 65) as

$$C_{max} = \frac{1000}{CN} - 10$$

Where CN = runoff curve number which can range between 30 and 100 with lower values indicating lower surface runoff potential. The curve numbers are first estimated at 30 m grid cells, the same resolution as the Landsat land cover data from which they are derived based on the classification suggested in the TR-55 Curve Number Tables.[21] The CN for each unit catchment is then estimated as the area-weighted average CN values from grid cells representing the unit catchment. This a priori estimate of C_{max} is then used in the calibration stage, which uses observational data from gauged catchments to obtain the optimal values of soil moisture capacity, while minimizing the differences in the observed and modeled quantiles.

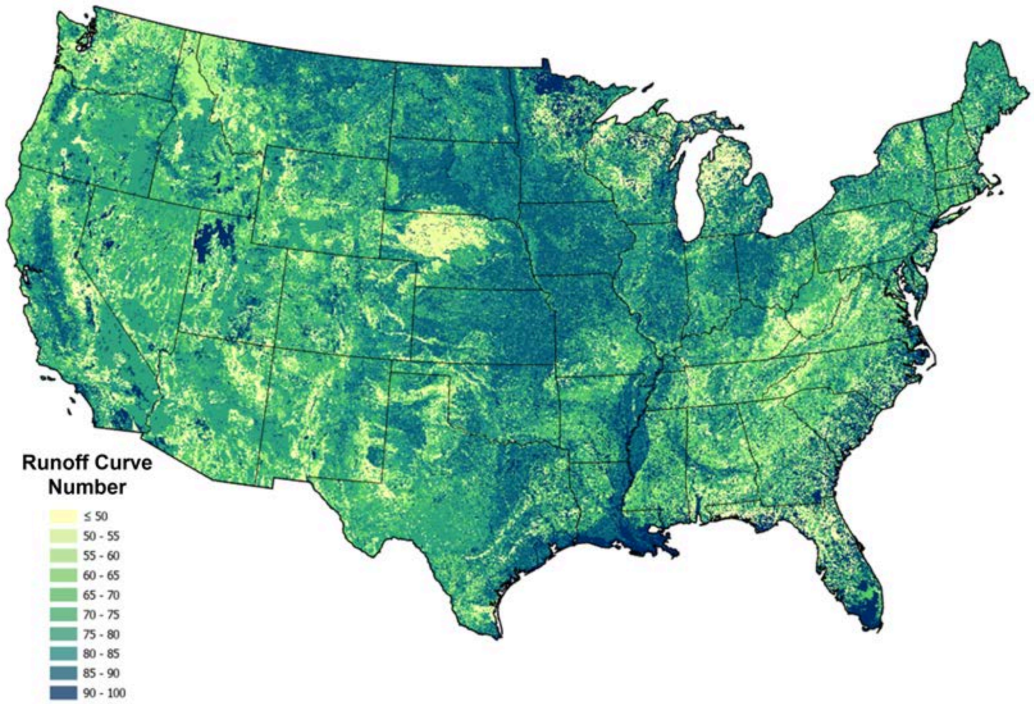

Figure 65. Runoff curve number across the model domain (USDA Natural Resources Conservation Service)

One of the strengths of the Verisk model is its modeling of the hydrological response to rainfall on a continual basis. By continuously accounting for, and tracking, the soil moisture conditions at every hour, the need to estimate initial moisture conditions at the beginning of each storm is avoided. Additionally, the uncertainty in the soil moisture conditions at the beginning of each year is minimized through the inclusion of a sufficient warming period of one year at the beginning of the simulation cycle.

See Also
Hydraulic Model—Estimating Flood Inundation Depths on the Floodplain
Local Intensity Off the Floodplain

Overland Flow at the Unit Catchment Scale

After determining surface runoff for each catchment, the model has to account for the smoothing effect that the overland flow asserts on the surface runoff until the discharge at the unit catchment outlet is obtained. A popular solution to this problem is the use of a

21 Example: https://www.wsdot.wa.gov/publications/fulltext/Hydraulics/HRM/App4B_2014.pdf

unit hydrograph (UH). Unit hydrographs describe the expected discharge at the outlet of a catchment, given a surface runoff input with infinitely small duration and unit rainfall intensity per unit area. The smoothing effect of the overland flow at the unit catchment outlet is then computed as the convolution of the surface runoff time-series with the unit hydrograph.

The Verisk model employs a kinked triangle UH (Kjeldsen, 2007), which uses one parameter - the time to peak (T_p). The initial estimate of T_p for each unit catchment was derived using the approach suggested by Cleveland, et al. (2008). Then these values were optimized based on observational data from gauged catchments while minimizing differences between observed and modeled flow quantiles. Such optimization, in fact, is done simultaneously for the time to peak flow and the maximum soil moisture capacity.

Non-Linear Baseflow

Following the framework provided by Moore (2007) and Moore and Bell (2002), the PDM model first distributes the runoff into surface runoff and groundwater recharge. The groundwater recharge adds to the groundwater storage S_g, which contributes to river flow due to the relatively slow-moving subsurface flow (baseflow). As shown in a flow hydrograph in Figure 66, the sudden increase in flow (the rising limb) characterizes the surface flow, while the end of the decreasing portion of the graph (the falling limb) characterizes the contribution of the baseflow. The Verisk model accounts for the physics of this flow process by incorporating a non-linear baseflow model given by:

$$q_b = K_b S_g^{M_b}$$

where q_b (mm/h) is the baseflow contribution per unit area, S_g (mm) is the groundwater storage depth, K_b (mm^{1-M_b} /h) is the storage rate coefficient and M_b is the storage exponent.

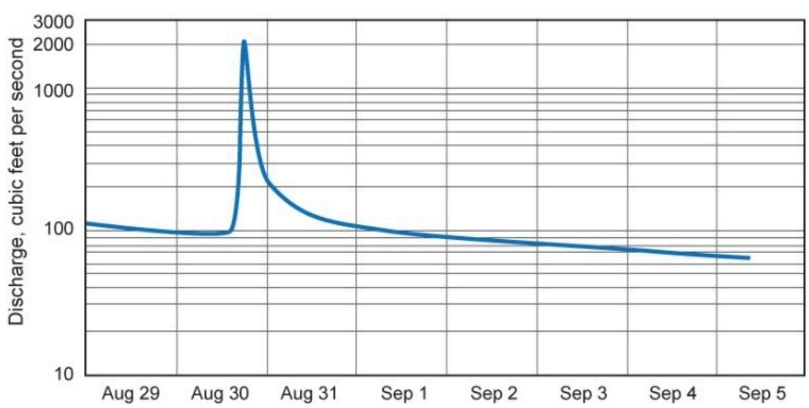

Figure 66. Example flow hydrograph

The parameters K_b and M_b are obtained for individual unit catchments using regionalized regression equations that relate these parameters to the geometry, topography, soil characteristics, land use, and baseflow index characteristics of the catchments. These relationships are developed by analyzing recession portions of the sub-daily observed river flow data, from many river gauging stations, and estimating the two baseflow parameters.

The relationships leverage the power law relationship between discharge (the flow volume rate) and its change per unit time (Kirchner, 2009) as:

$$-\frac{dq_b}{dt} = Aq_b^B m$$

where the parameters K_b and M_b are functions of coefficients A and B as:

$$M_b = \frac{1}{2-B} \text{ and } K_b = [A(2-B)]^{M_b}$$

See Also

Surface and Subsurface Flows

Modeling Snowmelt

Snowmelt and snow accumulation are important components of the hydrological cycle. Snow accumulation stores and delays the release of water from a catchment into a stream network. In the United States, snowmelt regularly contributes to flooding in many areas, particularly the Northeast, northern Midwest, and high mountains of the West. Although snowmelt-related floods are generally localized and less severe than those caused by excessive precipitation, many historical flood events in the United States have been associated with snowmelt.

The risk of snowmelt-driven flooding is highest during early spring, particularly in areas that receive runoff from the mountains. Melting snow cover can intensify runoff into larger rivers. A winter with heavy snowfall and accumulation, combined with a rainy spring and warmer temperatures, can significantly increase the potential for severe flooding.

Figure 67. Flooding and melting snow in Hendrum, Minnesota, Red River of the North flood, 2009
(Source: FEMA)

The Verisk model's downscaled precipitation, at 8 km x 8 km, includes both rainfall as liquid precipitation and snow as solid precipitation. Verisk's method first categorizes precipitation as snow or rain. Based on a temperature threshold, snow accumulates, but melts when the temperature rises above zero degrees Celsius. The snowmelt contributes to the total runoff depth, which is subsequently utilized as input for modeling the flood hazard, both on- and off-of the floodplain.

It is not possible to build a robust snowmelt model that is based only on stochastically generated precipitation because, in addition to simulated precipitation field, the model requires surface temperature to categorize the precipitation as snow or rain. An additional benefit of using NWP models is that the output contains the surface temperature variable.

To account for snowmelt in the model, Verisk scientists made use of the **degree-day model**. The degree-day model utilizes surface temperatures above a given threshold (usually 0° C) to determine if the modeled precipitation falls in the form of rain or snow. If the precipitation falls as snow, it is added to any existing snow cover at that time. The snowmelt rate, applicable for different regions, is determined based on a large amount of observational river flow data obtained at times when the flow is affected by snowmelt. To account for the increased snowmelt caused by liquid precipitation on existing snow cover, Verisk scientists used a modified version of the degree-hour model that is somewhat more complex and non-linear (Hirpa, 2005).

The snowmelt model's main inputs are the downscaled precipitation (at the 8 km x 8 km resolution), interpolated surface temperatures, and the estimated snowmelt rate. The state of the snowpack is monitored continuously by accounting for snow accumulation and snowmelt amounts on an hourly basis throughout the year. More precisely, the snowmelt at each location in time and space— *t*, *x*, *y* and time step Δt —is estimated as follows:

The snowmelt *SM* (in mm/hr) is estimated during the period $t : t + \Delta t$:

$$SM^{t:t+\Delta t,x,y} = min\begin{cases} SWE^{t,xy,y} \\ C_{sm}max\left(0, T_{surf}^{t:t+\Delta t,x,y}\right) \end{cases}$$

where *SWE* is the snow water equivalent of the snow cover (in mm), and T_{surf} is the surface temperature (in °C) of the air during the time interval. C_{SM} is the non-linear degree-hour factor, estimated as

$$C_{SM} = min\left(C_{max}, aP_{LIQ}^{t:t+\Delta t,x,y} + b\right)$$

where $P_{LIQ}$is the liquid precipitation in mm/hr. C_{max}, *a*, and *b* are parameters similar to those used in Hirpa, 2005.

$$SWE^{t+\Delta t,x,y} = SWE^{t,x,y} + SF^{t:t+\Delta t,x,y} - SM^{t:t+\Delta t,x,y}$$

The snow cover depth is updated at the end of the time interval,

where *SF* is the snow-water equivalent of the snowfall (non-liquid precipitation) in mm.

Once the snowmelt has been computed for each time step, it is added to the liquid precipitation and the total is used for the runoff generation module.

Flow Routing

After the discharges at the outlet of each unit catchment are computed, the model needs to convey them along the river network, working in the downstream direction. This modeling process is called flow routing (or river routing) and its purpose is to propagate the flood wave from each small unit catchment to the termination of the river network. The rivers may terminate in inland lakes, the Atlantic Ocean (including the Gulf of Mexico), the Pacific Ocean, in Canada or Mexico, or within the Great Basin of the United States.

The routing is applied recursively from upstream to downstream links, for all stream links that have at least one upstream link. The input to each modeled link is the lateral inflow (flow from that link's unit catchment distributed over the link) plus the flows from upstream links. The output from each stream link is then considered as input to the downstream link or to its terminus.

Flow Routing along a Single Stream Link

Verisk's runoff routing module employs a modified version of the widely-used Muskingum-Cunge flood routing scheme (HEC-HMS, 2000), an algorithm that accommodates the use of composite cross-sectional geometry to account for flood plain attenuation. Not only is this algorithm physically-based and suitable for a wide range of flow conditions, it is also efficient from a computational point of view without compromising theoretical precision and accuracy.

The Muskingum-Cunge flood routing scheme numerically solves the diffusion wave equation:

$$\frac{\partial Q}{\partial t} + c\frac{\partial Q}{\partial x} = \frac{Q}{2BS_0}\frac{\partial^2 Q}{\partial x^2} + cq_L$$

Where,

Q = discharge,

$c = \frac{\partial C_A}{\partial Q}$ and represents the wave speed (celerity),

C_A = the cross-sectional area of the channel

B = the top width of the water surface

S_0 = the channel slope

q_L = the lateral inflow per unit length

(See HEC-HMS, 2000 for technical details about the numerical implementation of the Muskingum-Cunge flood routing algorithm).

To compute the wave celerity at each time step requires a relationship between the cross-sectional area and discharge. This relationship is usually assumed to be a power law analogous to simple rectangular, triangular, and elliptical channel geometries which hold under the assumption of Manning's equation[22] for normal flow conditions.

Although simple and convenient for numerical implementations, the single-power-law relationship does not account for the effect of overbank flows (water flowing over the riverbank and out of the stream link in its floodplains), which introduces a significant attenuation effect on the flood hydrograph shape and, in particular, the peak flow.

Therefore, Verisk's routing model employs a double power law relationship with the assumption of a rectangular riverbed and a floodplain whose cross-sectional profiles are

[22] $Q = \frac{1}{n}C_A^{5/3}P^{-2/3}S_0^{1/2}$ where n is the resistance to the flow and P is the wetted perimeter (the part of the channel cross-section covered by water).

triangular in shape. The required parameters for the double-power-law relationship between the cross-sectional area C_A and the discharge Q are listed below:

S_0= channel slope

n_{CH} = channel bottom roughness

W = channel bottom width

Q_{BF} = bankfull discharge

S_{FP} = floodplain transverse slope

n_{FP} = floodplain surface roughness

The relationship has the form of two power laws connected with a sigmoid function:

$$C_A(Q) = exp\left\{ \left\{ 1 - \left[\frac{1}{1+e^{(-\ln Q + \ln Q_{BF} + w)/w}} \right] \right\} (0.6\ln Q + C_1) \right\} \times$$
$$exp\left\{ \left[\frac{1}{1+e^{(-\ln Q + \ln Q_{BF} + w)/w}} \right] \left[Q_{BF}(0.6\ln Q + C_1)/Q + (Q - Q_{BF})(0.75\ln Q + C_2)/Q \right] \right\}$$

Where the discharge $Q > 0$, and the transition width $w = 0.1$. C_1 and C_2 are the logs of the pre-exponents of the two power laws, which depend on the above parameters. The double-power-law relationship gives a result that is very close to the one of a piece-wise (two triangular and one rectangular) transverse integration using Manning's equation. However, it is differentiable everywhere, which is very convenient for an implementation in the Muskingum-Cunge flood routing algorithm, where one needs to estimate the wave celerity as the first derivative of the double-power-law relationship (i.e., $c = \frac{\partial C_A}{\partial Q}$).

In the left panel of Figure 68, a comparison between a double-power-law and a transverse integration based on Manning's equation is given for a channel with parameters listed below.

$S_0 = 0.0005$

$n_{CH} = 0.1$

$w = 30 \ m$

$D = 4 \ m$ (channel depth)

$Q_{BF} = 60 \ m^3/s$

$S_{FP} = 0.005$

$n_{FP} = 0.6$

At the point at which water flows over the bank (Q_{BF}), the speed of the flow within the channel, is suddenly and significantly reduced.

The right panel of Figure 68 shows two sample hydrographs routed using the Muskingum-Cunge method with single and double-power-law relationships, respectively, for a river reach with a length of 10 km. The effect of overbank flows on the peak flow and the shape of the hydrograph is clear—and in line with observation; single-peaked flood hydrographs measured at a gauging station often follow shapes similar to the shape in blue in Figure 68(b).

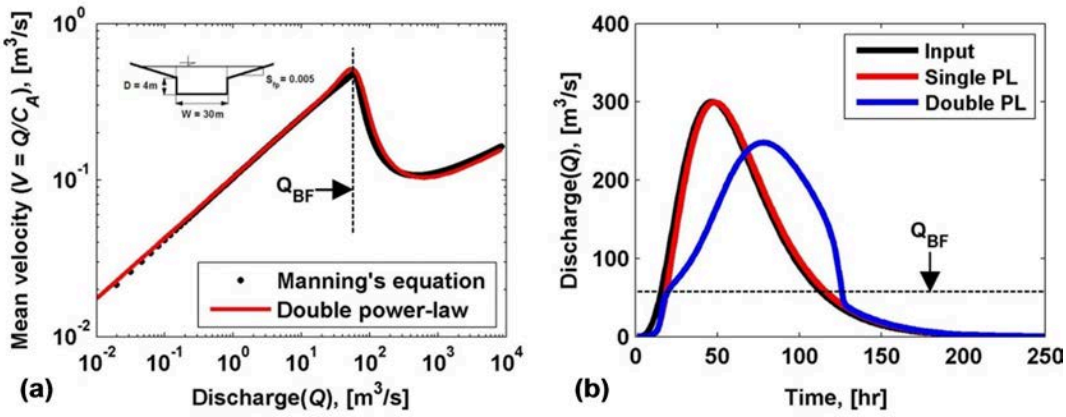

Figure 68. (a) Double power law relationship; (b) effect of the double-power-law on the flood hydrograph

The parameters S_O and $S_{FP}$are derived using Geographic Information Systems (GIS) from high resolution digital terrain model (DTM). The channel width, *W* is first obtained for a) a subset of gauge stations where these data are available from the USGS, and b) measured using aerial imagery and water body information. Regression models relating the channel width to contributing area is then used to extrapolate the width information to all the other stream links. The channel's and floodplain's Manning's *n* (n_{CH} and n_{FP}) were derived from the land use / land cover (LULC) data by using the methodology described by Arcement and Schneider (1989).

Accounting for the Attenuating Effects of Lakes and Reservoirs

Lakes and reservoirs mitigate flood risk as they control the flow of water, containing high flows and increasing low ones, or divert water from catchment outlets altogether. These water bodies exert an additional smoothing effect, or attenuation, by decreasing peak flows and increasing the time-to-peak and overall hydrograph duration.

The Verisk model incorporates over 21,000 lakes and reservoirs. Reservoir data comes from several sources, including the Global Reservoir and Dam (GRanD) of the Global Water System Project, and the International Commission on Large Dams (ICOLD). Additional information was obtained from elevation data maintained by NASA's Shuttle Radar Topography Mission (SRTM). Parameters collected for each modeled reservoir include the surface area, storage capacity, design discharge, and type of construction.

The model addresses lakes and reservoirs via two different approaches. For dams with sufficient historical storage state data available, Verisk employed a machine learning-based reservoir model. For the remaining dams, Verisk used linear reservoir routing.

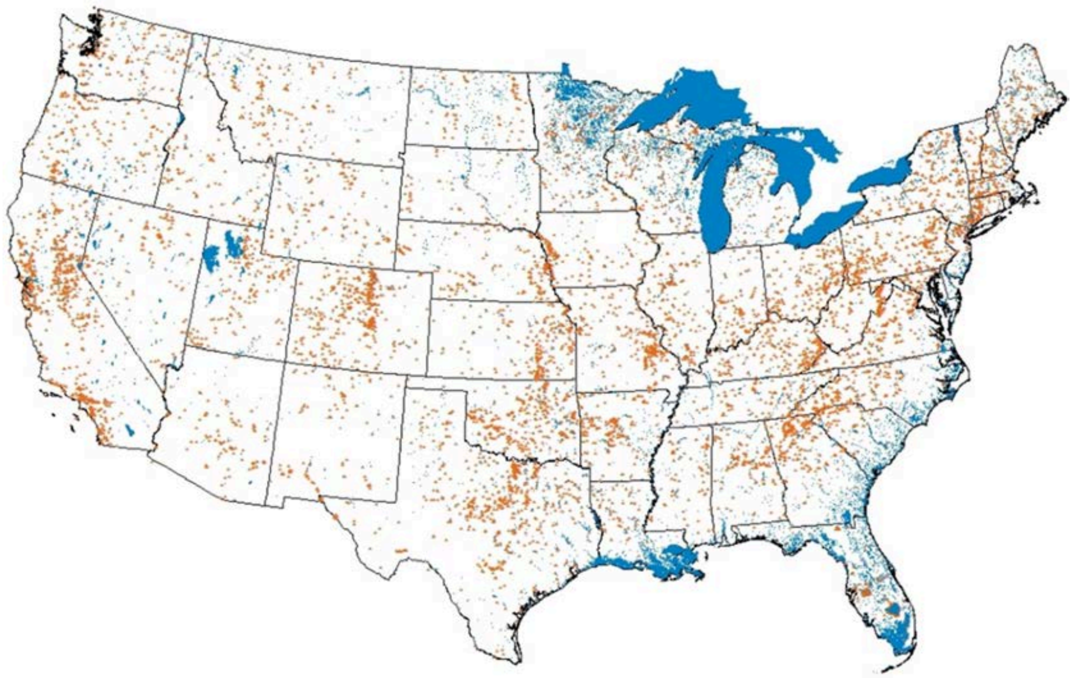

Figure 69. Modeled lakes (blue) and reservoir gauges (orange)

See Also
Event Generation Data Sources

Machine Learning-based Reservoir Model

Reservoirs are generally managed by employing operational rule curves (ORCs), which are based on characteristics such as climate and a reservoir's intended use. These ORCs are important input to simulate the outflow-regulation patterns of dams and reservoirs. However, this information is not readily available for every reservoir. Further, the large variability in ORCs between different dam types (e.g., irrigation, hydroelectric, etc.) and from year to year for the same reservoir makes it difficult to use generalized ORCs. In the absence of ORCs, Verisk developed an artificial neural network (ANN) model for about 250 reservoirs, using the storage state data from USGS, US Bureau of Reclamation, and precipitation data from the North American Land Data Assimilation System (NLDAS) to model ORCs across the United States.

Initially, 412 reservoirs with good storage state data were selected for training the ANN model. A separate neural network model was trained for each of the 412 reservoirs. Figure 70 provides a schematic representation of the ANN model. Fully-connected feed forward networks were used to develop these models. The architecture of the network (i.e., the number of hidden layers and the neurons in each layer) was optimized for every reservoir separately but limited to a maximum of three hidden layers and nine neurons per layer due to computation limitations. One enhancement Verisk introduced was the inclusion of two months of precipitation beyond the current modeled time step, which assumes reservoir operators will have information on precipitation forecasts and will be able to adjust the reservoir operations accordingly. This is suitable for stochastic simulation framework, as the precipitation for all months is readily available in advance.

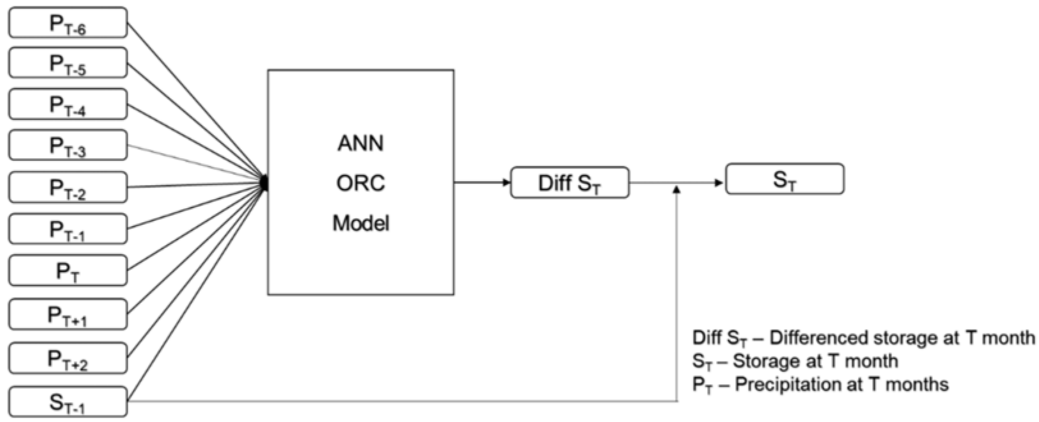

Figure 70. Neural network model architecture
(Source: Ghosh et al., 2019)

The models were trained using resilient back propagation or RPROP+ (Riedmiller and Braun, 1993) on the first 70% of the available time series. The remaining 30% was used for a testing phase, in which the models were run in a recursive multi-step forecast mode (Bontempi et al., 2013), where the predicted storage value at any time step served as an input for the next time step. The linear R-squared statistic was calculated as the primary metric for determining the model performance. To prevent overfitting of the model, Verisk also applied an early-stopping criteria (Prechelt, 2012) such that model calibration on the training data stops when performance of calibration begins to decrease.

To validate the model, Verisk used the trained ANN models to generate storage time series using historical rainfall data for 39 years from 1979 to 2017. Once generated for each reservoir, the storage time series were compared to the observed storage time series. Linear R-squared values between the two time-series served as performance metrics of the models. Figure 71 shows an example of such validation for the Lake Berryessa reservoir near Winters, CA. The observed data was present until 2009; after that the model simulates the storage time series using the observed precipitation. The scatter plot shows the model performance in testing phase.

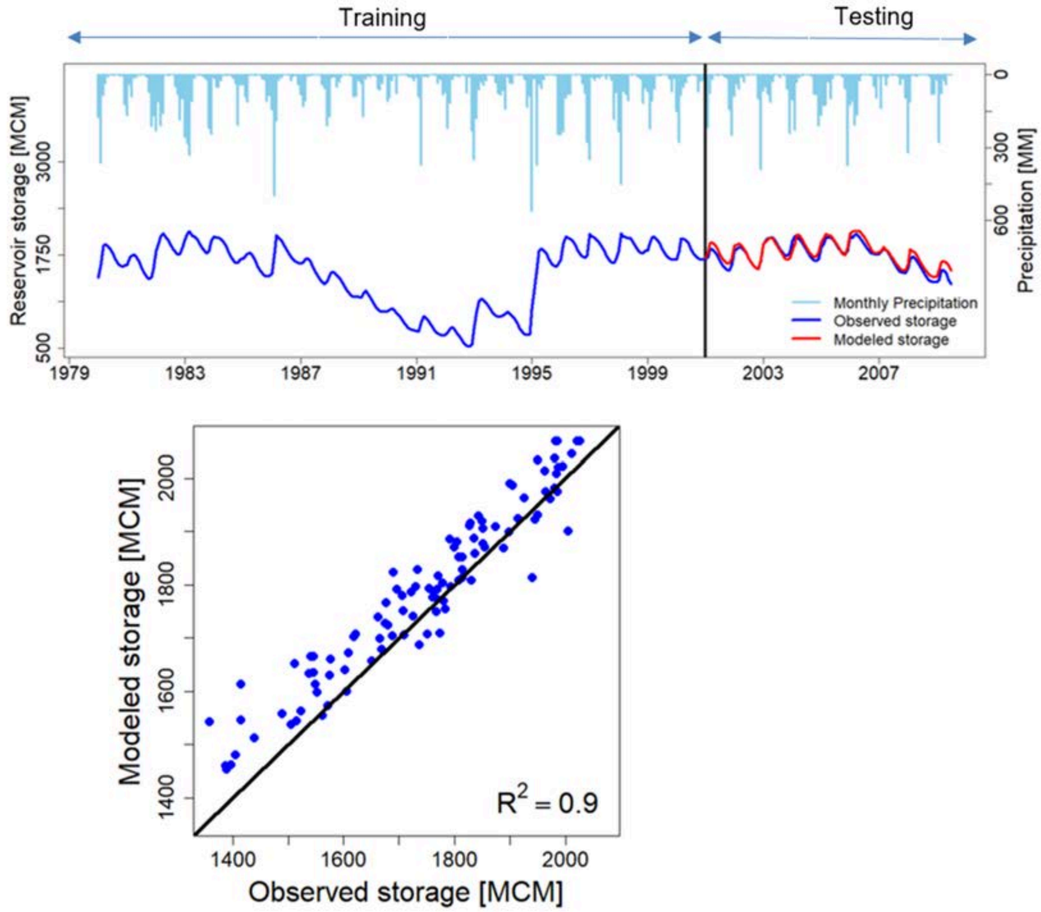

Figure 71. Example of model performance using precipitation and storage as inputs (Lake Berryessa)
The upper panel shows the observed storage (blue) and modeled storage (red in the testing period) in million cubic meters (MCM) and the corresponding monthly precipitation in millimeters. The light blue bars represent the monthly cumulative precipitation. The bottom panel illustrates the performance in the testing period as a scatter plot. (Source: Ghosh et al., 2019)

An ANN model was considered suitable if the R-squared value of the simulated storage time series vs. observed storage time series was more than 0.4. The median R-squared statistic varied between 0.4 to 0.6 for most of the reservoir types (Figure 72), except for reservoirs whose main function was navigation. Models for irrigation and flood control reservoirs performed better than others. Verisk selected ANN models for about 250 reservoirs in the stochastic simulation. More details about the implementation can be found in Ghosh et al. (2019).

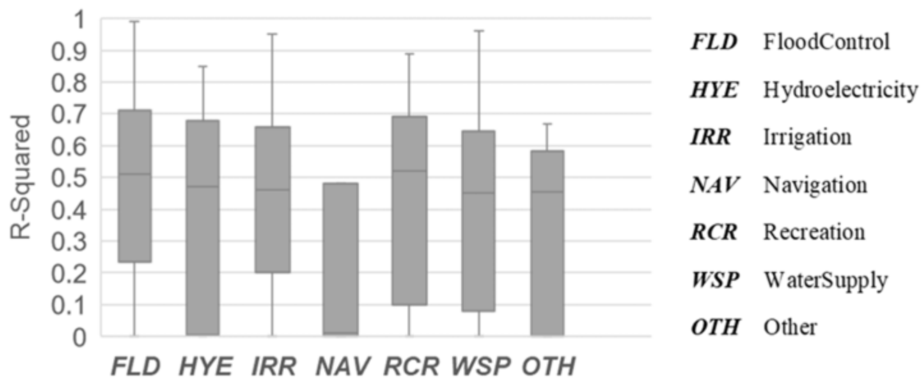

Figure 72. R-squared distribution from testing phase, grouped by the reservoir type (Source: Ghosh et al., 2019)

Linear Reservoir Modeling

For those reservoirs and lakes not modeled by the machine learning-based model—either because there were not sufficient training data or the ANN model did not result in a significant increase in performance when compared to a simple linear reservoir model—Verisk used the simpler linear reservoir routing approach. The linear reservoir routing assumes the reservoir storage S_R is linearly related to outflow Q_{out} by the equation:

$$S_R = K_R Q_{out}$$

where K_R is the reservoir's residence time (its storage capacity divided by its design discharge).

The equation for reservoir storage (S_R) is combined with the continuity equation:

$$Q_{in} - Q_{out} = dS_R / dt$$

where Q_{in} is the reservoir inflow at time *t*. An analytic solution of the reservoir outflow Q_{out} is obtained using a finite difference approach.

Validation of the Hydrological Model

Like all Verisk catastrophe models, the Verisk flood model is extensively validated. A selection of exhibits showing the validation of the hydrological component of the model is provided below.

Validation of Annual Maximum Discharges

The USGS collects annual maximum discharge data from over 26,000 streamflow gauge locations.[23] However, not all locations are useful for validating the model. Most have a very short period of record and many are discontinued and/or do not represent current conditions. After careful examination and a quality check, Verisk used over 9,000 gauge locations (Figure 73) to validate the modeled flows.

[23] https://waterdata.usgs.gov/nwis/sw

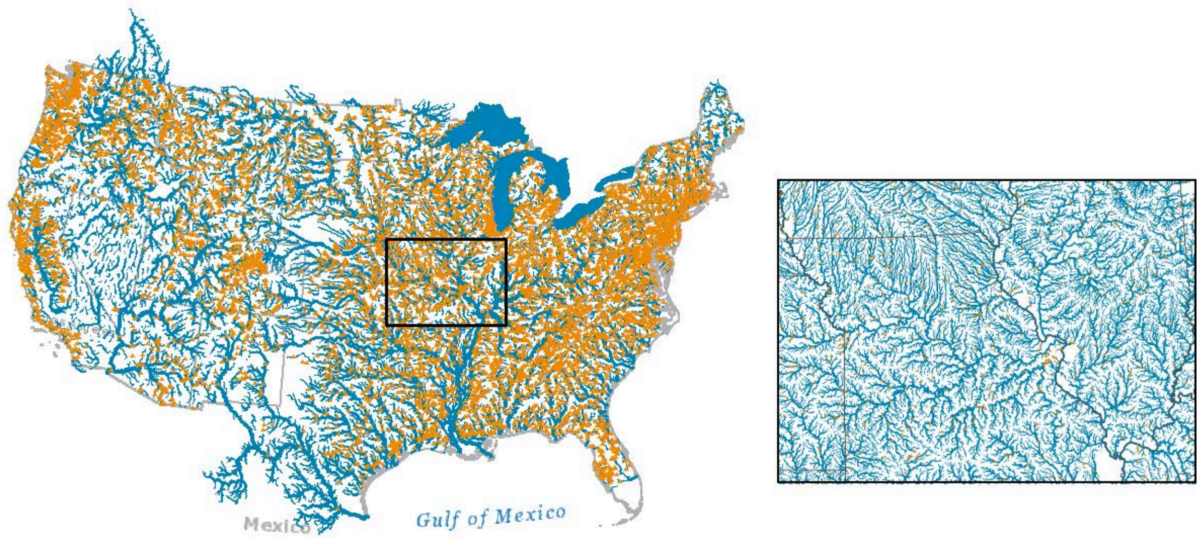

Figure 73. Locations of over 9,000 gauges (orange) used for validation of annual maximum discharges

For the selected gauges, the 2-, 10-, and 100-year return period flows were estimated using annual maximum flow values, following the standard flood frequency analysis procedures. Modeled 2-, 10-, and 100- year annual peak values were extracted from the 10,000-year catalog annual maximum series for the stream link corresponding to each gauge.

Figure 74 compares the modeled and distribution-fitted quantiles of observed peak discharges for the model domain at the return periods of 2-, 10-, and 100-years (exceedance probabilities of 50%, 10%, and 1%).

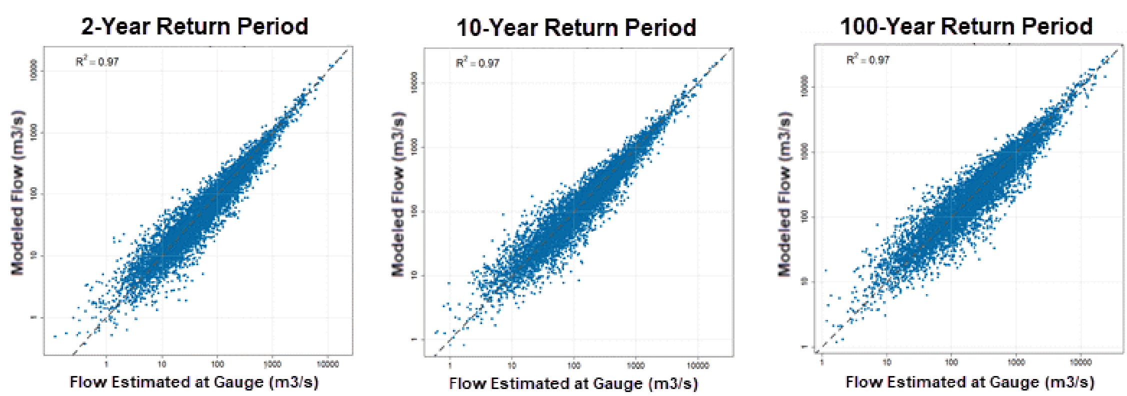

Figure 74. Comparison of modeled and distribution-fitted quantiles of observed annual peak flows for 2-, 10-, and 100-year return periods

Validation shown in Figure 74 was also carried out for each of the 17 hydrological regions[24] to ensure that there are no regional biases and the model performs reasonably well under

[24] For validation, Verisk combined the Tennessee and Ohio regions.

different climatological, geological, and soil conditions. Figure 75 provides an example of modeled flows compared with the distribution-fitted quantiles of observed peak flows in the New England region (Region 01) at the 100-year return period (1% exceedance probability).

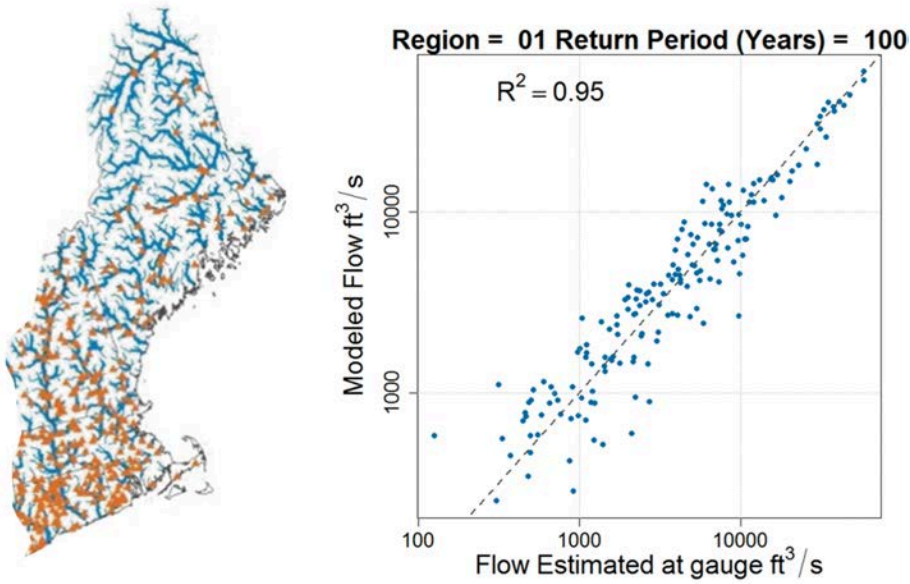

Figure 75. Comparison of modeled and distribution-fitted quantiles of observed annual peak flows in the New England region (Region 01), 100-year return period

Seasonality of Extreme Flows

Seasonality of the extreme flows is another important aspect that represents the robustness of the model's ability to realistically simulate the various facets of the hydrological cycle. Verisk compared the monthly frequency of annual maximum flows for each region, obtained based on the observed flows, with those based on modeled flows (Figure 76).

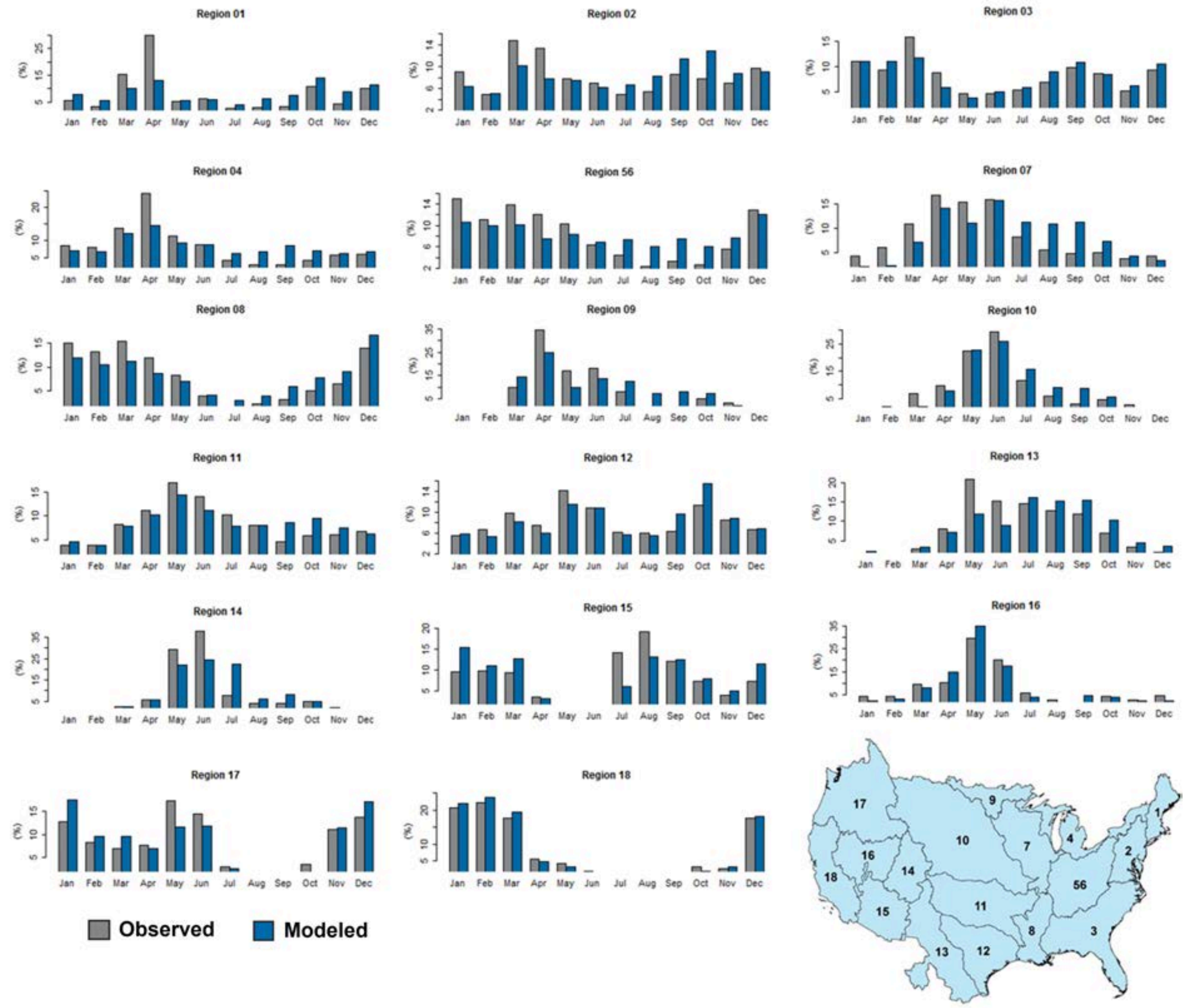

Figure 76. Modeled v. observed monthly frequency of annual maximum flows, by region

As illustrated, there is reasonable agreement across the regions.

Validation of Flows from Historical Flood Events

Verisk also validated a set of 20 significant historical flood events. For each event, the observed discharge at each gauge station within the impacted area was compared with the modeled discharge at each of the stream links corresponding to those stations.

Figure 77 and Figure 78 provide a comparison of observed and modeled data for the 2006 Northeast and the 2010 Tennessee floods, respectively. These plots illustrate that the model is not only realistically simulating the peak flow; in most cases, the entire pattern of the hydrograph is also reasonably simulated. The model is able to account for various hydrological processes such as soil saturation, snowpack and snow melt, evaporation, and flow routing. Although it is desirable to accurately simulate the entire hydrograph, it is not always possible, given the uncertainty in precipitation and other input data, as well as the simplistic nature of the conceptual hydrological models. Some of these challenges can be seen in plots of the Tennessee event (Figure 78) where the shape of the modeled hydrograph differs from the observed. Since maximum flow is proportional to the magnitude of the flood hazard, in cases where the hydrograph is not a complete match, the priority is given to simulating the magnitude of the maximum flow of the event accurately.

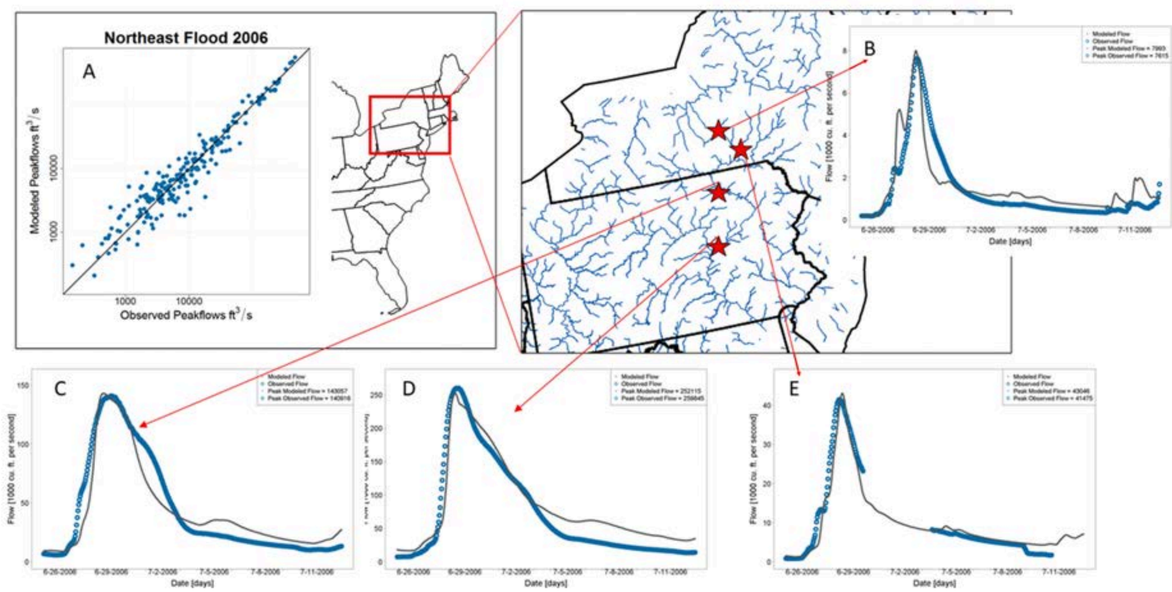

Figure 77. Validation of river flows for the 2006 Northeast flood events
A) Comparison of modeled and observed event peak flows for all gauges with flow data during the event
B) to E) Comparison of modeled and observed hydrographs at selected gauges

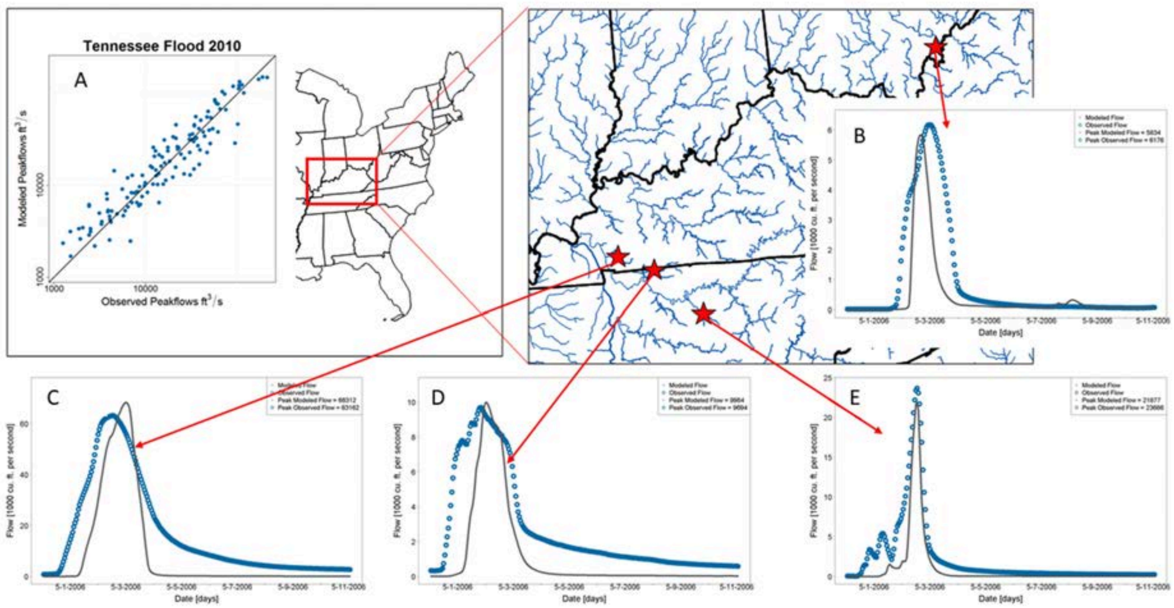

Figure 78. Validation of river flows for the 2010 Tennessee flood event
A) Comparison of modeled and observed event peak flows for all gauges with flow data during the event
B) to E) Comparison of modeled and observed hydrographs at selected gauges

3.4 Defining a Flood Event

Verisk has created distinct flood events in the stochastic catalog by grouping peak flows and peak 24-hour accumulated precipitation. However, due to the continuous nature of the flood peril in time and the structure of multiple converging river basins in space, the resulting flood event can be quite complex. The flood may consist of multiple initial conditions and sources of water (multiple storm fronts, snowmelt-induced flooding, etc.) across multiple drainage basins. It is a challenge to isolate a single source or condition that causes flooding at a macro-scale, and therefore an objective and robust method of defining flood events is needed. The Verisk model defines flood events in space and time through a multi-stage process based on several criteria, including characteristics of floods, industry needs, and a review of historical flood events.

To understand the complexities of an inland flood event, let's consider an example. In early 2017, a series of storm systems impacted California in quick succession, resulting in severe flooding across the state. The flooding lasted for about 47 days (January 7 to February 22). The observed rainfall and riverine peak flood instances for this event are shown in Figure 79. The top-left panel shows the footprint of observed total rainfall. The peak flow instances in this figure are based on the 2-year **peak-over-threshold** (PoT) flooding instances at the unit catchment level. It is apparent from the bottom-right panel of this figure that there is a lot of flooding activity throughout this period, particularly during the first 17 days (January 7-23) and the last 16 days (February 6-22). The highly publicized Oroville dam disaster unfolded from 7th to 14th February, corresponding to the second of two significant instances of flooding, starting on Day 30 as shown in the bottom-right panel. Another important element to note is that while there is a significant flooding in the California region during this time, there are several instances of flooding during the same time period in many other states across the country, such as Pennsylvania, Ohio, Georgia, Florida, Texas, Washington, Oregon, Idaho, and Nevada, among others. These peak flows, not classified as the California 2017 event, belong to one or more other events. This illustrates that deciphering and separating flood events from one other in continuous time and space is not a trivial exercise. Events like these suggest that inland floods unlike hurricane events can prolong for longer than a week. Furthermore, the event duration of the 20 historical events modeled as part of this model's marquee event catalog, as shown in Figure 80, suggests that the duration typically exceed 168 hours. These factors have been considered in the event definition algorithm to reflect inherent spatio-temporal continuity of flooding instances and to create longer inland flood events.

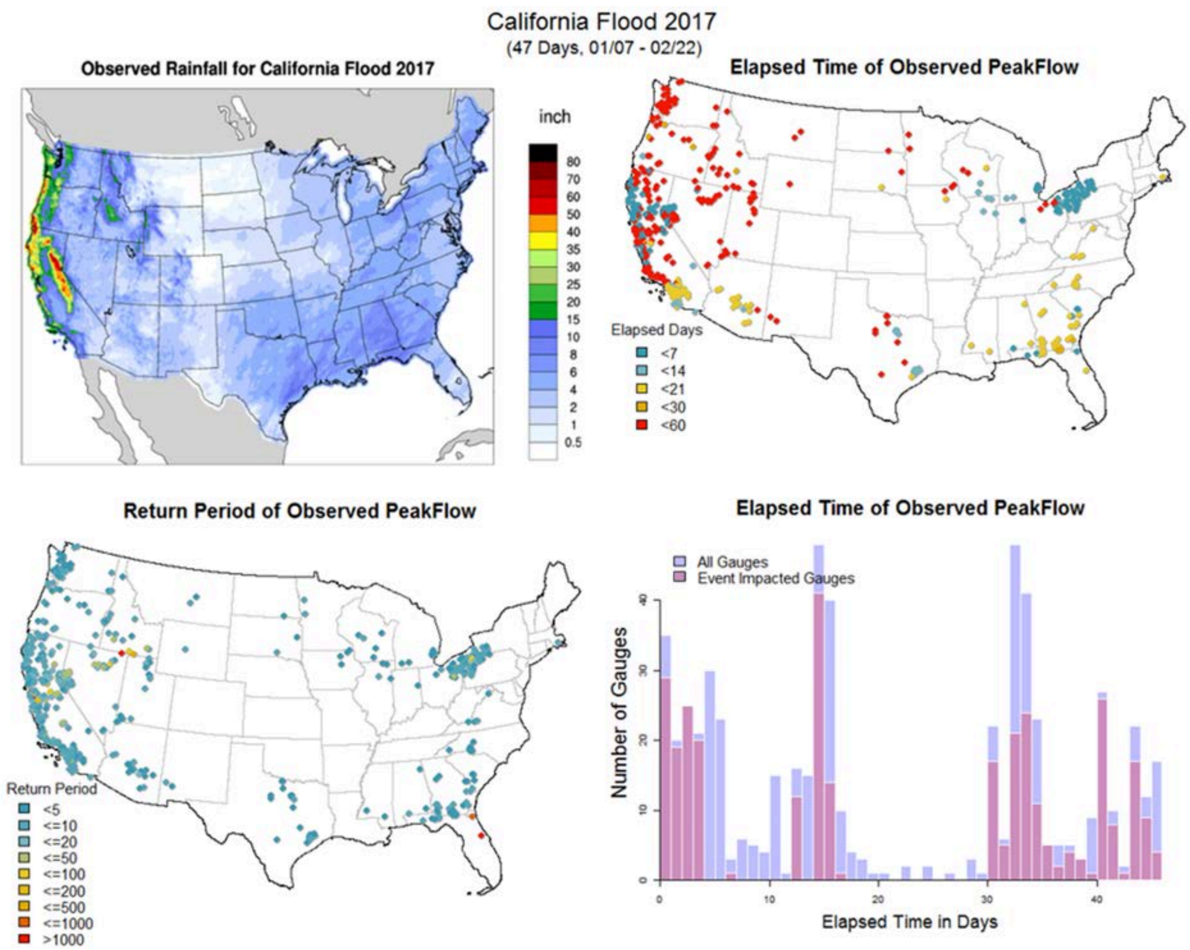

Figure 79. Extent, severity, and timing of flooding instances during the 2017 California Flood over the 47 day period (January 7 - February 22, 2017)
For the histograms in the bottom-right panel, the purple color reflects flooding throughout the country while the pink color represents only those river segments that are within the designated extent of this flood event (i.e., only the California region).

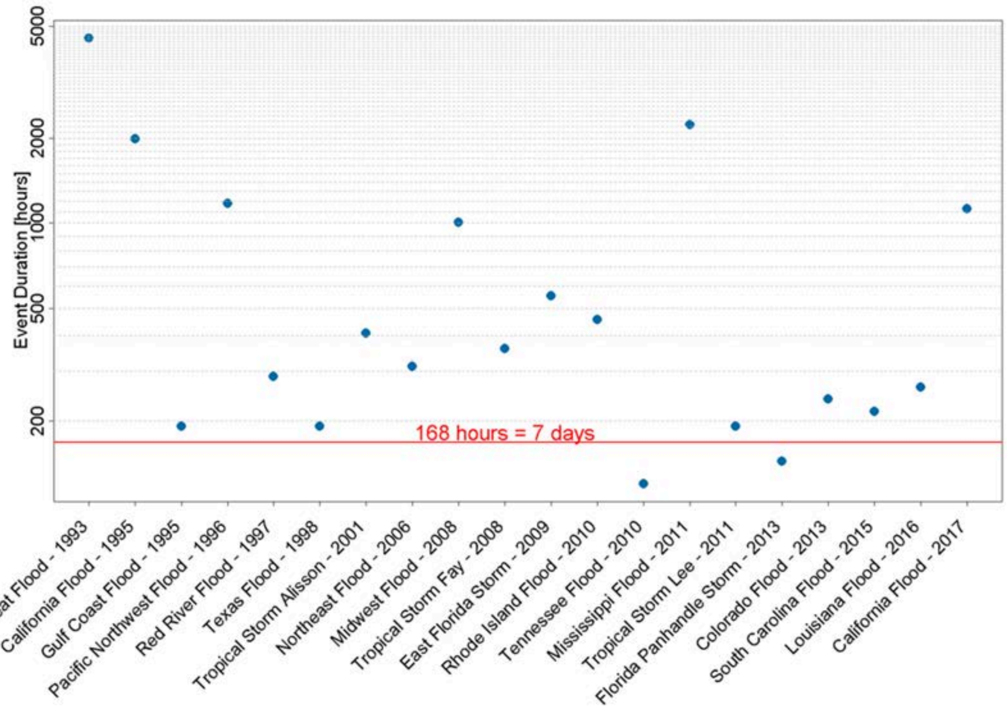

Figure 80. The duration of 20 significant historical events
All but two events have a duration that exceeds 168 hours.

Generation of Peak Flow and Peak Accumulated Precipitation

To model floods across the contiguous United States, the Verisk meteorological model simulates hurricane and non-hurricane precipitation together on a continual basis to best reflect real world processes. The Verisk hydrological model then utilizes the precipitation at hourly time steps to first store water in lakes, snowpack (accumulation and melting), or within the soil, and then route water through the subsurface or over land to each river segment. The response of the hydrological model to the precipitation will vary depending on the local antecedent conditions and terrain. The output of the hydrological model is the peak streamflow and peak 24-hour precipitation over a 5-year return period threshold (20% exceedance probability) for a river segment or unit catchment, respectively. For simplification, any peak flow or 24-hour accumulated precipitation over a 5-year return period threshold is considered a **flow peak over threshold (flow PoT)** or **precipitation PoT**, or simply **PoT** when both are considered. The 5-year threshold is used, as there is the expectation that any property would have nominal protection against low severity, but very frequent, hazard intensities.

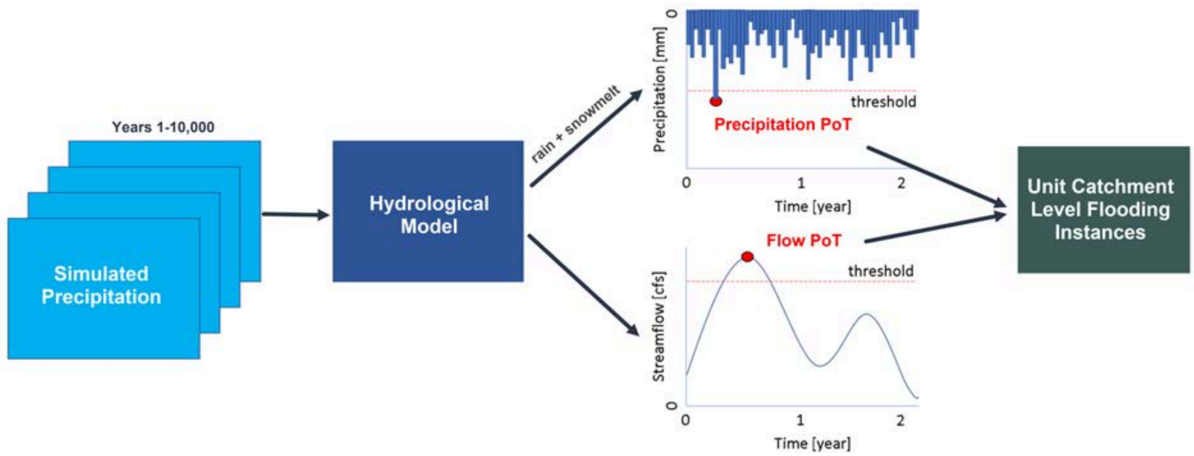

Figure 81. Verisk flood event development process

The Verisk stochastic catalog contains the magnitude and timing of each peak flow and 24-hour accumulated peak precipitation, organized by their respective flood events. For a given year, only a subset of catchments will have the flow and precipitation PoTs based on the expected frequency of exceeding the 5-year return period.

Flow and precipitation PoT patterns can be rather complex. The timing of flow and precipitation may differ. Multiple water sources may contribute to the same flood wave. A single source (meteorological system) may distribute water across multiple drainage basins over time.

Over a relatively small area, flow PoTs can be associated with a single storm system. However, for very large basins (e.g., the Mississippi River basin), the propagation of a flood wave may take months to travel from its head waters (in Minnesota) to its mouth (Gulf of Mexico). For example, the 1993 Mississippi flood event lasted nearly 200 days in some locations (Larson, 1997). During a flood event of this scale, a single flood wave along the Mississippi River can consist of excess water from multiple storm systems and release mechanisms (e.g., snowmelt). In this context, the vast combination of the location and timing of individual flow and precipitation PoTs presents a unique challenge that requires a multi-stage algorithm to realistically classify flood events at different scales in time and space.

Clustering Flow and Precipitation PoTs into Flood Events

To solve the challenge of defining events from flow and precipitation records, Verisk used a holistic approach to define a flood event, based on a multi-stage algorithm. The algorithm clusters the locations affected by precipitation and flow PoTs into flood events, according to their occurrence and distribution in time and space.[25]

The first stage involves grouping flow and precipitation PoTs together in time, based on the 168-hour clause and the temporal distribution and separation of PoTs as an initial metric.

[25] The stochastic catalog for the Verisk Inland Flood Model for the United States does not include events associated with hurricanes. These events are addressed in the Verisk Hurricane Model for the United States. Prior to applying the event definition algorithm, Verisk removed the flow and precipitation PoTs influenced by hurricanes, based on hurricane tracks and regions of influence.

However, since flood events typically exceed this duration, 168 hours should be considered a starting point to help organize the data and not indicative of the final maximum duration. The second stage uses a variance-based agglomerative hierarchical clustering approach (Müllner, 2013 and Reynolds et al., 2006) to find natural separation within a continuous space. Conducted iteratively, this stage proceeds until the maximum distance between PoTs is less than 3,500 km. Verisk selected this initial maximum distance based on the initial 168-hour duration constraint, the average propagation velocity of a flood wave [about 18 km/hr (11 mph)], and the average advection speed of a storm system over the United States [about 20 km/h (12 mph)].

Verisk then applied additional considerations for temporal overlap and spatial proximity of initial events to increase the robustness and flexibility of the algorithm. As such, the resulting flood events range from 1 hour to 1,200 hours (approximately 2 months) in duration and spatial extents that range from a few kilometers to over 3,500 km. Figure 82 provides an example of one year of flow and precipitation PoTs in space over the United States, and how these locations are grouped and separated into individual flood events. The statistical distributions of the defined events are shown in Figure 83.

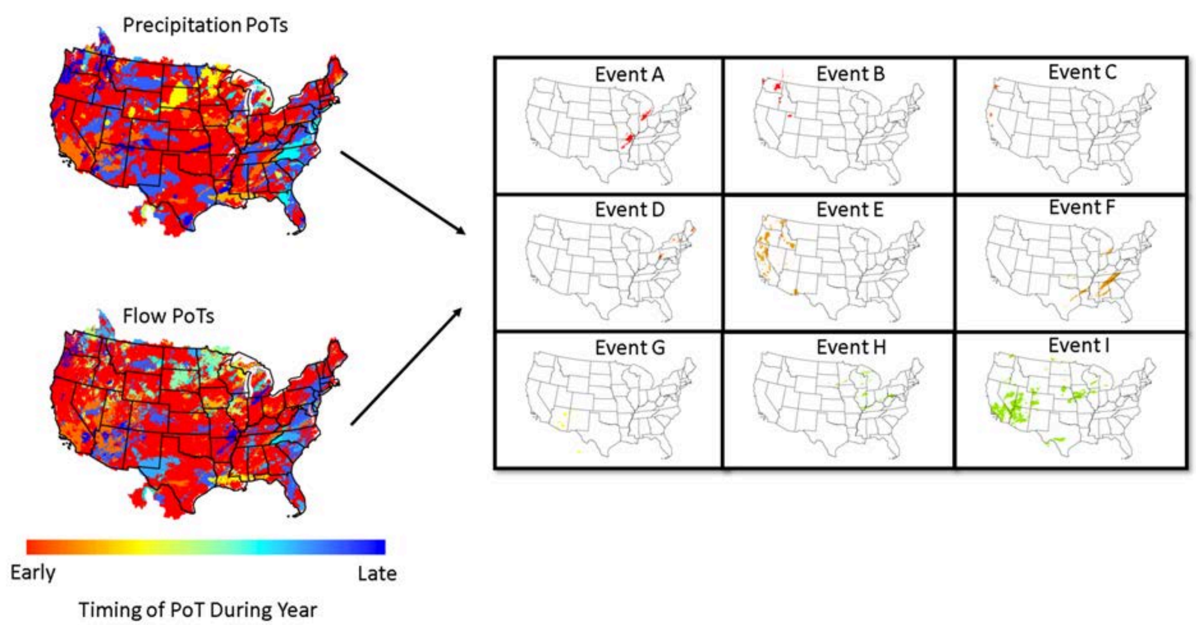

Figure 82. Flow and Precipitation PoTs over a given year (left) are fed through the Verisk event definition algorithm to classify unit catchment level flooding occurrences into flood events (right).

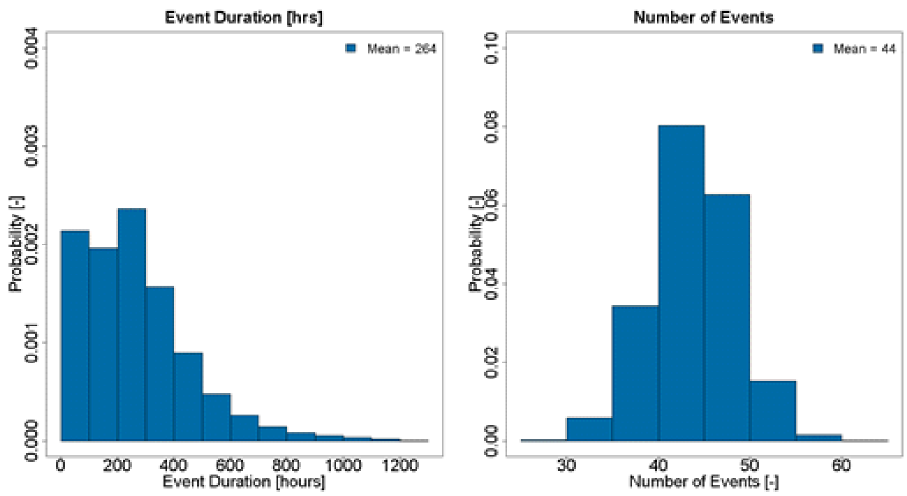

Figure 83. Statistical distributions of event definition, including the event duration and events per year

4 Local Intensity Calculation

The Verisk model determines flood intensity in terms of inundation (water) depth, at locations both on- and off-floodplain. The model employs two physically-based approaches, based on location and catchment size. A one-dimensional (1D) hydraulic model with a two-dimensional (2D) flood mapping tool is used for on-floodplain locations, and a 2D shallow water model is used for off-floodplain locations and small catchments.

For on-floodplain locations, the hydraulic model uses river discharge data (hydrographs) from the hydrological model to determine the water elevation at points along a river, as well as the extent of flooding. The model performs hydraulic calculations for over 4 million river cross sections, at approximately 500 m (0.3 mi) intervals along the course of the modeled rivers.

For off-floodplain locations, the pluvial model (2D shallow water model) computes the temporal evolution of surface runoff depth over a fine grid in response to intense precipitation.

The riverine or on-plain hydraulic model computes flood depths and extents for stream links with catchments larger than 10 km^2 (3.86 mi^2). The pluvial model computes flood depths and extents for locations over the entire model domain, including the floodplains of larger rivers. In locations where these analyses overlap, the model retains the greater of the two inundation depths to calculate losses and leave out the other depth.

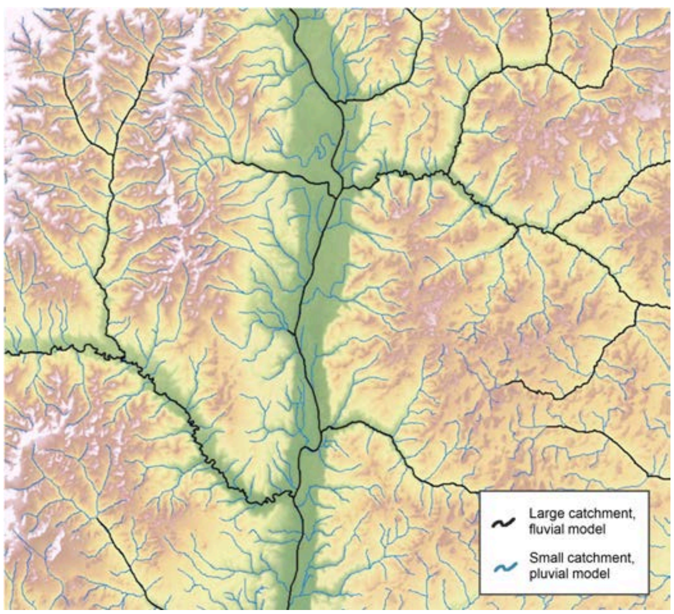

Figure 84. Stream links with catchments of various sizes

Details of the hydraulic model, pluvial model, and Verisk Flood Hazard Maps are presented in the following sections.

4.1 Local Intensity Data Sources

To develop the hydraulic model, Verisk obtained information from several agencies that gather original climatic and hydrological data. These data sources are listed below.

Water Bodies	USGS National Hydrography Dataset (NHD) https://www.usgs.gov/core-science-systems/ngp/national-hydrography/nhdplus-high-resolution Vintage: September 2017 Resolution: 0.25°
Digital Terrain Model (DTM)	USGS 3D Elevation Program (3DEP) https://www.usgs.gov/core-science-systems/ngp/3dep Vintage: 2017 Resolution: 10 m or better The data includes about 25% LiDAR-based areas and as per Verisk's industry exposure database (IED) it covers about 65% of country's exposures in terms of the replacement value.
Land Use / Land Cover (LULC)	USGS, Landsat data from the Multi-resolution Land Characteristics Consortium (MRLC) https://www.mrlc.gov/ Vintage: 2011 (released in 2014) Resolution: 30 m
Population	LandScan™ https://landscan.ornl.gov/, Vintage: 2011 Resolution: ~ 1 km
Stream flow	United States Geological Survey (USGS) https://waterdata.usgs.gov/nwis Vintage: 2017 Annual peak flow data, hourly flow data, concurrent stage-discharge field measurement data, and other data sets
Levees	USACE's National Levee Database https://levees.sec.usace.army.mil/ Vintage: June 2018

	~ 25,000 mi of levee information
Tides	National Oceanic and Atmospheric Administration (NOAA) Tides and Currents https://tidesandcurrents.noaa.gov/

4.2 Hydraulic Model—Estimating Flood Inundation Depths on the Floodplain

Water elevation typically increases with discharge, or flow. This relationship between water stage (water elevation above a specified reference point) and discharge is captured in a **rating curve**. Figure 85 provides an illustration of a typical rating curve.

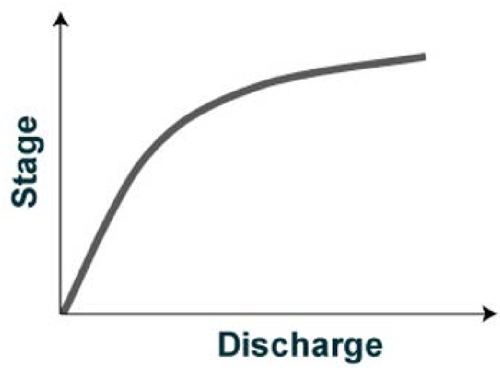

Figure 85. A typical rating curve

Rating curves are generally constructed, and periodically calibrated, at river gauging stations. They are not available for arbitrary points of interest. The role of the hydraulic model, therefore, is to develop a full set of rating curves for each 10-m grid cell, flooded up to a 100,000-year return period[26] level, across the model domain.

Once the hydraulic model has transformed peak discharges into water surface elevation, the model calculates inundation depth by subtracting the ground elevation (from the DTM) from the water surface elevation.

Determining Water Elevation

The hydraulic model developed at Verisk is based on a computational algorithm similar to the steady state mode of HEC-RAS, a widely-used physically-based hydraulic engineering model developed by the United States Army Corps of Engineers (USACE). In Verisk's hydraulic model, a one-dimensional energy equation is solved iteratively to compute a steady state water surface profile of a dendritic (branching) river network.

26 Exceedance probability of 0.001%

The total energy of the flowing water at a cross section along a river channel is defined as a combination of three forms of energy:

1. Potential energy due to the ground elevation
2. Static pressure energy due to the water depth
3. Kinetic energy due to the flow velocity

The energy balance equation dictates that from one cross section of the flow to the next, the total energy is conserved unless there is energy loss occurring between two cross sections. Invariably, there is energy loss due to surface roughness, and in some situations due to a lateral or vertical contraction or an expansion of the river channel.

The model estimates hydraulic parameters of a channel cross section by using, within each cross section, subdivisions in which the flow velocity is assumed to be uniformly distributed. By using these subdivisions, the hydraulic model provides reliable flow calculations for the main channel as well as floodplains. The subdivision units are based on changes in elevation (available from the DTM) and roughness (obtained from the high-resolution LULC data). Roughness coefficients may vary within a cross section.

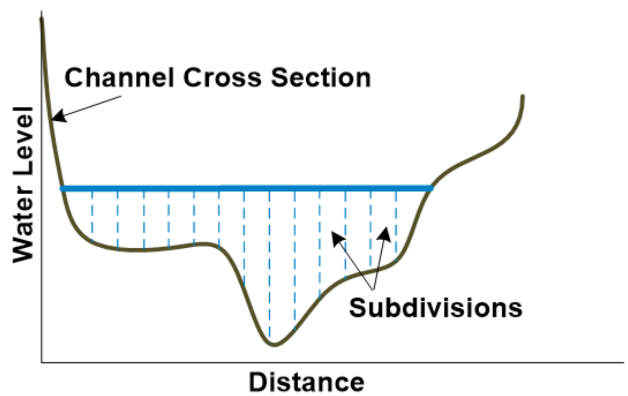

Figure 86. River channel cross section and its subdivisions
Flow velocity is assumed to be uniform within each subdivision.

Input Data for the Hydraulic Model

The hydraulic model uses three datasets as input, illustrated in Figure 87:

Water bodies	Water bodies include river networks, lakes, canals, etc. in the model domain. The model uses the dataset's river network to determine the center line for each stream in the river network. The total length of the modeled rivers is approximately 2.2 million km (1.4 million mi), with 335,000 distinct drainage catchments. All rivers with a contributing area of 10 km^2 or higher are modeled through the 1D hydraulic model followed by 2D flood mapping. The remaining rivers are modeled using the 2D shallow-water wave model.

Land use and land cover (LULC)	Verisk estimates surface roughness derived from satellite-based LULC data set. Surface roughness reflects the resistance of a surface to the flow of water over it. For example, the resistance of a smooth surface such as pavement, or even the sand or rock surface of a riverbed is much lower than the heavily-vegetated surface on a floodplain. As a result, the velocity, depth, and attenuation of the flow wave differ greatly over different surfaces. For this purpose of roughness estimation, LULC data at 30 m horizontal resolution are used.
Digital terrain model (DTM)	The DTM contains a database from which the channel shape— the geometry of the floodplain and the river channel above the surface of the water—is extracted. The results of the hydraulic model are mapped back to the same dataset to derive inundation depth. These inundation depths are obtained at high-resolution of 10 m.

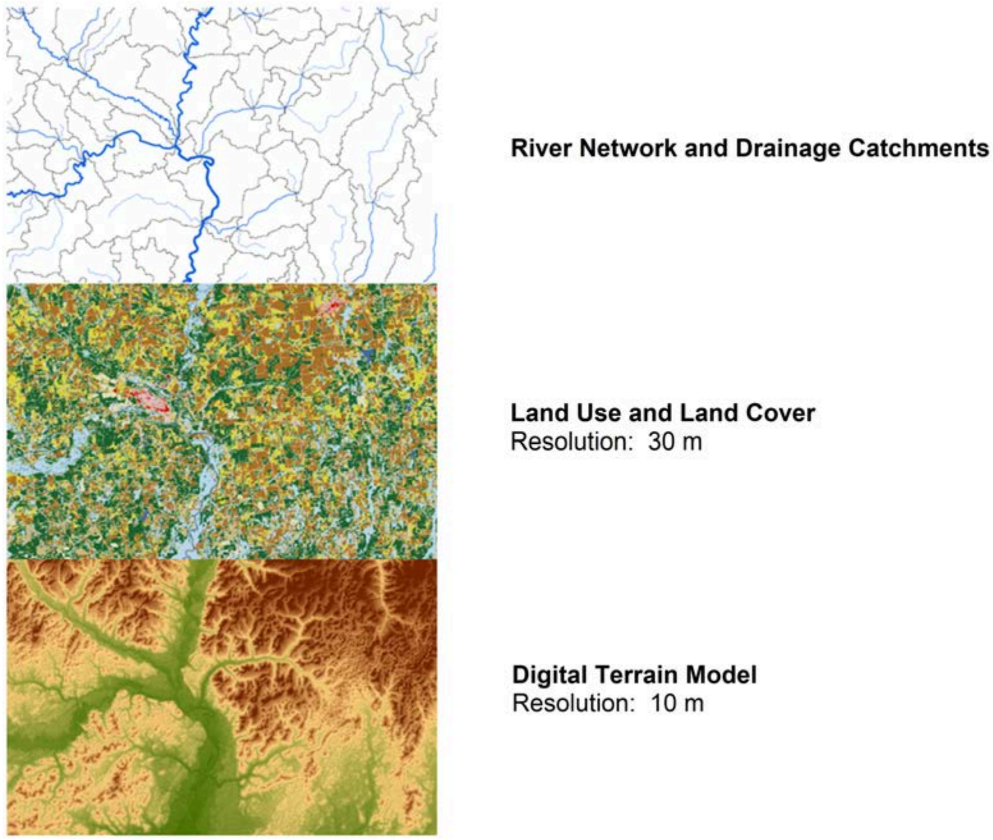

Figure 87. Underlying datasets used in the Verisk hydraulic model

See Also
Local Intensity Data Sources

Hydraulic Modeling Methodology

The hydraulic model requires the creation of cross sections along flowlines. Verisk developed a process to create cross sections for the entire model domain. First, to determine the maximum possible floodplain, Verisk scientists used hydraulic model inputs to obtain floodplain areas and the characteristics of the floodplain's environs (Figure 88). After obtaining the terrain and land information, Verisk estimated the flood extent that would occur if the water were 10 m (33 ft) above the normal water surface elevation. The hydraulic model uses this flood extent as the maximum possible domain for floodplains along the river network (Figure 88c).

After determining the hydraulic model domain for the river network, details of the domain's terrain are needed. To obtain these details, Verisk created cross sections at 500 m (0.3 mi) intervals along each stream segment/link within the domain (yellow lines in Figure 88c). This interval length is used as it is small enough to capture changes in the geometry and surface roughness of the floodplain, but large enough to be efficient from a computational standpoint. Along each cross section, the shape of the main channel (including the floodplain) is extracted from the DTM and the surface roughness from the LULC data.

As Figure 88 illustrates, the flow path may change when the peak flow is greater than the bankfull flow, as water will always take the shortest route. This change in flow path, which is captured by the model, is significant when modeling flow along meandering rivers because the flow path is shorter during a flood.

Figure 88. Terrain and river network
a) Center line of water course
b) Hydraulic model domain and cross section cutlines
c) Maximum flood extent

To calculate flood elevation data for each point where a cross section intersects the river, channel geometry and roughness data are used together with river flows/discharges for each stream link. For this, the discharge data are generated by the hydrological model.

To ensure a close match between modeled water levels and water level data from rated river gauges[27] across the model domain, the hydraulic model calibrates a set of parameters, which include the bankfull flow and roughness factor. This calibration is based on data collected from over 5,800 rated gauging stations located across the country (Figure 89). Verisk performed this calibration for the 10- and 100-year return period flows (10% and 1% exceedance probabilities).

27 A river gauge is rated if its discharge and corresponding water level measurements are available; preferably the gauge has an explicit discharge curve available for each stage.

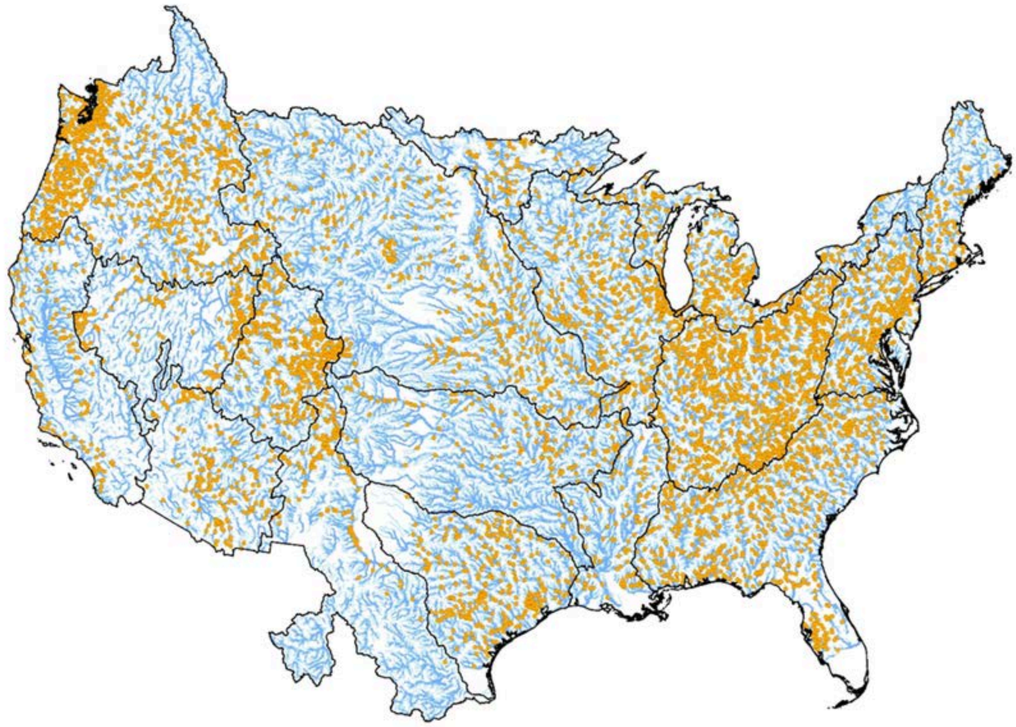

Figure 89. Locations of stream gauge stations (in orange) used for model calibration

For every point of interest, the model creates a relationship between a set of specified discharges and the corresponding simulated flood elevation in the form of rating curves. For a simulated event, these rating curves are used to estimate water levels from modeled flows/ discharges.

This calibration minimizes the root mean square error between the water levels from the gauge station rating curves and those generated by the model. The results for floods with a 100-year return period (an exceedance probability of 1%) are shown in Figure 90. As illustrated, the error distribution is centered on zero with the majority of the modeled water levels within 75 cm (30 in) of the observed levels from the gauge station rating curves.

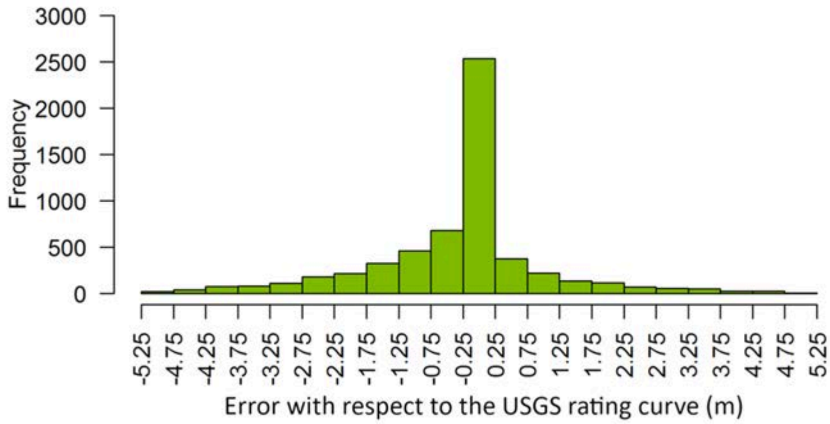

Figure 90. Calibration results for 100-year flood levels

Translating Water Elevation to Inundation Depth

In the Verisk model, flood intensity is determined by inundation (water) depth, or the difference in elevation between the water surface and the ground. During loss simulation, the model uses stored rating curves to compute flood depth for a given discharge in the pertinent river segment(s).

A Note on Bathymetry

An ideal DTM would represent the bare ground, excluding the height of vegetation, buildings, and standing water. In reality, most DTMs, including the one used in the Verisk model, do not include river bathymetry data. Instead, they provide the geometry of the main channel above the water surface, and the shape of the floodplain. The elevation provided over water bodies' surface is actually the water surface elevation, and the shape of the underlying channel remains unknown.

The model assumes there is a portion of the river discharge flowing at all times under the DTM elevation—between the DTM and the actual riverbed. To account for this, Verisk scientists have developed a two-layer hydraulic model in which the difference between the peak discharge and the discharge under the DTM surface, above the unknown riverbed, is used to calculate the flood elevation. This concept is shown in Figure 91 where part of the unknown riverbed is shown below the DTM surface.

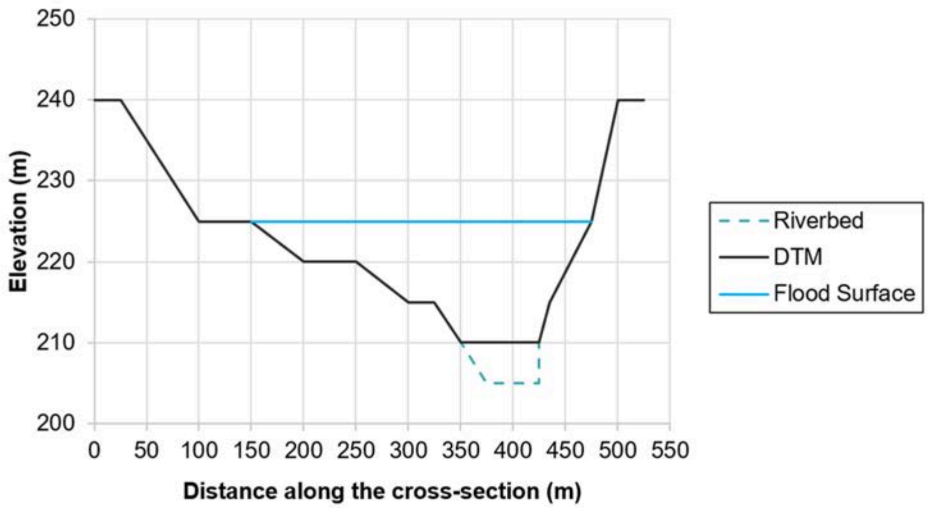

Figure 91. A typical river cross section in the hydraulic model

4.3 Modeling the Impact of Flood Defenses

The flood defense system in the United States is expansive and includes state and private levees as well as those managed by the U.S. Army Corps of Engineers (USACE). According to the USACE, there are an estimated 161,000 km (100,000 mi) of levees in the country. Levees are generally designed to protect an area against a flood with a certain return period. For example, a flood defense system in a heavily developed urban area may be designed to protect properties on the floodplain against a 100-year event.

The Verisk model includes approximately 47,000 km (29,000 mi) of levees along modeled flowlines, leveraging USACE's National Levee Database as a primary resource. Information for approximately 40,000 km (25,000 mi) of levees is obtained from this database. It includes the Midterm Levee Database, maintained by FEMA, as well as other state sources. The Midterm Levee Database focuses on levee accreditation and the flood protection status of communities that participate in the National Flood Insurance Program (NFIP). The model also includes approximately 6,400 km (approximately 4,000 mi) of levee lines digitized by Verisk, based on high-resolution aerial imagery and automated in-house DTM extraction procedures.

For leveed stream links where flood defense data are unavailable [approximately 23,000 km (14,000 mi)], the model uses the exposure replacement values, exposure counts, and USACE and FEMA protected area polygons to estimate the standard of protection that may be present in those river segments. In addition to known levee information, the Verisk model also employs estimation of standard of protection using other indicators.

Figure 92. Levees and levee-protected areas included in the Verisk model

The failure of flood defenses is modeled probabilistically using fragility curves such as Figure 93, which indicates the probability of failure given an intensity of loading. Although each flood defense is designed for a specific standard of protection (i.e., its design load), there is a probability that it can fail at load levels below that standard, as well as a probability that the defense will hold for loads greater than the standard. Ultimately, for most severe events the probability of defense failure reaches 100%. Such a probabilistic element in levee failure is due to the complex nature of the actual failure mechanism, as well as limited information on factor of safety in design and construction and levee maintenance.

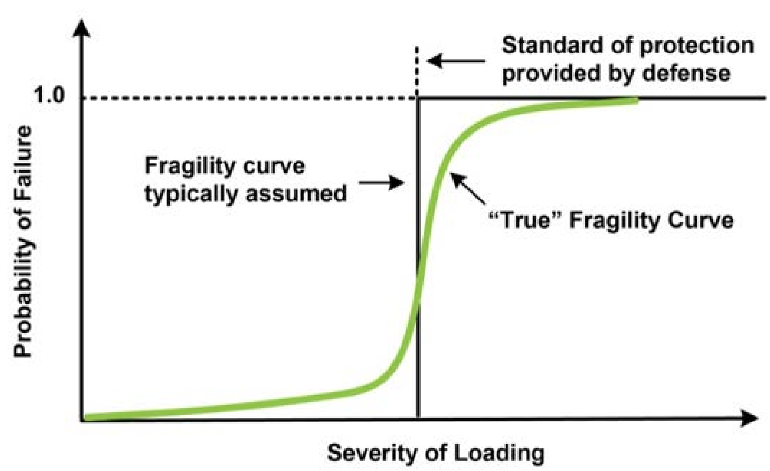

Figure 93. Flood defense fragility curve

For each flood event, the model uses fragility curves to determine whether a flood defense fails along a protected stream link in the river network. The flood severity at a given link is indicated by the return period of the water flow at that link. Failure conditions are sampled probabilistically based on the event flow and the fragility curve for a given stream link. Within each area protected by a flood defense, the fragility curves are used to determine if and when a defense fails. If it does fail, losses are calculated for the event, using the modeled flood depths, in areas impacted due to the failed river link under consideration.

Figure 94. Levee breach along the Sacramento River during the 1997 California floods
(Source: California Department of Water Resources)

Flood protection along river segments is not always achieved by constructing levees. Other options include deepening, channelizing, and/or paving/lining river channels (e.g., the Los Angeles River in Los Angeles, CA and the bayous of Houston, TX). Flood defense fragility curves are not applied to the 127,000 km (79,000 mi) of modeled river links protected by alternative flood protection measures. The model uses exposure replacement values and exposure counts to estimate the standards of protection for stream links with such alternative protection. For areas protected from flooding using river channel modification, Verisk uses modified rating curves to increase the main channel capacity and conveyance so that flows less than the estimated protection levels are contained in the main channel. Figure 96 illustrates two example rating curves: one for a natural river section and another for the same river channelized to convey 25-year return period flow, as simulated in the Verisk model. The impact of the channelization on the river stage (or water level) decreases as the discharge increases.

Figure 95. Example of a lined river channel, Los Angeles River, Los Angeles, CA
(Source: USACE)

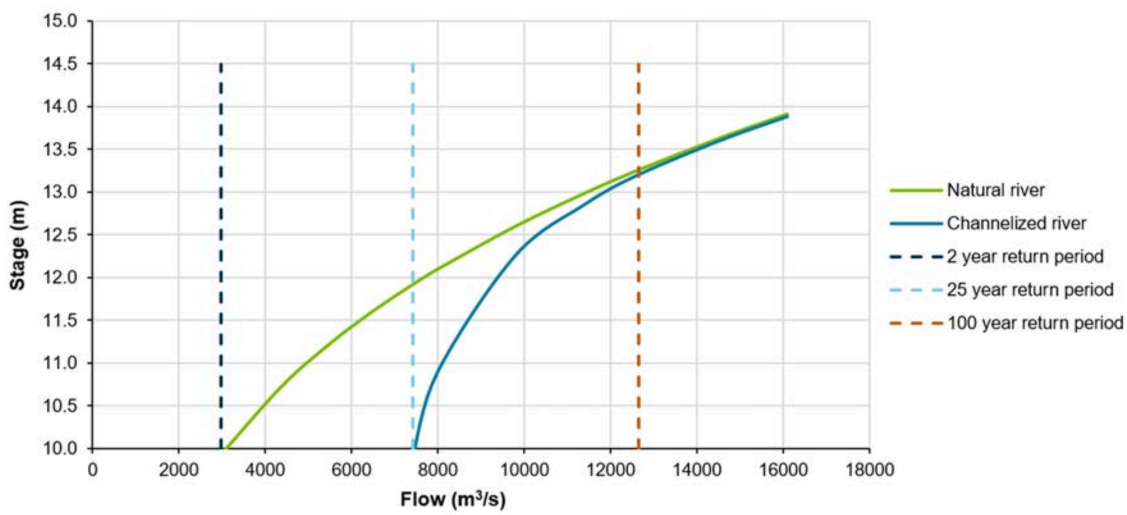

Figure 96. Rating curve for a natural river and a river channelized to carry 25-year return period flow

See Also
Local Intensity Data Sources

4.4 Modeling Tidal Effects

Tidal effects are explicitly considered in the Verisk flood model as tides affect a large number of rivers along the U.S. coastline. The hydrological routing model determines the time of peak discharge for each stream link. This time is then used to calculate the astronomical tide and its effect on water elevations in the tidal zone at peak discharge. Harmonic constants for tides have been obtained from the National Oceanographic and Atmospheric Administration (NOAA).

The majority of tidal gauge stations in the United States are located along the eastern seaboard although stations are located throughout the Gulf States and along the west coast as well. The model includes data from 512 tidal gauge stations (Figure 97).

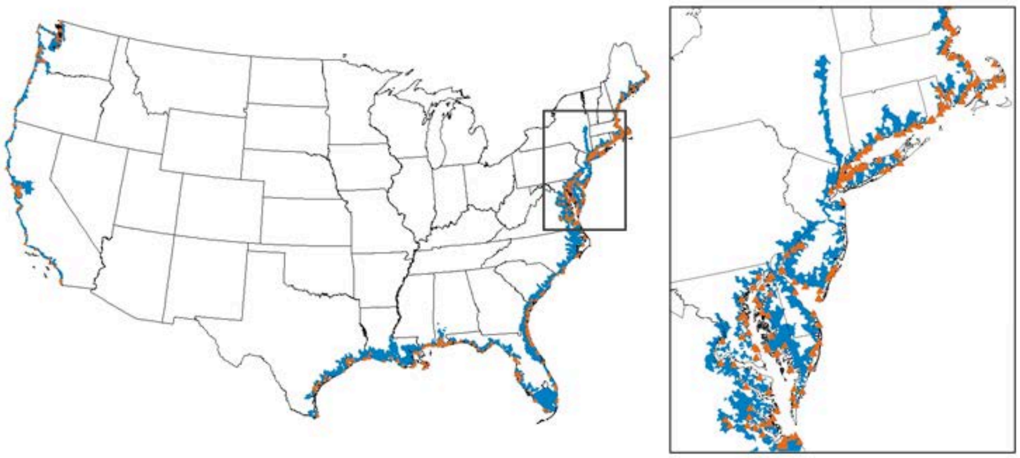

Figure 97. Tidal gauge stations (orange) and tidal zones (blue) along the U.S. coastline

See Also
Event Generation
Flow Routing

4.5 Local Intensity Off the Floodplain

Damage data from recent flood events in the United States indicate that a significant portion of flood losses occur in off-floodplain locations. Affected areas are often a considerable distance from large rivers and their floodplains. For example, in August 2016 central Louisiana (Lafayette to Baton Rouge) experienced flooding from intense rainfall

The percentage of loss attributable to off-floodplain events can vary considerably for each state. A list of the contribution to the insurable aggregate average annual loss due to on-floodplain and off-floodplain events, by state, is included in Chapter 1.

Off-floodplain losses typically occur when very intense rainfall causes high levels of surface runoff. This can occur at locations outside the floodplain, and also within the floodplain at a location where the river did not overflow but a property flooded due to intense rainfall. For this reason, off-floodplain damage is more frequent in urban areas where the large percentage of paved areas significantly increases the runoff coefficient. Sewer backups and pump failures, insufficient drainage capacities, and clogged street gutters are common causes of off-floodplain flooding. In urban areas, aging drainage systems can be easily overwhelmed (or fail altogether) during heavy downpours, causing water to accumulate in local depressions on the land surface.

The contiguous United States covers a geographic area of approximately 8 million km^2 (3 million mi^2) and contains over 35,000 cities. It is not feasible to explicitly model the specifics of each city's storm water and sewer drainage network (i.e., the operating details of each network's pipes and pumps). However, the Verisk model accounts for the design capacity of urban drainage facilities in the off-floodplain model. This data has been collected from states, counties, and cities across the country.

See Also

[Insurable Aggregate Average Annual Losses](#)
[2016 Louisiana Flood](#)

Physically-based Pluvial Flood Model

To explicitly determine off-floodplain inundation depths, Verisk researchers developed a Graphics Processing Unit (GPU)-based, 2D shallow-water wave model. Using precipitation intensity, the DTM, land use, and drainage capacity as input, this model dynamically simulates the flux (change in volume of water over time) and accumulation of water over each grid cell (Figure 98). Unlike the hydraulic on-floodplain model, which calculates inundation depth based on a river's flow rate, the off-floodplain model calculates inundation depth directly. The model uses the maximum 24-hour precipitation accumulation in a unit catchment to calculate inundation depths for each affected cell within that catchment. Since the off-floodplain model calculates inundation depths directly, loss estimates are computed using the same damage functions used for on-floodplain flooding.

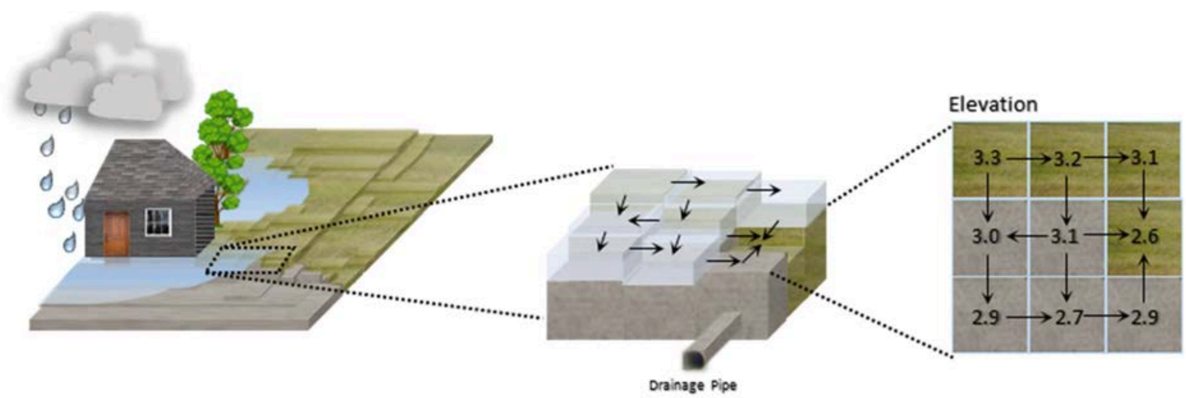

Figure 98. Schematic representation of the 2D pluvial flood model

In addition to off-floodplain areas, the shallow-water wave model also models inundation depths along streams with cumulative catchment areas smaller than 500 km^2 (193 mi^2) to varying degrees. During intensity calculation for a given event, in locations where both on-floodplain and off-floodplain models overlap, the model uses the greater of the two inundation depths for obtaining hazard estimates and omits the second one.

Storm Drainage Capacity

Urban storm drainage networks are designed to mitigate the most frequent precipitation intensities. Drainage networks may include storm drains, swales, culverts, ditches, and other structures designed to handle certain flood frequencies. Drainage capacity standards differ by city, county, and state. In addition, standards are not always uniform, depending on the year built, and available data are limited. For areas without known information, Verisk researchers assumed storm drainage design capacities based on land use and population density (Figure 99).

The model estimates precipitation intensity as a 24-hour maximum from the precipitation catalog, at the unit catchment level. To account for drainage, the model removes a certain precipitation depth (corresponding to drainage water) from the precipitation intensity, for each grid cell, prior to calculating flood intensity. To calculate the water removed, the model uses the precipitation intensity corresponding to the drainage design frequency as shown in Figure 99.

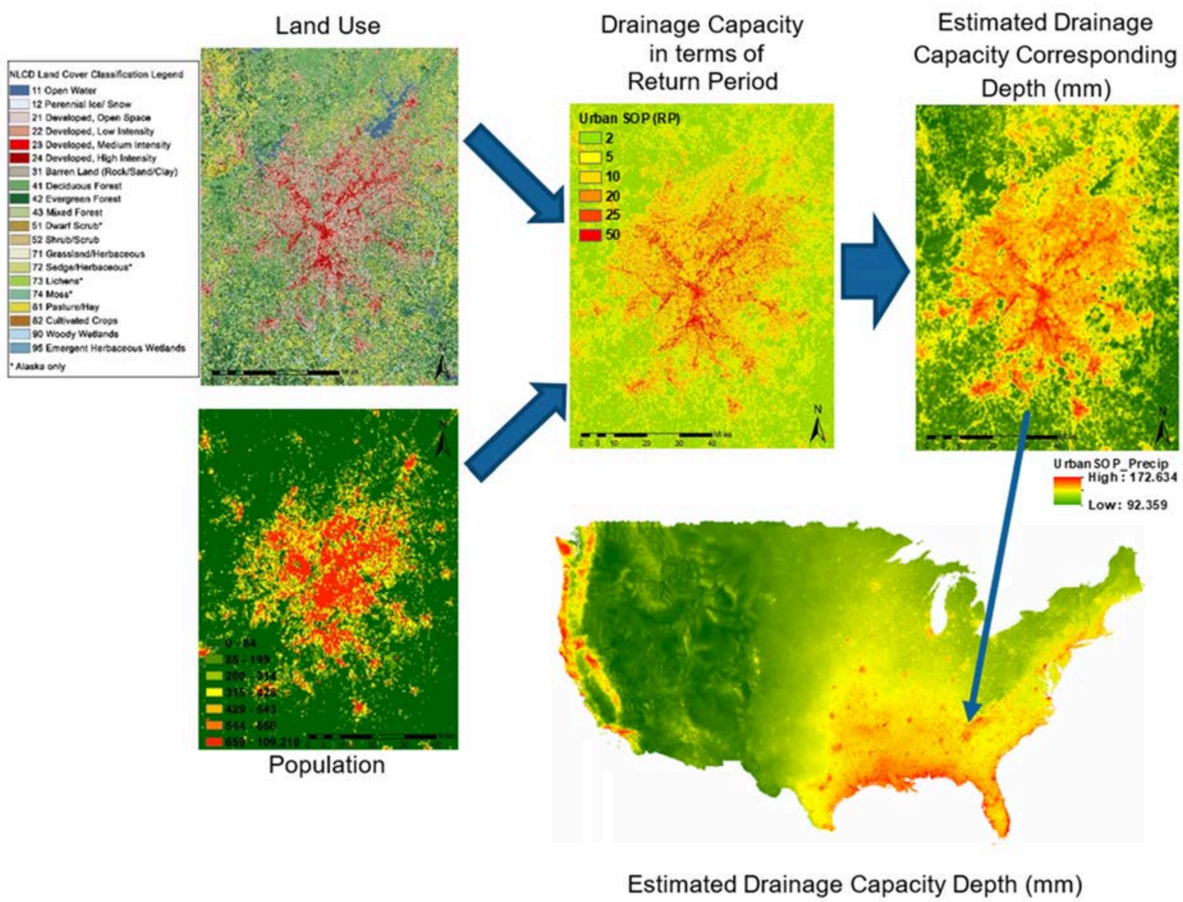

Figure 99. Development of drainage capacity

See Also
Simulating Precipitation

4.6 Flood Hazard Maps

The Verisk model is a fully probabilistic, event-based model. For model development, Verisk leverages the hydraulic module to create flood hazard maps as a complementary solution for managing flood risk in the United States. Six maps—corresponding to the 25-, 50-, 100-, 200-, 250-, and 500-year return periods—are available for use in the Geospatial Analytics Module of Touchstone. These maps reflect the combined on-plain and off-plain flood hazard and are provided in terms of specified depth bins of 0-1, 1-3, 3-6, 6-9, and 9+ feet. These unified flood hazard layers are based on the maximum of on-floodplain and off-plain/pluvial return period depths at any given 10 m grid.

It is important to distinguish the hazard represented by the flood hazard maps from the modeled output of a particular event footprint. Flood hazard maps provide the flood extent at a certain return period that would occur if every affected river simultaneously carried the flow corresponding to that return period. They do not show the footprint of any given flood event. The flood hazard maps provide an envelope of the maximum potential flood hazard at that return period. For example, in the Lower Mississippi Region, the flood hazard maps represent the envelope of maximum flood extent that would occur if a breach, corresponding to the return period of interest, occurred anywhere along the lower Mississippi River, in addition to flooding extents of the smaller rivers in the area.

The hazard for a region includes areas behind flood defenses like levees; therefore, the flood hazard maps do not include the effects of flood defenses. Figure 100 illustrates the differences between the flood hazard provided by the hazard maps and a modeled footprint of a given flood event.

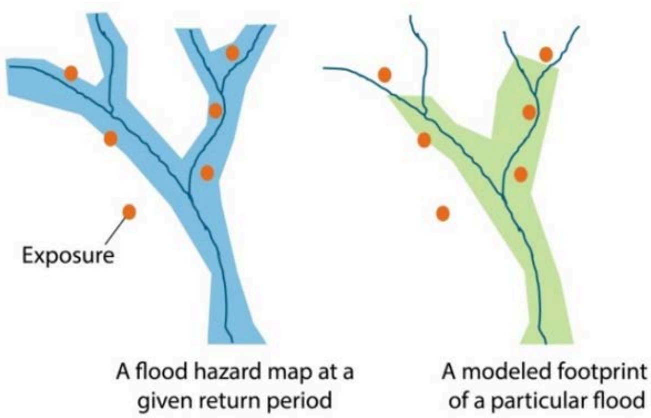

Figure 100. Example of a flood hazard map at a given return period (left) and a footprint of a particular flood event (right)

See Also

Flood Mapping of the lower Mississippi River: A Special Case

Verisk's Methodology for Creating Flood Hazard Maps

Once the hydraulic model calculates the flood elevation at each river cross section, these data are used to generate flood maps. To provide an accurate view of the hazard at a high resolution, the model generates 20 flood extent maps with return periods ranging from 2 to 10,000 years (exceedance probabilities from 50% to 0.01%). Six of these maps—corresponding to the 25-, 50-, 100-, 200-, 250-, and 500-year return periods—are available in Touchstone.

In order to generate the maps, the model exports the flood elevation data into Verisk's flood mapping tool, which employs a multi-source point expansion approach to provide realistic flood extents. This methodology applies diffusive and kinematic wave equations, in two dimensions, from given points on the water surface while incorporating the dataset from the DTM. This process delineates the flood extent two-dimensionally across the entire floodplain, creating a continuous water surface represented at the same resolution as the underlying DTM.

Figure 101 presents an example of the computed water surface elevation and resulting flood extent. The computed water surface elevation points are located along the river centerline, at each cross section.

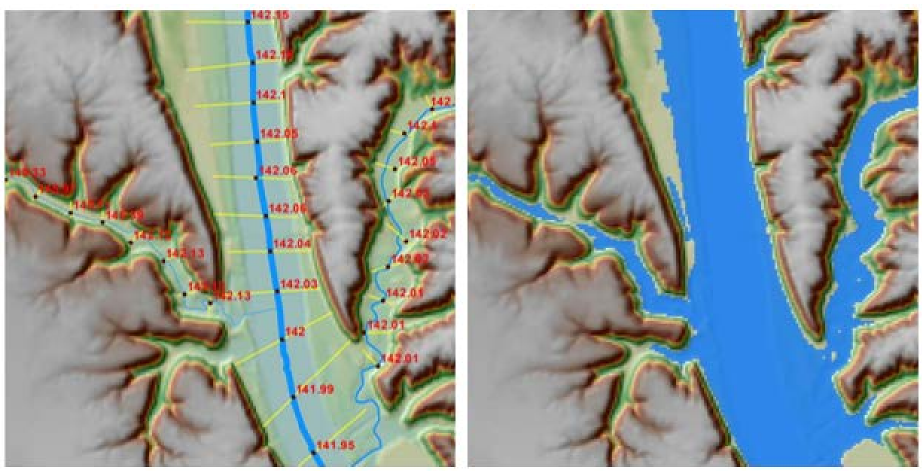

Figure 101. Cross sections and their water levels along the river (left) and corresponding flood extent (right)

The water surfaces produced by the flood mapping tool correspond to specific discharges for 20 return periods and every stream link along the river networks in the model domain. Once these surface levels have been obtained, the rating curves (the relationships between water elevation and discharge) can be constructed for any point of interest. Figure 102 illustrates this process. The top panel (Figure 102a) provides five example water surfaces, whose surface levels are represented in Figure 102b. Figure 102c shows the rating curve constructed using these surface levels. In the Verisk model, rating curves are developed at every point location (latitude-longitude) within the model domain.

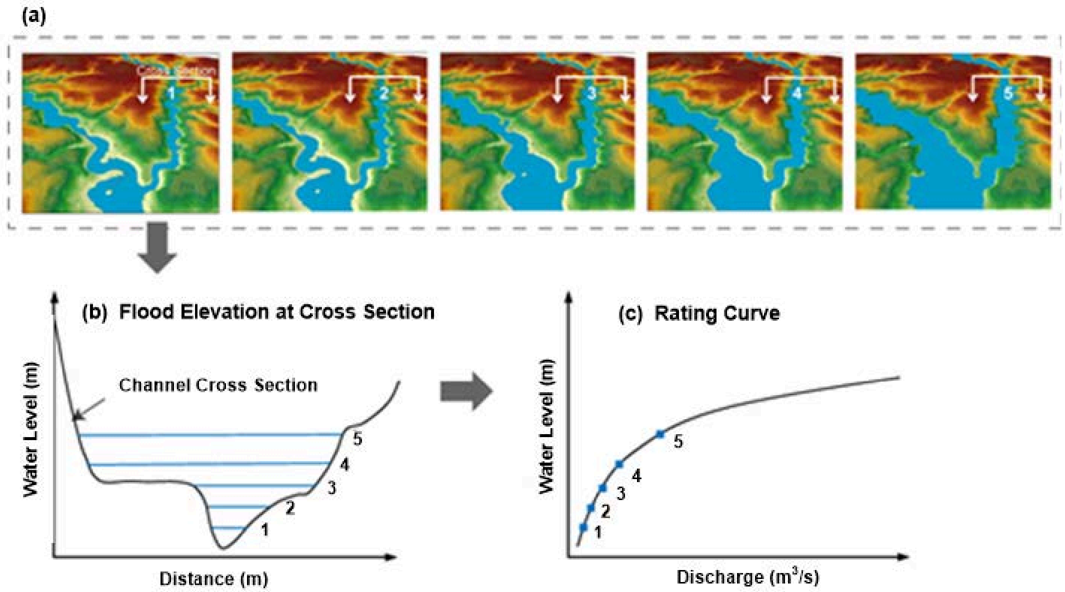

Figure 102. Rating curve produced by the hydraulic model

Flood Mapping of the lower Mississippi River: A Special Case

The lower Mississippi River is defined as the stretch of the Mississippi that runs from its confluence with the Ohio River at Cairo, Illinois, to the Gulf of Mexico. This section of the river feeds an alluvial valley of about 91,000 km^2 (35,000 mi^2). Over 80% of this floodplain relies on levees for protection. Approximately 1.5 million homes, along with thousands of agricultural buildings, are situated within this historically flood-prone region.

The extensive system of levees and floodways along the Lower Mississippi, maintained by the USACE, effectively controls flood waves well in advance of their arrival to this stretch of the river. The main stem system is 3,545 km (2,200 mi) long: 2,586 km (1,607 mi) lie along the Mississippi River itself, while 959 km (596 mi) lie along the south banks of the Arkansas River, the Red River of the South, and in the Atchafalaya Basin (Figure 103). Over time, sediment deposits in the river have caused the river bed to rise – to the extent that the river surface is well above the level of the floodplain on the either side of the levee.

Figure 103. Lower Mississippi River and tributaries

In addition to the Mississippi River, the large lower Mississippi floodplain includes smaller, local rivers. Levees confine the main river, isolating it from the remainder of the river network. Unlike other areas of the United States, flood protection along the lower Mississippi River cannot be defined in terms of river catchments.[28] Due to the length of the river stretches confined by levees, when flood defenses are broken the river flows out of its unit catchment areas. For this region, the Verisk model simulates levee failure scenarios on selected breach points along the river. The model simulates a total of 162 breach points. For each point, the 2D shallow-water wave model dynamically simulates the flood propagation resulting from a potential breach for several return period flows. The model estimates the flow hydrograph through the breach, based on the flow hydrograph in the river and the geometry of the levee breach.

Figure 104 shows the modeled flood extents resulting from a modeled levee breach along the lower Mississippi River. The levee breach was simulated to test the final flood extent, which

[28] In regions outside of the lower Mississippi River, the failure of a flood defense structure along a river affects mainly the catchment of that stretch of the river.

corresponds with a 250-year flood. Verisk validated this methodology by comparing modeled flood extents of the 2011 Mississippi River floods with historical Landsat[29] images.

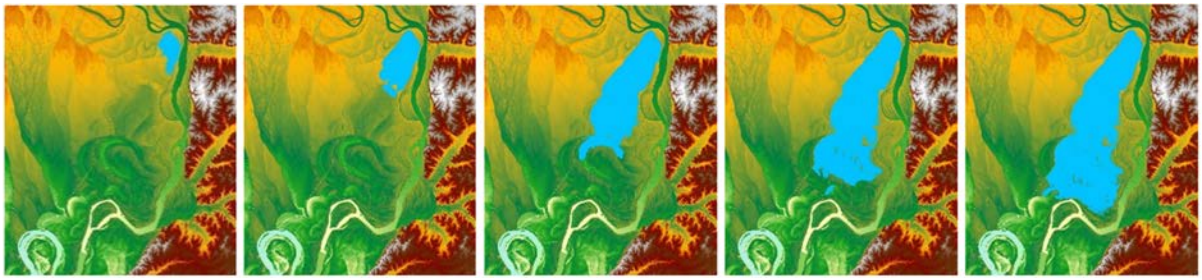

Figure 104. Modeled levee breach producing a 250-year flood extent along the lower Mississippi River at the New Madrid Floodway, Missouri

See Also

The Mississippi River
Validation of Levee Breach Modeling

A Comparison with FEMA Maps

Like Verisk's flood hazard maps, FEMA's flood hazard maps are based on a model. While the Verisk and FEMA models differ in terms of DTM, river flow data, methodology, and assumptions for flood defenses, it is still useful to compare their results. When results from different models show agreement, this can provide additional assurance of the robustness of the results, although some differences are expected. Another significant difference between Verisk and FEMA maps is that FEMA maps, in most cases, do not account for pluvial flooding. The Verisk maps are unified (on-plain and off-plain) hazard maps. Furthermore, the Verisk maps provide an undefended view of the flood risk, while FEMA maps incorporate the effects of levee protection and often demarcate the protected areas behind levees.

Figure 105 shows the FEMA 100-year flood hazard extent side by side with Verisk's 100-year unified on-floodplain and off-floodplain flood extent for a small area near Houston, TX area. Verisk's flood extent includes greater coverage of the smaller rivers. These rivers are modeled using Verisk's pluvial model, based on 2D shallow water wave equations.

[29] Landsat is a joint venture of the USGS and NASA. It provides the world's most comprehensive set of space-based land remote sensing data.

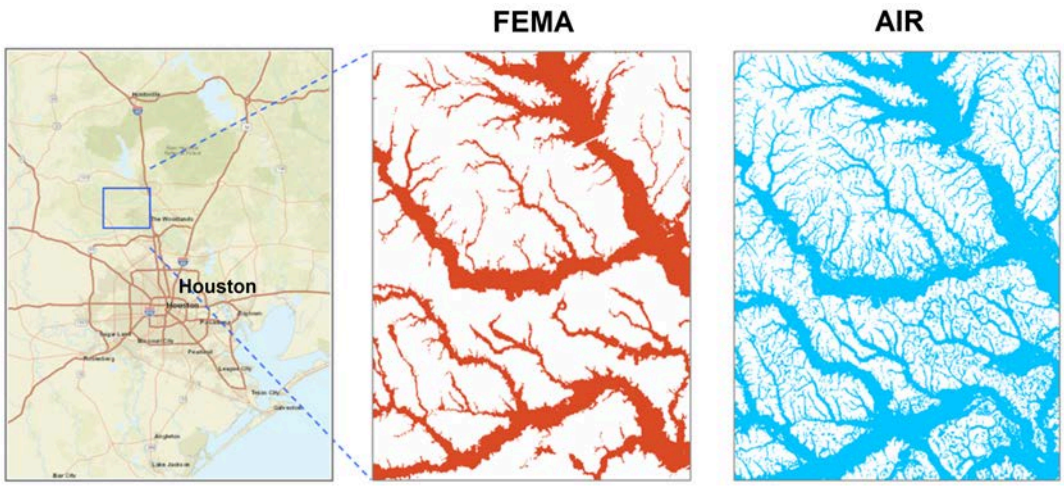

Figure 105. FEMA 100-year flood extents compared to the Verisk 100-year on- and off-floodplain unified flood extents
The Verisk map denser coverage of small streams.

Verisk compared its modeled undefended flood footprints with those produced by FEMA, for AE zones. Figure 106 through Figure 108 compare the modeled flood extent for the 100-year return period (1% exceedance probability) from the Verisk model with the extents in FEMA flood maps for the same location. As illustrated, there is significant agreement.

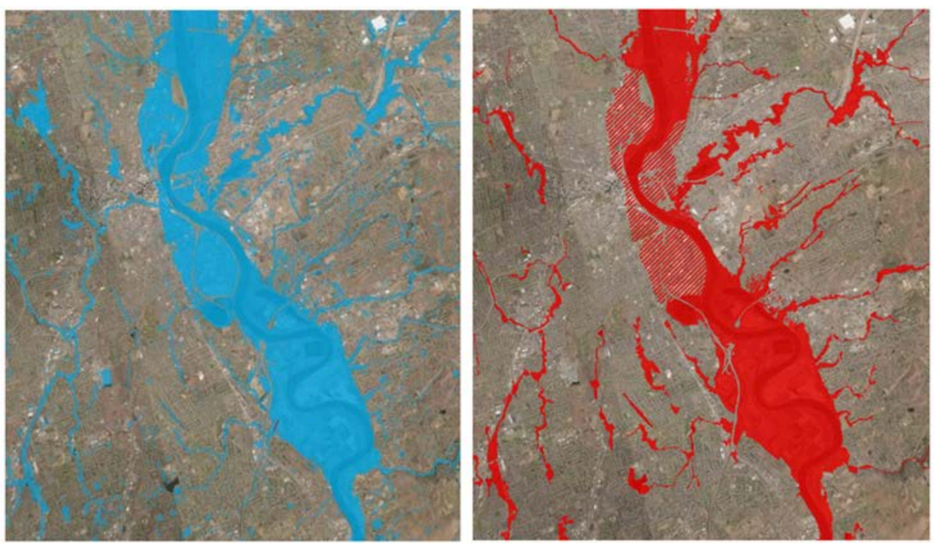

Figure 106. Comparison of the Verisk modeled undefended on-plain and off-plain unified 100-year flood extent (left) and the FEMA AE zone (right) for Hartford, CT
Hatched areas in the FEMA map indicate protected areas behind levees.

Figure 107. Comparison of the Verisk modeled undefended on-plain and off-plain unified 100-year flood extent (left) and the FEMA AE zone (right) near Columbia, MO

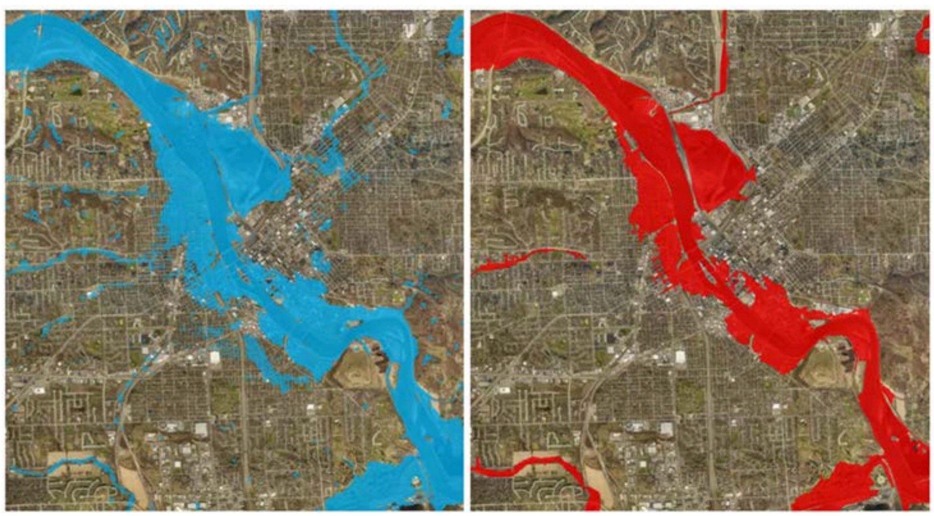

Figure 108. Comparison of the Verisk modeled undefended on-plain and off-plain unified 100-year flood extent (left) and the FEMA AE zone (right) for Cedar Rapids, IA

4.7 Validating Local Intensity

Verisk has performed a variety of validation exercises for this model, comparing modeled flood extents to observation data. These comparisons provide the assurance of robustness and reliability in the Verisk model.

Historical Event Footprints

Figures Figure 109 and Figure 110 compare the Verisk-modeled maximum on plain flood extent for the Great Flood of 1993 with Landsat imagery for flooding at St. Louis and Jefferson City, Missouri, respectively. Both figures show very good agreement with the observed flood extents from the USGS.

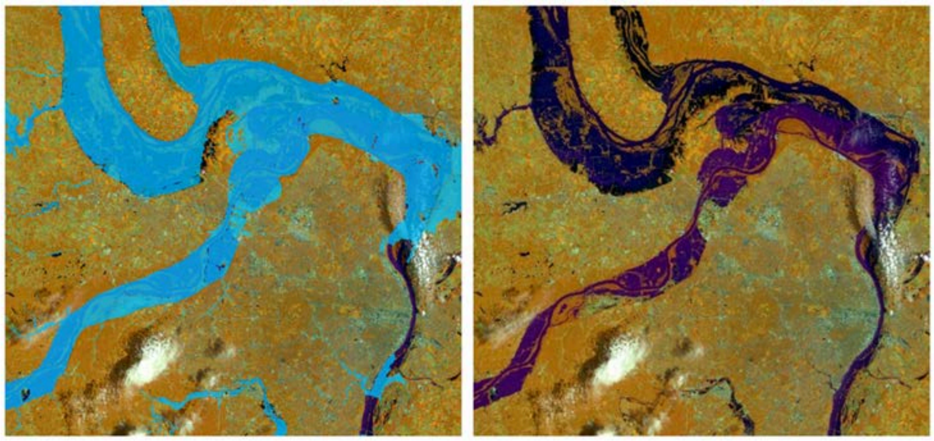

Figure 109. Comparison of the Verisk modeled maximum on plain flood extent (left) and observed flood from Landsat 5 imagery (right) of St. Louis, MO during the 1993 Great Flood

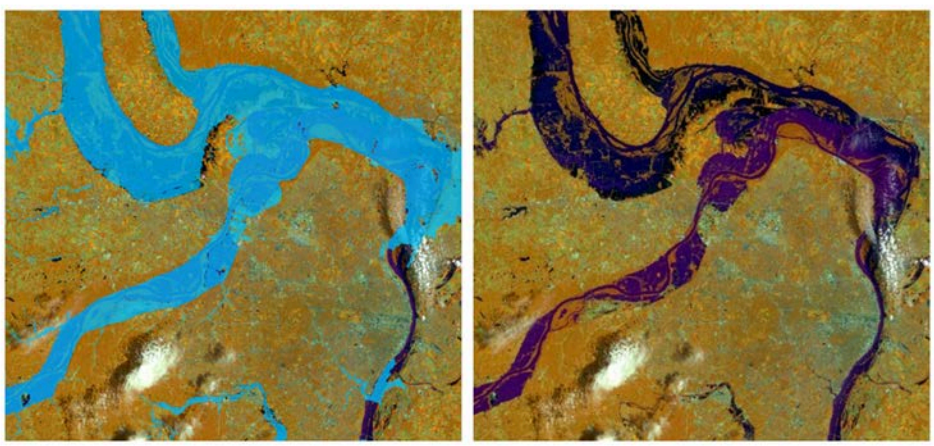

Figure 110. Comparison of the Verisk modeled maximum on plain flood extent (left) and observed flood extent from Landsat 5 imagery (right) near Jefferson City, MO during the 1993 Great Flood

Figure Figure 111 compares the Verisk modeled maximum on plain flood extent of the Cedar River in Cedar Rapids, IA with Linn County (GIS Division) imagery for flooding during the 2008 Midwest floods.

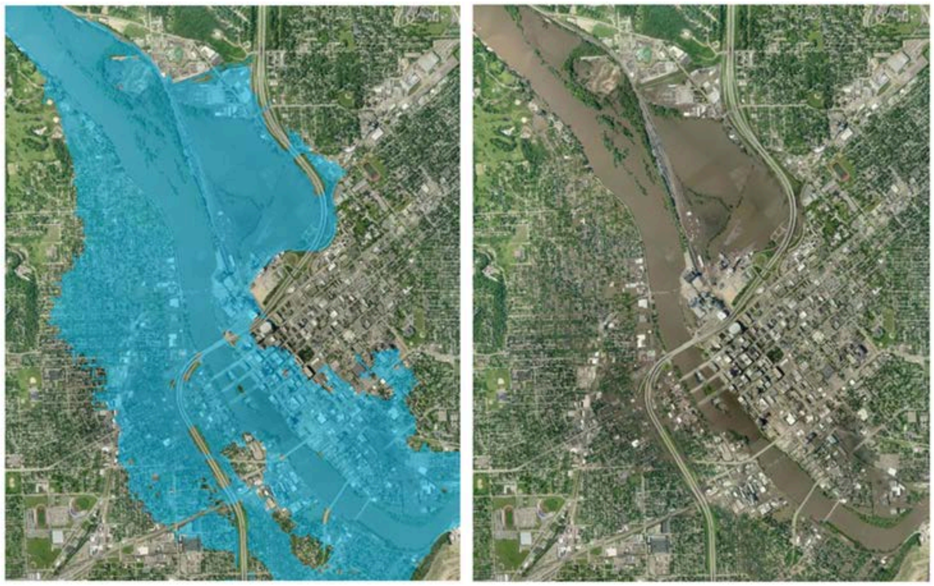

Figure 111. Comparison of the Verisk modeled maximum on-floodplain flood extent (left) and observed flood extent from Linn County, IA GIS Division (right) for Cedar Rapids, IA during the 2008 Midwest floods

Validation of Flood Extents

Figure 112, Figure 113, and Figure 114 compare the Verisk-modeled maximum on-plain flood extent for the Midwest 2008 floods with USGS aerial photos for flooding at Gays Mills, WI, Cedar Rapids, IA, and Iowa City, IA, respectively. All three figures show very good agreement with the observed flood extents from the USGS.

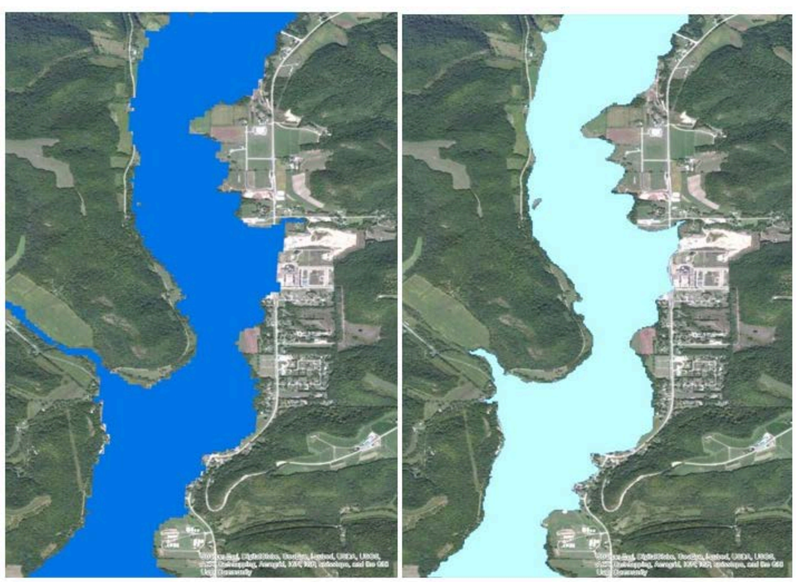

Figure 112. Comparison of the Verisk modeled maximum flood extent (left) and the USGS observed maximum on-plain flood extent (right) at Gays Mills, WI during the 2008 Midwest flood

Figure 113. Comparison of the Verisk modeled maximum flood extent (left) and the USGS observed maximum on-plain flood extent (right) in Cedar Rapids, IA during the 2008 Midwest flood

Figure 114. Comparison of the Verisk modeled maximum flood extent (left) and the USGS observed maximum on-plain flood extent (right) in Iowa City, IA during the 2008 Midwest flood

Figure 115 shows the Verisk-modeled maximum on-plain flood extent near Ashland City, TN during the 2010 floods along the Cumberland River in Tennessee. The bottom panel shows the observed flood extent from DigitalGlobe.

Figure 115. Comparison of the Verisk modeled maximum flood extent (left) and the DigitalGlobe observed maximum on-plain flood extent (right) near Ashland City, TN during the 2010 Cumberland River floods

Figure 116 shows, in the lefthand panel, the Verisk-modeled maximum on-plain flood extent at Cranston, RI during the 2010 Rhode Island floods. The righthand panel shows the observed flood extent from NOAA.

Figure 116. Comparison of the Verisk modeled maximum flood extent (left) and the NOAA observed maximum on-plain flood extent (right) in Cranston, RI during the 2010 Rhode Island floods

4.8 Validation of Levee Breach Modeling

Figure 117 compares Verisk's modeled flood footprint with a Landsat image for the intentional levee breach at the New Madrid Floodway in Missouri, south of Cairo, Illinois, during the 2011 Mississippi River floods.

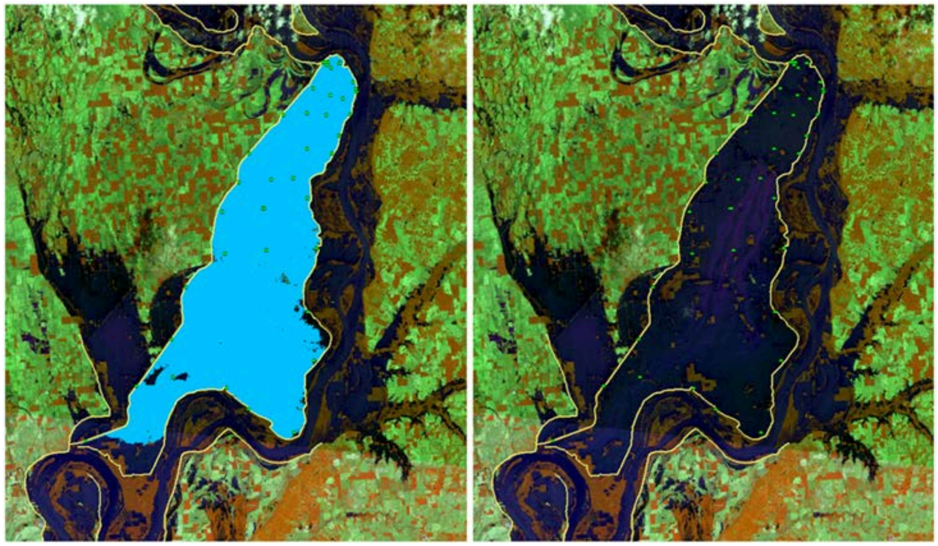

Figure 117. Modeled (left) and Landsat image (right) of the flood footprint from the levee breach at the New Madrid Floodway, MO during the 2011 Mississippi River floods
Green dots represent USACE gauging stations; yellow lines represent USACE-accredited levee. Only modeled extents from the breach are shown.

5 Damage Estimation

The vulnerability module of the Verisk model estimates damage to buildings, appurtenant structures, contents, as well as business interruption (downtime) losses. The intensity parameter used to calculate damage and losses from both on-floodplain and off-floodplain flooding is the inundation or water depth.

When determining damage, the Verisk model accounts for primary building characteristics, including construction and occupancy classes, building height, and building age. Secondary risk features account for other risk characteristics such as foundation type, first floor height, base flood elevation, and others. All these aspects, pertinent to damage estimation in the Verisk model, are discussed in detail in the following sections.

5.1 Common Types of Flood Damage

Observations and studies indicate that, in general, damage due to flooding is primarily non- structural; it is typically found in interior finishes, such as drywall, plaster, insulation, and flooring (Figure 118). Basements, which are quite common in many areas of the United States, contribute significantly to flood vulnerability. Buildings with basements are susceptible to varying degrees of structural damage due to high hydrostatic and hydrodynamic forces in cases of high velocity floodwaters (due to the overtopping of a nearby levee or stream), which leads to the inundation of interiors and contents. Finished basements are typically equipped with interior finishes (drywall, plaster, insulation, and flooring) and service equipment (mechanical, electrical and plumbing systems). These elements make finished basements more vulnerable than their unfinished counterparts.

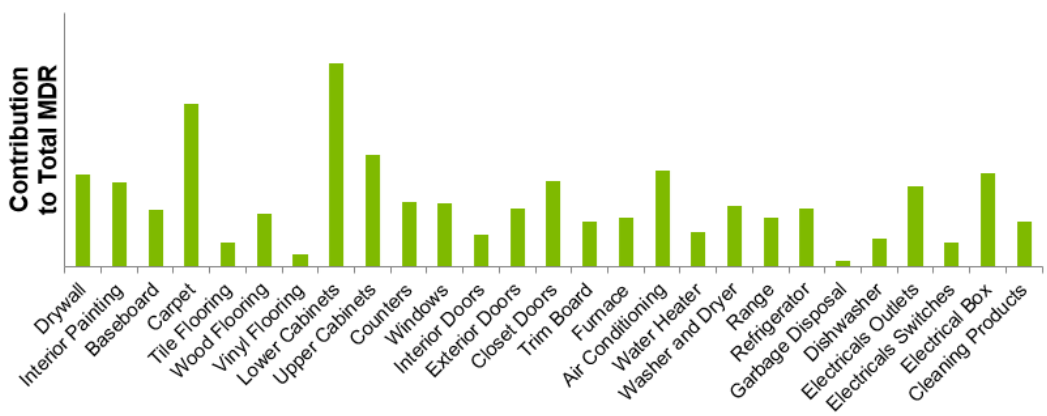

Figure 118. Relative contribution of various building elements to the total mean damage ratio of a low-rise single family home at a flood depth of 1.5 m

Figure 119. Basement wall damage due to hydrostatic pressure in 2008 Midwest Floods
Masonry wall basement damaged in Iowa (left), and collapsed foundation wall in Wisconsin (right).
(Source: FEMA)

In addition to water damage, the associated cleanup after a flood event can be substantial. Mold growth can be a source of loss, particularly for floods that do not subside quickly.

5.2 Building Classifications and Resistance to Flood Damage

Building characteristics and attributes that affect flood vulnerability can be divided into two broad categories:

Primary	Characteristics such as the occupancy, construction type (material), height, and age (year built) of the building
Secondary	Characteristics that define the building envelope and the building's environs (e.g., foundation type, first floor height, etc.)

Embodied within these are other attributes, such as the degree of flood mitigation applied to certain building types, regional construction practices, and role of building codes as they pertain to flood. Verisk has obtained information on the relative impact each component has on vulnerability from a variety of sources, including published research, post-disaster surveys, and loss experience.

Engineered and Non-engineered Buildings

The model captures the difference between engineered and non-engineered buildings, which has a great effect on the flooding vulnerability. How well a building is engineered, what key building features it contains, and which codes were in effect at the time of construction, vary according to occupancy, construction, height and year built. For example, the foundation type and presence of a basement are important determinants of flood vulnerability for low-rise residential structures. However, in high rise buildings —which are assumed to be better engineered—foundation type is not as important as other features (e.g., the location of vulnerable mechanical equipment).

This important distinction stems from the role foundation type plays depending on the construction type, which helps distinguish buildings as engineered vs. non-engineered. For non-engineered buildings, while foundations help transfer loads from the building to the ground, they can also be used to elevate the building to the desired height above the ground. Piles/stilts, walls, crawlspaces, etc. offer varying elevations for the first floor, above the local ground surface. For engineered buildings, the sole purpose of the foundation is to transfer building loads to the ground. Pile foundations, or deep rooted piles in engineered buildings, are different from pile foundations in non-engineered buildings. Deep rooted piles are typically very expensive and used when site conditions are poor, as they effectively transfer the building's weight to the underlying bedrock.

Table 6 summarizes how non-engineered and engineered structures are defined in the model, based on occupancy, construction, and building height.

Table 6. Non-engineered and engineered occupancy and construction classes

Occupancy Codes	Construction Codes	Height Class	Temporal-spatial Variation	Engineered or Non-engineered
300, 301-306, 311-319,331-381	101-120	All	Yes	Non-engineered
	131-140, 151, 153-159	All	Yes	Engineered
	152, > 181-187	All	No	n/a
	100	1-3 Stories	Yes	Non-engineered
		> 3 Stories	Yes	Engineered
		Unknown	Yes	Non-engineered
321-330, ≥400	All	All	No	n/a
All	200 Series	All	No	n/a

Residential Buildings

The vulnerability of residential buildings, which include single- and multi-family homes as well as condominiums and apartment buildings, varies regionally (Figure 120). In part, this variation is related to construction type. Single-family home (SFH) building stock across the contiguous United States is dominated by wood frame and masonry construction. Wood frame buildings make up approximately 98% of the single and multi-family building stock in the western and northeastern regions. The next common residential construction type prevalent in United States, primarily in Florida is masonry (Figure 120). While both wood and unreinforced masonry buildings are vulnerable to flooding, a masonry building with a slab foundation is more resistant to water pressure and buoyancy forces than a comparable wood frame building.

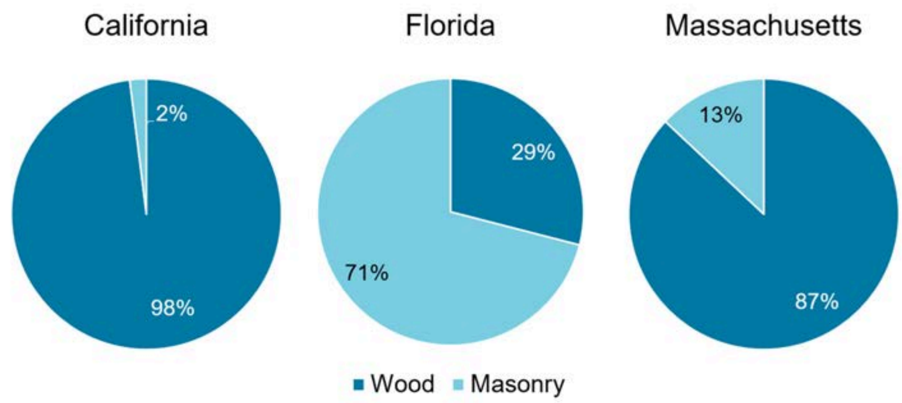

Figure 120. Distribution of single-family home construction types in California, Florida, and Massachusetts

Apartment buildings and condominiums tend to have a more diversified construction mix than single family homes. While lower rise buildings may be made of wood or masonry, taller buildings are more likely to be constructed with reinforced concrete or steel. Apartments and condominiums are often built to strict engineering standards and their vulnerability is similar to large commercial buildings.

Apart from construction type, the foundation type and elevation of the livable floor(s) are critical determinants of flood damage in residential buildings. It has been observed, from both Verisk damage surveys and FEMA reconnaissance studies, that buildings with an elevated first floor perform better than buildings with a first floor at street level.[30] However, some elevated homes can experience significant damage depending on the foundation, particularly perimeter walls or center-block foundations. Houses built on stilt-type foundations with their first floors elevated above the base flood elevation (BFE) experience minimal damage in most flooding situations (Figure 121).

[30] Evaluation of the National Flood Insurance Program's Building Standards (American Institute of Research Study): https://www.fema.gov/media-library-data/20130726-1602-20490-5110/nfip_eval_building_standards.pdf, Natural Hazard Mitigation Saves (National Institute of Building Sciences Study):https://www.fema.gov/media-library-data/1516812817859-9f866330bd6a1a93f54cdc61088f310a/MS2_2017InterimReport.pdf

Figure 121. House elevated above the based flood elevation (BFE) in Wisconsin that had minimal damage in 2008 Midwest floods
(Source: FEMA)

Typical foundations for single-family homes include concrete crawl space, basement, slab-on-grade, and spread concrete footings (particularly in older wood frame houses) . While crawl space foundations offer some elevation to buildings, slab foundations made of poured concrete offer little or no elevation. Shallow spread footing foundations are concrete blocks that support a column or wall and are slightly below ground or below the basement. Basements are common in many areas, particularly in older homes. They are particularly prevalent in northeastern states like Massachusetts (Figure 122), which has a higher number of older buildings than other regions of the country. As mentioned earlier, buildings with basements are more vulnerable due to the structural make-up and the value of a basement's contents and equipment.

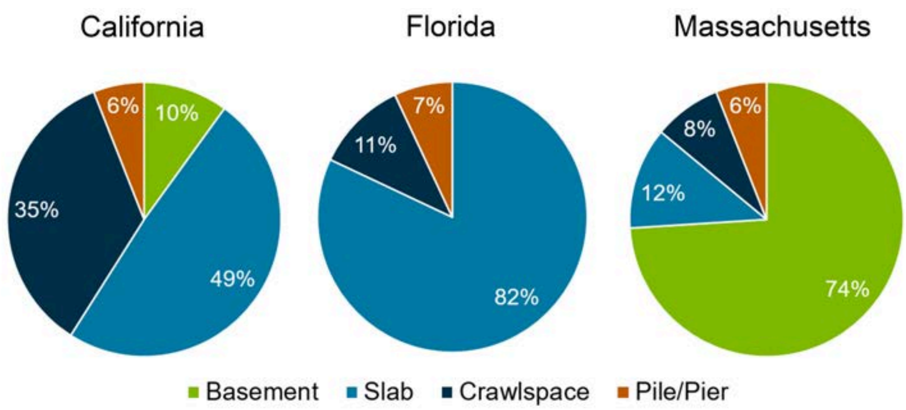

Figure 122. Regional distribution of common single family home foundation types in California, Florida, and Massachusetts

Figure 123. Flood damage to residential properties
Top: Damage and sediment in the interior of homes from the Great Flood of 1993;
Bottom: Foundation damage to home from the 2001 Mississippi River flooding (left) and total damage to home from the Great Flood of 1993 (right)
(Source: FEMA)

Commercial and Small Industrial Buildings

Damage to nonstructural mechanical, electrical, and plumbing (MEP) systems is the most common type of damage commercial buildings experience from a flood event. The failure of these systems can cripple building operations, increasing downtime. The presence of basements, which usually house MEP systems, can increase a commercial building's vulnerability, particularly in buildings that are not substantially impermeable.

As with residential buildings, construction materials used for commercial buildings vary regionally. Along the West Coast, in states like California and Oregon, concrete and masonry are the predominant construction choices. Steel, concrete and masonry are common in Texas, Louisiana, and other states along the Gulf Coast, while steel is more common in the Northeast and along the East Coast (Figure 124). Low-rise commercial structures are generally comparable to single-family homes, and are often made of wood or masonry. For smaller commercial buildings, foundation types are also similar to residential buildings. Small industrial assets (300-series occupancy classes) usually consist of multiple buildings, often with different construction types.

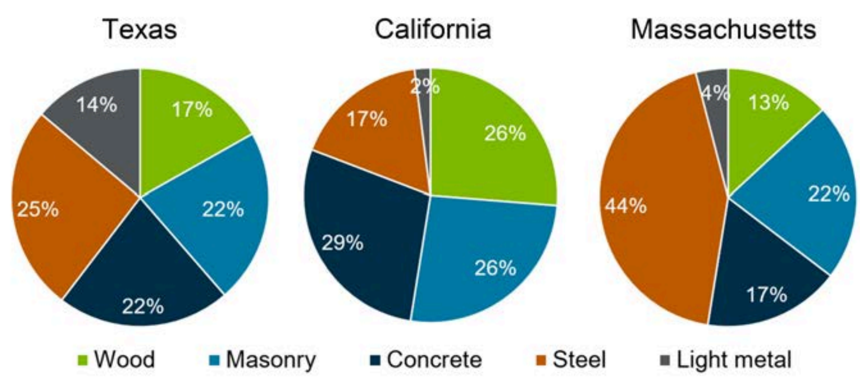

Figure 124. Distribution of small commercial and industrial construction types in Texas, California, and Massachusetts

Mid-rise and high-rise commercial buildings (like large apartment and condominium buildings) are usually built of reinforced concrete or steel. These buildings typically follow stricter standards and are built under the supervision of an engineer, resulting in structural systems that are less vulnerable to flooding. However, large commercial buildings may contain one or more basement levels, typically used for underground parking garages or to store mechanical or electrical equipment. Flooding of basements can damage the equipment, rendering the building inoperable, even if the structure itself was not damaged structurally.

Figure 125. Flooded commercial buildings
Top: East Grand Forks, MN during the 1997 Red River flood;
Bottom: School in Minot, ND submerged during the 2011 Souris River flood
(Source: FEMA)

Agricultural Buildings

The agricultural building classification refers to farm buildings only; it does not include crops or other non-building property. Buildings covered under this line include all buildings on the property except residences, which are covered under separate lines of business.[31]

Agricultural buildings may include barns, silos, buildings that house farming vehicles such as tractors, and any other buildings that are located on an orchard, farm, or other agricultural property.[32] Although this class includes a wide variety of buildings, they tend to be roughly

[31] To achieve reliable loss estimates, Touchstone Re clients should input data by lines that correspond to the Verisk definitions. However, analysis of client data suggests that "agriculture" books also include residential, commercial and industrial risks together with pure agricultural risks. Clients should take care in preparing their data.

[32] While Verisk estimates agricultural risk counts and their values according to the definition provided above, the datasets used for the industry exposure do not make a clear distinction between greenhouses, farming-related properties, and other physical assets on a farm holding. Therefore, the Verisk loss estimates for this line are subject to uncertainty due to different definitions of this classification.

similar in construction type to residential buildings. While most agricultural buildings are low-rise and built of masonry, agricultural buildings employ a wider range of construction materials than residential buildings.

Figure 126. Flooded agricultural buildings from the flooding of the Cedar River during the 2008 Midwest flood
(Source: FEMA)

5.3 Flood Damage Functions

The Verisk model uses the same damage functions for all precipitation-induced flooding, regardless of source[33] or location (on- or off-floodplain). Damage is modeled as a function of the flood depth (intensity) and the mean damage ratio (MDR). The MDR represents the average repair-to-replacement ratio for an exposure when subjected to a certain flood depth. Other hazard variables such as water contamination, water velocity, and flood duration at a given location, are not modeled explicitly. However, the impact of these variables is captured implicitly, as modeled losses are calibrated to and validated against actual claims.

The flood damage functions incorporate important characteristics of each location that affect susceptibility to flood damage. They account for the physical response of structures to flood and incorporate findings from observational data and engineering analysis. The primary building characteristics that determine damage are the construction, occupancy, building height, and year built. Foundation type, presence of basement, first floor height, among others, are also important secondary characteristics for modeling flood damage. The model also incorporates regional variations in building codes and practices, including variability in construction type and foundations. The model also supports 14 individual secondary risk characteristics.

[33] The same damage functions are used for the Verisk Inland Flood Model for the United States and the Verisk Hurricane Model for the United States

Assessing Flood Damage at the Component Level

The building flood damage functions have been designed using a component-based approach. This method provides a unique advantage as it considers the structure a granular level, rather than to the building as a whole. This approach is particularly well-suited to water damage since impacts are confined to the levels of the building below the water level, which contain different building components. To build the component damage functions, Verisk engineers primarily used the results of studies conducted by the New Orleans District of the USACE (GEC, 2006), as well as other USACE studies (Davis and Staggs, 1992; FEMA, 2018), on flood losses to single-family homes and commercial buildings.

The model considers the following six key building components, plus clean-up and miscellaneous costs, to arrive at the total replacement cost:

Foundation	The foundation forms the part of the building that transmits the loads from the building to the ground below. The types of foundations used for residential buildings vary and may be in the form of a basement, crawlspace, slab, or others.
Structure	The structure includes all load-carrying parts of the building, including the roof frame, structural envelope, and exterior walls.
Interior	The interior component refers to walls inside the building (e.g., partition walls and drywall), flooring and floor coverings, and other interior finishes.
Mechanical Systems	Mechanical systems typically include the heating, ventilation, and air conditioning (HVAC) systems, ducts, and elevators.
Electrical Systems	The electrical systems component includes electrical switchboards, meters, distribution panels, switches, circuit breakers, and control and utilization systems, such as lighting and wiring.
Plumbing Systems	Plumbing systems consist of water piping and sewage treatment and disposal systems, including septic tanks, bathroom drains, sinks, and interior pipes.
Clean-up and Miscellaneous	This component includes remediation and other activities associated with repair and mold removal.

To produce a damage function for a building, the individual component-level damage functions are combined in proportion to their contribution to the overall building replacement value. The proportion of component contribution can vary, based on building type as well as building height.

Figure 127 shows an example of the seven component-level damage functions and the overall building damage function for a one-story single-family home, of wood-frame construction on a slab foundation. In this illustration, flood depth refers to the water depth measured from the floor level and not the ground level.

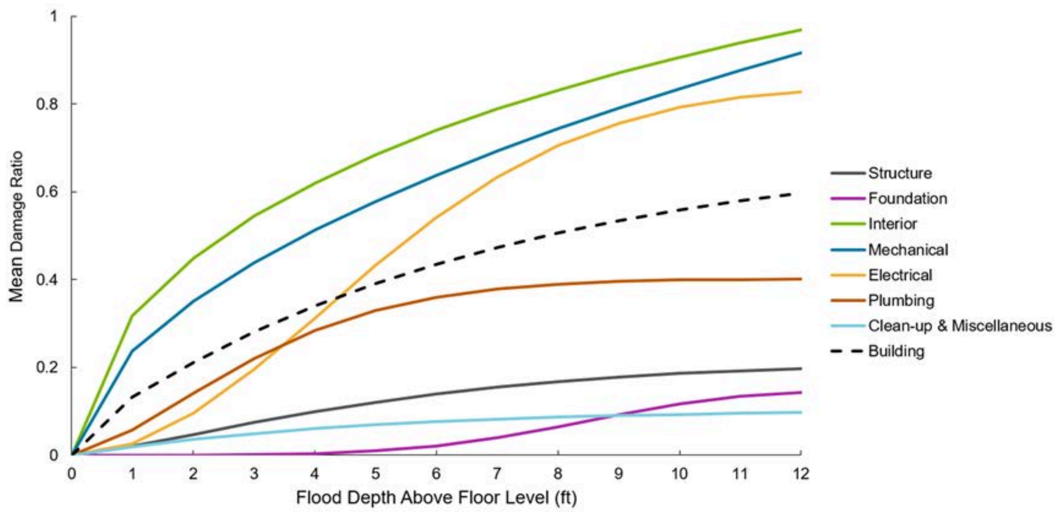

Figure 127. Component-level and overall building damage functions for a one-story, wood-frame, single-family home

The relative contribution of a component's replacement cost to the overall replacement value of the building depends on the building's characteristics. Table 7 shows an example of component-level cost breakdowns for one-story, single-family wood-frame homes with different foundation types.

Table 7. Component-level cost breakdowns for one-story, wood-frame, single-family homes with different foundation types

Component	Foundation Type			
	Basement	Crawlspace	Slab/Mat	Piles/Stilts
Foundation	15%	9%	11%	17%
Structure	44%	48%	43%	43%
Interiors	24%	26%	27%	27%
Mechanical	6%	6%	7%	7%
Electrical	5%	5%	6%	6%
Plumbing	5%	6%	6%	6%

For multi-story residential buildings, components are distributed across the building levels. The foundation and electrical and mechanical fittings, for example, are generally located on the lower floors or basement and therefore have a high vulnerability to flood damage. Table 8 compares the vertical distribution of the six key building components for a three-story reinforced concrete professional building with a basement and pile foundation.

Table 8. Distribution of component costs across a three-story commercial reinforced concrete building, for basement and pile foundations

Foundation Type	Story	Components						
		Foundation	Structure	Interiors	Mechanical	Electrical	Plumbing	Total
Basement	**Basement Level**	5.0%	4.8%	0.7%	5.3%	4.5%	2.0%	**22.3%**
	Story 1	0.0%	6.4%	7.8%	5.3%	4.5%	2.0%	**25.9%**
	Story 2	0.0%	6.4%	7.8%	5.3%	4.5%	2.0%	**25.9%**
	Story 3	0.0%	6.4%	7.8%	5.3%	4.5%	2.0%	**25.9%**
	Total	**5.0%**	**24.0%**	**24.0%**	**21.0%**	**18.0%**	**8.0%**	**100.0%**
Pile	**Story 1**	22.0%	6.7%	7.3%	3.0%	7.3%	1.7%	**48.0%**
	Story 2	0.0%	6.7%	7.3%	3.0%	7.3%	1.7%	**26.0%**
	Story 3	0.0%	6.7%	7.3%	3.0%	7.3%	1.7%	**26.0%**
	Total	**22.0%**	**20.0%**	**22.0%**	**9.0%**	**22.0%**	**5.0%**	**100.0%**

The component level damage functions are aggregated at the story level to yield the corresponding building damage function. These are then aggregated vertically over the height of the building based on component cost breakdowns, such as ones shown in Table 8. The process can be described mathematically as:

$$DF_{Building} = \sum_{j=1}^{N}\left(\sum_{i=1}^{6} \alpha_i \beta_j DF_{comp,i}\right)$$

Where, $DF_{Building}$ is the building damage function, DF_{comp} is the component level damage function, N is the number of stories in the building, α is the component cost breakdown for a given component, β is the distribution factor for a component at a given story/floor level. The product αβ for different components at different floor levels is shown in Table 8. Note that:

$$\sum_{j=1}^{N}\left(\sum_{i=1}^{6} \alpha_i \beta_j\right) = 100\,\%$$

The process is illustrated in Figure 128. The functions are not a smooth curve; rather, they tend to be "lumpy" due to the variable rate at which damage increases over different flood depths. For example, even if only the lower portion of a wall has been affected, generally the entire wall will need to be re-plastered. Since the damage functions are built per floor and flood depth measured from floor level, the flood damage functions for buildings with a basement can easily accommodate depths below zero (ground level) with non-zero MDRs (Figure 128a).

While individual floor level damage functions are aggregated based on flood depth from floor level, the final damage function for the overall structure is a function of flood depth from the ground level. Hence, in Figure 128a, the livable floor (basement) floor is at -8 feet (8 feet below ground), and the building damage function starts at -8 feet. Similarly, in Figure 128b, the first floor starts 3 feet above the ground level; therefore, the building damage function remains zero until the effective water depth (x-axis) exceeds 3 feet. This further demonstrates the importance of first floor height.

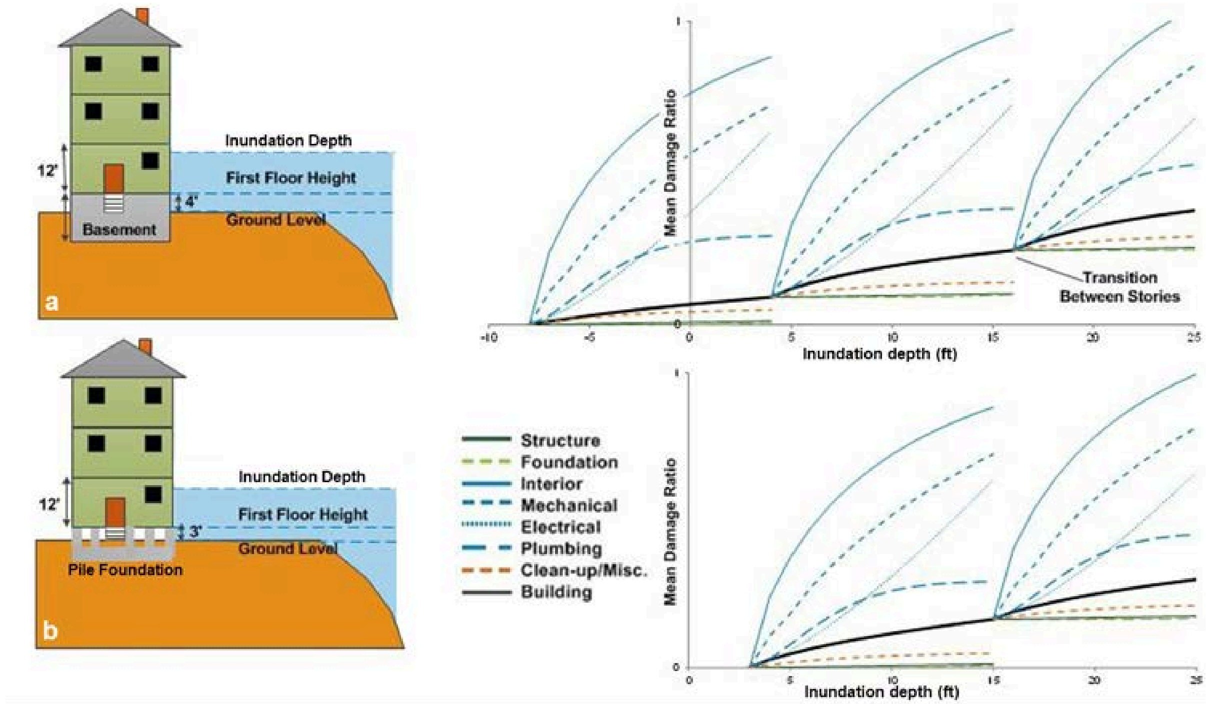

Figure 128. Illustration of the component-level approach to developing flood damage functions for buildings, for a basement and pile foundation

The building damage functions have been calibrated and validated against damage observations from past events as well as location level claims data.

Effects of Building Height on Flood Damage

Flood is a peril where building height, or number of stories, plays a significant role in determining the level of damage. Flood damage in one story buildings tends to be much higher than damage in two story buildings. The concentration value on one floor, versus the distribution of value across both the floors, makes single story buildings prone to flood damage. Similarly, high-rise buildings are typically well engineered, including better flood defenses. However, even though a flood primarily affects the lower floors, significant portions of the electrical and mechanical fixtures for a high-rise building might be located in the basement or ground floor and they pose a greater loss potential.

Flood damage functions vary explicitly by the number of stories for construction types 100-183, for the 300-series occupancy classes. For other construction types, there is no variation in vulnerability by height. The height vulnerability by construction type is summarized in Table 9.

Building height is also correlated with the construction type. The construction materials used for high rises, such as steel and concrete, have lower porosity and higher strength than masonry and wood construction, and thus have lower vulnerability.

Table 9. Variations in vulnerability by height for different construction and occupancy classes

Occupancy Codes	Construction Class	Construction Codes	Height Vulnerability
300-373	Wood frame	101-104	Damage functions vary by the number of stories
	Masonry	111-119	
	Concrete	131-140	
	Steel	151-160	
	Wind Resistive	181-183	
	Unknown	100	
300-373	Manufactured homes	191-194	Same vulnerability for all height bands
	200 Series[34]	201-261	
400-482	All	All	Same vulnerability for all height bands

Figure 129 shows the effect of building height on the damage function for residential wood-frame buildings of one, two, and three stories, with a slab foundation. As shown in the figure, the single-story building has a much greater vulnerability than the two- or three-story structures.

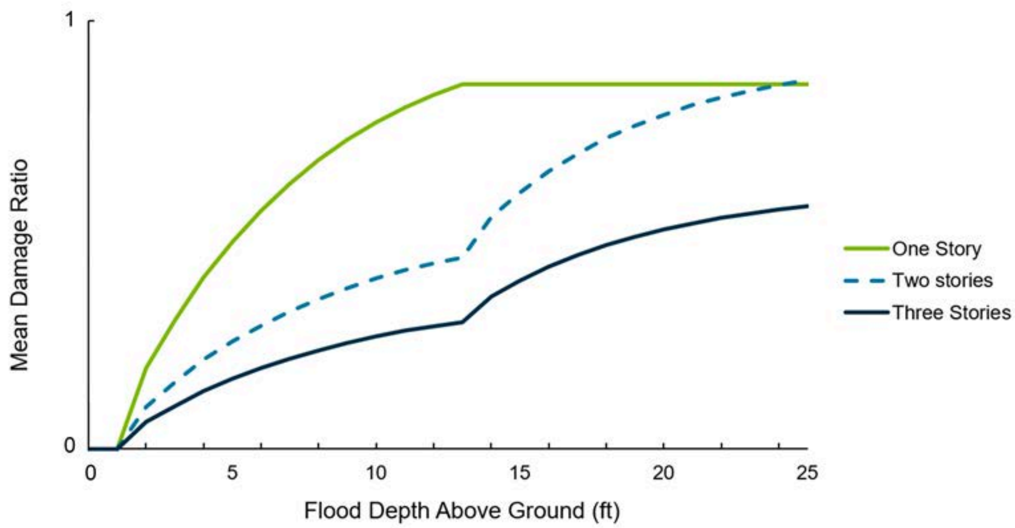

Figure 129. Damage functions for residential wood-frame buildings of different heights, with a slab foundation

Buildings with Unknown Characteristics

Building vulnerability, and therefore losses, can vary considerably by location, which is significant when modeling unknown combinations. For modeling unknown characteristics

[34] The 200-series of construction classes includes bridges, storage tanks, pipelines, chimneys, towers, equipment, cranes, compressor stations, and waterfront and offshore structures.

and combinations, the Verisk model captures the geographic and temporal variability of exposure distribution by accounting for local building attributes and year built.

Verisk engineers developed "unknown" damage functions for all combinations of primary characteristics, including unknown construction, occupancy, and height classes at the state and flood zone level, and for certain secondary features, including foundation type. These damage functions are weighted averages of damage functions for buildings for which these characteristics are known, using a state- and flood zone-level building inventory weight, derived from Verisk's Industry Exposure Database. The state and flood zone level de-aggregation of the exposure inventory captures two key components of flood vulnerability:

- Regional- and flood zone-specific construction practices (e.g., requirements related to building within a 100-yr floodplain)
- Variation in construction type

Different damage functions are used, depending on how many variables, and which ones, are unknown. For example, the damage function for a single-story, low-rise, commercial building of unknown construction type founded on a mat/slab in Texas along the Gulf of Mexico would be a weighted average of the damage functions of a single-story low-rise commercial building of each construction type founded on a mat/slab (Figure 130). The weights used in this computation are derived from the proportion/distribution of construction types in the Gulf of Mexico. If the height is also unknown for the building, then the weighted averaging is completed for all combinations of construction types and height bins for the building type.

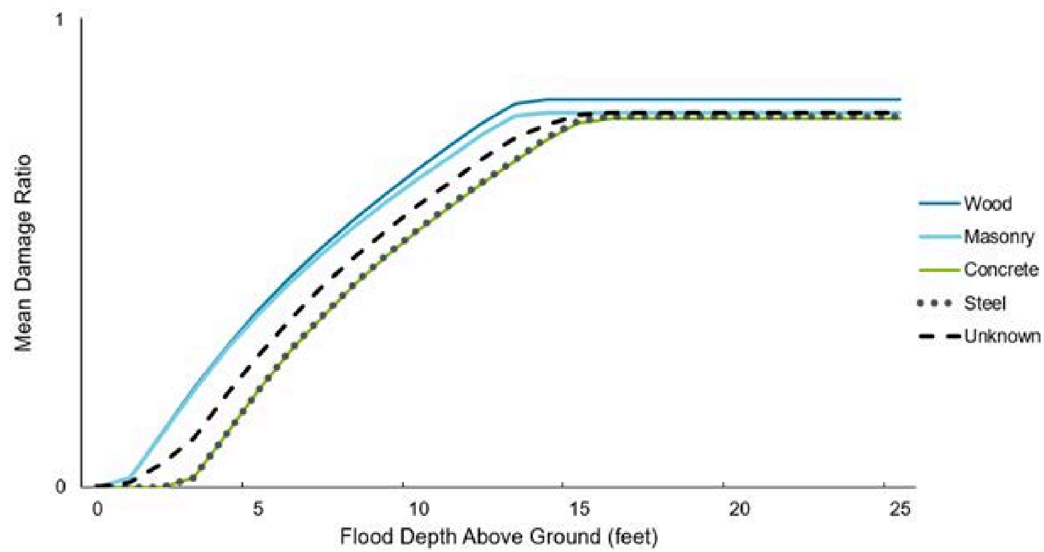

Figure 130. Damage functions for one-story general commercial buildings of different construction classes on a mat/slab foundation

Similarly, the damage function for unknown building height is the weighted average (weighted by total value) of low-rise, mid-rise, and high-rise heights for each construction and occupancy class. These weighting factors are then used when developing the unknown damage functions. In the Verisk flood model, the damage functions also reflect a weighted average of year built and selected secondary risk characteristics, including foundation type, first floor height, among others.

In developing these unknown damage functions, states with similar building inventory in the Industry Exposure Database were combined, resulting in ten regions with distinct building vulnerabilities (Figure 131). These regional distributions were used to derive region-specific damage functions for buildings of unknown construction, occupancy, or height classes.

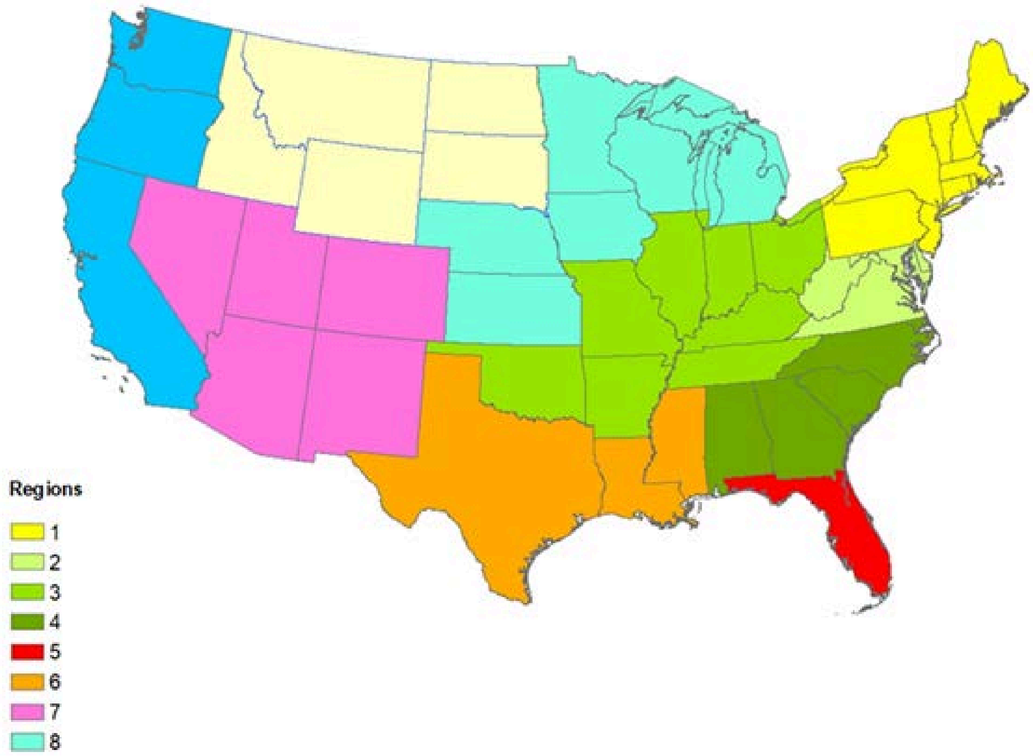

Figure 131. Verisk building vulnerability regions for unknown construction, occupancy, or height class

Including Flood Depth and Elevation Uncertainty in the Final Damage Functions

Mean damage functions are most appropriate when there is little uncertainty in the estimation of flooding intensity. For example, they can accurately assess losses suffered by buildings that have recorded water depth data, since the uncertainty at those sites is fairly limited. In other cases, a more realistic loss assessment is achieved when elevation/DTM uncertainty and the resulting inundation depth uncertainty are considered.

For any flooding there is a significant amount of variability in the inundation depth intensity at a given site. To account for this uncertainty, Verisk researchers final damage functions are "integrated" damage functions in which expected damage is directly estimated from the mean inundation depth by considering the uncertainties in the digital terrain model. These functions estimate the expected damage for events in the stochastic catalog as well as events in the Verisk historical catalog.

The mean damage function gives the MDR at different levels of flooding (depth) intensity. The flooding intensity is the mean value of a distribution of possible flooding intensities that can be generated at a site by an event. Each level of flood depth in that distribution, if it were to occur, would generate a damage ratio that is generally different from the MDR.

By taking the variability of flood depth into account, the final damage function used in the loss calculation module is not as steep as the original damage function, especially at low inundation depth as shown in Figure 132. The integrated damaged function and initial damage function are identical for most flood depths, except the low flood depths.

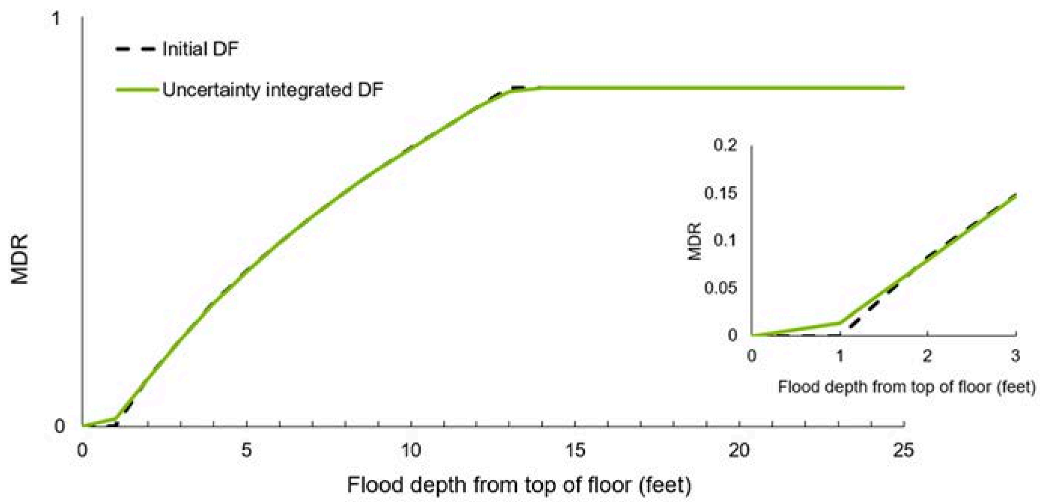

Figure 132. Integration of uncertainty

Uncertainty Around the Mean Damage Ratio

The secondary uncertainty distributions for flood are based on available European claims from four historical flood events between 2002 and 2007 from two insurance companies. The approximately 67,000 claims cover the residential line of business. In addition to being informed by claims data, the distributions were constructed using the inflated transformed beta family of distributions. Distributions based on these claims were created for the Residential and Commercial lines of business for Coverages A through D.

The secondary uncertainty distribution represents a distribution around a mean damage ratio (MDR) of a location, that is due variability of claims data. It typically has two discrete spikes at 0% damage ratio and 100% damage ratio, that represent the probability of no damage or full damage, respectively, as well as the main part of the distribution for the damage ratios in between those two extremes (Figure 133 and Figure 134.)

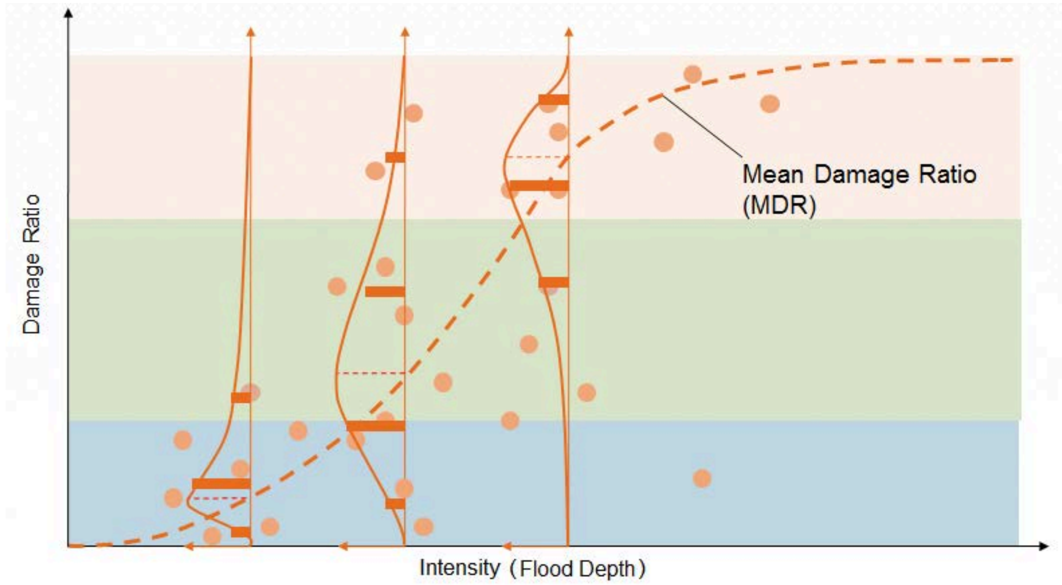

Figure 133. Representation of secondary uncertainty distributions around a given mean damage ratio, defined by claims data (data points)

The distributions are characterized by smoothly transitioning shapes of the spikes and the main body of the distribution, as MDR increases. Figure 134 shows that the distributions transition in a natural manner from monotonically decreasing to bell-shaped, with the main part of the distribution moving towards the spike at total damage.

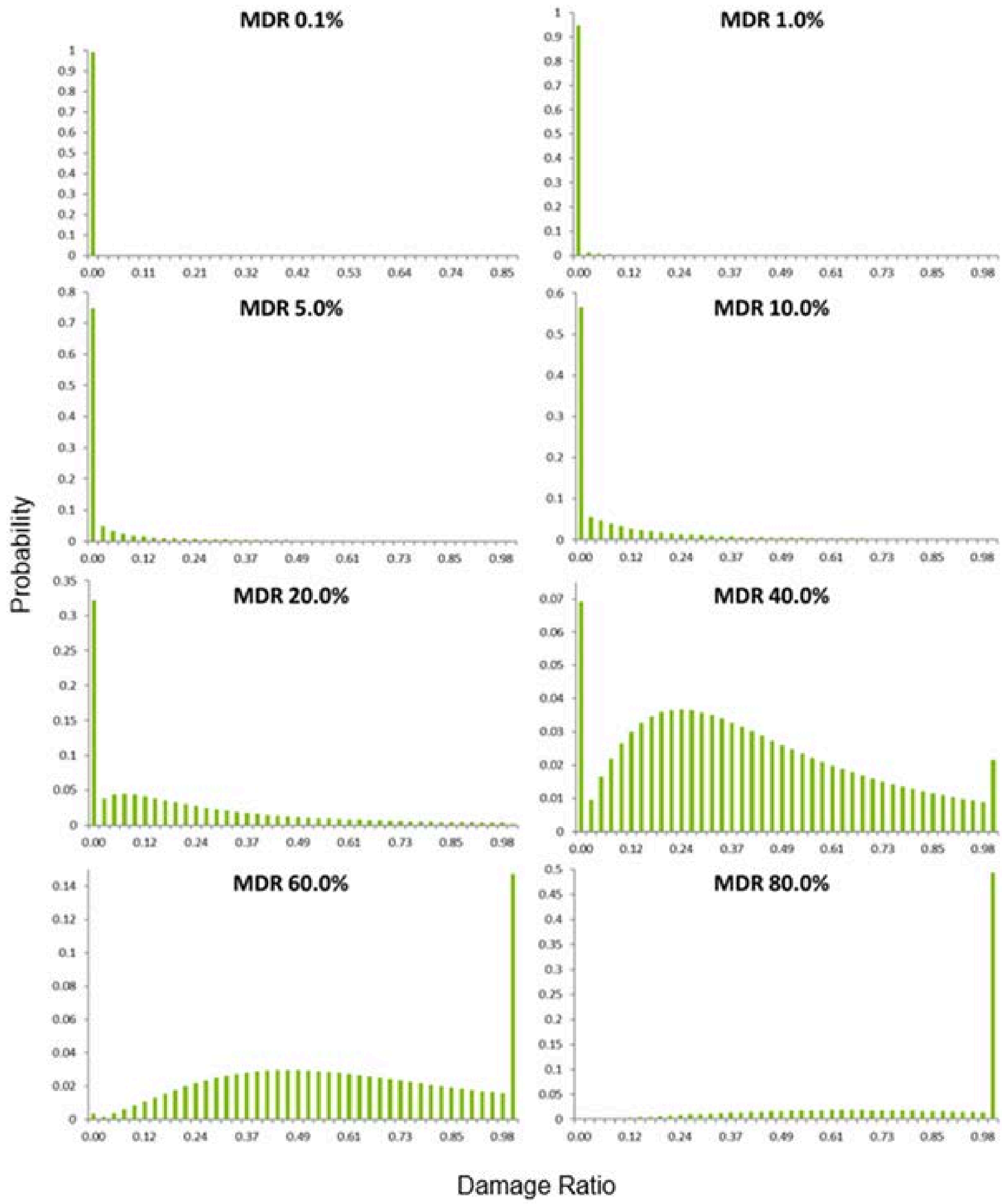

Figure 134. Smoothly transitioning shapes of the Residential Coverage A distributions

A key element of the flood distributions is the use of inflated transformed beta distributions for fitting of the claims data. This 5-parameter family of distributions affords great flexibility in producing a variety of shapes represented by claims data at different MDRs, and particularly in reproducing the interior part of distributions exhibited by data.

To ensure smooth transitioning of the shapes of the distributions, a smooth functional relationship for the parameters of the transformed beta distribution is imposed. Because the large majority of the claims have low or moderate MDR (Coverage A MDR is less than 15% for 90% of claims), the fitting of distribution parameters to data (i.e., determining the functional form mentioned above) was performed in this MDR range. In other MDR ranges, extrapolation of the parameters was used to determine the shape of loss distributions.

The fitted distributions are shown in Figure 135, for selected MDRs with sufficient amounts of data. The interior part of the fitted distributions matches well with the distributions of the claims.

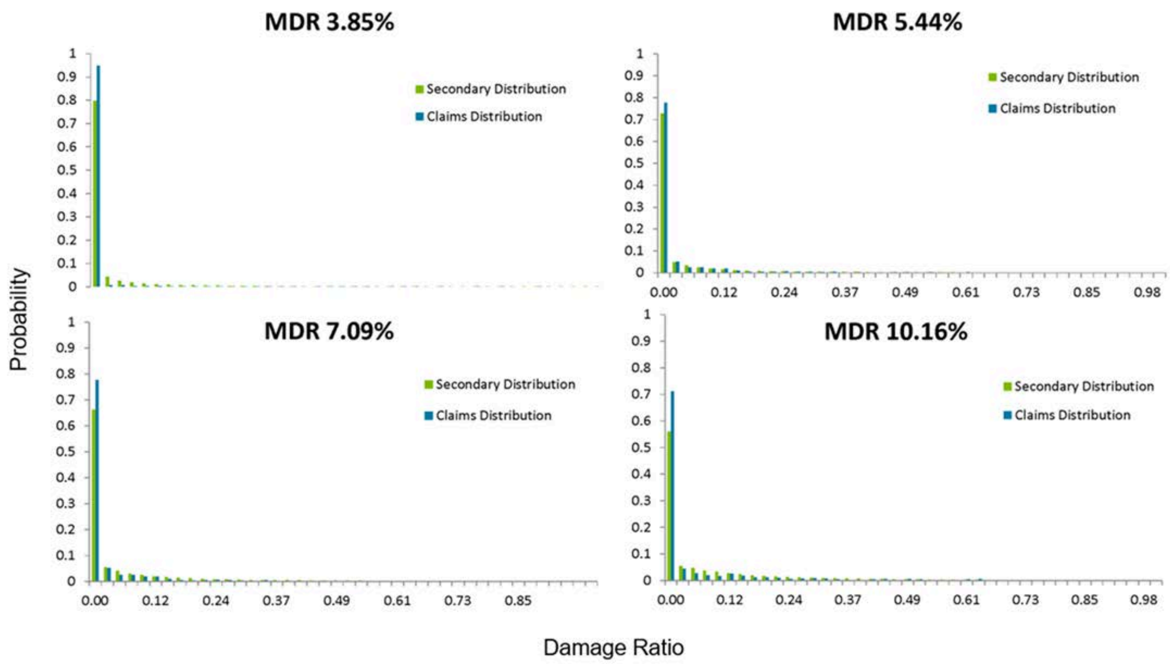

Figure 135. Smoothed parametric fit of Coverage A distributions to claims data, for selected MDRs with sufficient amounts of data

The procedure described above for fitting the distributions is performed for Residential Coverages A and C. Additionally, intuitive relationships between different Coverages' distributions are enforced.

Some assumptions can be drawn about the differences between the behavior for certain coverages and construction types, and these assumptions can be used to derive distributions from the Residential Coverage A uncertainty distribution, as illustrated in Figure 136. For Coverage B, the following conditions regarding the distribution of uncertainty are used:

- Because appurtenant structures are likely built to a lower construction standard than the primary building, the probability of total loss (P1) for Coverage B is higher than for Coverage A.
- Due to policy conditions, the replacement value of Coverage B is often given as a percentage of the replacement value of Coverage A. In claims data this suggests that the secondary structure went undamaged. Thus, the probability of zero loss (P0) for Coverage B is higher than for Coverage A.
- The less stringent enforcement of construction standards for Coverage B relative to Coverage A implies that the standard deviation (SD) will be higher for Coverage B than for Coverage A.

Using a similar method implemented for the derivation of the uncertainty distribution for Coverage B from Coverage A, the following conditions are used to derive the distribution of uncertainty for commercial structures relative to uncertainty for residential buildings:

- Probability of zero loss (P0) and total loss (P1) for a commercial building is equal to that of a residential structure, since we do not expect commercial buildings to provide significantly different resistance to flood damage.
- Since there are more variable construction types for commercial structures than standard residential homes, standard deviation (SD) is higher for commercial buildings than residences.

For Coverage C, residential and commercial distributions are identical because the vulnerability of contents to flood damage does not depend on the building's construction type. Finally, because data on Coverage D for flood is not available, the distributions are informed by other atmospheric perils.

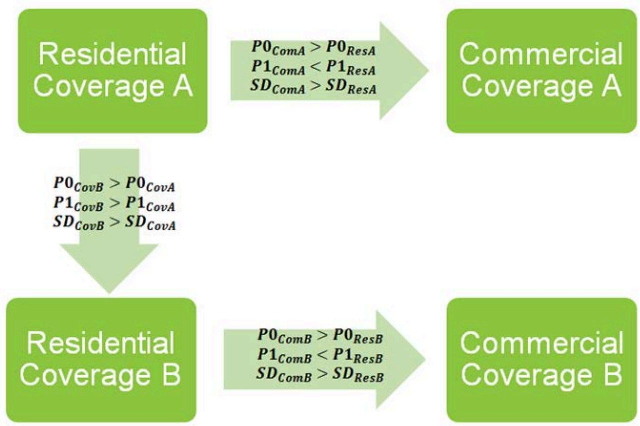

Figure 136. Relationships between residential and commercial distributions for Coverages A and B

As part of the fitting procedure explained above, the distributions were validated against the claims data for agreement on some basic statistics, such as the standard deviation. Another important statistic to validate is the behavior of gross losses (GR) relative to ground up losses (GU). At a given location,

$$\textit{Gross-to-Ground Up Loss Ratio} = \frac{\textit{Mean GR Loss}}{\textit{Mean GU Loss}}$$

where the gross loss is calculated based on a deductible that is given as a proportion of the replacement value. For residential claims, the limit is typically equal to the replacement value.

Figure 137 shows a good match between the loss ratios produced by the new distributions and the claims data, including for some of the most common deductible proportions of 1%, 2%, and 5%.

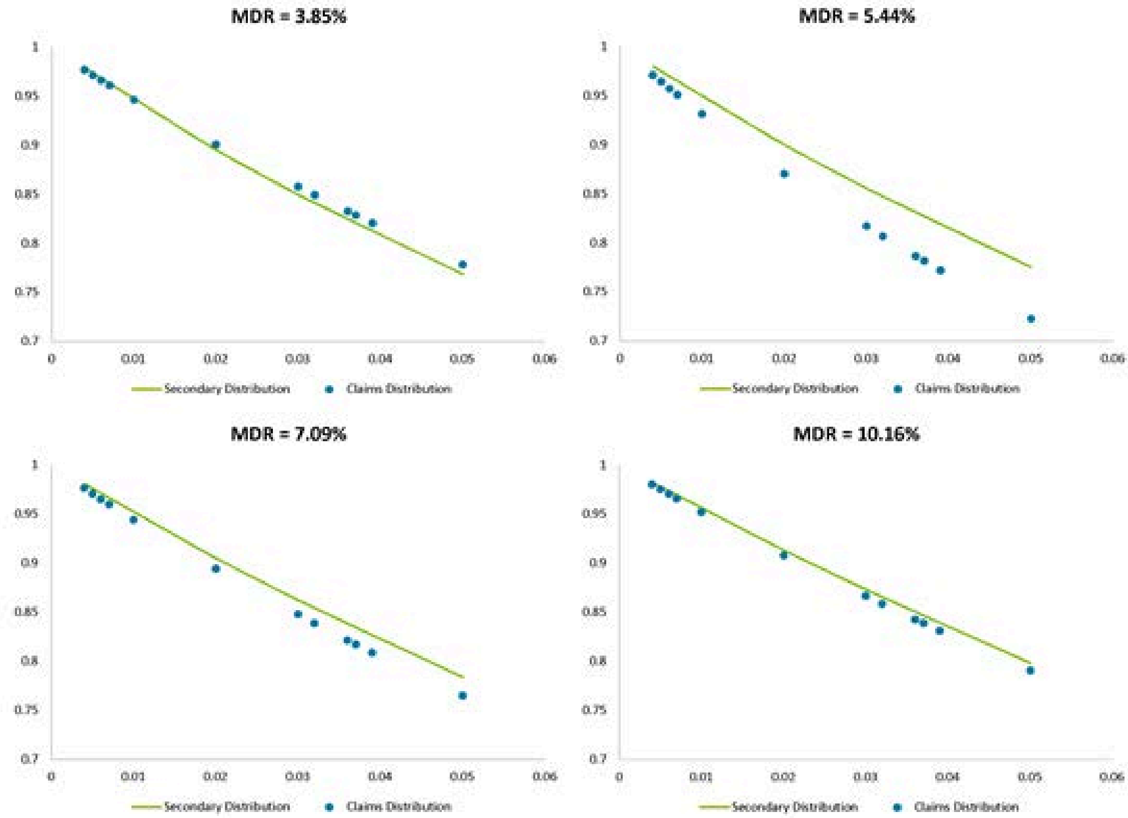

Figure 137. Validating the gross-to-ground up loss ratio for Residential Coverage A, at varying MDRs and deductible proportions

The secondary uncertainty distributions have impacts on flood losses, some important properties of which are listed below. The effects of these properties can be seen in Table 10 at select commonly used deductible proportions.

- The loss ratios for both residential and commercial distributions are monotonically increasing with MDR, and monotonically decreasing with deductible proportion.
- The loss ratio is the same for commercial and residential for lower values of the deductibles. The reason is that the two distributions have the same probability of zero losses.
- For a given MDR and sufficiently high deductible proportion, the loss ratio for the commercial distribution is greater than that for residential distribution.
- For any fixed and sufficiently high deductible proportion, the difference between the loss ratios of the new commercial and residential distributions decreases as MDR increases.

Table 10. Gross-to-ground up loss ratios for Residential and Commercial Coverage A Distributions, at varying MDRs and deductible proportions

	Deductible = 0.5%		Deductible = 1%		Deductible = 2%		Deductible = 5%	
MDR	**Res**	**Com**	**Res**	**Com**	**Res**	**Com**	**Res**	**Com**
0.001	0.970	0.970	0.940	0.940	0.880	0.880	0.749	0.752
0.005	0.973	0.973	0.946	0.946	0.893	0.893	0.769	0.771
0.010	0.973	0.973	0.947	0.947	0.893	0.893	0.769	0.772
0.050	0.975	0.975	0.949	0.949	0.899	0.899	0.773	0.777
0.100	0.978	0.978	0.957	0.957	0.913	0.913	0.798	0.800
0.200	0.983	0.983	0.966	0.966	0.932	0.932	0.836	0.837
0.500	0.990	0.990	0.980	0.980	0.961	0.961	0.902	0.902
0.800	0.994	0.994	0.988	0.988	0.975	0.975	0.938	0.938

5.4 Flood Damage Functions for Buildings

Flood Damage Functions for Residential Buildings

The vulnerability of buildings varies by occupancy and construction class. Residential buildings have a higher vulnerability due to their low height and lack of engineering. Smaller, multiple-family homes perform similarly to single-family homes. Large apartment or condo complexes are typically steel or reinforced concrete and have a higher level of engineering than residential buildings, which results in a vulnerability that is closer to commercial buildings than residential.

Figure 138 presents the damage functions for a two-story, residential building in Florida with a crawlspace foundation, for wood-frame, masonry, and unknown construction classes. Since masonry is a heavier building material, it allows for increased flood resistance, making it less vulnerable than wood. However, damage to both construction types can be considerable at higher flood depths, since these buildings are relatively small, and a large portion is submerged at higher flood depths.

The unknown construction damage function, built as a weighted average, closely mirrors the masonry damage function, as masonry is the predominant construction material in Florida. The assumed first floor height (from ground) for a crawlspace foundation type is around 3 to 4 feet. Incorporating uncertainty around this height and the hazard level leads to little damage below 3 feet. The damage function has a “kink” around a story height of 15 feet, which implies flood waters have begun to damage the second floor of the structure.

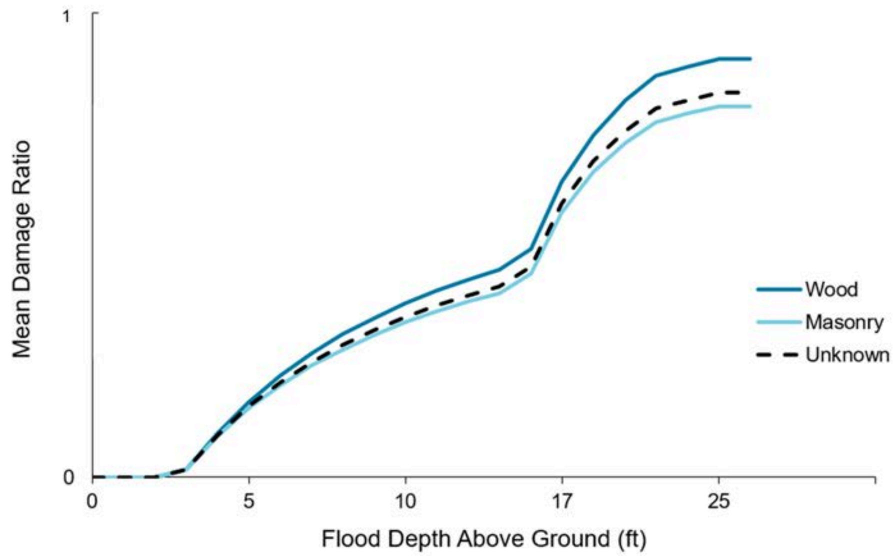

Figure 138. Damage functions for two-story residential buildings in Florida with different construction types for a crawlspace foundation

The effects of building height are shown in Figure 139, which presents the damage functions for reinforced concrete apartment buildings of different heights, on a mat/slab foundation. As previously described, taller buildings are usually better engineered, resulting in a lower MDR. The unknown height is a weighted average of other height classes, and the specific weights depend upon the state or region in which the building is located.

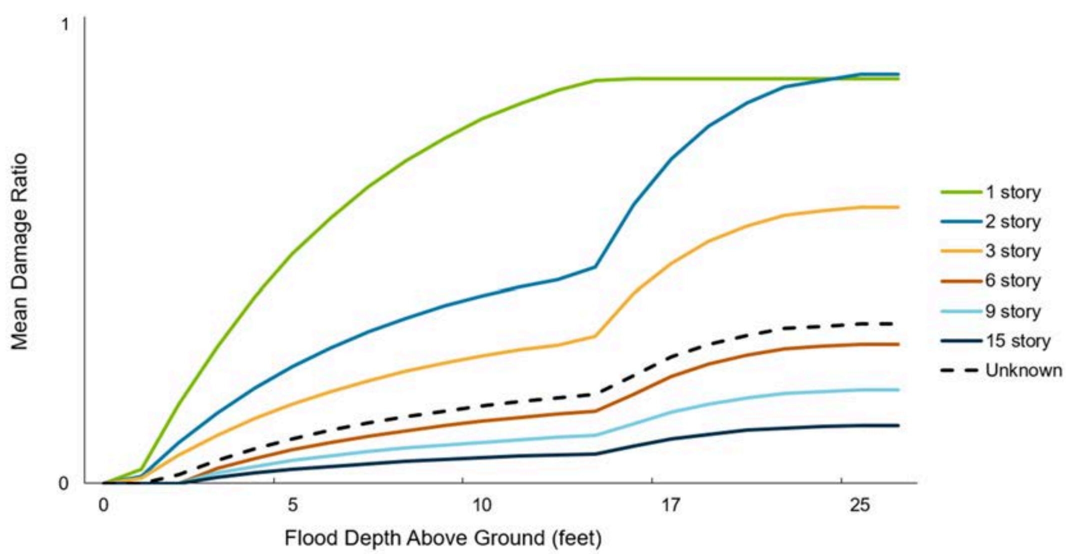

Figure 139. Damage functions for apartment buildings of different heights

The impact of foundation type, specifically the presence of basement, is shown in Figure 140. The figure compares the damage functions for a one-story, masonry, single-family home, with different foundation types in Florida and New York. Foundation type affects the first floor elevation. Slab foundations are assumed to have an elevation of 1-2 feet above ground. Crawlspace foundations typically have a height of 3-4 feet, and buildings on pile foundations are typically elevated 6-9 feet. Hence, the damage functions for these foundation types have non-zero values only if the flood depth exceeds the first floor elevation (Figure 140).

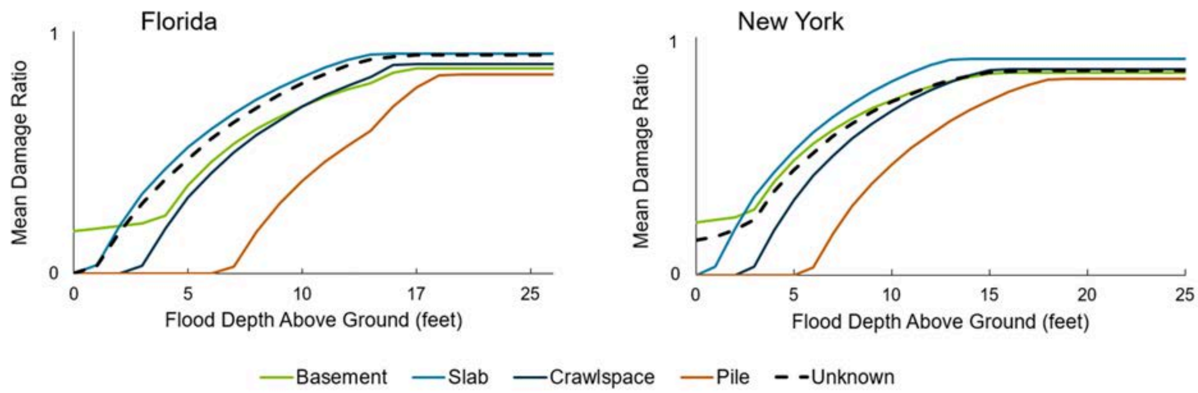

Figure 140. Damage functions for a one-story, masonry, residential building, for Florida and New York, with and without basements

For buildings with basements, however, some part of the lowest floor (basement) is below ground level, resulting in a non-zero MDR even at 0 ft depth of flood water. The model assumes the height of the floor above the basement is 3-4 ft above ground for both Florida and New York. At this water depth, there is a sharp increase in MDR (Figure 140), below which damage is mainly restricted to the basement. All the damage functions with known foundations are identical across the two states as the assumptions for first floor elevations are similar. In Touchstone, first floor height is available as a secondary risk characteristic and can be customized.

While the known foundations are identical for both states (Figure 140), the unknown foundation damage function is influenced by the distribution of foundations in each region. In Florida, non-basement foundation types are most common, especially slab foundations, and the unknown foundation damage function is very similar to the damage function for a slab foundation. In New York, however, basements are prevalent; therefore, the unknown foundation damage function is dominated by the basement function.

See Also

Residential Buildings
Secondary Risk Characteristics
Buildings with Unknown Characteristics

Flood Damage Functions for Commercial Buildings

Figure 141 and Figure 142 show sample damage functions for two commercial buildings, for different construction classes, with mat-slab foundations. Figure 141 provides sample damage functions for a one-story general commercial building, and Figure 142 presents sample damage functions for an eight-story healthcare facility. Because of the height and the level of engineering for high-rise buildings, the vulnerability of the eight-story structure (Figure 142) is much lower than the low-rise buildings in Figure 141.

As illustrated in Figure 141 (single story building), wood and masonry have a higher vulnerability than reinforced concrete or steel. In addition, damage for wood and masonry structures starts accumulating at a water depth below 1 foot, while damage for the concrete and steel structures does not start 2-3 feet. Concrete and steel structures are assumed to be better engineered and hence the damage starts accumulating at a greater inundation depth.

For the eight-story healthcare facility (Figure 142), only reinforced concrete, steel, and unknown construction types are shown since wood and masonry are not commonly used for taller buildings. The damage functions for reinforced concrete and steel are almost identical, which leads to a very similar unknown damage function. Regardless of construction type, the mean damage ratio is low, even at high flood depths, as design requirements for healthcare facilities include flood mitigation.

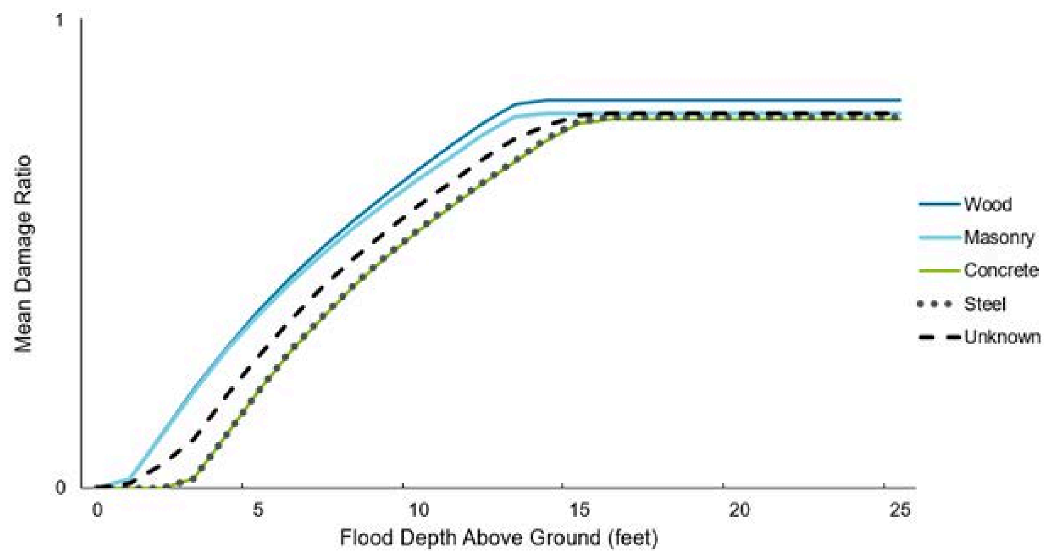

Figure 141. Damage functions for one-story general commercial buildings of different construction classes on a mat/slab foundation

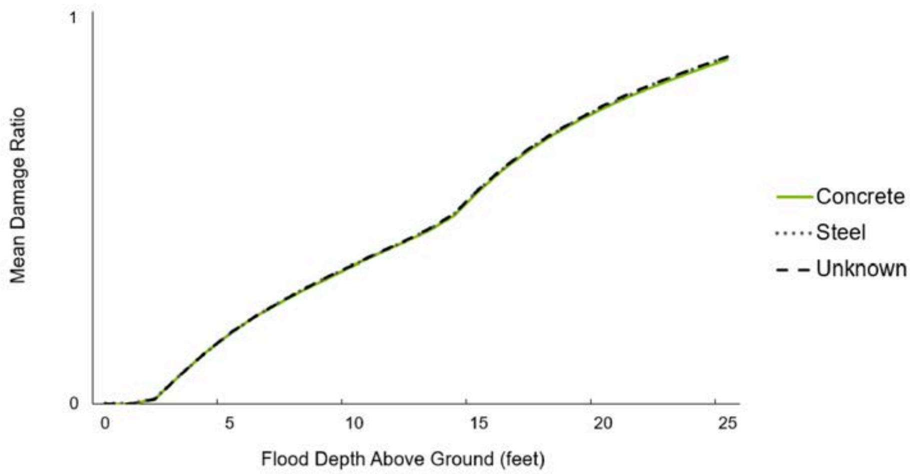

Figure 142. Damage functions for an eight-story healthcare facility of different construction classes on a mat/slab foundation

Figure 143 shows the effect of occupancy class on the damage functions for several commercial and small industrial occupancy types, with unknown heights, construction class, and foundation, in New York. At higher water depths, a general industrial building has much higher flood vulnerability than the other occupancies, followed by food and drug processing plants. This is mainly due to the dominance of low-rise structures for these facilities.

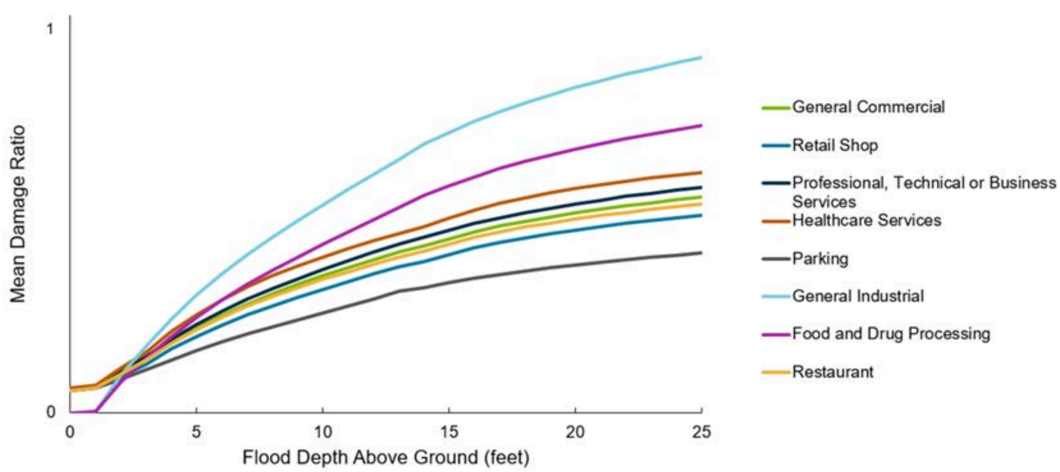

Figure 143. Damage functions for commercial buildings of different occupancy classes in New York
The construction, height, and foundation type are unknown.

Parking structures are the least vulnerable at high depths. However, at low water depths, they are quite vulnerable, due to the presence of underground parking in New York, and the effect of these parking structures on the unknown foundation function.

For the unknown foundation damage function, the presence of basements in the prevalent foundation mix leads to a non-zero mean damage ratio at zero flood depth for most commercial occupancies. Industrial occupancies such as general industrial, and food and drug processing facilities typically do not have basements, thereby leading to a zero mean damage ratio at zero flood depths.

5.5 FEMA Regulations and the National Flood Insurance Program (NFIP)

The year a building was constructed can have a significant impact on its vulnerability as it reflects the regulations in place at that time. Older buildings are often more vulnerable, due to age as well as older building practices. Some older buildings lack a continuous load path; a construction with a continuous load path allows all loads, including lateral and uplift, to be transferred to the foundation and then the ground.

To determine the time periods that affect vulnerability, Verisk obtained information from communities that participate in FEMA's National Flood Insurance Program (NFIP).[35] These communities tend to follow building regulations and mitigation practices, which usually specify the type of foundation and its resistance to buoyancy forces, the use of waterproof materials in the walls, the elevation of the lowest floor, and protection of service equipment. From this data, Verisk obtained the proportion of flood mitigated structures in a community that complies with the Flood Insurance Rate Maps (FIRM). Hence, the year built can be considered as a proxy in the Verisk model to capture the temporal variation in community adoption of FIRM and NFIP regulations.

Verisk engineers undertook a comprehensive study of the evolution of flood regulations, building codes, and building construction practices across the country and incorporated their findings into the damage and loss estimation modules. For a given occupancy, construction, and height combination, the model features different damage functions for each state, foundation type, and time period

NFIP Flood Hazard Zones and Building Standards

Building codes for flood resistance vary widely across the United States. Some NFIP zones [e.g., Special Flood Hazard Areas (SFHAs) and others] have additional, more stringent, building requirements. While participation in the NFIP program is voluntary, construction in SFHAs mandates the minimum design and construction requirements of the NFIP, per the International Code Series, which includes the International Building Code (IBC), the International Residential Code (IRC), and the International Existing Building Code (IEBC) as well as ASCE 24: *Flood Resistant Design and Construction*, by the American Society of Civil Engineers (ASCE).

[35] 44 CFR 59 through 44 CFR 80

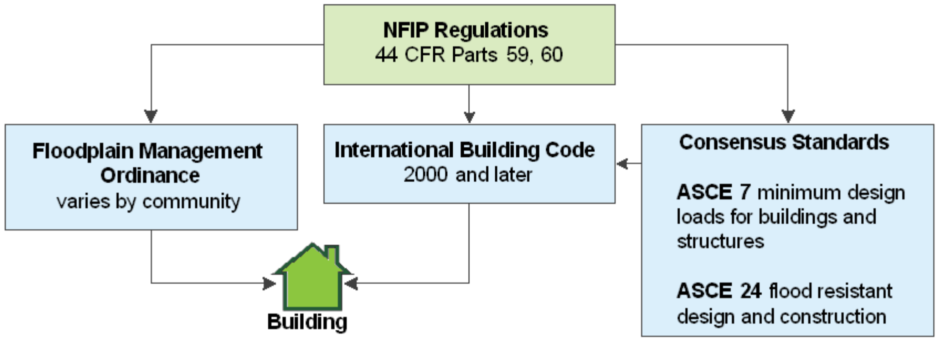

Figure 144. Standards and regulations associated with NFIP floodplain management in the United States

These SFHAs are defined as areas that have a 1 % or larger chance of flooding in any given year and are demarcated on the FIRM maps. Typically, FEMA flood zones V and coastal A zones are designated as SFHAs. The water elevation for a 100-year flood (1% exceedance probability) is defined by FEMA as the **Base Flood Elevation** (BFE). Flood regulations determines the elevation of the lowest floor of a building or structure relative to the BFE. For example, new buildings in SFHAs are designed with a first floor elevation of the BFE plus a freeboard. Freeboard values are typically in the range of 1 or 2 feet above the BFE.

Figure 145 shows the impact of FIRM practices on first floor elevation in two buildings - one built before FIRM adoption (pre-FIRM), and an elevated building that follows FIRM practices (post-FIRM).

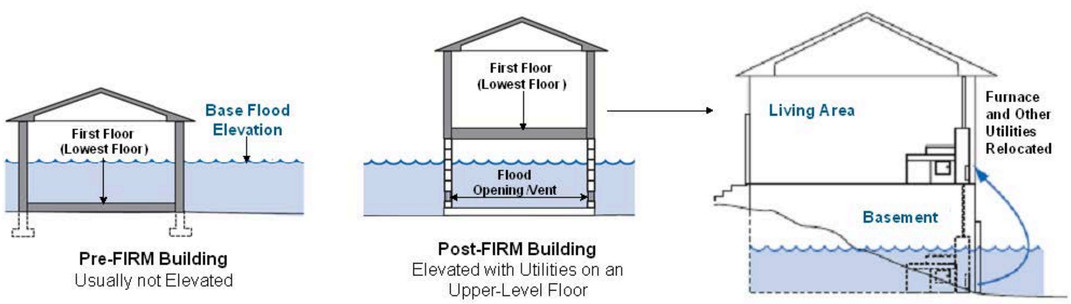

Figure 145. Elevating a building and relocating its contents in accordance with FIRM regulations significantly decreases flood vulnerability.

In addition to elevation of the lowest floor, NFIP regulations also include requirements for foundation type, equipment location, and presence of flood openings or enclosures in the building envelope.

Year Built and FEMA Regulations

FEMA periodically updates their FIRMs as part of the NFIP. These maps delineate areas designated by FEMA as special risk areas. NFIP standards account for foundation design and resistance to buoyancy forces, the use of waterproof materials in walls, the elevation of the first floor, and protection of service equipment. Studies show a difference in the vulnerability of buildings built before the implementation of FIRMs (pre-FIRM buildings) and those built afterwards (post-FIRM buildings). FEMA flood zone V and some coastal flood zone A areas are considered SFHAs and most buildings in these zones are post-FIRM buildings, built according to IBC or IRC. However, the majority of the buildings not in V or A zones tend to be pre-FIRM. Low flood risk communities (e.g., buildings in FEMA flood zone X, beyond the 500-year water level) may not have adopted NFIP policies.

Table 11 shows the structural characteristics of a residential and commercial building that meet NFIP flood resistance requirements.

Table 11. Structural characteristics two structures built to NFIP requirements - a single-family, wood-frame building and a commercial masonry building

Occupancy	First Floor Elevation	Example of Allowable Foundation	Enclosures below the Lowest Floor	Use of Flood-Resistant Materials
Single-Family, Wood-Frame	One foot above Base Flood Elevation (BFE)	Crawl Space	Flood openings are necessary. The bottom of them must be no more than 12 inches above grade	Required below the Base Flood Elevation (BFE)
Commercial, Masonry	Two feet above Base Flood Elevation (BFE)	Slab	None	Required below the Base Flood Elevation (BFE)

Verisk engineers performed an extensive study to understand where FIRM adoption and NFIP regulations are enacted across the country. The implementation of FIRM standards changes at community level (Figure 146). As illustrated, most of post-FIRM buildings that were built in 1980 or later.

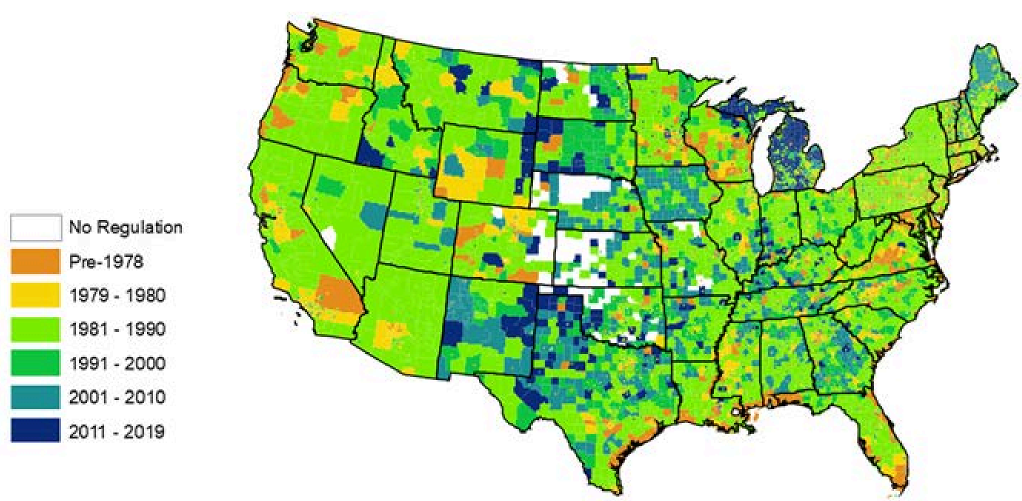

Figure 146. Community level FIRM year built, based on BCEGS® data and FEMA community data
BCEGS® is ISO's Building Code Effectiveness Schedule.

The Verisk model uses community level FIRM year adoption maps (Figure 146) to capture the impact of changes in building codes inside the A and V FEMA flood zones. The community level FIRM adoption map allows the Verisk model to accurately reflect granular changes in community adoption of NFIP regulation changes.

For example, for a particular geocode the Verisk model uses a FEMA flood zone layer to determine if a property falls in or outside of the flood hazard area. If the location is assigned FEMA A and V zones and the year exceeds the FIRM year maps for the community that encompasses the exposure location, the model will apply a year-built variation by accounting for minimum FEMA regulation requirements. Touchstone users can overwrite this assumption by using the custom flood zone and/or the FIRM Compliance secondary risk characteristics.

Figure 147 shows damage functions for a one-story, wood-frame, single-family home in Massachusetts with an unknown foundation, for pre-FIRM, post-FIRM and unknown year built. As the pre- /post-FIRM status affects the elevation and prevalence of certain foundation types in a given area, the effect of year built (or FIRM) is more pronounced at lower water depths (Figure 147). The effect diminishes as the flood depth increases.

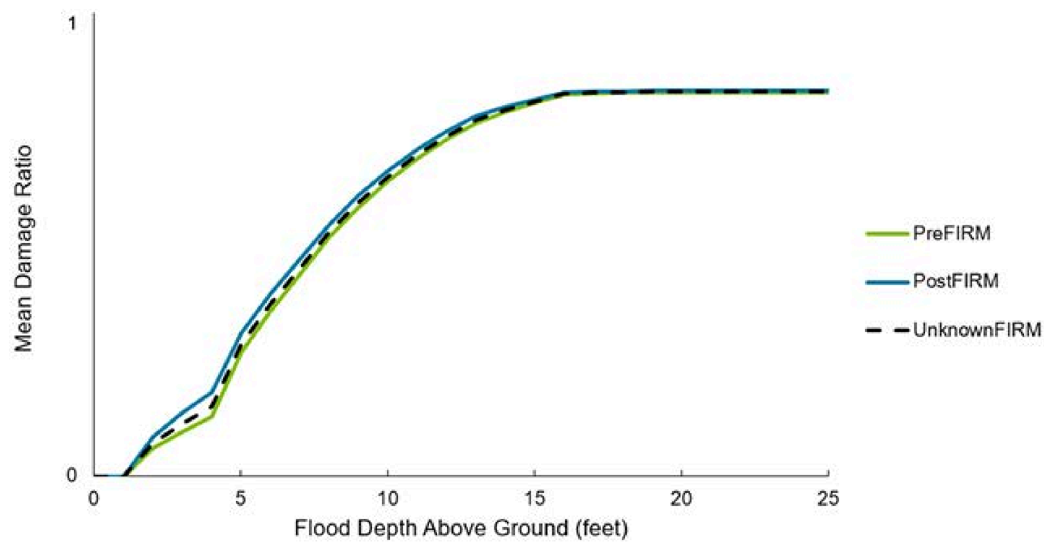

Figure 147. Pre-FIRM, post-FIRM, and unknown year-built damage functions for a one-story, wood-frame, single-family home with an unknown foundation type in Massachusetts

See Also

Secondary Risk Characteristics

NFIP Regulations and the Presence of Basements

NFIP flood regulations and the timing of their implementation have had a significant impact on building practices. This is evident in the spatial and temporal (year built) variation in the presence of basements and foundation type.

Flood regulations enacted in 1968 have had a major impact on the prevalence of basements in the United States. Since NFIP policy adoption is mandated in the special hazard zones, FEMA flood zones A and V have seen a decrease in the presence of basements in post-firm construction. This impact is visible in Figure 148, which presents the distribution of basements in residential buildings. Unlike flood zones A and V, the presence of basements in flood zone X, where NFIP regulations are voluntary, has remained consistent pre- and post-FIRM. To account for this variation, the Verisk flood model considers foundation distribution by both region or state as well as flood zone, and incorporates year built variations of these trends for all occupancies.

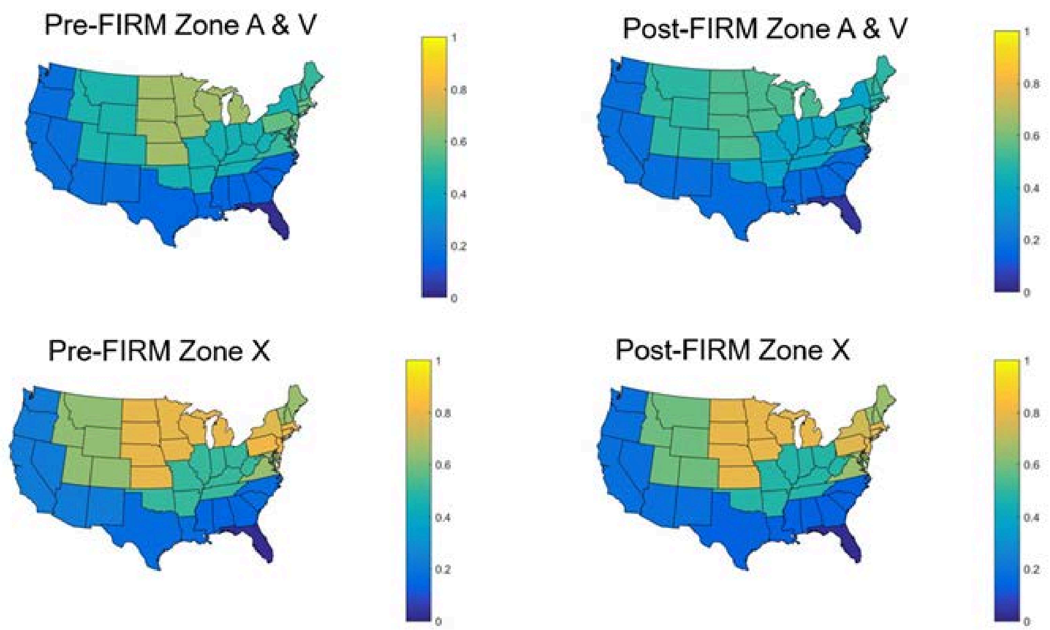

Figure 148. Proportion of residential buildings with basements before and after FIRM adoption

In addition, Touchstone users may further customize property settings by using the foundation type and FIRM compliance secondary risk characteristics. For example, if a building in flood zone X was built according to NFIP regulations, users can account for this by turning on FIRM Compliance even if the community is not FIRM compliant.

If the foundation type is not specified, the model uses the unknown damage function, which reflects a weighted distribution for the state and flood zone where the exposure is located. For example, buildings in southern states are often built on slab foundations that are designed to withstand flotation, collapse, or lateral movement from flood. In the northeast, basements are much more prevalent. The current distribution of all foundation types among residential buildings in the modeled states in FEMA flood zone A is illustrated in Figure 149.

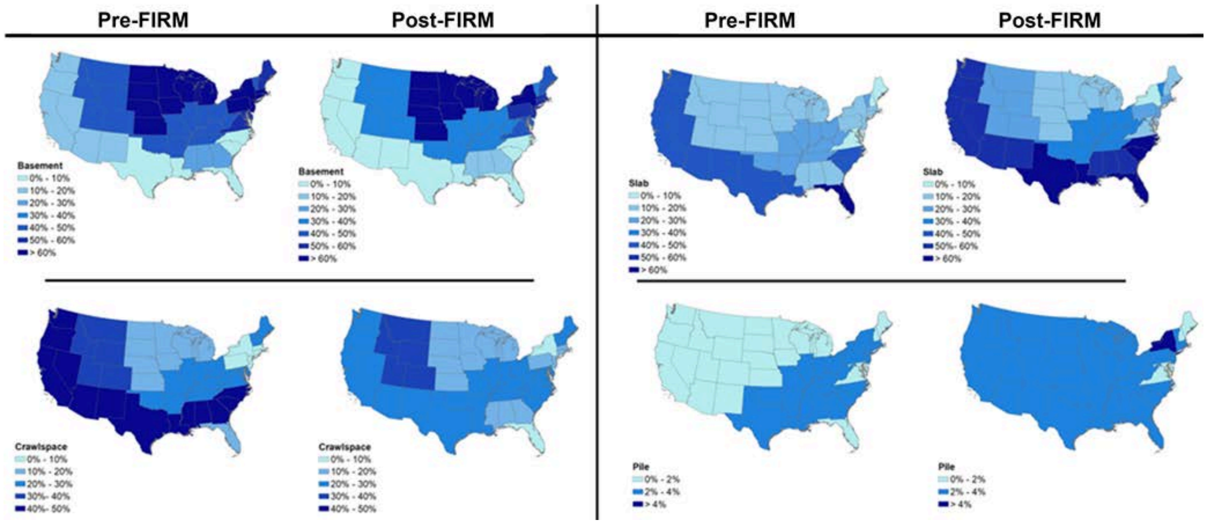

Figure 149. Distribution of all foundation types among residential buildings, in the modeled states, before and after FIRM adoption (flood zone A)

To account for the regional variations in flood-resistant characteristics, Verisk engineers determined the relative vulnerability of buildings, by state and flood zone. These relative vulnerabilities indicate the types of secondary risk characteristics (e.g., foundation type, first flood height, and FIRM Compliance) that buildings are likely to include, for each region. The presence of these modifiers has a direct relation on whether the building was built before or after the introduction of FIRMs.

Figure 150 shows the relative vulnerability across the model domain, for residential and commercial buildings of the same construction and height. The relative changes shown represent the change in the average mean damage ratios that characterizes their respective damage functions within the flood depths of 0 to 7 feet. In both maps, the relative vulnerability values are calculated with the Florida region as the base. It can be observed that residential buildings have a wider range of flood vulnerability due in part to the varying percentage of homes with basements. The flood vulnerability of commercial buildings is more homogeneous since most of these buildings have a slab foundation, and a higher level of engineering.

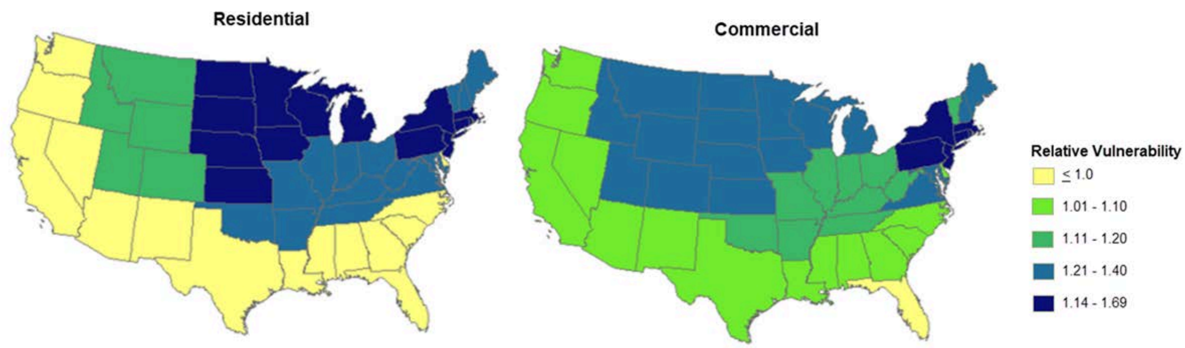

Figure 150. Relative building flood vulnerability across the United States, for 1-story residential and commercial structures inside flood zone A

See Also
Secondary Risk Characteristics

Foundation Type and First Floor Height

In addition to the primary characteristics of a building, secondary characteristics play a significant role in determining a building's vulnerability to flooding. Two key secondary characteristics for flood resistance are foundation type and first floor height, or elevation of the lowest floor above ground level. Foundation type generally dictates the elevation of the first floor. In addition, these characteristics have changed significantly due to NFIP regulations, and are therefore also correlated with the year built.

In the Verisk model the first floor height is correlated with foundation type. In addition, the foundation type has implications for the component cost breakdowns and their vertical distribution over the building height. Table 12, Table 13, Table 14 show the maximum number of stories assumed for a building based on the occupancy and construction type. The tables also show the first floor height associated with different foundation types in the model, for buildings built before FIRM and after FIRM, by flood zone. For buildings inside flood zone X the model assumes the same first floor height regardless of year built.

Table 12. First floor height assumed in the model based on occupancy class, construction class, height, and foundation type for flood zone V

Occupancy Code	Construction Code	Height Band	Foundation Type	First Floor Height (ft)	
				Pre-FIRM	Post-FIRM
301-303	101-104 111-119	Low-rise (1-3 Stories)	Basement, Masonry	4.0	4.0
			Basement, Concrete	4.0	4.0
			Crawlspace, cripple wall	3.0	4.0

Occupancy Code	**Construction Code**	**Height Band**	**Foundation Type**	**First Floor Height (ft)**	
				Pre-FIRM	**Post-FIRM**
			Crawlspace, masonry	3.0	4.0
			Post and pier	5.0	8.0
			Footing	1.0	1.0
			Mat/slab	1.0	1.0
			Pile	7.0	8.0
			Crawlspace, raised (wood)	3.0	4.0
304-306 311-373	101-104 111-119	Low-rise (1-3 Stories)	Basement, Masonry	4.0	4.0
			Basement, Concrete	4.0	4.0
			Footing	1.0	1.0
			Mat/slab	1.0	1.0
			Pile	7.0	8.0
301-306 311-373	131-140 151-160	Low-rise (1-3 Stories)	Basement, Masonry	4.0	4.0
			Basement, Concrete	4.0	4.0
			Footing	1.0	3.0
			Mat/slab	1.0	3.0
			Pile	1.0	3.0
304-306 311-373	111-119 131-140 151-160	Mid-rise (4-7 Stories)	Basement, Masonry	2.0	2.0
			Basement, Concrete	2.0	2.0
			Footing	3.0	3.0
			Mat/slab	3.0	3.0
			Pile	3.0	3.0
304-306 311-373	131-140 151-160	High-rise (8+ Stories)	Basement, Masonry	2.0	2.0
			Basement, Concrete	2.0	2.0
			Footing	3.0	3.0
			Mat/slab	3.0	3.0
			Pile	3.0	3.0

Table 13. First floor height assumed in the model based on occupancy class, construction class, height, and foundation type for flood zone A

Occupancy Code	Construction Code	Height Band	Foundation Type	First Floor Height (ft)	
				Pre- FIRM	Post-FIRM
301-303	101-104 111-119	Low-rise (1-3 Stories)	Basement, Masonry	3.0	3.0
			Basement, Concrete	3.0	3.0
			Crawlspace cripple wall	3.0	4.0
			Crawlspace masonry	3.0	4.0
			Post and pier	3.0	4.0
			Footing	1.0	1.0
			Mat/slab	1.0	1.0
			Pile	6.0	7.0
			Crawlspace-raised (wood)	3.0	4.0
304-306 311-373	101-104 111-119	Low-rise (1-3 Stories)	Basement, Masonry	3.0	3.0
			Basement, Concrete	3.0	3.0
			Footing	1.0	1.0
			Mat/slab	1.0	1.0
			Pile	6.0	7.0
301-306 311-373	131-140 151-160	Low-rise (1-3 Stories)	Basement, Masonry	3.0	3.0
			Basement, Concrete	3.0	3.0
			Footing	1.0	2.0
			Mat/slab	1.0	2.0
			Pile	1.0	2.0
304-306 311-373	111-119 131-140 151-160	Mid-rise (4-7 Stories)	Basement, Masonry	2.0	2.0
			Basement, Concrete	2.0	2.0
			Footing	2.0	2.0
			Mat/slab	2.0	2.0
			Pile	2.0	2.0

Occupancy Code	Construction Code	Height Band	Foundation Type	First Floor Height (ft)	
				Pre- FIRM	Post-FIRM
304-306 311-373	131-140 151-160	High-rise (8+ Stories)	Basement, Masonry	2.0	2.0
			Basement, Concrete	2.0	2.0
			Footing	2.0	2.0
			Mat/slab	2.0	2.0
			Pile	2.0	2.0

Table 14. First floor height assumed in the model based on occupancy class, construction class, height, and foundation type for flood zone X

Occupancy Code	Construction Code	Height Band	Foundation Type	First Floor Height (ft)
				Pre-FIRM
301-303	101-104 111-119	Low-rise (1-3 Stories)	Basement, Masonry	3.0
			Basement, Concrete	3.0
			Crawlspace cripple wall	3.0
			Crawlspace masonry	3.0
			Post and pier	3.0
			Footing	1.0
			Mat/slab	1.0
			Pile	5.0
			Crawlspace-raised (wood)	3.0
304-306 311-373	101-104 111-119	Low-rise (1-3 Stories)	Basement, Masonry	3.0
			Basement, Concrete	3.0
			Footing	1.0
			Mat/slab	1.0
			Pile	5.0
301-306 311-373	131-140 151-160	Low-rise (1-3 Stories)	Basement, Masonry	3.0
			Basement, Concrete	3.0
			Footing	1.0

Occupancy Code	Construction Code	Height Band	Foundation Type	First Floor Height (ft)
				Pre-FIRM
			Mat/slab	1.0
			Pile	1.0
304-306 311-373	111-119 131-140 151-160	Mid-rise (4-7 Stories)	Basement, Masonry	2.0
			Basement, Concrete	2.0
			Footing	2.0
			Mat/slab	2.0
			Pile	2.0
304-306 311-373	131-140 151-160	High-rise (8+ Stories)	Basement, Masonry	2.0
			Basement, Concrete	2.0
			Footing	2.0
			Mat/slab	2.0
			Pile	2.0

Touchstone users may specify the first floor height using the secondary risk characteristics.

See Also

Secondary Risk Characteristics

5.6 Flood Damage Functions for Building Contents

By calculating contents damage separately, the Verisk model accommodates flood policies that cover contents only or provide no contents coverage at all. The contribution of contents damage to the total damage for a building can be considerable. The severity of damage depends on the flood depth and contents' susceptibility to water damage.

Contents damage functions are also explicitly modeled. Verisk built the contents damage functions based on a function that represents the losses of vulnerable contents for a given floor. The one-story content damage function is then aggregated vertically over the height of the building based on the interior component cost breakdowns.

Like the building damage functions, contents damage functions come from the results of studies conducted by USACE and vary by occupancy type. Similarly, the content functions account for the presence of primary and secondary attributes such as first-floor height and presence of basement to name a few. The final content damage functions have been calibrated and validated against historical flood losses and claims analysis.

Figure 151. Flood-damaged appliances and furniture in Waverly, Iowa after the 2008 Midwest flood (Source: FEMA)

Figure 152 provides an example of the relative vulnerability of contents for a residential structure. The vulnerability is not based on the likely location of the contents, but rather their damageability should they become flooded.

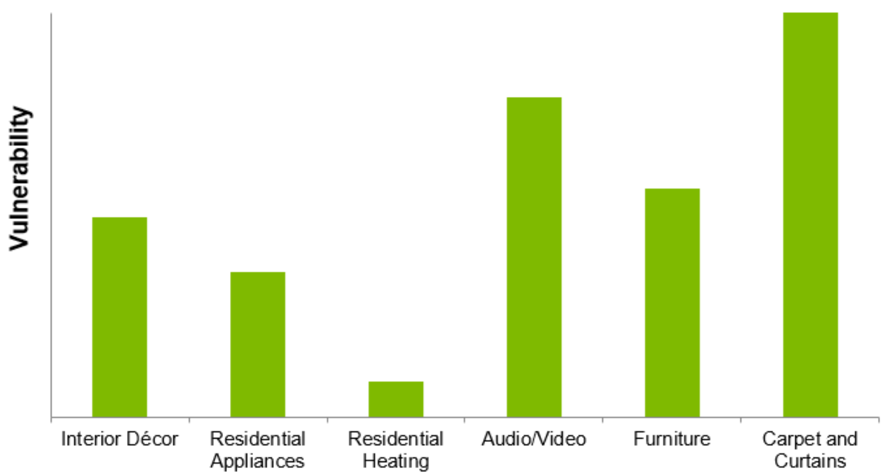

Figure 152. Relative vulnerability of contents for residential buildings

Contents damageability varies with occupancy since certain types of contents are more vulnerable than others. Figure 152 compares building and contents damage functions for a single-family home and a general small commercial structure. Both structures are one-story wood structures on slab foundations. While the building envelope of the commercial structure is less vulnerable than the single-family home, its contents are more vulnerable than the residential contents. In addition to interior décor and appliances, commercial buildings typically include stock and goods that are perishable upon contact with floodwaters. Such vulnerability leads to a content MDR of 1.0, while the building MDR remains significantly lower.

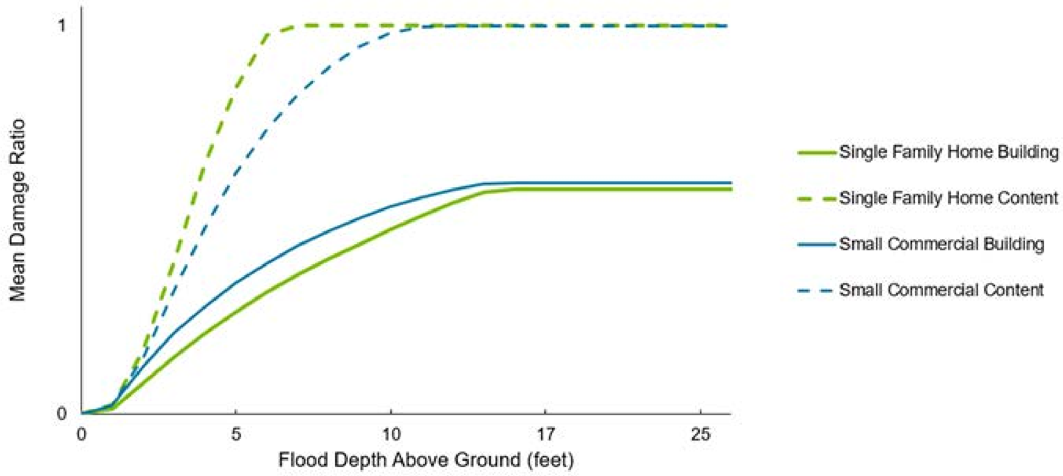

Figure 153. Building and contents damage functions for one-story wood buildings on slab, residential and commercial occupancy

Figure 154 compares the relative vulnerability of building and contents for some key commercial occupancy classes and single-family home. As illustrated, in all cases, the contents are significantly more vulnerable than the structure.

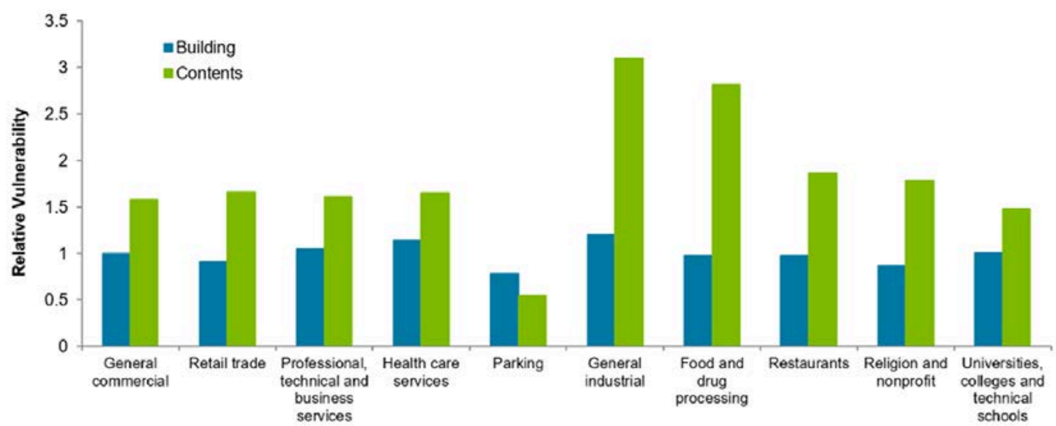

Figure 154. Relative vulnerability of building and contents for selected commercial occupancies

In addition to primary characteristics (construction, occupancy, height), Touchstone users can further modify contents damage functions by providing details of secondary risk characteristics (e.g., the presence of a basement, floor of interest, and content vulnerability etc.).

See Also

Secondary Risk Characteristics

5.7 Flood Damage Functions for Appurtenant Structures

Verisk models support separate damage functions for appurtenant structures. Appurtenant structures encompass a wide variety of assets including storage sheds, detached pool enclosures, gazebos, picnic pavilions, boathouses, among others. In general, appurtenant structures include any structure other than the main building. While there have been major advancements in data collection and value estimation for buildings, the majority of insurance companies still use approximate methods to estimate the value of appurtenant structures. It is a common practice to value appurtenant structures as a certain percentage of the building's replacement value. Further, on the claims side, many companies lump the paid-out claims for appurtenant structures together with the loss paid out for building coverage. Given this method of replacement value and claim attribution, Verisk models the damageability of appurtenant structures along the same lines as property damage, albeit with some addition assumptions.

While the primary building might be founded on basements, the structures that characterize appurtenant structures are assumed to be founded on shallow slab foundations. They are also assumed to be of standard height, close to that of a one-story building, irrespective of the height of the primary building. Further, secondary features including foundation type, first floor height, base flood elevation, service equipment protection, etc. do not necessarily apply to these structures. Custom elevation and custom standard of protection are the only secondary features that impact the flood vulnerability of appurtenant structures.

See Also

Secondary Risk Characteristics

5.8 Damage Functions for the Time Element

Time Element for Residential Buildings

Time element damage functions for residential buildings are a function of the mean building damage and the time it takes to repair or reconstruct the building. Time element losses reflect the cost of providing alternative housing to displaced residents. These losses depend on estimates of the time that will lapse before the property is habitable.

Time estimates include the number of days needed to complete the following tasks:

- Damage assessment
- Drying
- Cleaning
- Repairing the property

Drying and cleaning times contribute significantly to the total time it takes before a building can be reoccupied. Repair costs do not increase significantly after the first meter of water;

the costs to repair a building with one and a half meters of water are not very different than they would be if the water level were one meter.

Figure 155 shows the average amount of time needed to restore a building to full functionality.

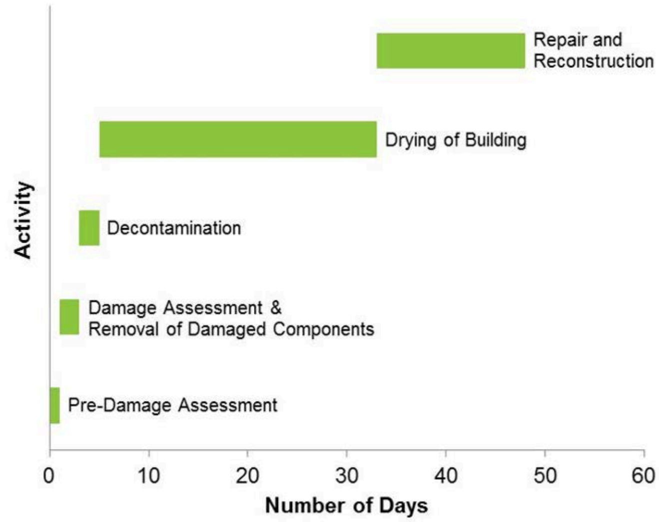

Figure 155. Time associated with different repair activities for minor building damage

Business Interruption

Business interruption (BI) functions represent per-diem expenses and losses due to downtime, or the expected number of days that a building is unusable. The functional relationship between building damage and loss of use is based on published building construction/restoration data and expert engineering judgment. Verisk's methodology uses an event tree approach (Figure 156), and incorporates the latest research and extensive claims analysis.

For each damage state, the model assigns a probability to two possible outcomes for a location:

- Continued operations
- Cessation of operations

If operations cannot continue at a location, the model assigns a probability to the likelihood of relocation. This probability varies by occupancy. For example, while relocation is feasible for an office, it is not feasible for a hotel. The two occupancies will take different paths to recovery, and experience different downtimes.

In addition to calculating direct BI due to building damage, the model estimates BI from indirect sources like actions taken by civil authorities, loss of business income from dependent properties, and utility service interruption.

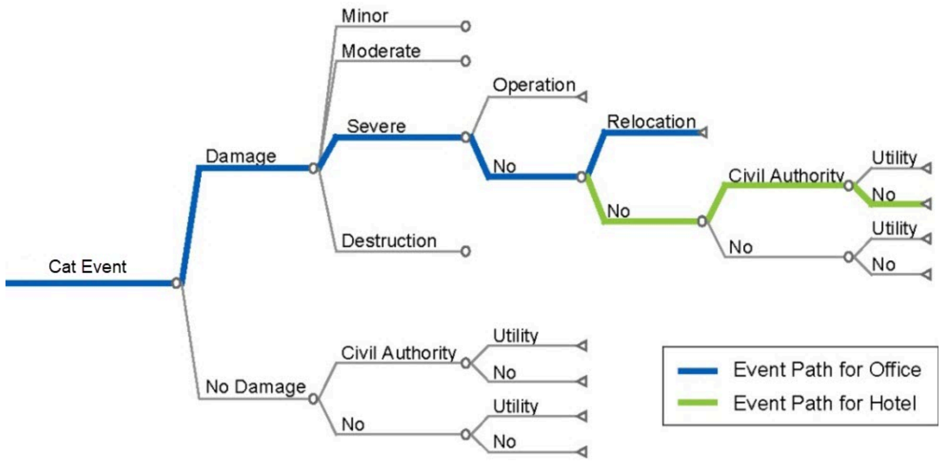

Figure 156. Hypothetical business interruption event tree (office and hotel)

The model calculates downtime for activities conducted during each stage of the recovery process:

Pre-repair / Damage assessment	• Evaluate damage • Negotiate repair costs with contractors • Obtain building permits
Repair / Relocation	• Clean up and repair property, or • Relocate business
Post-repair / Post-relocation	• Regain market share • Rebuild work force

The time needed to fully restore a business's operations depends on several key factors:

Damage	The level of damage sustained
Building size	For a given damage ratio, a 2,500 m^2 hotel will take significantly longer to repair than a 450 m^2 office building.
Architectural complexity	For a given building size, structures with significant architectural complexity will require more time to repair than a simple structure. For example, a warehouse may be large, but it can be repaired quickly, due to the building's architectural simplicity.
Interior finishes	Higher quality interior finishes require longer repair or reconstruction time. For example, it will take longer to restore a

five-star hotel than a standard office building of comparable size, due to the quality of the hotel's interior finishes.

Business resiliency

Some types of businesses (e.g., hospitals) are more resilient than others and may be able to resume operations before repairs are finished. Resilient businesses may also have disaster management plans, which allow them to quickly relocate selected operations. For other businesses (e.g., hotels), location is crucial and relocation is not an option.

The model calculates BI based on the level of damage sustained, occupancy class, and building height. Since many parameters critical to determining BI may not be available for input into the model, Verisk uses occupancy class to approximate building size, complexity, and business resiliency. Similarly, Verisk uses building height to estimate floor area. To consider BI at dependent buildings, the model relies on occupancy class, loss experience data, and expert judgment, as detailed information on businesses' locations and their interdependence is rarely available.

The functional relationship between building damage and loss of use is based on published construction/restoration data and expert engineering judgment. Figure 157 shows the relationship between downtime and the geometric mean of building and contents damage for a variety of occupancy classes.

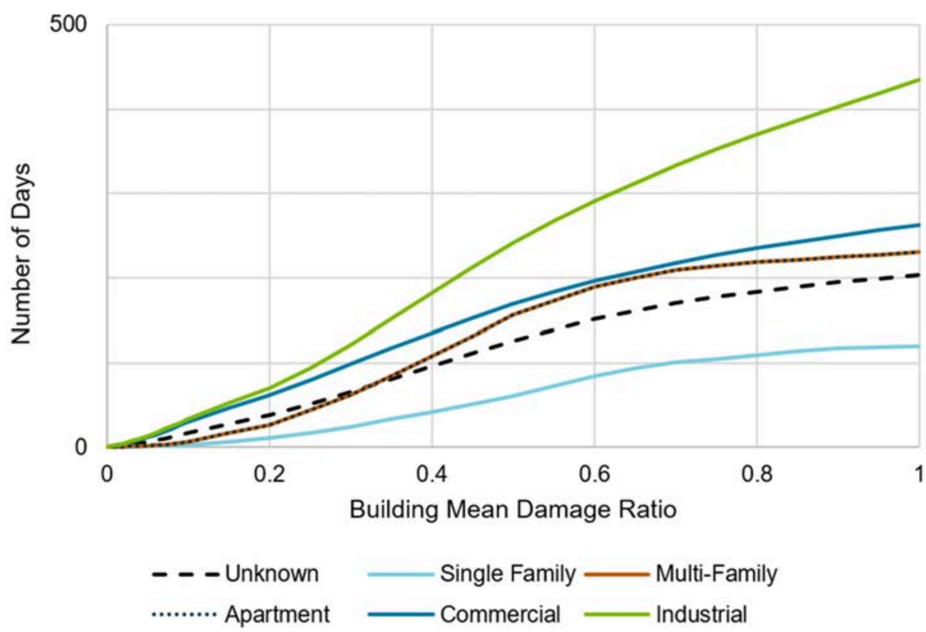

Figure 157. Business interruption damage functions for different occupancy classes

5.9 Damage Functions for Automobiles

The Verisk model considers two classifications of automobiles (personal and commercial), and accounts for the likelihood of flood warnings. Verisk created the damage functions for automobiles to represent an average vehicle type, validated with historical loss data from Property Claims Services (PCS).[36]

The model incorporates separate damage functions for personal vehicles and commercial such as car dealerships, parking lots, etc. The commercial damage function considers the amount of damage associated with large numbers of automobiles parked within a limited area, and the likelihood that such vehicles will not be moved following a flood warning.

As presented in Figure 158, there are "steps" in the damage functions, where the MDR levels off at certain water depths due to the characteristics of automobile damage. No damage occurs at shallow depths below the exhaust pipe, from 0 to about 1 ft above the ground surface. Damage increases as the water level rises, and stabilizes at a high level. Once the engine compartment is submerged and electrical systems, and electronic and computer components are destroyed, the vehicle is likely to be considered a total loss.

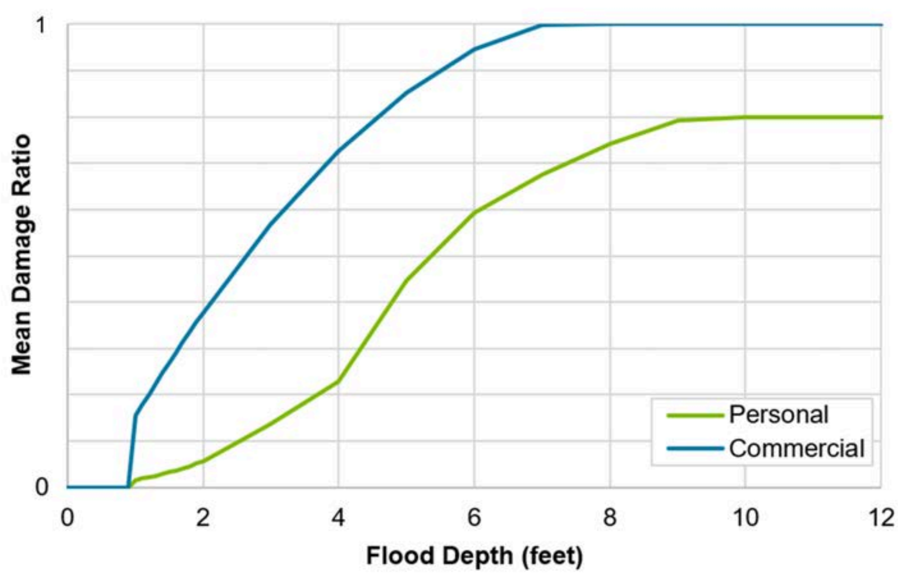

Figure 158. Damage functions for automobiles

Figure 158 also indicates that in the Verisk model commercial auto damage functions are more vulnerable than residential. The model does not account for any evacuation of commercial autos, while the personal auto functions account for evacuation of vehicles. The rate of evacuation differs by county.

[36] Verisk Property Claim Services available at https://www.verisk.com/insurance/products-and-services/product-category/pcs/

Accounting for Flood Evacuation/Warnings in Personal Auto

Advanced flood warnings can have a significant impact on personal vehicle losses; 100% of the loss can easily be avoided by moving the vehicle well away from the inundation area. When determining the number of vehicles that are likely to be in a flooded area at the time of the event, the Verisk model accounts for the likelihood of advanced warnings for the location.

In urban areas, large number of automobiles parked in garages are not easily evacuated. Furthermore, evacuation plans are typically not enforced in large cities due to forecast limitations and to mitigate the loss of life. In suburban and rural areas, the chances of evacuation increases, which lowers the risk of flood damage. As a result, the model includes regionality to account for the potential evacuation of personal automobiles.

Verisk engineers developed the auto damage functions for urban and non-urban areas, which consider decreases in automobile vulnerability as the population density decreases. Figure 159 and Figure 160 show the relative personal auto vulnerability to flooding by county in the contiguous United States and some northeastern counties. As illustrated, vulnerability decreases in rural areas (e.g., the central plains).

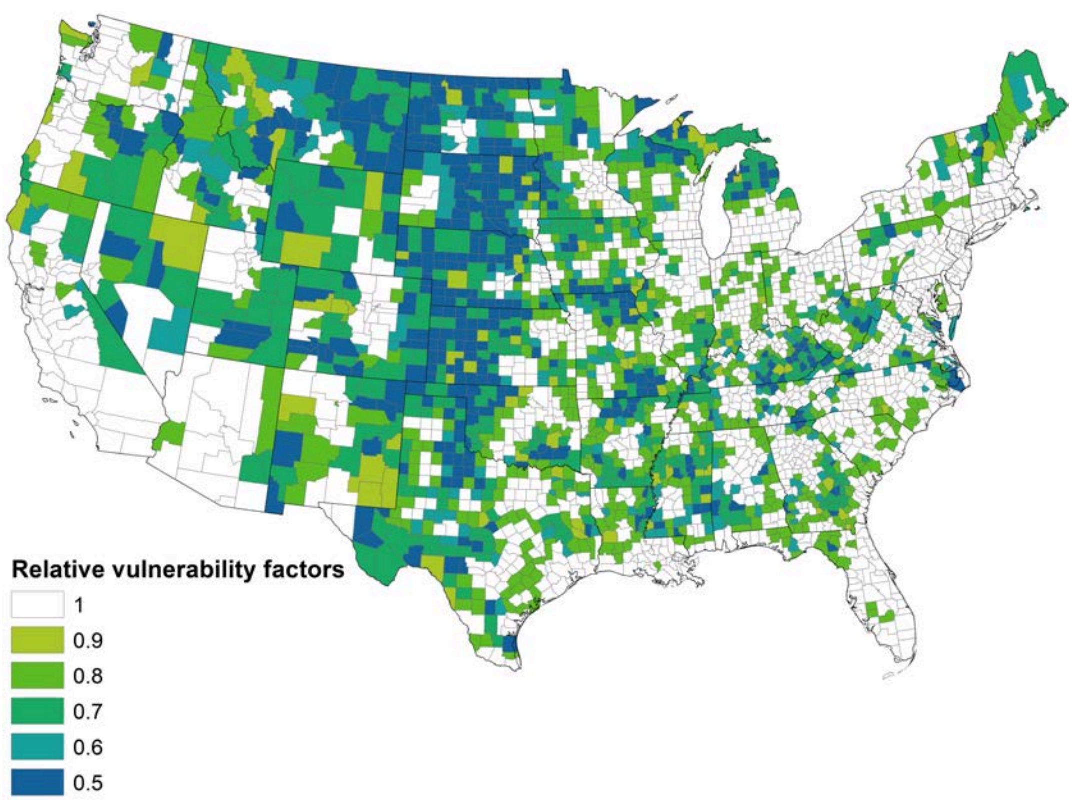

Figure 159. Relative automobile vulnerability to flooding by county in the contiguous United States

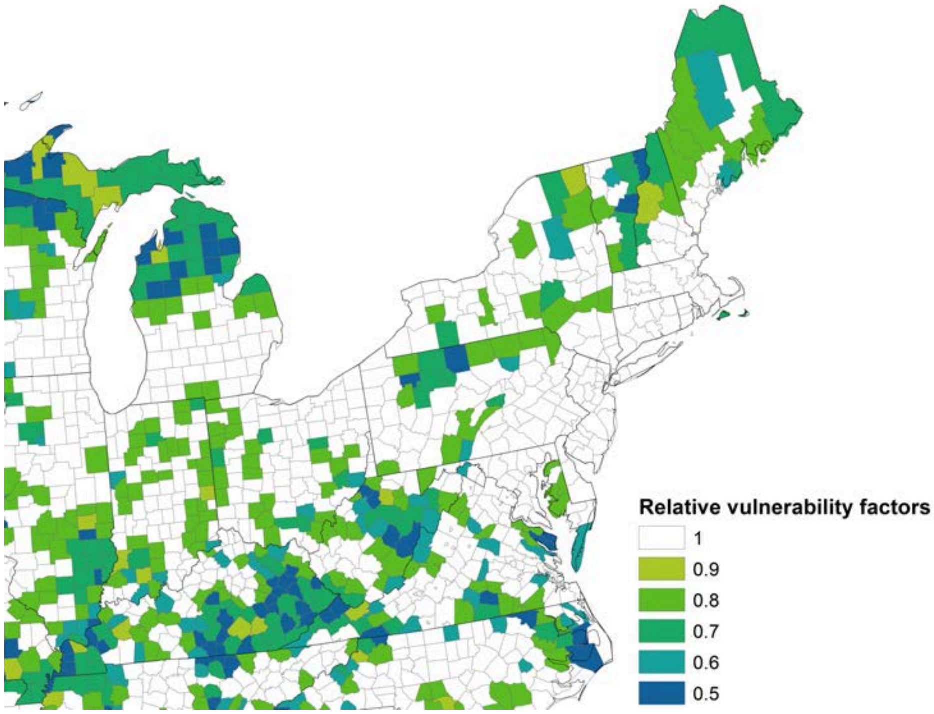

Figure 160. Relative automobile vulnerability to flooding by county in the northeastern United States

5.10 Damage Functions for Specialty Lines of Business

The Verisk flood model supports specialty risks, as listed below.

- Large industrial facilities
- Pleasure boats and yachts
- Marine Cargo and Inland Transit
- Marine Hull
- Builders risk
- Infrastructure

Large Industrial Facilities

Verisk employs a component-based approach to evaluate damage and loss to an entire industrial facility. This method accounts for the primary components of an industrial facility as well as their interconnectivity. Primary components have been categorized into classes and sub-classes to account for variations in vulnerability within each component class. Verisk has developed more than 400 damage functions for approximately 550 distinct industrial components and subcomponents.

Figure 161 and Figure 162 provide examples of types of large industrial facilities and industrial facility components.

Figure 161. Examples of large industrial facilities
Top left to lower right: steel mill,[58] wastewater treatment plant,[59] paper mill,[60] hydroelectric power plant,[61] aluminum plant,[62] electric substation,[63] chemical plant,[64] petroleum refinery,[65] and cement plant.[66]

58 Source: Kobe Steel, Ltd-Kakogawa Works 1172657 by Matsuoka Akiyoshi, CC BY-SA 3.0
59 Source: Marlborough East Wastewater Treatment Plant Aerial by Nick Allen, CC BY-SA 4.0
60 Source: Rumford paper mill 2 by Alexius Horatius, CC BY-SA 3.0
61 Source: Ožbalt Hydroelectric power plant by Josef Moser, CC BY-SA 3.0
62 Source: Bogoslovsky aluminum plant by Kostya Wiki, CC BY-SA 2.5
63 Source: MLGW electric substation Person Ave Memphis TN 01 by Thomas Machnitzki, CC BY-SA 3.0
64 Source: Polymer plant along the Ohio River near the settlement of Apple Grove in Mason County, West Virginia by Carol M. Highsmith, Library of Congress Prints and Photographs Online Catalog
65 Source: Anacortes Refinery 31911 by Walter Siegmund, CC BY-SA 3.0
66 Source: Lafarge, ZI Horizon Sud, Frontignan, Hérault 01 by Christian Ferrer, CC BY-SA 3.0

Figure 162. Examples of large industrial facility components
Top left to lower right: buildings,[67] open frame structures,[68] cooling towers,[69] processing towers,[70] distillation towers,[71] flare towers,[72] tanks,[73] conveyors,[74] pipe racks,[75] transformers,[76] high voltage circuit breakers,[77] and transmission towers.[78]

To develop damage functions for an industrial facility, Verisk made assumptions regarding the characteristics of individual components. Aggregated functions based on component and subcomponent damage functions were developed for each industrial facility type. Each component and subcomponent damage function was assigned a weighting factor, based on

67 Source: Volkswagen factory in Wolfsburg, Germany by Andreas Praefcke, CC BY 3.0
68 Source: Modular, portable GTL plant outside Houston Texas by Serge Zolotukhin, CC BY-SA 4.0
69 Source: Industrial cooling towers for a power plant by Cenk Endustri, CC BY-SA 3.0
70 Source: Petroleum refinery in Anacortes, Washington, United States by Walter Siegmund, CC BY 2.5
71 Source: A double effect distillation plant by Luigi Chiesa, CC BY 3.0
72 Source: Gas flare, PetroChina Jabung field, Jambi, Indonesia by Darmawan Kwok, CC BY-SA 4.0
73 Source: Spherical gas tank farm in the petroleum refinery in Karlsruhe MiRO by Michael Kauffmann, CC BY 2.0
74 Source: Large sulfur pile at North Vancouver, B.C., Canada, by Leonard G., CC SA 1.0
75 Source: Pipe rack constructing by Pbujair, CC BY-SA 4.0
76 Source: Trafostation Alter Hellweg by Rainer Knäpper, CC BY-SA 2.0
77 Source: Circuit Breaker 115 kV by Wtshymanski, Public Domain
78 Source: High voltage switchgear at a transmission substation by Dingy, CC BY-SA 3.0

its replacement value relative to the replacement value of the industrial facility, in order to determine the damage function for the industrial facility as a whole.

This approach provides damage estimates that are transparent, realistic, and consistent for a variety of facilities. Further, the component-based approach is essential for a reliable assessment of business interruption (BI) losses, which depend on numerous interactions between a facility's various components and lifelines.

Damage Functions for Large Industrial Facility Components

The Verisk model can be used to estimate damage to 550 different industrial components and their many associated subcomponents. Each of these individual components can have varying levels of vulnerability due to the differences in their physical characteristics. By using a component-based methodology to develop the damage functions for industrial facilities, the Verisk model captures the wide variation in vulnerability that can be observed across a facility. Table 15 lists some of the many components that were analyzed when developing the damage functions for industrial facilities.

Table 15. Large industrial facility components used in the model

Industrial Facility Components		
Air Handling Units	Distribution Panels	Open Frame Structures
Baffles	Electric Power Backup	Paddles
Basins	Electric Transmission Towers	Pipe Racks
Battery Chargers	Elevated Pipes	Pipes and Pipelines
Battery Racks	Engine Generators	Potential Transformers
Boiler/Pressure Vessels	Equipment	Pressurized Reactors
Boilers	Fans	Process Towers
Buildings	Filter Gallery	Pumps
Chillers	Flares	Scrapers
Chlorination Equipment	Generators	Sediment Flocculation Equipment
Circuit Breakers	Equipment	Silos
Commercial Backup Power	Highways/Runways/Railroads	Stacks/Chimneys
Compressors	Large Horizontal Vessels	Switch Gears
Control Panels	Large Motor-operated Valves	Tanks
Cooling Towers	Large Vertical Vessels with Formed Head	Transformers
Coupling Capacitors	Lightning Arrestors	Tunnels
Current Transformers	Loading Structures (Cranes/Cargo Handling/Conveyors)	Wells
Dams	Motor Control Centers	Valves
Disconnect Switches	Motor-driven Pumps	

Verisk engineers used many different types of data to develop mean damage ratios over a range of flood depths. When possible, damage data or available research for a specific component was used; however, other sources were often needed in cases where this information was not available. Some of these additional sources of information include historical damage data, scientific literature, site-specific measurements, and structural analyses. All analysis took into account the complexity of each component and its characteristic response to flood levels.

For a given flood level, the damage ratio for a particular component falls within a range of damage ratios that depend not only on the level of flood intensity, but also on the type of component. The reason for this is that often, seemingly identical components experience different levels of damage during the same flood event; this variation is due to several factors such as differing quality in materials and construction, and in the level of building maintenance. Therefore, when developing the damage functions for a particular component, Verisk engineers considered a range of characteristics and behaviors within the particular component class or subclass and are intended to represent the average damage ratio for a group of many individual components.

Among the components that are not as resistant to flood are storage tanks, whose flood vulnerability varies, depending on each tank's aspect ratio (the ratio of height to diameter), its fill level, and the type of anchorage at its foundation. Anchorage systems prevent tanks from floating, which can happen if the flood depth exceeds the liquid level within the tank.

Many industrial facility components have a low vulnerability to flooding over a large range of water depths. For example, open frame structures are usually built from steel and they tend to have substantial cross-sectional areas, which helps them maintain stability during a flood.

Damage Functions for Large Industrial Facilities

In the model, the facility-level damage function for a large industrial facility is the weighted average of the damage functions for individual components at that facility. The weight assigned to each component damage function is the ratio of the replacement value of the component/subcomponent class to the total replacement value of the facility. Verisk's weighting conventions for different industrial facilities are based on scientific research, Applied Technology Council report ATC-13 (1985), and HAZUS data.

For certain components and subcomponents, Verisk has made reasonable assumptions about their typical characteristics based on the type of facility (e.g., different percentages of anchored and unanchored tanks or different filling levels and aspect ratios for tanks).

Figure 163 presents the component- and facility-level damage functions for a sample industrial facility.

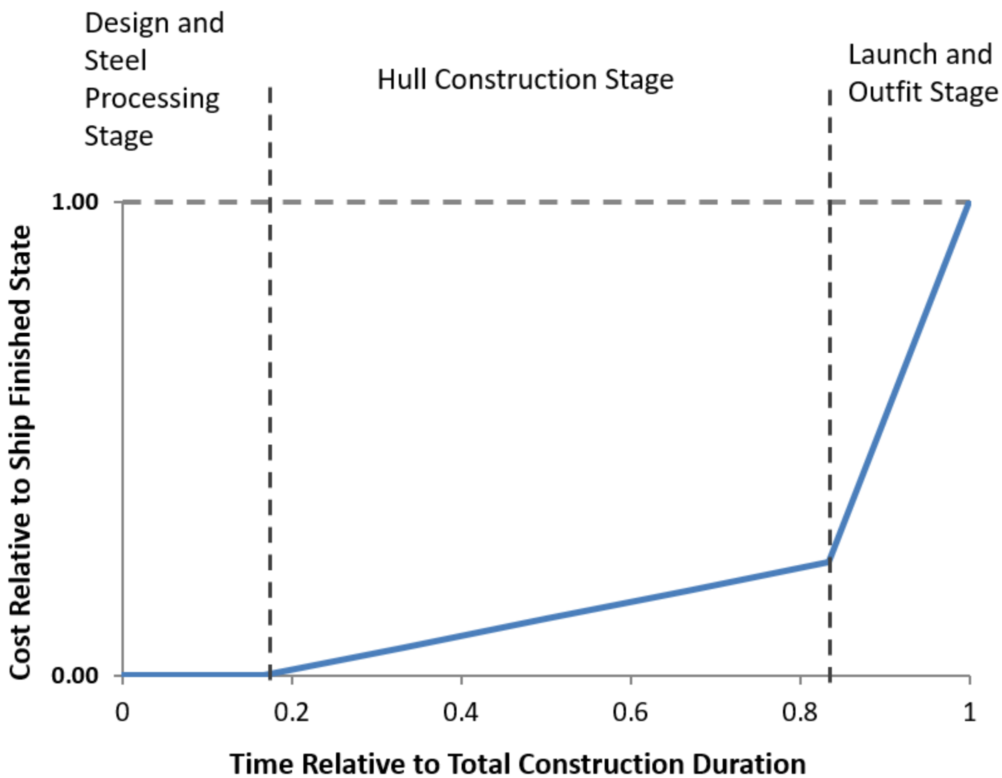

Figure 163. Damage functions for a sample industrial facility
(X%) indicates the weight assigned to the component class.

Figure 164 shows the flood damage functions for selected industrial facilities. The facility level damage function is a weighted average of the damage functions of the individual components. Damage functions for the unknown (general) facility type, indicated with a dotted black line, are based on the weighted average of the damage functions.

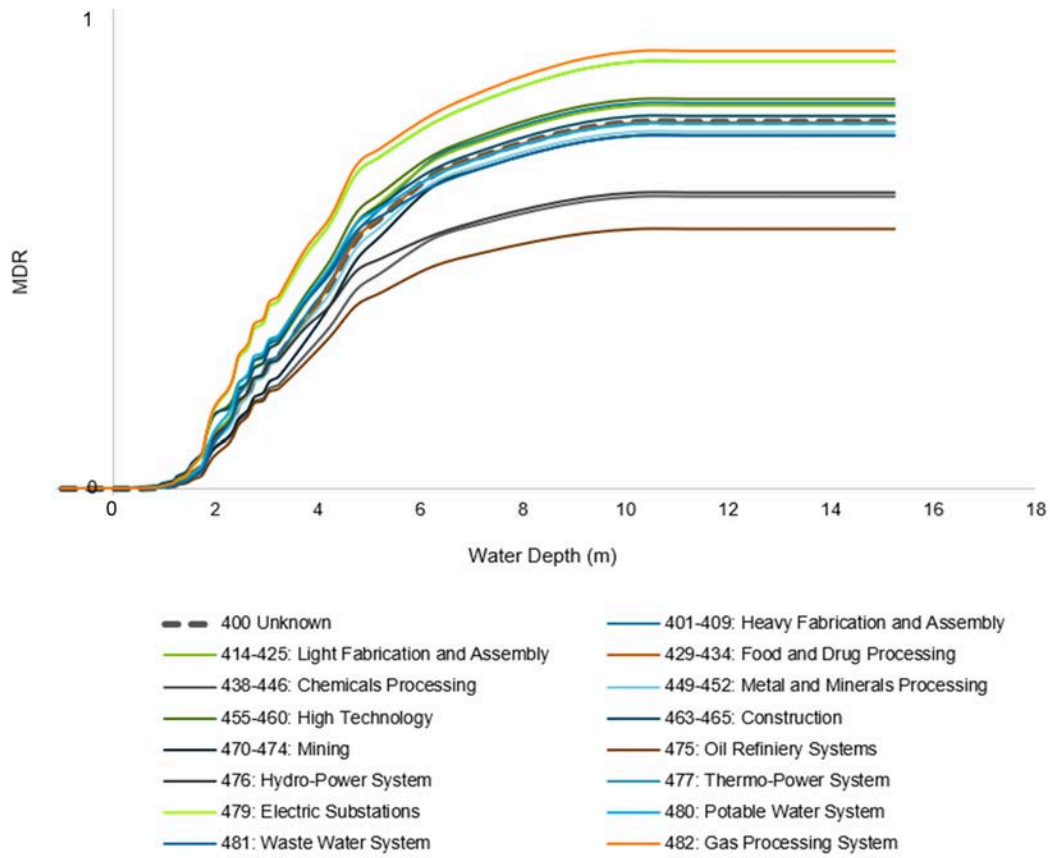

Figure 164. Flood damage functions for selected industrial facilities

Accounting for Flood Protection in Large Industrial Facilities

Building regulations in the United States require that the design for essential facilities such as large industrial facilities, must consider a 100-year return period flood load, at a minimum. Facilities, like chemical plants and power plants, which pose a higher contamination potential, are required to consider higher loads. The Verisk model accounts for the different levels of mitigation inherent in construction of these facilities by assigning a minimum custom level of protection, based a facility's potential contamination risk category (Table 16). The model categorizes facilities as low/moderate (Risk Category III) or high (Risk Category (IV), as outlined in ASCE 7.

Table 16. Contamination potential risk categories for large industrial facilities, based on ASCE 7

	Contamination Potential (ASCE 7 Risk Category)	
Occupancy Class	**Low/Moderate (III)**	**High (IV)**
Unknown Industrial Facility (400)	X	
Heavy Fabrication and Assembly (401-409)	X	

	Contamination Potential (ASCE 7 Risk Category)	
Occupancy Class	**Low/Moderate (III)**	**High (IV)**
Light Fabrication and Assembly (414-425)	X	
Food and Drug Processing (429-434)	X	
Chemical Processing (438-446)		X
Metal and Minerals Processing (449-452)		X
High Technology (455-460)	X	
Construction (463-465)	X	
Mining (470-474)	X	
Petrochemical (475)		X
Power Generation & Distribution (476-479)		X
Utilities (480-481)		X
Gas Processing System (482)		X

In addition to a minimum custom level of protection based on the contamination potential risk category, the model assigns a freeboard value to facilities that fall inside the Verisk 100-year water level. The freeboard value varies by FEMA flood zone and risk category (Table 17).

Table 17. Freeboard by Facility Risk Category

FEMA Flood Zone	Low and Moderate Contamination Potential Freeboard above 100-year Water Level	High Contamination Potential Freeboard above 100-year Water Level
Zone A	+1 ft	+2 ft
Zone V or Coastal A Zone	+3 ft	+4 ft
Zone X	0 ft	0 ft

Failure of the custom level of protection is modeled probabilistically using fragility curves (Figure 165), which indicate the probability of failure given an intensity of loading. The model accounts for failure of the custom defense level at load levels below the standard, as well as the probability that the defense will hold for loads greater than the standard. Ultimately, however, for severe events, the probability of defense failure reaches 100%.

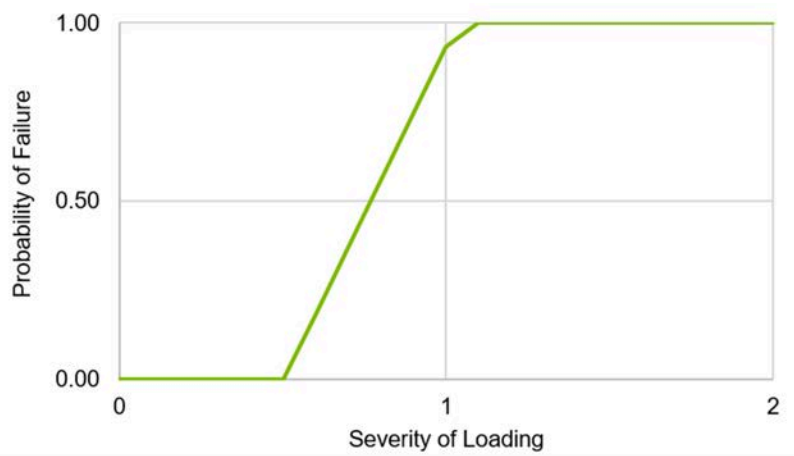

Figure 165. Large industrial facility fragility curve

Business Interruption for Large Industrial Facilities

Assessing business interruption (BI) loss for industrial facilities is complex, particularly in the case of highly integrated facilities. The main contributor to BI losses is the loss of revenue incurred when product chains are rendered completely or partially non-functional (downtime). Loss of functionality can occur due to physical damage to components, component interconnectivity, or lifelines (electricity, water systems, etc.). Verisk has derived the model's facility-level BI damage functions from component distribution information and individual component and subcomponent downtime functions.

To assess BI losses for an entire industrial facility, the model uses BI damage functions for each facility component at each stage of the damage assessment and repair process (pre-repair, repair, and post-repair). Verisk employs a "network model" that simulates the interconnections between components, processes, lifelines, and product changes, and accounts for components to be idle even if undamaged or already repaired if other components or lifelines remain down. The model accounts for the high degree of site-specific connectivity and the complexity of the product chains that exists at most plants. It is a many-faceted calculation involving numerous operations, including evaluations of onsite process interactions, bottlenecks, and redundancies, offsite interdependencies, and revenue generators.

The time element damage functions for flood are illustrated in Figure 166.

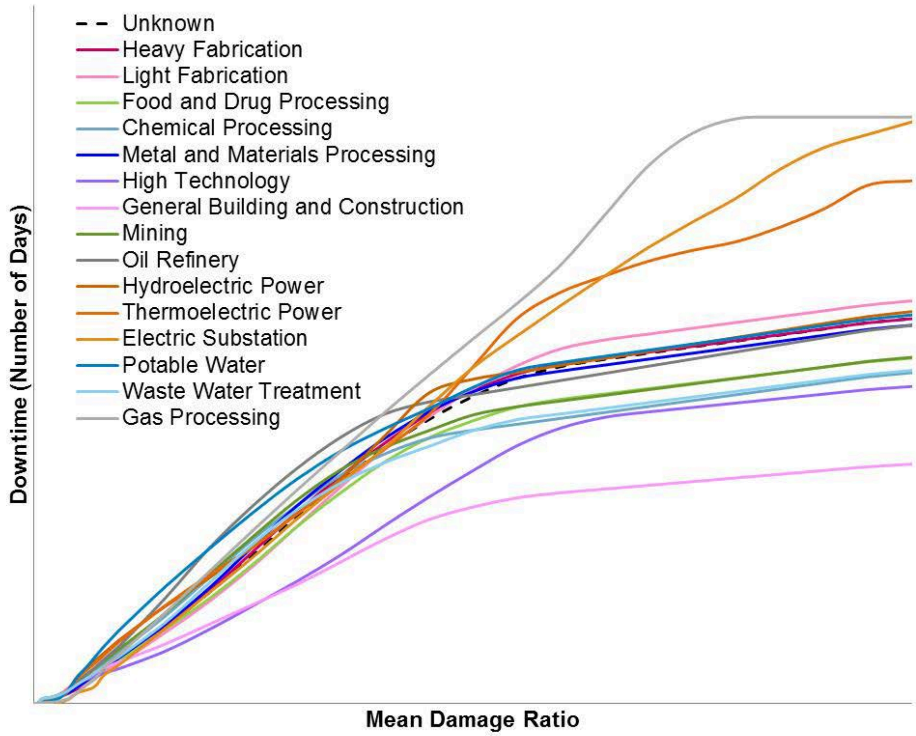

Figure 166. Flood time element damage functions for selected industrial facilities

Marine Risks

The marine line of business comprises a heterogeneous mix of products and assets. It includes products transported over water, typically referred to as ocean-going cargo, as well as when transported over land (via truck or train) and warehoused, typically referred to as inland transit. The assets themselves, such as marine hull, are also included in the marine line of business. Marine assets and products are typically mobile and change in value over time.

The Verisk model explicitly models damage due to precipitation-induced flooding for marine risks, which include the following:

- Pleasure boats and yachts (construction codes 265-267)
- Marine cargo inland transit (construction codes 270-276 and 259)
- Marine hull (construction code 260)

The model does not support secondary risk characteristics for marine risks. There is no spatial or temporal variation in vulnerability for marine risks, nor is there any year built variation in vulnerability.

Pleasure Boats and Yachts

Precipitation flooding can cause water levels in lakes and rivers to rise, allowing boats to become undocked and float freely. Boats may collide with anything in their erratic path, including other marine craft, docks, pilings, or the ground. This can damage many components of the boat including the hull, which increases the possibility of sinking.

Flood damage to pleasure boats and yachts varies according to the level of intensity - at low inundation depths the damage is negligible, but as the water level increases the machinery components inside the hull may be inundated and thus becomes more damageable.

Boat Characteristics

The Verisk model includes damage functions for sail and motor-powered pleasure boats and yachts, as well as for those whose source of power is unknown. Different style boats contain distinct components that are vulnerable to damage. For example, sailboats have additional components (i.e. sails, masts, and riggings) as compared to power boats.

Mitigation Factors

Boat damage can be mitigated by transporting the vehicles out of the water and into dry stack storage, or by moving them to inland water areas such as canals. Another mitigation technique is to moor boats to a floating dock, since floating docks change height in high waves along with the boat, decreasing the likelihood of boats being torn from their moorings. The effects of mitigation are implicitly captured in the model to the extent that such practices are represented in the actual reported losses used for validation purposes.

Marine Cargo Risks

Marine cargo risks include physical damage to cargo and related liabilities while the cargo is in transit by sea and for up to 60 days while the cargo is in storage. Marine cargo risks are classified using occupancy code 354 (Sea and Inland Waterways) and the supported construction codes listed in Table 18.

Table 18. Construction codes for supported marine cargo risks

Construction Code	Category and Description
270	Carpool: Cars parked in open areas near harbors before shipment in car containers
271	Cargo Containers (General and Refrigerated): Used to transport freight (including electronic equipment) on ships. The containers are approximately 20-40 ft long by 8 ft wide by 8 ft high.
272	Heavy Cargo: Oversized items and machinery that are too large to fit into general cargo containers (e.g. construction machinery, harbor equipment, luxury yachts). Heavy-lift ships, barge tows, and dock ships typically transport heavy cargo.
273	Refrigerated Cargo: Cargo shipped in containers that have additional electrical equipment to keep the cargo cool
274	Dry Bulk Cargo: Grains and solid materials such as coal, metal ore, and lumber that are stored on the ground in an open yard
275	Liquid Bulk Cargo: Oil, liquid natural gas, and liquid chemicals that are stored in onshore tanks
276	General/Unknown

The Sea and Inland Waterways occupancy code 354 is supported for ocean-going cargo risks.

The replacement value of the ocean-going cargo is classified as coverage A. Users should enter the risk location as the location of the residence or the business location of the insured, and the exposure value as the daily exposure.

See Also

Marine Cargo, Fine Art, and Specie Modeling

Carpools

Carpools are more vulnerable than the conventional automobile line, as carpools involve large numbers of vehicles parked in a lot. Their evacuation requires logistics that may not be feasible in the event of a flood. Individually owned vehicles, however, can easily be relocated once an owner receives a flood warning.

Inland Transit Cargo

Inland transit cargo refers to risks that are in transport, in transit warehouses awaiting distribution, and the warehouses themselves. Transit warehouses temporarily store various commodities, such as food, clothing, medicine, or construction machinery, prior to distribution. These warehouses are typically one-story buildings of light steel-frame construction.

Warehouses are very susceptible to flooding at high water depths, and the cargo inside is very susceptible to flooding if water reaches the inside of the structure.

The model includes damage functions for model cargo stored in warehouses as well as the warehouses themselves. The supported occupancy codes for these inland transit warehouse risks (construction code = 259) are listed in Table 19.

Table 19. Occupancy codes for supported transit warehouse risks

Occupancy Code	Category
300	Unknown
313	Wholesale
322	Heavy Fabrication
323	Light Fabrication
324	Food and Drug
325	Chemical Processing
327	High Technology

The cargo risks are coverage C. The replacement value of the warehouse itself is coverage A.

Ocean-going Cargo

Ocean-going cargo risks in the model include general container, heavy cargo, refrigerated containers, dry bulk cargo, and liquid bulk cargo. General cargo containers transport freight on ships, trains, or airplanes. These containers are usually box-shaped and are approximately 2.5 m (8 ft) wide, 2.6 m (8.5 ft) tall, and 6-12 m (20-40 ft) long.

Electronic equipment is generally packed tightly within general cargo containers for shipment over long distances. While some forms of heavy cargo can be shipped in general containers, most heavy cargo consists of machinery that does not fit into standard containers, such as construction machinery, harbor equipment, or luxury yachts. Semi-submersible heavy-lift ships, conventional heavy-lift ships, barge tows, or dock ships are used to transport these forms of heavy cargo.

Refrigerated cargo is similar to general containerized cargo, but requires additional electrical equipment to maintain temperatures to preserve the commodities they hold. Dry bulk cargo, which refers to grains and solid materials, such as coal, metal ore, and lumber, are usually stored on the ground in an open yard. Liquid bulk cargo refers to onshore tanks that store oil, liquefied natural gas, and other liquid chemicals.

Refrigerated cargo and heavy cargo containers both involve machinery, which may be located on the exterior of the container, increasing their vulnerability to flood. In contrast, container cargo and liquid tank cargo are less vulnerable, as they are completely enclosed in a containment vessel, which prevents their direct contact with flood waters.

Marine Hull

The marine hull line of business includes the hull of a ship (the structure of the vessel) and the vessel machinery (equipment that generates the power to move the vessel and control the lighting and temperature systems, such as the boiler, engine, cooler, and electricity generator). Marine hull does not include cargo. In the model, this risk can be modeled whether the vessel is at port, at a shipyard under construction, or at a shipyard undergoing regular maintenance and/or repair.

Marine Hull at Port

Damage to marine hull risks at port is primarily caused by collision with other ships or a barge, dock, or pier. The marine hull at a port risk generally has a higher vulnerability compared to marine hull at a shipyard, due to the unprotected nature of exposure.

Marine Hull at Shipyard, under Construction

Damage to marine hull risks under construction at a shipyard may occur due to fire, tidal waves, capsizing, failure in launch, collision, and sinking on a trial trip. This risk has a damage mechanism similar to marine hull under repair.

The value and vulnerability of marine hull under construction risks changes throughout the construction process. On an annual basis, the vulnerability of a marine hull under construction risk is lower than marine hull under repair, because the risk's value is much lower during construction.

The insured value is the contract price, or the estimated completed value of the vessel if there is no contract price. The period of insurance is from the construction start time to the time of vessel delivery.

Marine Hull at Shipyard, under Repair

Damage to marine hull risks under repair at a shipyard are typically caused by collision with the block or pier, or by flooding due to precipitation. Marine hull at shipyard under repair risks generally have a lower vulnerability than marine hull at port, due to the protected nature of their exposure (in dry-dock).

Marine Hull Flood Damage

In general, the flood risk for marine lines is low, compared to surge and tsunami perils. Marine properties are usually well protected and their design involves a higher level of engineering than most conventional lines (residential and commercial).

Marine hull at port has a lower flood vulnerability, since the machinery is protected within the ship. The marine hull at shipyard under repair has higher flood vulnerability since the machinery can get damaged during repair and construction.

The supported occupancy codes for these marine hull risks (construction code = 260) are listed in Table 20.

Table 20. Occupancy codes for supported marine hull risks

Occupancy Code	Category
300	Unknown
314	Marine Hull at Repair
354	Marine Hull at Port
381	Marine Hull Under Construction

The replacement value of the vessel and its machinery is classified as Coverage A. Enter the exposure value at the time of the event into the software in terms of the average daily exposure. For occupancy code 381 (marine hull under construction), use the total replacement value.

Builders Risk

The builders risk line of business determines potential losses resulting from flood damage to buildings while they are still under construction. Modeling builders risk is supported for the majority of the 100-series construction classes and 300-series occupancy classes included in the model, for all height and age bands. Contractor equipment is not modeled under builders risk; it is modeled using existing construction and occupancy classes.

In the model, builders risk can be modeled as a secondary risk characteristic. Users are required to input policy start and end dates to estimate losses for different construction phases, average annualized project loss, and worst case loss.

To develop damage functions for buildings whose replacement value and vulnerability vary during construction, Verisk engineers conducted extensive structural analyses of buildings, for each occupancy and construction class, during the four phases of construction:

Phase I	Foundation and substructure
Phase II	Superstructure
Phase III	Walls and roofing
Phase IV	Finishing, mechanical, and electrical installation

Damage functions have been developed for two classes of construction type: engineered and non-engineered. For these analyses, Verisk used statistical data from RS Means (Reed Business Information), United States Construction 2010 Census, and the National Building Construction Manual for 2009.

See Also

Secondary Risk Characteristics

Duration of Building Phases

The building phases overlap one another, with the timeline of each dependent on the type of building. For commercial buildings, phase IV will be much longer than it would be for residential ones. To determine the phase duration, Verisk engineers used engineering cost estimation data, project duration data, and input from construction management engineers. Figure 167 shows an example of the phase timeline for a mid-rise (four to seven stories) commercial building. The duration for each phase is presented as a percentage of the total amount of time to complete a building.

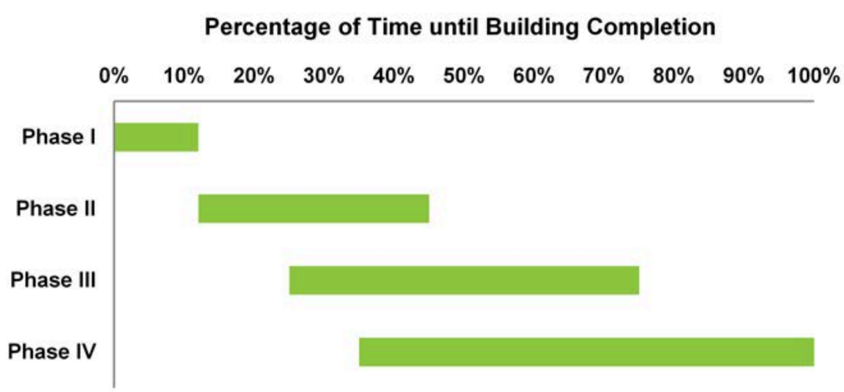

Figure 167. Duration of phases for a mid-rise commercial building

Verisk researchers also took into consideration the subcomponents at each phase. For example, to determine the vulnerability curves for phase III, the vulnerability of the roofing, windows, and exterior walls were all considered. Figure 168 illustrates the duration of some of the subphases for a mid-rise commercial building. The figure includes the duration and overlap of the main four phases, illustrating how the many subphases are included in more than one main phase.

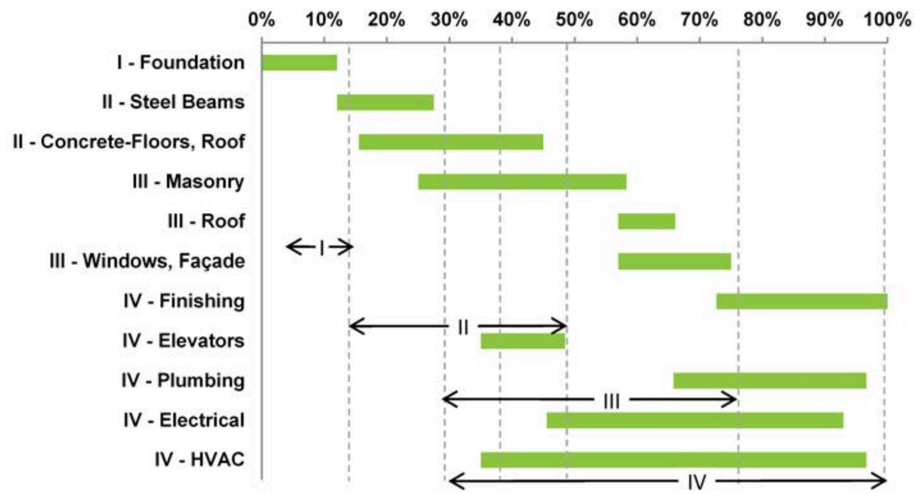

Figure 168. Duration of some sub-phases for a mid-rise commercial building

Variations in the Replacement Value during Construction

The relationship between the building cost, or replacement value, and project duration is captured in a cost ramp-up curve, which shows the evolution of a total project cost over time. The slope of this cost ramp-up curve is largely affected by building height and occupancy class[79] (the effect of construction class is negligible). Note that cost ramp-up curves remain constant across perils.

For example, the effects of height on building costs can be illustrated by examining the percentages of the total cost at each construction phase, for buildings of the same occupancy type at different heights. Table 21 compares the percentage of the total cost at each construction phase between apartment buildings of different heights. For each height band, the cost of each phase is presented as a percentage of the total cost; therefore, a change in the costs at particular phase causes the costs of other phases to be adjusted.

For low-rise buildings, the foundation and substructure account for a larger percentage of the entire building (and its cost) than they would for a mid-rise building. This is because the absolute cost of phase II in mid-rise buildings has a higher increase over phase I than it does for low-rise buildings, making the percentage of the phase I cost lower. The cost percentage for high-rise buildings is greater since these buildings require a more elaborate foundation than shorter buildings.

The cost percentages at phase II increase steadily with height, with a larger increase from phase I for taller buildings. This is to be expected since the columns and other elements of the superstructure are more elaborate for taller buildings than lower ones. It is also the

[79] Only a subset of the model occupancies is supported in builders risk. The main occupancies modeled with unique phase durations are residential and commercial buildings; they do not include industrial facilities.

reason for the decrease in the percentage of cost with height at phases III and IV. Due to the large increase in the costs of phase II for mid-rise and high-rise buildings, the percentages of the total cost at phases III and IV are diminished.

Table 21. Percentage of the total cost at each construction phase for apartment buildings of different heights

Construction Phase	Low-rise (1 – 3 Stories)	Mid-rise (4 – 7 Stories)	High-rise (8+ Stories)
I. Foundation and Substructure	6%	5%	7%
II. Superstructure	9%	12%	13%
III. Walls and Roofing	14%	12%	10%
IV. Finishing, Mechanical and Electrical Installation	71%	71%	70%
All Phases	**100%**	**100%**	**100%**

The cost ramp-up curve in Figure 169 shows the changes in the replacement value for commercial buildings of different heights. The sharp bend in the curves indicate the beginning of phase IV when the interior work occurs, mechanical and electrical systems are installed, and the finishing touches are applied. The replacement value then levels off slightly once the finishing touches begin since the costliest parts of this phase are complete at that time.

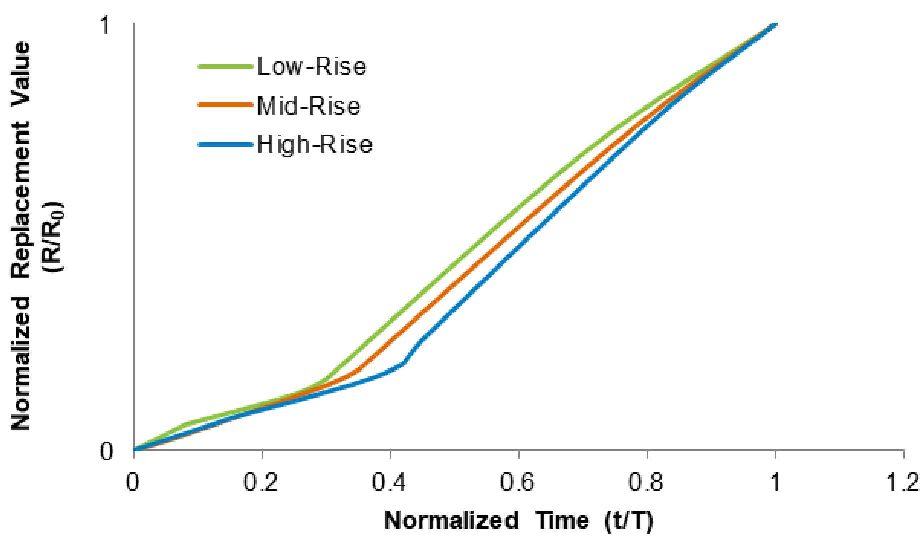

Figure 169. Changes in replacement value during construction of a commercial building, for different heights

Figure 170 compares the cost ramp-up curves for low-rise buildings of different occupancy classes. After phase IV, the curve ramps up more sharply for apartment buildings. Apartment buildings have a larger amount of interior work and finishing, which have to be done in each unit. In addition, the materials used for kitchens and bathrooms are of a higher quality than in commercial and industrial buildings. While commercial and industrial buildings have more wall partitions, facilities, and fixtures, the materials are not as costly as those in apartment buildings.

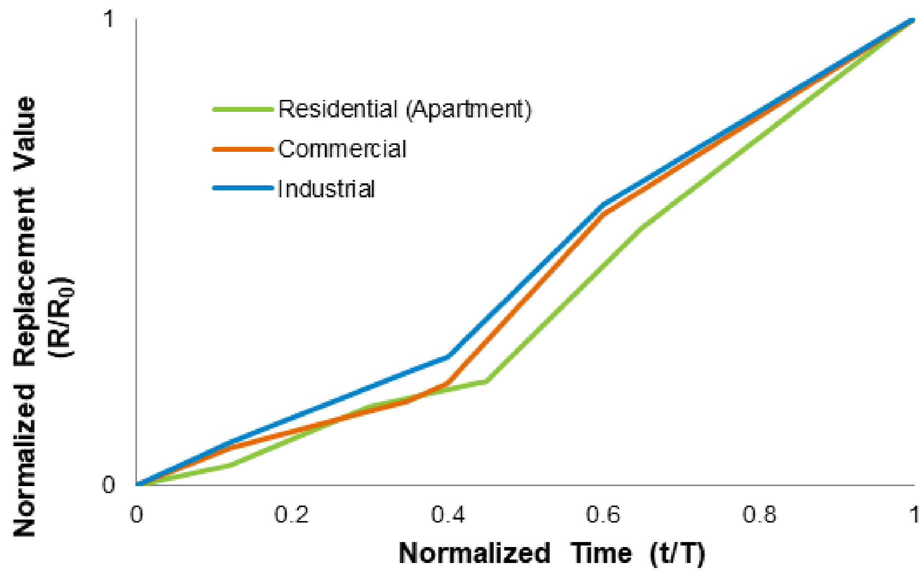

Figure 170. Changes in replacement value during construction of low-rise buildings with different occupancy classes

The various occupancy types within each class can have a significant effect on the variations in replacement value during construction, as shown in Figure 171. For example, phase IV of a hospital can take up a significant percentage of the total cost compared to other buildings, due to the extensive electrical and mechanical fittings that are required for a hospital. For other large structures, such as wholesale trade centers, costs are more concentrated in phases II and III due to the extensive walls, roofing, and other elements of the superstructure. Phase IV is less important in these cases since the interior walls and fixtures are not as costly as in other buildings.

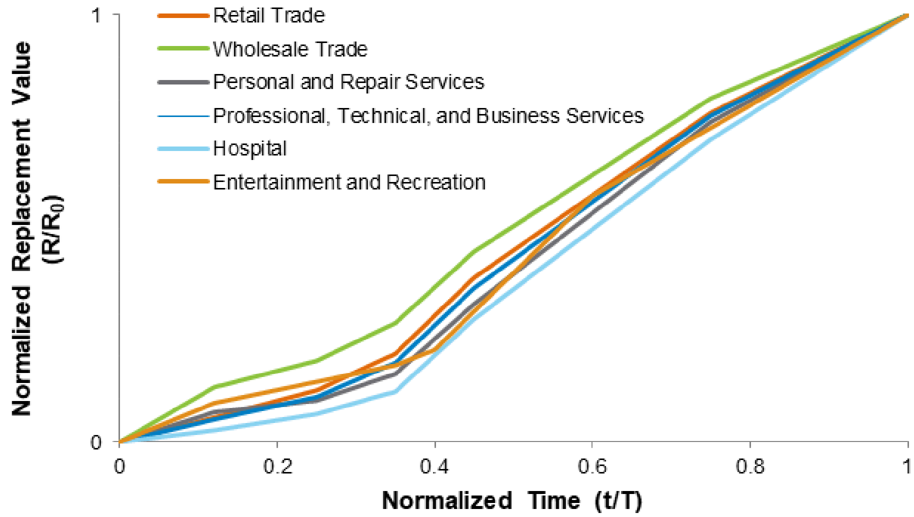

Figure 171. Changes in replacement value during construction of mid-rise commercial buildings with different occupancy type

Vulnerability to Flood

As building progresses, the changes in vulnerability must be considered along with the replacement value. The vulnerability of a building under construction to flooding generally increases with building phase. At phase I, flooding may erode and scour a building foundation, where a shallow foundation is more susceptible to damage. Flood waters can also stress building columns and walls, lead to water pooling, debris accumulation, and soil subsidence. The level of damage experienced at phase II is lower than that of phase I. At this point, flooding exerts force onto a building skeleton rather than on a more vulnerable incomplete building foundation; phase II damage is largely related to debris. Types of flood damage observed in phase III are similar to that in phase II; one key difference includes damage to completed walls and the building interiors. At phase IV, potential building flood damage is similar to that of a completed building. Figure 172 shows a flood damage function by building phase for an engineered mid-rise commercial building.

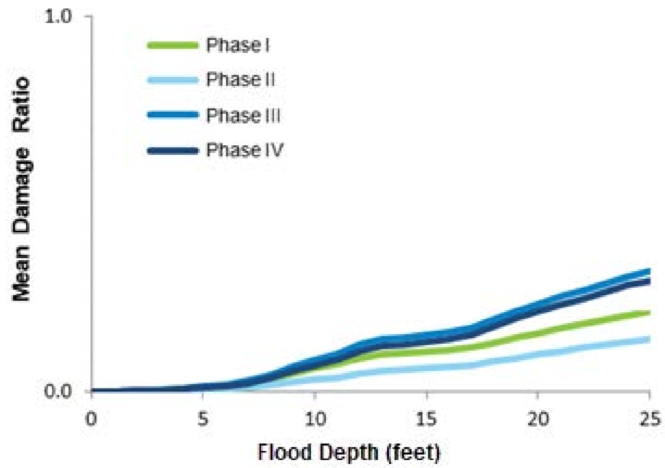

Figure 172. Flood damage functions by building phase for an engineered mid-rise commercial building

Modeling the Effects of Seasonality on Building Construction Phases

To ensure accurate damage calculations for buildings under construction, the model explicitly accounts for seasonality. Each month of the year has been assigned frequency value.

Using user input policy start and end dates, the model determines which construction phases overlap with the season for each project and then only calculates losses for those phases. During the loss calculation process, frequency is considered along with building phase, replacement value, and peril vulnerability.

Infrastructure

The Verisk flood model supports damage functions for a wide variety of infrastructures, including, but not limited to, bridges, railroads, dams, chimneys, towers, tunnels, storage tanks, and residential and commercial building equipment. Damage assessments for these risks are challenging, because the response to precipitation-induced flood is not universal across all types of infrastructure. For example, modern bridges that are constructed mainly out of concrete or steel are relatively vulnerable to precipitation-induced flood due to the buoyancy and lateral forces acting on the bridge. In addition, railroads and highways are vulnerable to water since scour and inundation can inflict substantial damage or make them impassable. Towers (e.g., electrical transmission and broadcast towers), however, are relatively resistant to flood. Some examples of typical infrastructures supported in the model are shown in Figure 173 below.

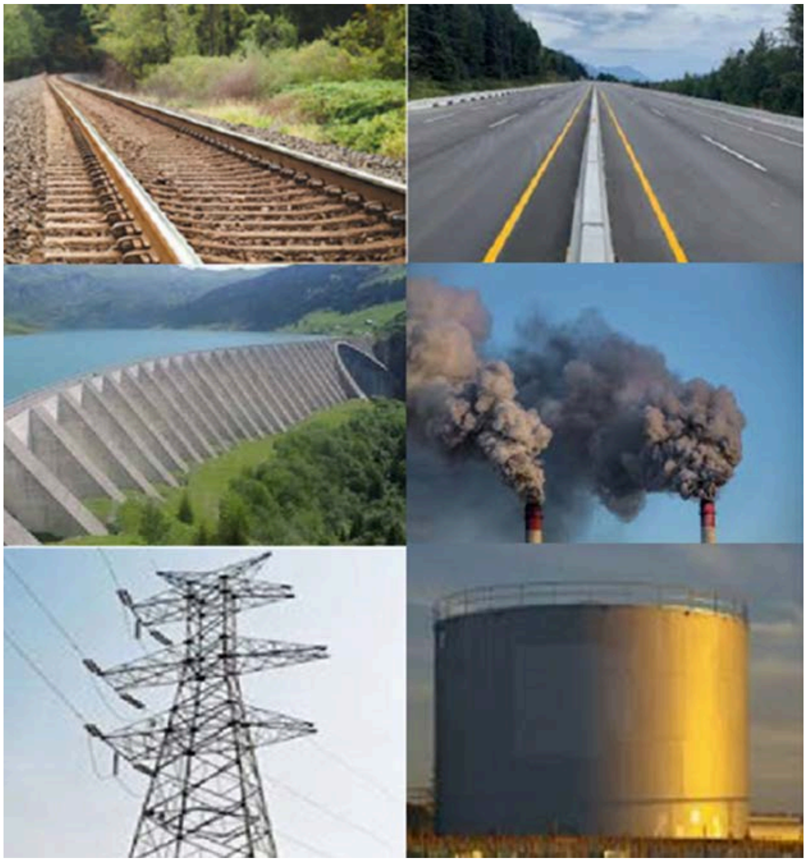

Figure 173. Examples of typical infrastructure risks
Left to right, top to bottom: railroad, highway, concrete dam, concrete chimney, transmission tower, and a water tower

Considerations for Modeling Marine Cargo and Inland Transit Risks

The following notes are important to consider when modeling the marine cargo and inland transit risks in Touchstone:

- Similar to marine hull risks, the model requires that users enter exposure values for marine cargo at the time of an event, not the monthly or yearly aggregates. Since cargo is constantly moving, average daily amounts (taking into account accumulations) should be used in Touchstone to estimate flood losses.
- Oceangoing cargo: Only Coverage A (building) is supported for occupancy 300 (Sea and Inland Waterways) and construction classes 271-276.
- Carpool: Only Coverage A is supported for occupancy 300 and construction class 270 (Carpool).
- Inland transit cargo: Both Coverage A and Coverage C (content) are supported for the combination of construction class 259 (Transit Warehouse) and occupancy classes 300, 313, 322-325, and 327. However, to appropriately model the cargo, the exposure should be coded as Coverage C. Coverage A represents the building exposure (i.e., the warehouse).

In addition, an inland transit modifier is introduced for Coverage C based on different inland transit cargo damageability.

5.11 Secondary Risk Characteristics

In addition to the primary determinants of vulnerability, the Verisk model supports secondary risk characteristics (SRCs). These individual risk modifiers are features of a building or its environment that affect resistance to damage. The use of SRCs can significantly impact losses sustained by residential, commercial, and industrial properties.

Verisk strongly encourages the collection of relevant exposure data, as the inclusion of SRCs in loss analysis can yield more accurate results and have a major impact on the view of risk.

The SRCs supported in this model are presented below.

See Also

Flood Damage Functions

Foundation Type

The type of building foundation has a significant impact on its flood vulnerability. Basements can greatly increase the susceptibility to flood damage at low water depths, while cripple wall crawl spaces can easily buckle or be damaged from water. The foundation type SRC is available for all residential (except mobile homes) and commercial buildings. The following foundation types are supported:

- Unknown
- Masonry basement
- Concrete basement
- Crawl space - cripple wall
- Crawl space - masonry
- Crawl space - raised (wood)
- Post and pier
- Footing
- Mat/slab
- Pile
- No basement
- Engineered foundation

Number of Basement Levels

While basements increase flood vulnerability, multiple basement levels are usually found in high-rise and other large commercial buildings or apartment complexes. These buildings also have a higher level of engineering and are therefore equipped with better flood protection systems.

Used in conjunction with masonry or concrete basement foundation types, this feature indicates the number of basement levels. For general residential, single family homes, or multi-family homes, only one level is supported. For all other residential (except mobile homes) and commercial buildings, multiple levels can be entered, indicated by a number.

Basement Finish

Used in conjunction with masonry or concrete basement foundation types, this feature uses a numerical designator to indicate if the basement is unfinished or finished. Finished basements are equipped with interior features such as drywall, plaster, insulation, and flooring, and also contain more valuable contents than unfinished basements.

Custom Elevation

The elevation of the local ground surface (in feet) can be entered for this feature, which will override the underlying modeled digital terrain elevation. The model uses 10-meter digital terrain data to represent ground elevation. A higher surface elevation can significantly reduce flood damage and loss.

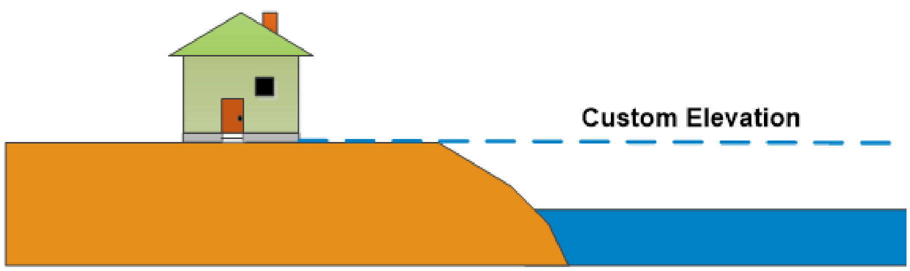

Figure 174. Custom elevation

Base Flood Elevation (BFE)

FEMA defines the base flood elevation as the "water surface elevation corresponding to a flood having a 1% probability of being equaled or exceeded in a given year." Thisis essentially the water elevation (in feet) expected for a 100-year flood. When this information is provided, the model will assume that the building has its lowest floor (including the basement, if any) at the base flood elevation. Base flood elevation is supported for all residential, commercial, and small industrial buildings and is typically measured/referenced with respect to the datum (NAVD88).The model then subtracts the ground elevation (default model assumed value or user input custom elevation value) determine the height of the first floor above the local ground surface.

Note: Any input for First Floor Height (described below) will override BFE values.

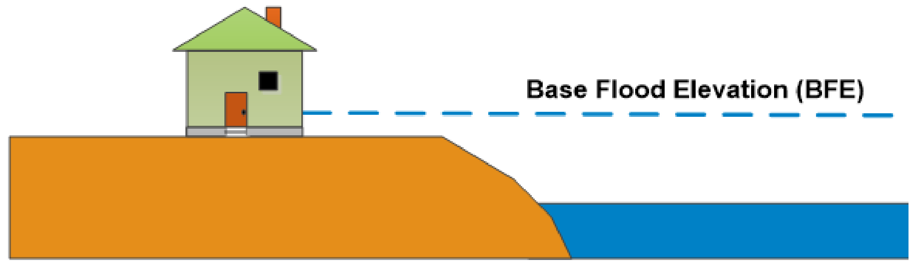

Figure 175. Base flood elevation

First Floor Height (FFH)

The height of the first floor (in feet), above the ground surface can be entered for all residential, commercial, and small industrial buildings. This overrides the BFE entry. A raised first floor significantly reduces a building's vulnerability to flood damage.

Note: User input FFH (in feet) is with respect to the local ground surface, while user input BFE is with respect to the datum (NAVD88).

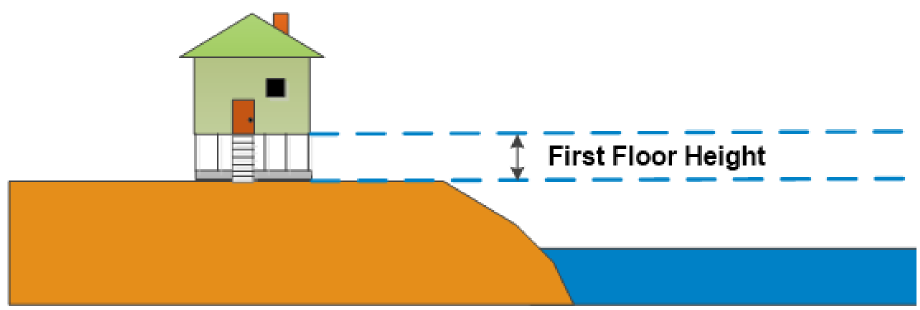

Figure 176. First floor height

Custom Flood Protection

For buildings that are protected by a custom flood protection system such as a levee or flood wall, this feature provides the height of the custom flood protection system (in feet), above the ground surface.

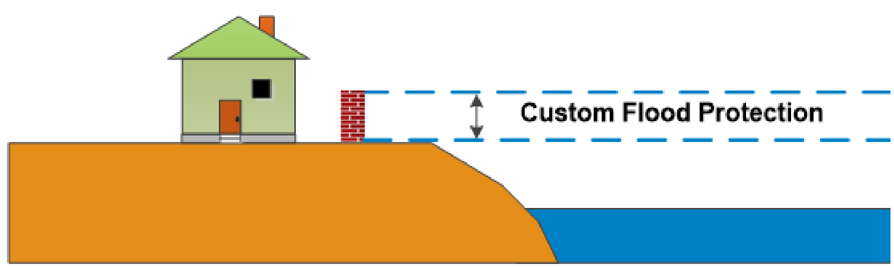

Figure 177. Custom flood protection

Service Equipment Protection

Mechanical, electrical, or plumbing service equipment can be designated as protected or unprotected using a numerical designator. Protection can be provided by elevating the equipment, or having some type of flood-proofing. This is supported for all residential, commercial, and small industrial buildings.

Floor of Interest

In cases where the entire building is not covered under the insurance policy, the floor of interest (including a basement) can be entered with a numerical input. Replacement values (building, contents, and business interruption) and policy terms will be applied for the floor of interest only. This is supported for all residential (except mobile homes) and commercial buildings.

Contents Vulnerability

If some of a building's contents are resistant to water damage, or have flood protection, then an indication of the portion of contents that have a low vulnerability can be entered for all residential, commercial, and small industrial buildings. The following options are available for contents vulnerability:

Low	An unusually large percentage of the contents are water-resistant or protected against flood damage
Moderate	A typical percentage of the contents are water-resistant or protected against flood damage
High	A low percentage of the contents are water-resistant or protected against flood damage
Very High	Almost none of the contents are water-resistant or protected against flood damage

Builders Risk

Project phase code and project completion may be entered as secondary risk characteristics. Users are required to input policy start and end dates to estimate losses for different construction phases, average annualized project loss, and worst case loss.

See Also

Builders Risk

Custom Flood Zone

Verisk damage functions vary by flood zone. Users can specify which flood zone the exposure lies in by specifying one of the following FEMA flood zones:

0	Unknown (Default)
1	Zone A (within the 100-year floodplain)
2	Zone V (coastal flood zone)
3	Zone X (area with no flood hazard map or outside the 500-year floodplain)
4	Zone X500 (beyond the 100-year floodplain and inside the 500-year floodplain)

If data are not specified, the model uses a FEMA flood zone layer.

In order to map the Verisk Custom Flood Zone Value, Verisk recommends users use Table 22.

Table 22. Verisk Custom Flood Zone Values

Custom Flood Zone	FEMA Flood Zone	Description
0		Data unavailable. This is the default value.
1	A	An area inundated by 100-year flooding, for which no Base Flood Elevations have been determined.
1	AE	An area inundated by 100-year flooding, for which Base Flood Elevations have been determined.
1	AH	An area inundated by 100-year shallow flooding (usually an area of ponding), for which Base Flood Elevations have been determined; flood depths range from 1 to 3 feet.
1	AO	An area inundated by 100-year shallow flooding (usually sheet flow on sloping terrain), for which average depths have been determined; flood depths range from 1 to 3 feet.
1	AOVEL	An alluvial fan inundated by 100-year flooding (usually sheet flow on sloping terrain), for which average flood depths and velocities have been determined; flood depths range from 1 to 3 feet.
1	AR	An area inundated by flooding, for which Base Flood Elevations or average depths have been determined. This is an area that was previously, and will again, be protected from the 100-year flood by a Federal flood protection system whose restoration is federally-funded and underway.
1	A99	An area inundated by 100-year flooding, for which no Base Flood Elevations have been determined. This is an area to be protected from the 100-year flood by a federal flood protection system under construction.
1	100IC	An area where the 100-year flooding is contained within the channel banks and the channel is too narrow to show to scale. An arbitrary channel width of 3 meters is shown. Base Flood Elevations are not shown in this area, although they may be reflected on the corresponding profile.

Custom Flood Zone	FEMA Flood Zone	Description
2	V	A coastal flood zone, inundated by 100-year flooding with velocity hazard (storm-induced waves); no Base Flood Elevations have been determined.
2	VE	A coastal flood zone, inundated by 100-year flooding with velocity hazard (storm-induced waves); Base Flood Elevations have been determined.
2	FPQ	An area designated as a “Flood Prone Area” on a map prepared by USGS and the Federal Insurance Administration. This area has been delineated based on available information on past floods. This is an area inundated by 100-year flooding for which no Base Flood Elevations have been determined.
2	FWIC	An area where the floodway is contained within the channel banks and the channel is too narrow to show to scale. An arbitrary channel width of 3 meters is shown. Base Flood Elevations are not shown in this area, although they may be reflected on the corresponding profile.
2	IN	An area designated as within a “Special Flood Hazard Area” (or SFHA on a FIRM. This is an area inundated by 100-year flooding for which Base Flood Elevations or velocity may have been determined. No distinctions are made between the different flood hazard zones that may be included within the SFHA. These may include Zones A, AE, AO, AH, A99, AR, V, or VE.
3	X	Zones B, C, and X are low-risk areas that are outside the 100- and 500-year floodplains or are protected by levees. These zones have a 1% annual change of sheet flow flooding where average depths are less than one foot, and 1% annual chance of stream flooding where the drainage area is less than 1 square mile. There are no base flood elevations or depths in these zones.
3	OUT	An area designated as outside a “Special Flood Hazard Area” (or SFHA on a FIRM. This is an area inundated by 500-year flooding; an area inundated by 100-year flooding with average depths of less than 1 foot or with drainage areas less than 1 square mile; an area protected by levees from 100-year flooding; or an area that is determined to be outside the 100- and 500-year floodplains. No distinctions are made between these different conditions. These may include both shaded and un-shaded areas of Zone X.
3	500IC	An area where the 500-year flooding is contained within the channel banks and the channel is too narrow to show to scale. An arbitrary channel width of 3 meters is shown.
4		A body of open water, such as a pond, lake ocean, etc., located within a community’s jurisdictional limit, that has no defined flood hazard.

Custom Flood Zone	FEMA Flood Zone	Description
4	X500	An area inundated by 500-year flooding; an area inundated by 100-year flooding with average depths of less than 1 foot or with drainage areas less than 1 square mile; or an area protected by levees from 100-year flooding.
4	D	An area of undetermined but possible flood hazards.
4	UNDES	A body of open water, such as a pond, lake ocean, etc., located within a community's jurisdictional limit, that has no defined flood hazard.

See Also

NFIP Flood Hazard Zones and Building Standards

FIRM Compliance

FIRM compliance indicates if a building's design and construction comply with NFIP guidelines and requirements. The following options are available in the model:

Unknown	If FIRM compliance is entered as unknown but a year-built is specified, compliance is assumed based on the community FIRM adoption.
Yes	A value of yes will override any model assumption of the exposure's age or year built and the software will model the structure as a post-FIRM building. If the exposure falls inside a SFHAs and has a BFE the model will enable the Base Flood Elevation secondary feature; for locations without BFE the model will use the default assumptions of first floor height as explained in the Foundation and First Floor Height section of this document.
No	A value of no will override any model assumption of the exposure's age or year built, and the software will model the structure as a pre-FIRM building.

See Also

Foundation Type and First Floor Height

Wet Floodproofing

Wet floodproofing indicates the level of floodproofing or mitigation measures at the location of interest. Protection can be in the form of the equipment and stock protection, it also accounts for the use of flood openings in the foundation wall, such as vents. The following options are available:

Unprotected	No protection
Low protection	Up to 1 ft elevation
Medium protection	Up to 3 ft elevation
High protection	Above 3 ft elevation

5.12 Validating the Model's Damage Functions

Verisk developed the flood damage functions based on a large volume of published research, engineering analyses, aggregate and detailed insurance loss experience data, and economic loss data. Data sources include FEMA and its affiliated agencies such as the Federal Insurance and Mitigation Administration (FIMA), the U.S. Army Corps of Engineers (USACE) and claims data from the NFIP program available through the OpenFEMA program.[80]

As discussed previously, the model's damage functions provide the mean damage ratio (MDR) for increasing water depth, where the MDR is the ratio of the repair cost to replacement value. Therefore, validating the damage estimation component of the model is inextricably intertwined with validating modeled losses.

USACE Damage Functions and NFIP Claims Data

USACE has conducted many studies that include both expert opinion-based and survey-based damage functions. Sources used to validate the damage functions include the USACE Louisiana report (USACE, 2006) and a catalog of USACE functions (Davis and Skaggs, 1992). Some of the USACE functions were also incorporated into FEMA's HAZUS flood loss methodology (FEMA, 2018).

In addition to these empirical and survey-based functions, Verisk engineers used NFIP flood claims published by OpenFEMA to validate the damage functions. The NFIP claims data include a claim's value as well as the coverage for the corresponding flood insurance policy. A ratio of the actual claim paid to coverage serves as the proxy MDR used for comparisons presented below. An advantage of NFIP claims data, over USACE data, is the availability of data for use in validation of additional secondary features such as flood zone, impact of FIRM compliance, and foundation types.

Validation of Damage Functions for Residential Buildings and Contents

Figure 178 compares the Verisk damage function for a single-story residential building on slab with the USACE function and the NFIP claim-derived MDR. Since NFIP includes a large number of claims, there is a large degree of uncertainty associated with the NFIP MDR as shown by the 95% confidence interval bounds around the mean (Figure 178). Figure 178 shows the possible uncertainty around the NFIP MDR.

Survey data as well as claims data show that even within a flood footprint, there will be buildings that escape damage altogether. The model's damage functions provide estimates of the mean, or expected, damage ratios corresponding to the hazard at each site. These mean damage ratios reflect the average of damaged and undamaged properties as a result of hazard uncertainty, flood resistance, preparedness, and early warning. In the NFIP claims data and USACE function, all the properties are damaged (Figure 178). Hence, the Verisk damage function is lower than the mean claims and the USACE function at lower depths. At

80 https://www.fema.gov/media-library/assets/documents/180374

higher depths, the Verisk function gets closer to the USACE function. This is expected, since at high levels of hazard intensity the proportion of the buildings that are undamaged are low.

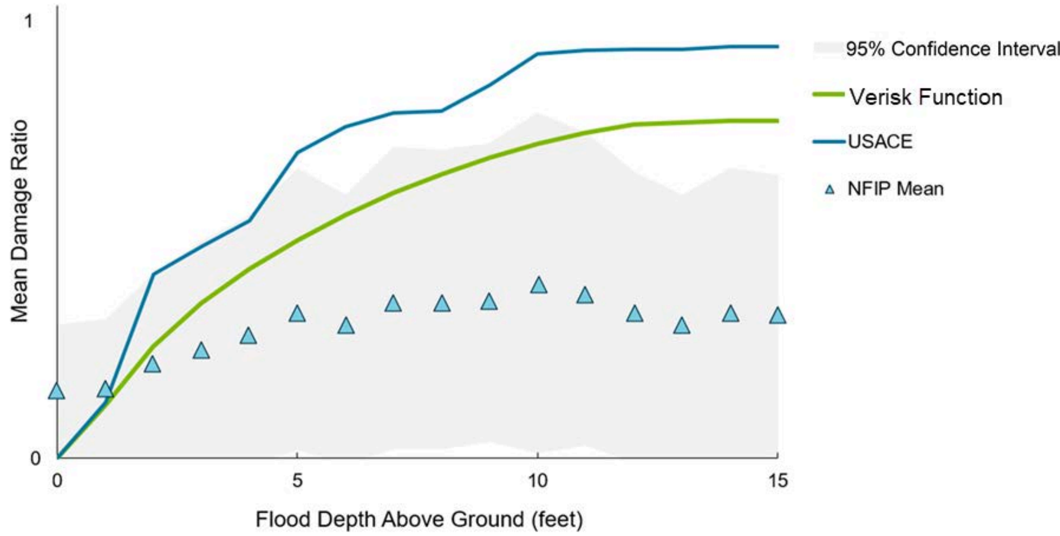

Figure 178. Verisk damage function for single-family homes on slab, USACE function and NFIP Claims

Verisk also used these data sources have also been to understand relative vulnerabilities of different features. Figure 179 shows the relative vulnerability of the Verisk damage function for a single-family homes with and without a basement compared with other data sources, such as USACE, HAZUS, FIA as well as NFIP claims. The relative vulnerability is expressed here as a ratio of the MDR of a single-family home with a basement to the MDR of a single-family home without a basement. Hence, a MDR ratio of above 1 for most flood depths confirms the model assumption that the presence of a basement increases flood vulnerability. NFIP claims, however, do not exceed an MDR ratio of 1 (Figure 179). This is largely due to the fact that NFIP often does not insure all components in basements, resulting in claims that show a lower vulnerability for a single-family home with a basement. As illustrated in the figure, the Verisk damage functions are in agreement with the USACE and HAZUS sources.

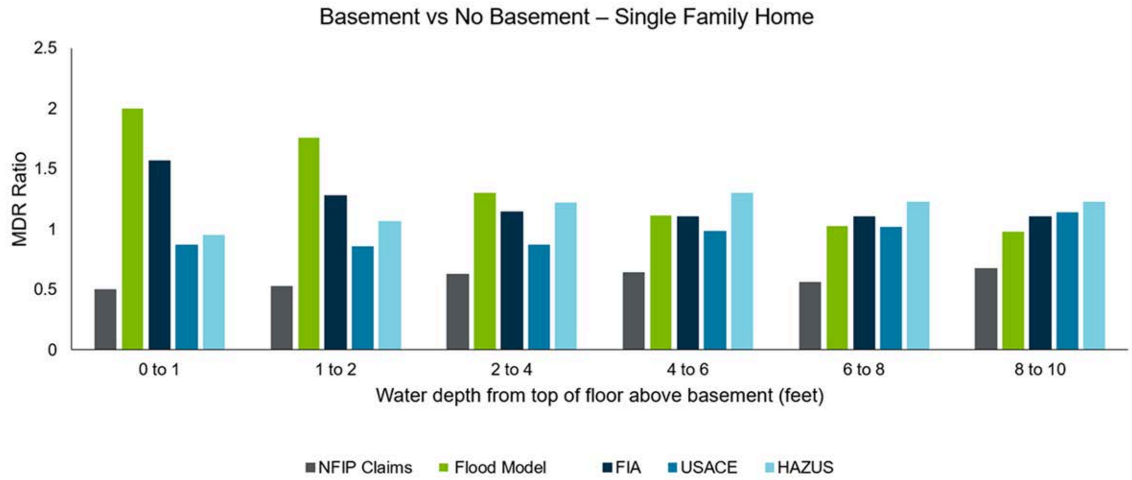

Figure 179. Relative vulnerability comparison for single-family homes with basement to single-family homes with no basement

Figure 180 and Figure 181 present relative vulnerability comparisons for flood zone X and FIRM compliance, respectively. Both figures present modeled MDRs for one-story, single-family homes with no basement, compared to NFIP claims data. Figure 180 compares MDR ratio of a single-family home in flood zone X to flood zone A. At lower flood depths, a single-family home in flood zone X is more vulnerable than a single-family home in flood zone A, as is evident from the greater than 1 ratio. The relativity between flood zones shows a good agreement between claims data and Verisk model at most depths. The Verisk model, again, show larger relativities between 0 to 2 feet because the model accounts for more presence of finish basements in flood zone X than what is observed in the NFIP exposure.

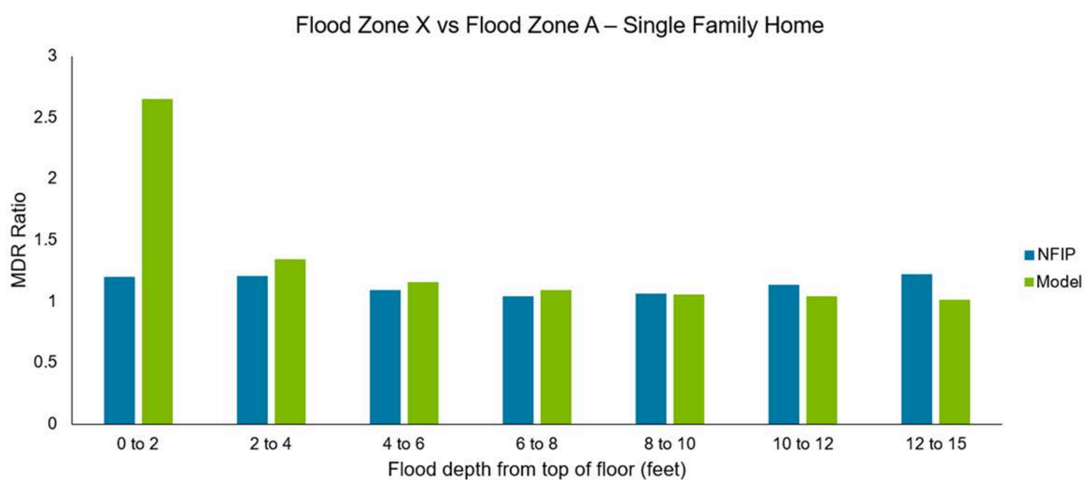

Figure 180. Relative vulnerability of one-story, single-family homes in flood zone X with respect to flood zone A, modeled (Verisk) v. observed (NFIP)

Figure 181 compares the MDR ratio of a post-FIRM single-family home to a pre-FIRM single-family home. One of the most important FIRM-complaint guidelines is to elevate the first floor, which results in an MDR ratio less than 1 at lower flood depths. As flood depths increase, the impact of FIRM compliance is less.

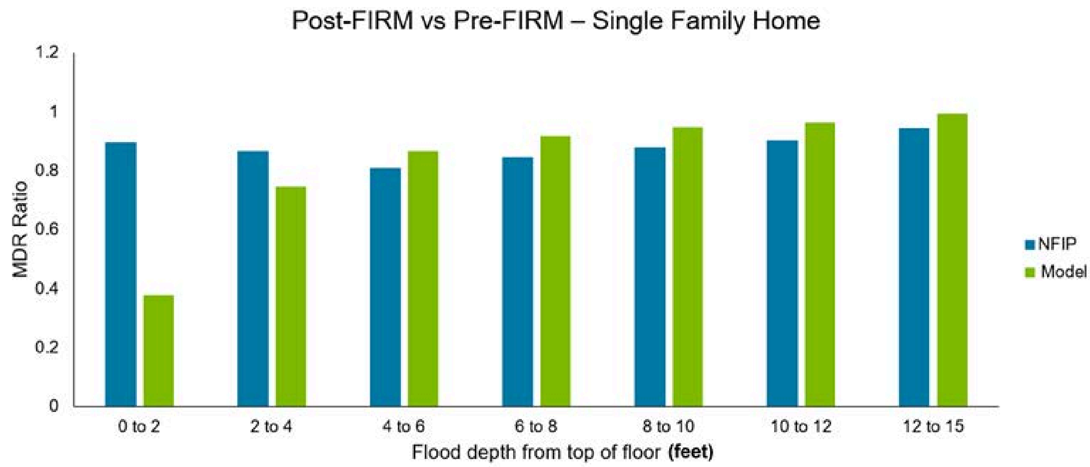

Figure 181. Relative vulnerability of one-story, post-firm, single-family homes and pre-firm single-family homes, modeled (Verisk) v. observed (NFIP)

Verisk also validated damage functions for residential contents with USACE and NFIP claim data. Figure 182 shows the relative vulnerability of contents with respect to the building damage function for different flood depths. Contents are typically more vulnerable to flood damage than the building, as reflected in Figure 182, where the MDR ratio (building MDR to content MDR) is less than 1.0 for most water depths.

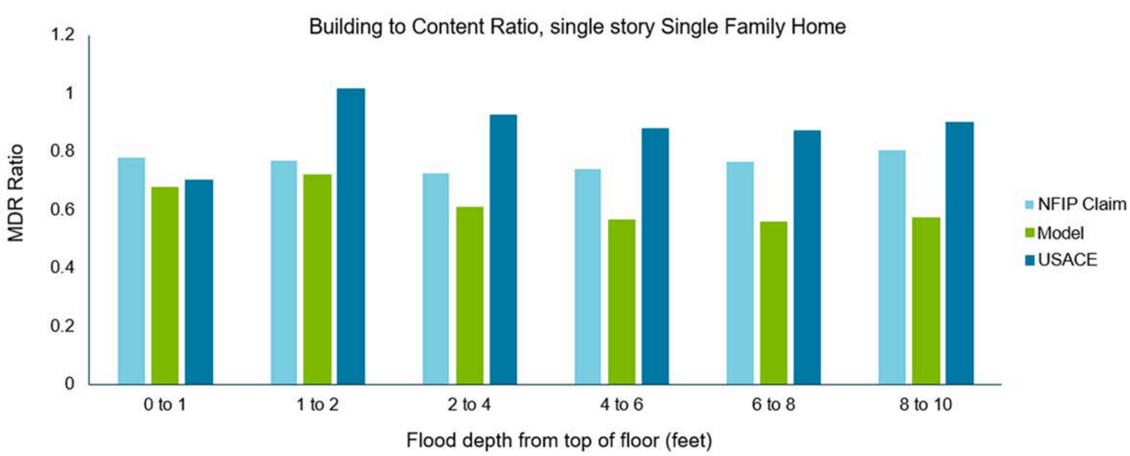

Figure 182. Relative vulnerability of contents and buildings for a one-story, single-family home, modeled (Verisk) v. observed (USACE and NFIP)

See Also

Uncertainty Around the Mean Damage Ratio

Validation of Damage Functions for Commercial Buildings and Contents

Verisk validated damage functions for commercial and small industrial (300-series) buildings, using claims data for similar occupancy types when available. Figure 183 shows the Verisk damage function for an unknown commercial occupancy along with the USACE damage function and NFIP flood claim mean MDR. The Verisk damage function is built from a combination of various commercial occupancies, whereas the USACE damage function and NFIP claims focus on small commercial properties only. It can be observed that our commercial damage function resembles the USACE source.

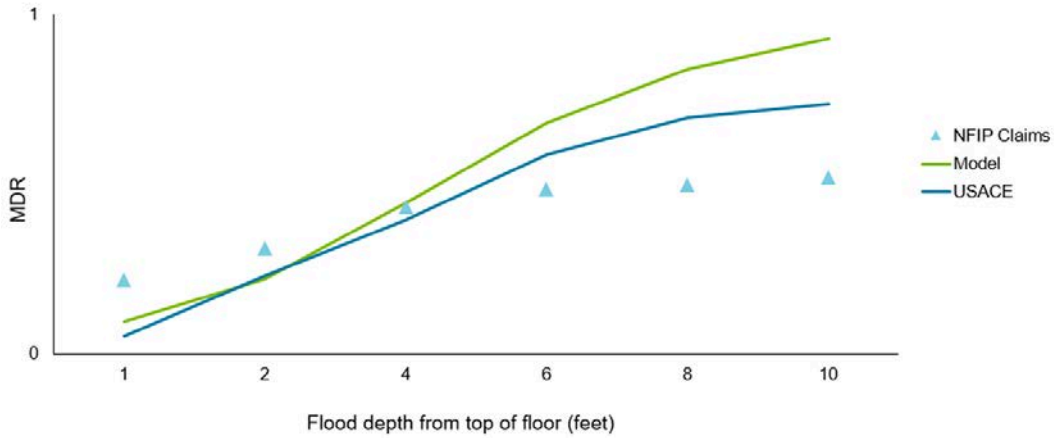

Figure 183. Verisk damage function for an unknown commercial building and comparison with USACE damage function and NFIP claims data

Figure 184 shows the relative vulnerability of commercial contents, comparing the Verisk model with USACE and NFIP claims data. Similar to residential occupancies, the building to contents MDR ratio is less than 1 for commercial occupancies and the Verisk model shows a good agreement with the data.

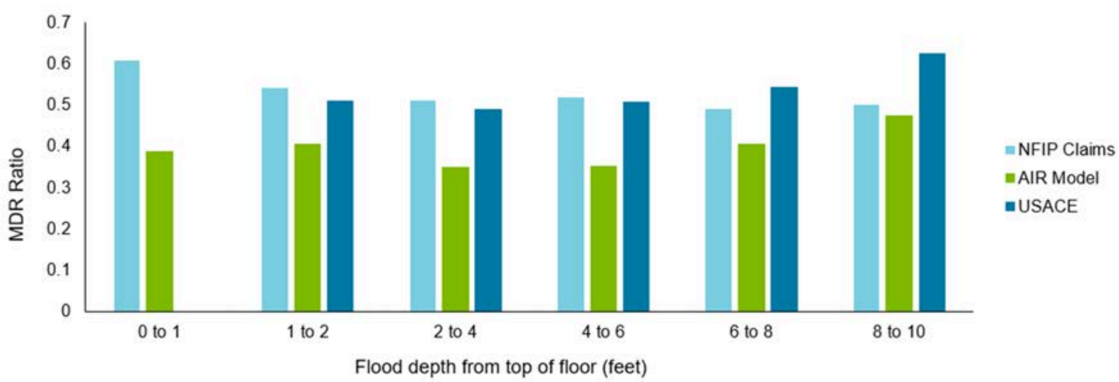

Figure 184. Relative vulnerability of building to contents for commercial occupancy

Figure 185 shows relative vulnerability of commercial to residential occupancies for a single-story building and comparison with USACE and NFIP claims data. While commercial buildings are less vulnerable than residential buildings (MDR ratio less than 1) at all flood depths, the contents relativity shows the opposite trend. The Verisk model relativities are consistent between the claims data and published USACE damage functions.

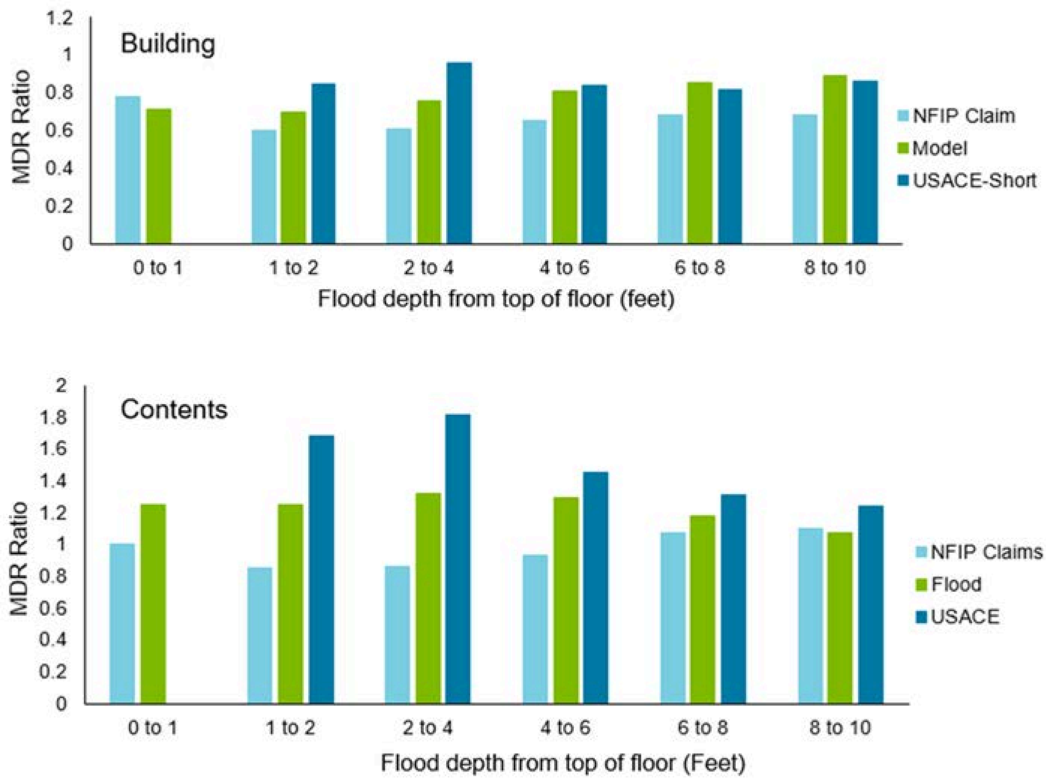

Figure 185. Relative vulnerability of commercial and residential MDRs for building and content

6 Insured Loss Calculation

In this component of the Verisk Inland Flood Model for the United States, ground-up damage is translated into financial loss. Insured losses are calculated by applying the standard FEMA National Flood Insurance Program (NFIP) and private market flood policy conditions to the total damage estimates resulting from the damage estimation module. The standard NFIP policy conditions do not include either time element (business interruption) or automobile coverage. Policy conditions may include franchise deductibles, coverage limits, loss triggers, and risk-specific reinsurance terms.

6.1 Aggregating Losses Probabilistically

Post-disaster surveys and actual claims data reveal an inherent variability in the damage that results from a given flood depth. Loss estimates generated by the Verisk Inland Flood Model for the United States capture this variability by accounting for both primary and secondary uncertainty. Primary uncertainty derives from the uncertainty associated with the event generation process (i.e., the stochastic catalog), while secondary uncertainty describes the uncertainty in damage resulting from a given event. This secondary uncertainty captures the uncertainty in damage *and* in the local intensity estimation. The uncertainty in building damage arises due to inherent randomness in the response of buildings of similar construction to a given intensity, as well as from variability in building characteristics, construction materials, workmanship, etc. The uncertainty in local intensity of the hazard can be attributed to unmodeled phenomena, local site factors, and the presence of small-scale processes within atmospheric systems.

Damage is calculated by damage functions that provide, for a given event intensity, a mean damage ratio (MDR) and a probability distribution around the mean that captures the variability in damage. For the Verisk Inland Flood Model for the United States, the transformed beta family of distributions combined with empirically derived probabilities of 0% and 100% damage levels are used to model the uncertainty around the mean damage. The damage functions are used to produce, for each event, a distribution of ground-up loss by location and coverage. Limits, deductibles, and reinsurance are applied in the financial module to the ground-up loss distribution to produce gross and net loss estimates.

In the financial module there clearly is a need for probabilistically aggregating losses at various levels. Specifically, computational techniques are developed for statistically aggregating non-parametric distributions. Even though the ground-up, coverage-level damage distributions typically use parametric distributions, after the application of location and policy terms, the distributions cannot be represented in a parametric way. Further aggregations of such loss distributions are achieved using numerical algorithms.

Convolution is a method used to statistically derive the probability distribution of the sum of losses. The convolution of two independent random variables X and Y with discrete probability density functions p_X and p_Y , respectively, can be computed as:

$$p_S(s) = p_X \oplus p_Y = \sum_x p_X(x) p_Y(s-x)$$

where $S = X + Y$.

The Verisk models employ an efficient and accurate numerical algorithm for "convolving" any number of non-parametric loss distributions. However, extreme care must be taken when combining distributions with differing loss sizes. This convolution technique allows the shape of the loss distributions to be correctly represented throughout the financial loss estimation process. Preserving the right shape is particularly important when insurance terms apply to the "tails" of the distributions.

The financial module within Verisk's software applications allows for a wide variety of location, policy, and reinsurance conditions. Location terms may be specified to include limits and deductibles by site or by coverage. Supported policy terms include blanket and excess layers, minimum and maximum deductibles, and sublimits. Reinsurance terms include facultative certificates and various types of risk-specific and aggregate treaties with occurrence and aggregate limits. For additional information, see the product-specific documentation available from the Client Support section of Verisk's website (http://www.air-worldwide.com/) as well as details on the industry standard UNICEDE data format (www.unicede.com).

6.2 Demand Surge

Demand surge is the sudden, and usually temporary, increase in labor and materials costs driven by high demand following a catastrophe and widespread property damage. An affected area might also experience increased demand for services and resources (e.g., transportation, equipment, and storage). The greater and more widespread the damage, the greater the resulting demand surge and insured losses.

Scarce resources can also increase the time required to repair or rebuild. Such delays may affect business interruption losses and living expenses. Infrastructure damage, delayed building-permit processes, and a shortage of available building inspectors also increase time-element loss. These factors can result in insured losses that exceed expectations for a particular event and portfolio.

Verisk developed the default demand surge function using economic principles, and validated the function against U.S. loss levels and component cost analyses. Details can be found in The Verisk Demand Surge Function, available on the Client Portal.

6.3 Validating Modeled Losses with Historical Data

Modeled losses calculated by the Verisk Inland Flood Model for the United States have been validated through extensive analysis of both insurable and insured aggregate annual loss data as reported by several sources. Sources of insured losses include FEMA's NFIP, private market losses from Verisk's sister companies Xactware® and ISO Property Claims Services (PCS®), and company claims data. Insurable ground-up losses are reported by multiple sources, including the National Oceanic and Atmospheric Administration's (NOAA's) National Center for Environmental Information's (NCEI's) Storm Events Database[81]. As a result, close to USD 70 billion in NFIP loss data over four decades (1978-2018) and more than USD 14 billion of commercial claims data (with more than USD 4 billion in policy level claims from 4,200 policies) were used in this model's validation.

Leveraging NFIP Data for Inland Flood Model Validation

NFIP exposure and claims data are a major source of benchmark data used to validate the Inland Flood Model for the United States. These NFIP data from 1978 to 2012 were collected as part of a rigorous location-level Flood Insurance Risk Study (FIRS; *National Flood Insurance Program: Report to Congress,* 2015). This database was augmented with 2013-2018 publicly available NFIP exposure and claims data released by FEMA in 2019[82]. The resulting NFIP claims dataset includes inland flood losses modeled by the Verisk Inland Flood Model for the United States (i.e. all precipitation-induced flood events other than hurricanes) and the Verisk Hurricane Model for the United States (hurricane storm surge and precipitation-induced flood), as well as losses from unmodeled perils (e.g., storm surge caused by winter storms). Prior to using this dataset for validation and calibration, flood losses were grouped into flood sub-peril cause of loss (e.g., storm surge, non-hurricane precipitation-induced flood, hurricane precipitation-induced flood). Next, storm surge and unmodeled events were removed, and the remaining modeled event losses were trended to present-day loss values.

Identifying Historical Events

Verisk researchers grouped the NFIP dataset into historical events based on their temporal and spatial distributions. By leveraging information from FEMA's Significant Flood Events Report, significant events that resulted in at least 1,500 paid losses were first identified. Since FEMA's report only provides the month in which a given event occurred, Verisk researchers plotted the total number of claims filed within a loss date spanning from one month prior to one month after the report's listed date. Any substantial increase in the total number of claims filed over a short time period were identified and mapped to determine if these claims corresponded to the reported event's location. The geographic extent of an event was hand-selected based on the clustering of claims data. The resulting subset of loss data within this geographical region were assigned an event for additional analysis. This process was repeated for the entire NFIP database.

Next, Verisk researchers grouped the NFIP loss claims data based on cause of the loss. Tropical storms and hurricanes associated with location-level inland flood claims between 1978 and 2012 were identified using the National Oceanic and Atmospheric Administration's (NOAA's) National Hurricane Center's (NHC's) HURricane DATabase 2nd generation (HURDAT2). This database includes tropical cyclone information on the location, central pressure, and maximum winds on all known historical tropical cyclones at six-hour intervals

[81] NOAA's NCEI's Storm Events Database: https://www.ncdc.noaa.gov/stormevents/
[82] FEMA significant events website: https://www.fema.gov/significant-flood-events

from storm formation through dissipation. Using these data, tropical storm and hurricane tracks were plotted. Next, a region defined by the geographical extent of tropical storm force windspeed was applied to the track to determine the geographic area likely impacted by each storm. Historical NFIP claims were assigned to a given storm event if they met the following criteria:

- Located within a region defined by the geographical extent of tropical storm force winds
- Occurred within a time period extending from 2 days before landfall through the storm's dissipation
- Filed within one year of the event

Verisk researchers relied on additional data (e.g., PCS and the NCEI) to identify non-location level claims data associated with tropical storms and hurricanes post-2012. Post-2012 PCS claims that occurred in one of the impacted states and within a specified date range of a known tropical storm or hurricane were labeled as tropical storm or hurricane losses, respectively.

Figure 186 below shows the yearly NFIP flood loss claims data (blue) and the subset of non-hurricane precipitation-induced flood loss (green) claims data modeled by Verisk's Inland Flood Model for the United States compared to all sources of NFIP losses. It is evident that non-hurricane precipitation-induced flood losses have been a signficant contributor to the total amount of NFIP loss claims in the last few decades.

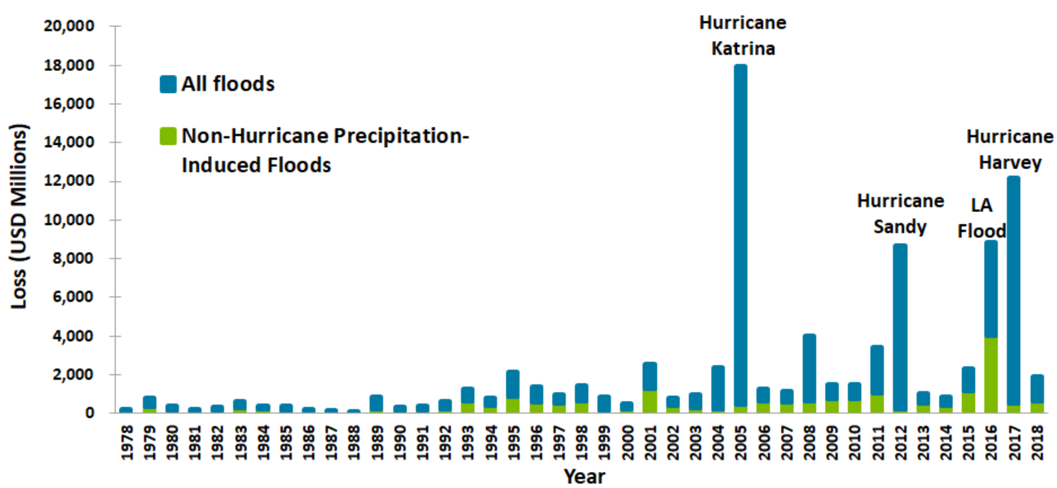

Figure 186. NFIP untrended claims paid by year due to non-hurricane precipitation-induced floods that are modeled in the Verisk Inland Flood Model for the United States (green) and for all floods combined (blue).

Since floods produced by hurricanes result from either storm surge or rainfall, Verisk researchers assigned a cause of loss to the NFIP claims associated with hurricanes. Verisk-developed storm surge inundation footprints were used to identify storm surge losses by intersecting the claims locations with these footprints. Claims located within the footprint of a given hurricane were labeled as hurricane storm surge losses; all other claims associated with this hurricane were labeled as hurricane precipitation losses. For post-2012 data, Verisk's storm surge footprints were used to identify a list of impacted ZIP codes. Claims that fell within these ZIP codes were labeled hurricane storm surge losses.

Grouping historical claims by weather event type and cause of loss provides a comprehensive understanding of the contribution each peril has on the total NFIP's historical losses. As seen in Figure 187 below, at 65%, storm surge losses represent the greatest percentage of total NFIP claims paid between 1978 and 2018 followed by inland flood (all precipitation-induced flood events other than hurricanes and tropical storms) losses at 24%. Unmodeled losses, at 1%, include storm surge losses resulting from Nor'easter storms. Verisk researchers validated the Verisk Inland Flood Model for the United States using claims data identified as non-tropical cyclone precipitation-induced flood and tropical storms. Verisk researchers used hurricane precipitation claims data to validate the precipitation-induced flood component of the Verisk Hurricane Model for the United States.

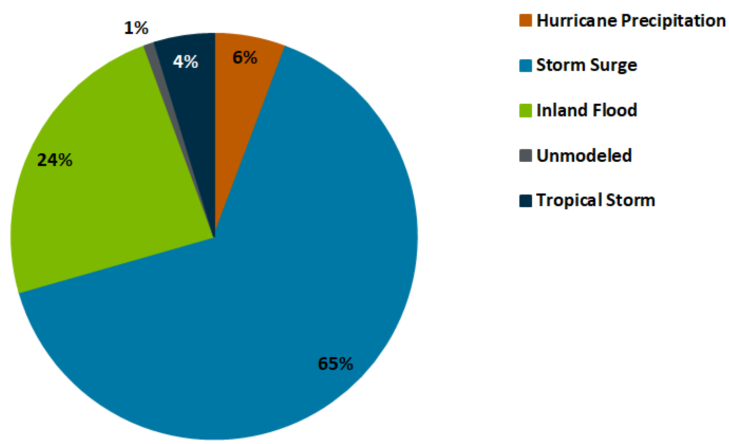

Figure 187. Distribution of NFIP untrended loss claims by cause of loss as well as the percentage of unmodeled losses (including attritional losses) between 1978 and 2018. The total amount paid includes building and contents losses.

Trending Losses

Historical losses need to be trended to present loss values by accounting for various factors, including changes in building stock, premium, vulnerability, and inflation over time, such that the modeled and industry-reported loss values can be compared. To account for these factors, Verisk researchers developed an exposure growth index based on regional changes in FEMA's portfolio growth and on increases in annual number of exposure growth ("risk count") from the event loss year to the end of 2019. Annual exposure risk count was estimated by ZIP code and by occupancy for each year from 1994 to 2017. Next, trending factors for a given year-of-interest from 1994 – 2017 (TF_x) were estimated by taking the ratio of the 2018 risk count to the given year-of-interest's (x) risk count and multiplying by an inflation factor, as shown in the following equation:

$$(TF)_x = \frac{(Risk\ \ Count)_{2018}}{(Risk\ \ Count)_x} \times (Inflation\ \ Factor)$$

The Inflation Factor is measured in terms of implicit price deflator and is defined as the yearly average inflation and median home value change between 2019 and the year-of-interest, as shown in the following equation:

$$Inflation\ \ Factor = \frac{(Inflation)_{2019}}{(Inflation)_{year\ x}} \times \frac{(Median\ \ Home\ \ Value)_{2019}}{(Median\ \ Home\ \ Value)_{year\ x}}$$

Note that prior to 1994, FEMA-reported total policy count data[83] were used as a proxy for state-level risk count due to lack of exposure data. This count was used to trend the NFIP loss claims data between 1978 and 1993 to the equivalent 1994-dollar values. Then, these 1994 values were trended to 2019 using the equations above.

Figure 188 below shows a comparison between the original and 2019-trended yearly NFIP loss claims for non-hurricane precipitation-induced flood losses included in the Verisk Inland Flood Model for the United States.

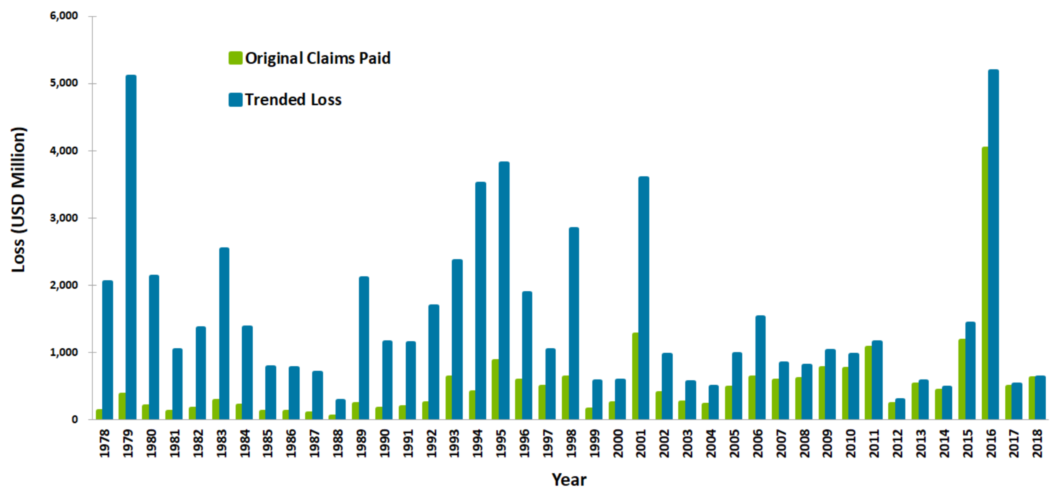

Figure 188. NFIP original (untrended; green) and 2019-trended (blue) yearly paid loss claims, including building and contents losses, for non-hurricane precipitation-induced flood losses included in the Verisk Inland Flood Model for the United States

Figure 189 below shows a distribution of 2019-trended NFIP losses by cause of loss as well as the percentage of unmodeled losses. These loss percentages are similar to the untrended NFIP loss percentages presented earlier. At 58%, storm surge losses still represent the greatest percentage of total NFIP claims paid between 1978 and 2018 followed by inland flood (all precipitation-induced flood events other than hurricanes and tropical storms) losses at 31%.

[83] FEMA-reported Policies in Force: https://www.fema.gov/statistics-calendar-year

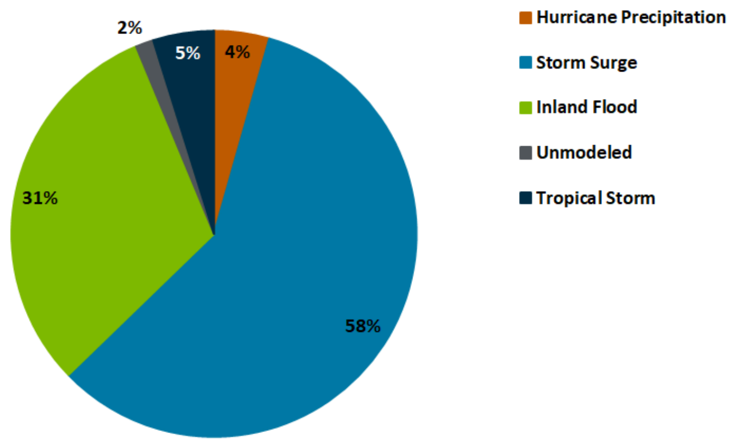

Figure 189. Distribution of 2019-trended NFIP losses claimed by cause of loss as well as the percentage of unmodeled losses (including attritional losses) between 1978 and 2018. The total amount paid includes building and contents losses.

Loss Validation Using NFIP Data

The loss module of the Verisk Inland Flood Model for the United States is extensively validated by comparing modeled historical event losses with NFIP insured non-hurricane pecipitation-induced flood losses trended to 2019. In order to obtain modeled view of insured losses, Verisk developed an exposure dataset that replicates NFIP's portfolio in force as of 2019. NFIP policy conditions by specific lines of business are applied to every exposure in the 2019 Industry Exposure Database, and take-up rates are estimated for each line of business based on flood zone and county to develop this NFIP-specific exposure view.

Figure 190 below compares Verisk-modeled and NFIP-observed (trended to 2019) non-hurricane precipitation-induced flood losses for the 20 storms available in the Verisk Inland Flood Model for the United States historical event set. It is evident that there is very good agreement between Verisk-modeled and observed losses for these 20 events.

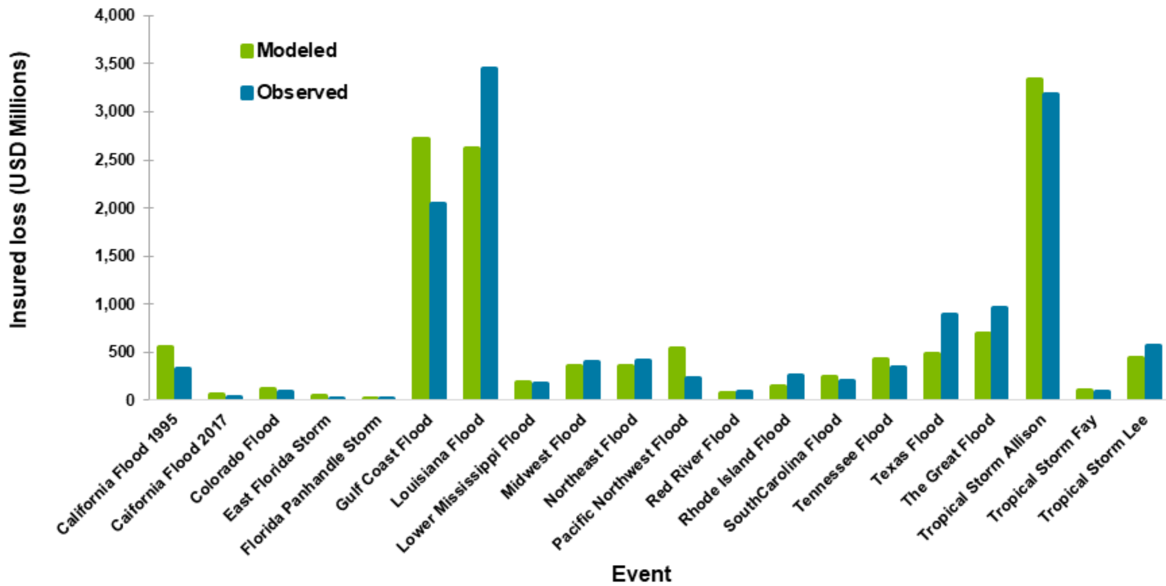

Figure 190. Comparison of Verisk-modeled (green) and observed (blue; source: NFIP claims data trended to 2019) insured non-hurricane precipitation-induced flood losses for the 20 events available in the Verisk Inland Flood Model for the United States' historical event set

Figure 191 below compares Verisk-modeled and 2019-trended NFIP-observed insured inland flood losses for the Midwest Flood of 2008, by state.

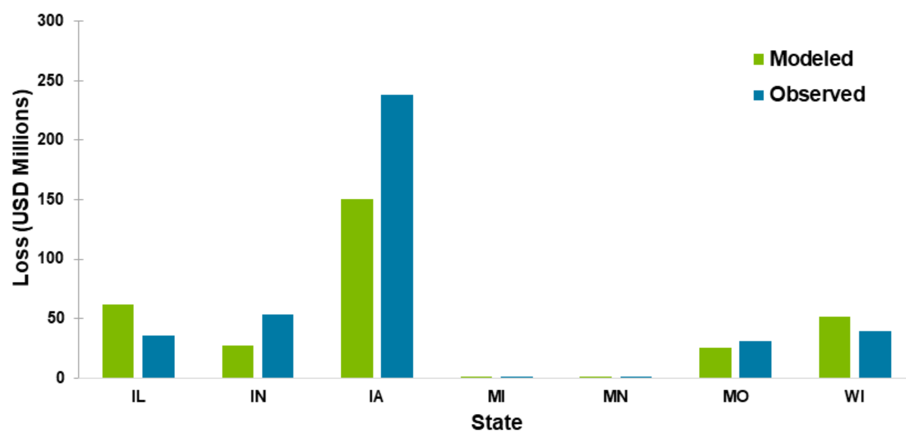

Figure 191. Comparison of Verisk-modeled (green) and observed (blue; source: NFIP claims data trended to 2019) insured inland flood losses, by state, for the Midwest Flood of 2008

The most plausible explanation for the modeled versus observed loss differences in Iowa (Figure 191) is the different exposure assumptions. Buildings that experience significant loss from a given event may be bulldozed or relocated to areas farther from the affected river to prevent such loss in the future. These changes are reflected in the Verisk Industry Exposure

Database and are used to model historical events. However, actual observed claims data include losses sustained by these buildings during the event. As a result, modeled losses often will be lower than observed losses for this historical event.

The two areal images of Cedar Rapids, Iowa in Figure 192 below depict the effect changing exposures has on losses. The image on the left was taken in 2008, and the image on the right was taken in 2013. As depicted, in 2008, there were more exposures located close to the river, as compared to 2013. Thus, resulting insured losses from claims data in 2008 in Iowa are greater than the modeled losses, which use the latest exposure data from the 2019 Verisk Industry Exposure Database.

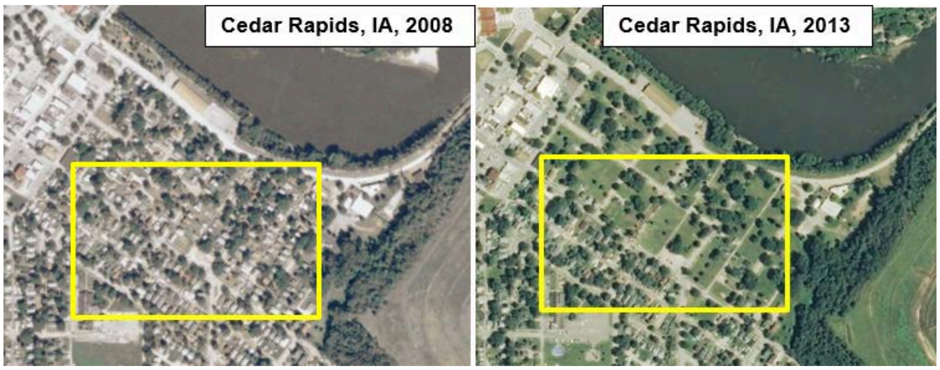

Figure 192. Two areal images of exposures in Cedar Rapids, Iowa from 2008 (left) and from 2013 (right; Source: US Department of Agriculture)

Figure 193 below shows the state-level contribution to the total insured loss for two significant loss-causing inland flood events: the 2016 Louisiana Flood and 2001 Tropical Storm Allison. This figure compares the modeled and observed (NFIP claims data trended to 2019) total insured inland flood losses. As illustrated, there is good agreement in total loss values for both the Louisiana Flood (left) and for Tropical Storm Allison (right). In addition, the Verisk Inland Flood Model for the United States accurately captures the high proportion of losses experienced in Texas from Tropical Storm Allison.

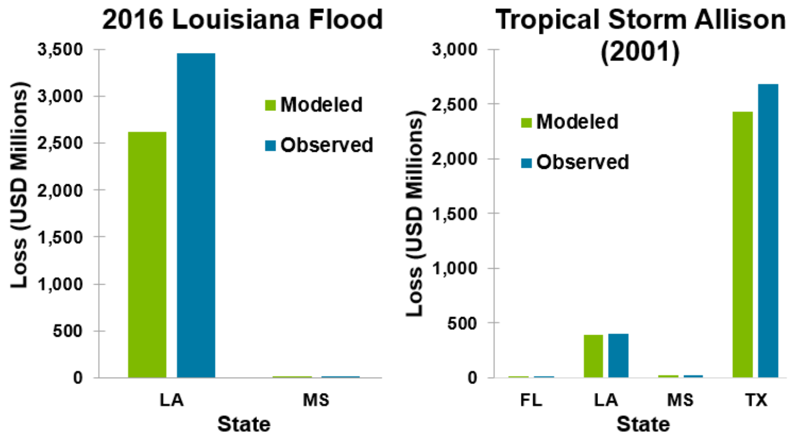

Figure 193. Comparison of modeled (green) and observed (blue; source: NFIP claims data trended to 2019) insured inland flood losses for the 2016 Louisiana Flood (left) and for 2001 Tropical Storm Allison (right), by state

Figure 194 below compares the percent contribution of Verisk-modeled and observed (NFIP claims data trended to 2019) total insured inland flood losses by lines of business for the 2016 Louisiana Flood and Tropical Storm Allison (2001). Lines of business include single-family homes (denoted "SFH"), apartment buildings, and commercial buildings, for buildings and contents combined.

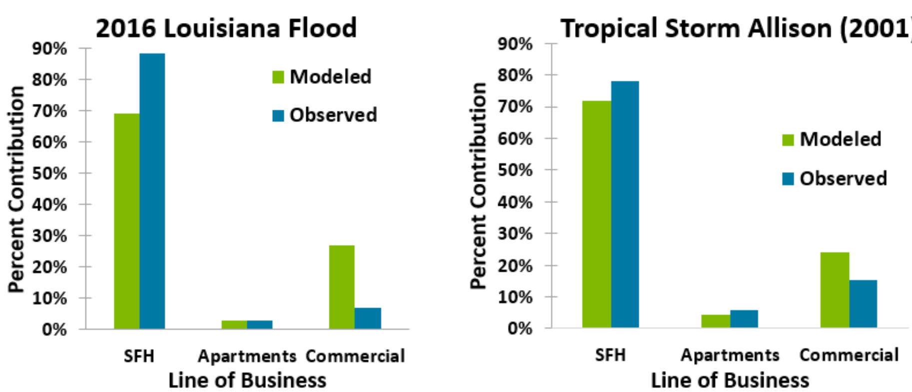

Figure 194. Comparison of the percent contribution of modeled (green) and observed (blue: source: NFIP claims data trended to 2019) total insured inland flood losses for the 2016 Louisiana Flood (left) and 2001 Tropical Storm Allison (right), by line of business and for buildings and contents combined. Single-family homes are denoted "SFH" in the above figure.

County-Level Historical Event Validation

Verisk compared modeled and observed (NFIP claims data trended to 2019) county-level insured non-hurricane precipitation-induced flood losses for several historical events. An example of this type of comparison performed for the 2016 Louisiana Flood is shown in Figure 195 below. As illustrated, there is good agreement between the observed and modeled losses at the county level, particularly for the counties surrounding Baton Rouge. Such comparisons of modeled and observed loss footprints at higher spatial resolutions are important to ensure that the model is capturing historical loss signatures at the most detailed level.

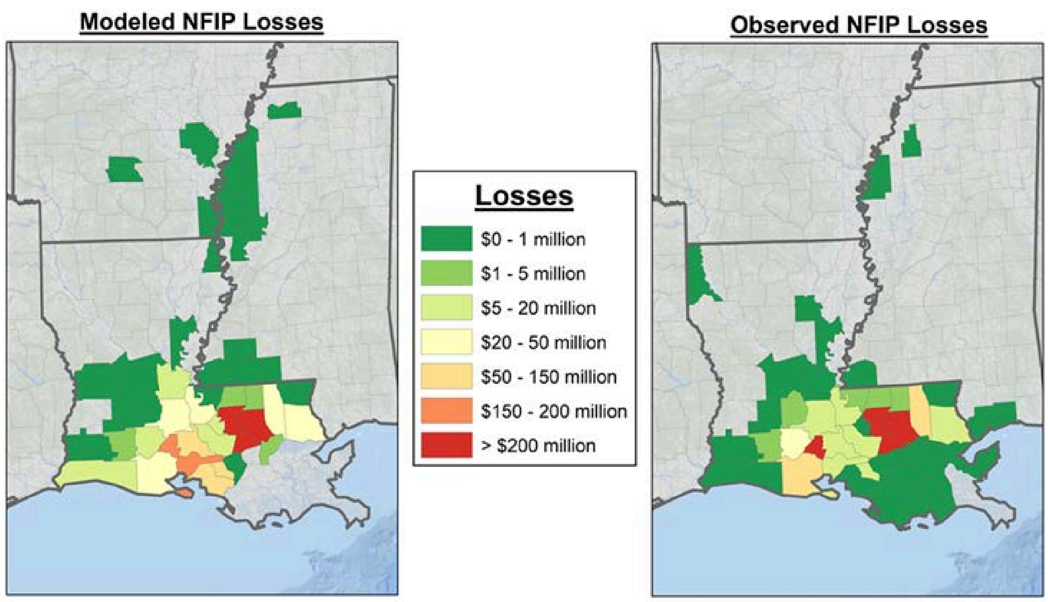

Figure 195. Comparison between Verisk-modeled (left) and observed (right; source: NFIP claims data trended to 2019) insured inland flood losses, at county-level

Average Annual Loss (AAL) Validation

In order to validate losses generated from the stochastic catalog, particularly the average annual loss (AAL), Verisk researchers compared the Verisk-modeled to NFIP-observed (trended to 2019) insured AAL due to non-hurricane precipitation-induced flood (Figure 196). The modeled AAL (USD 2 Billion) compares well to the NFIP AAL (USD 1.5 Billion) considering NFIP is a limited dataset of 40 years (1978 – 2018), whereas the modeled dataset uses a 10,000-year stochastic catalog. It is expected that the modeled AAL would be larger than the observed AAL because high-end events (e.g. a levee failure that results in extensive inland flooding) that are not captured in a limited observed dataset are included in the modeled dataset.

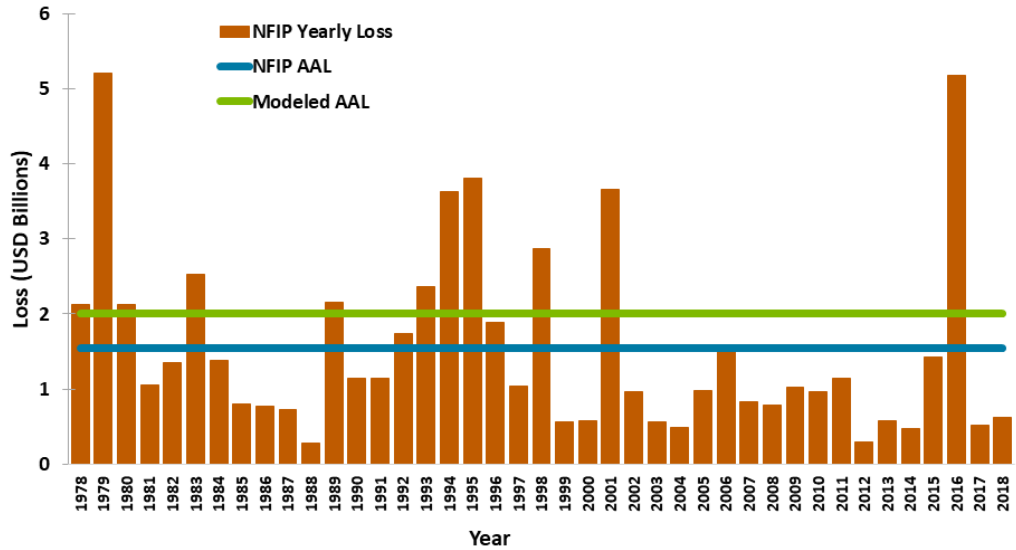

Figure 196. Comparison of Verisk-modeled (green) to observed (blue; source: NFIP claims data trended to 2019) insured non-hurricane precipitation-induced flood average annual loss (AAL). The NFIP observed yearly losses from 1978 to 2018, trended to 2019, are plotted in orange.

Exceedance Probability Validation

Verisk researchers benchmark the predicted frequency of losses that result from simulated floods as captured in the stochastic catalog. The reasonability of the modeled loss frequency is evaluated by comparing the simulated return period losses with actual loss experience.

To generate the historical exceedance probability (EP) curves, an extensive historical flood catalog created from a variety of sources is run in the model. Modeled losses rely heavily on the accuracy of the modeled vulnerability of the building stock as well as the frequency of floods and, particularly for occurrence losses, the model's ability to accurately detect individual storms that cause flood losses.

Figure 197 below presents modeled and observed (NFIP claims data trended to 2019) aggregate return period curves and gross aggregate average annual loss (AAL) for Texas and Florida. The modeled losses were calculated by running Verisk's 2019 Industry Exposure Database with NFIP's policy conditions, and the observed losses were generated using 40 years (1978 – 2018) of available NFIP claims data. Texas and Florida were chosen because they both have experienced significant non-hurricane precipitation-induced flood-related losses in last 40 years.

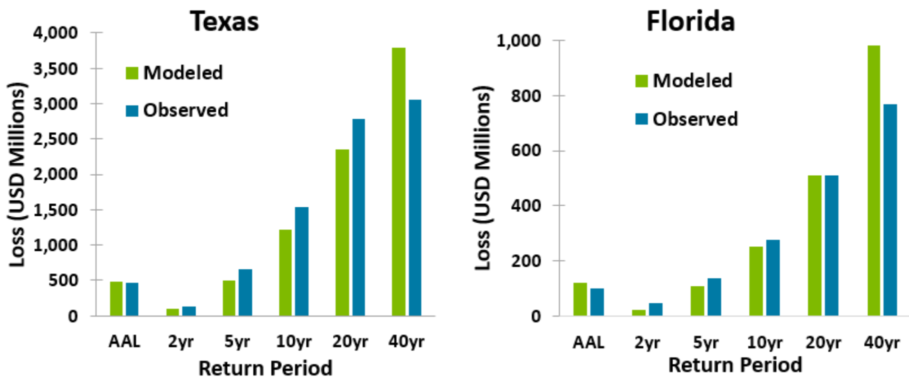

Figure 197. Non-hurricane precipitation-induced flood modeled (green) and observed (blue; source: NFIP claims data trended to 2019) gross insured aggregate average annual loss (AAL) and aggregate return periods for Texas (left) and Florida (right).

Loss Validation Using ISO Property Claims Services (PCS) Data

For additional validation, Verisk researchers compared modeled non-hurricane precipitation-induced flood losses to Verisk's ISO Property Claims Services (PCS) industry insured property loss data. The modeled insured losses are calculated based on Verisk's 2019 Industry Exposure Database. The PCS losses have been trended to 2019 values, and some policy conditions and take-up rate assumptions have been made to obtain industry-level insured losses.

Verisk's loss normalization methodology used to trend PCS losses is at state level and incorporates inflation, wealth, and changes in exposure. Inflation adjustments are based on the implicit price deflator for gross domestic product from the Bureau of Economic Analysis. Wealth adjustments are determined from the state-level median home value and exposure growth in terms of number of housing units.

Figure 198 below compares private market Verisk-modeled to PCS-observed (trended to 2019) gross insured industry non-hurricane precipitation-induced flood losses for various historical events. There is very good agreement between modeled and observed losses for riverine flood-dominated events such as the 2010 Tennessee Flood and the 2006 Northeast Flood. Observed 2019-trended losses tend to be larger than modeled losses for non-riverine flood-dominated events (e.g., Tropical Storm Allison (2001)). A major reason for this difference is because PCS-reported losses represent the sum total of losses from multiple perils (e.g. wind and/or hail, in addition to non-hurricane precipitation-induced flood), whereas modeled losses only include losses due to non-hurricane precipitation-induced flood. Two addtional plausible reasons for lower modeled losses compared to trended PCS-based observed estimates are: 1) the everchanging landscape of a built environment in terms of exposure locations, and 2) adoption of floodplain management and mitigation strategies in the aftermath of these disastrous flood events.

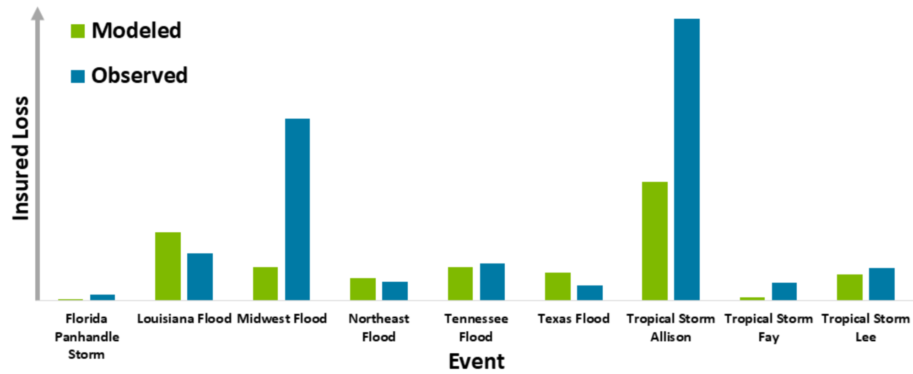

Figure 198. Comparison of modeled (green) private market and observed (blue; PCS claims data trended to 2019) gross insured industry non-hurricane precipitation-induced flood losses for various historical events in the historical event set

Figure 199 below compares the percent contribution of each state's modeled private market and PCS-observed (trended to 2019) gross insured industry inland flood losses for the 2016 Louisiana Flood and Tropical Storm Allison (2001). As illustrated, there is good agreement between the modeled and observed state contribution percentages.

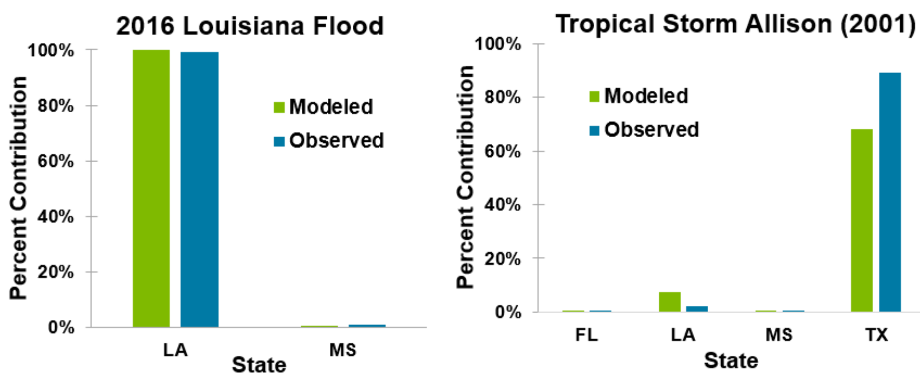

Figure 199. Comparison of the percent contribution of each state's modeled (green; private market) and observed (blue; source: PCS claims data trended to 2019) gross insured industry inland flood losses for the 2016 Louisiana Flood (left) and Tropical Storm Allison (2001; right)

Figure 200 below compares the modeled and PCS-observed (trended to 2019) automobile line of business percent of industry insured inland flood loss claims made as a result of the 2016 Louisiana Flood and Tropical Storm Allison (2001).

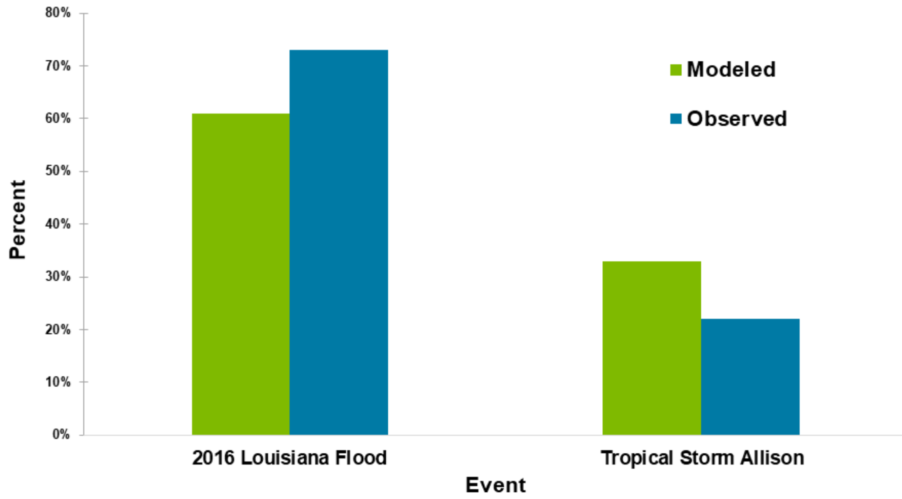

Figure 200. Comparison of the modeled (green) and observed (blue; source: PCS trended to 2019) automobile line of business percent of industry insured inland flood losses resulting from the 2016 Louisiana Flood and Tropical Storm Allison (2001)

Loss Validation Using Private Insurance Claims Data

In addition to actual losses from NFIP and industry insured losses from the private insurance market, Verisk collected company-specific claims and exposure data for a few significant non-hurricane precipitation-induced flood events including the 2013 Colorado Flood and the 2016 Louisiana Flood. The actual losses from these events exceeded USD 72 Million. The exposure portfolios were modeled for these events and the policy level modeled losses were then compared to actual losses, as shown in Figure 201 below. This figure along with several others that were presented in previous sections demonstrate the robustness of the updated model in replicating historical loss experience, not only for NFIP and the private flood insurance market at large, but also for specific companies in an unbiased fashion.

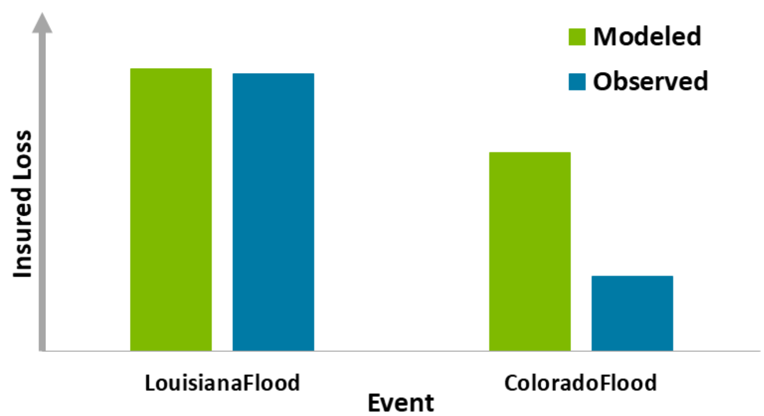

Figure 201. Comparison between modeled (green) and observed (blue; source: private insurance claims) insured commercial and industrial inland flood losses for the 2016 Louisiana Flood (left) and the 2013 Colorado Flood (right)

7 Accounting for Climate Change

In an effort to capture the effects of climate change on extreme weather events, Verisk strives to incorporate the current and near-present climate into its catastrophe models. For precipitation-induced flood models, that means understanding how extreme rainfall events have and will change, and how the Verisk models capture such trends.

In general, as the atmosphere warms, it can hold more water vapor. This well-known theoretical Clausius Clapeyron relationship states that the amount of water vapor the atmosphere can hold increases approximately seven percent per degree Celsius increase in air temperature. It is also understood that not every location will experience this same increase. There is agreement for some of the regional texture, but not all. There are also discrepancies in terms of which areas of the planet will see more, as opposed to less, precipitation, based on how climate models simulate climate-related changes to large-scale circulations (e.g., Hadley Circulation).

Verisk researchers have carefully analyzed precipitation trends over the past 60 years in an effort to account for any possible climate change signal and how that signal may be incorporated into the generation of a stochastic precipitation catalog. Independent Verisk research indicates that heavy rainfall days are not only increasing in the United States, but the magnitudes of these extrema are also increasing. Using completely independent datasets – Climate Prediction Center (CPC) and gauging station data with a longer temporal coverage – Verisk has identified sensitive locations, like the Houston, TX area, where this signal is particularly strong. By utilizing newer and higher-resolution data in the calibration – PRISM[84] and NOAA Atlas 14 – the Verisk Inland Flood Model for the United States captures more recent trends in the changing extrema. With this analysis, Verisk can also say with confidence that the model's precipitation catalog is equipped to handle extreme rainfall events that may occur over the next ten years.

7.1 Trends in Hydroclimatology and Extreme Precipitation over the United States

Through a combination of literature review and internal research, Verisk has identified the extent to which, and the locations where, trends in the frequency of extreme precipitation events are evident.

Literature Review

Many studies have shown that heavy precipitation events, more than annual precipitation totals, have increased over the last several decades and may continue to do so as the climate warms. For example, Myhre et al. (2019), find that the frequency of intense rainfall events will increase. The paper also states, via observations and climate modeling, that the rarer (or

[84] Parameter-elevation Regressions on Independent Slopes Model Climate Group

more extreme) the event is, the more likely its precipitation total is to increase. The authors conclude that if historical trends continue, for every additional one degree Celsius of global warming, the frequency of today's most intense precipitation events would more than double.

Additional work has shown that extreme precipitation will increase more strongly than mean precipitation with increased global mean surface temperature (e.g., Kharin et al., 2013; Berg et al., 2013; Fischer, 2016). These modeled or theoretical predictions correspond with the observed record over Europe and the United States (e.g., Papalexiou and Montanari, 2019).

Verisk Research

Verisk conducted independent research to evaluate trends in the frequency of heavy rainfall days in the United States. This research was performed using the CPC's gridded daily rainfall dataset [at 0.25-degree (~ 25 km) resolution] for the United States. Although this is not the data used to build the model,[85] the longer temporal resolution of the CPC rainfall data makes it easier to identify trends over regions of the United States.[86] The CPC dataset incorporates rain gauge data to construct a continuous view of precipitation from 1948 to present, across the continental United States. In this analysis, Verisk used the data from 1948 to 2018. First, the record was divided into two distinct time periods 1948-1984 and 1985-2018. Then, Verisk thresholded the daily precipitation at 1-inch and 3-inch cutoffs and counted the number of times the threshold was met or exceeded for each grid cell in the model domain. Verisk then normalized the data by the number of years to calculate an average annual frequency, or days per year (Figure 202).

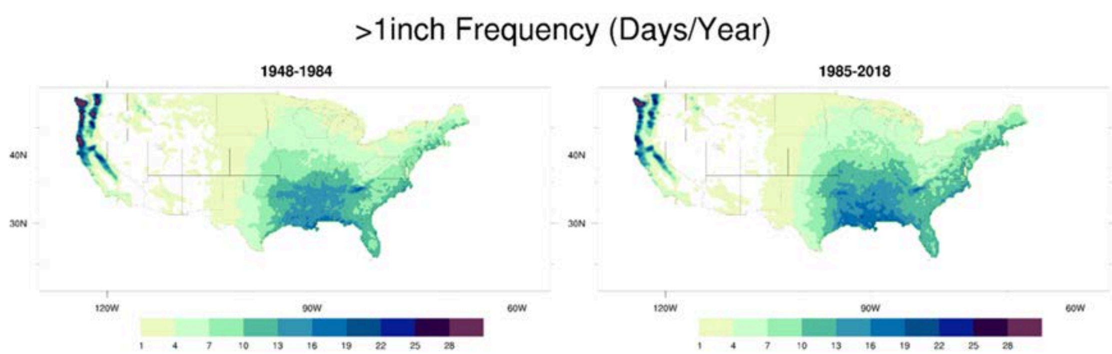

Figure 202. Comparison of average annual frequency of daily rainfall exceeding 1 inch (CPC data) for two periods: 1948-1984 and 1985-2018

As illustrated, the basic hydroclimatology of the country is preserved in terms of the average annual frequency of days with more than one inch of daily rainfall. The spatial maximum of the heaviest annual precipitation occurs in the same locations where heavy rainfall days occur—the Southeast, Gulf of Mexico, and Pacific Northwest/Sierra Nevada. However, a sharp negative gradient occurs moving west across the Rocky Mountains and desert Southwest, with a distinct void in between. This spatial signature is evident in both 1948-1984 and

85 The model relies on adjusted PRISM data for the precipitation catalog.
86 Both CPC and PRISM are gridded products based on gauging station data. Verisk regridded the PRISM and CPC datasets to the resolution of the Verisk catalog (8 km) prior to comparing datasets.

1985-2018 records. However, upon closer examination, the 1985-2018 record clearly exhibits an increase in the average number of days exceeding 1 inch of rain across a significant portion of the eastern half of the United States. This magnitude and spatial pattern are highlighted in Figure 203, which shows the absolute and relative differences between the average annual frequency from the last 34 years (1985-2018) versus the previous 37 years (1948-1984).

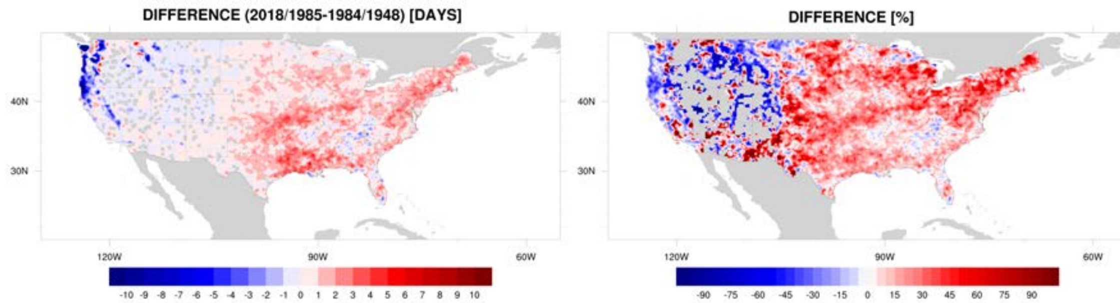

Figure 203. Absolute (left) and relative (right) differences in average annual frequency of greater than one inch daily precipitation for 1948-1984 compared to 1985-2018 (CPC data)

Clearly a large increase in the number of days receiving ≥ 1 inch of rain has occurred across the southeastern United States, particularly Texas and Louisiana. The pattern is also pronounced across the Northeast and parts of the Midwest (Figure 203). However, the spatial pattern in the change of average frequency does not necessarily match the overall pattern of frequency. There appears to be a northward expansion of more heavy rainfall days. Moreover, the increases are on the order of 25% to 75% in the number of days per year, which is quite a remarkable signature, with statistical significance at a 95% confidence interval for much of the region (Figure 204). This pattern, however, is not found west of the Rocky Mountains. In fact, there are large decreases across the Pacific Northwest and Sierra Nevada region where ≥ 1 inch rainfall days have decreased by 5 to 10 days/year or 25% to 50%.

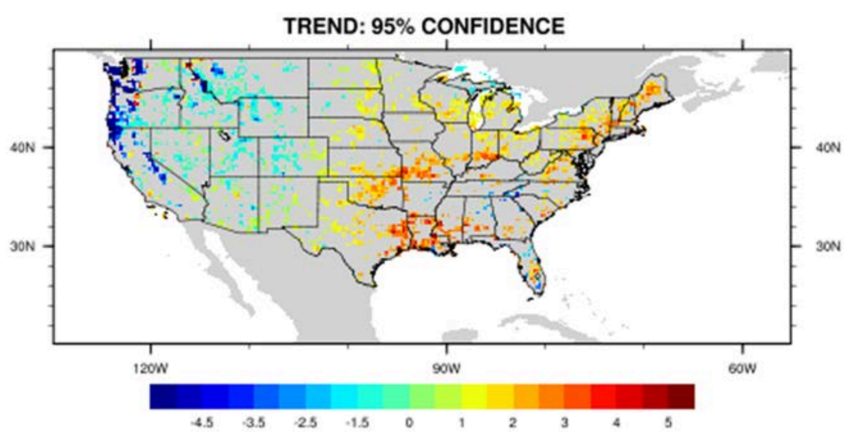

Figure 204. All differences/trends in average annual frequency (days per year) of greater than one inch daily precipitation for 1985-2018 compared to 1948-1984 that are statistically significant at the 95% confidence level (CPC data)

Examining days with ≥ 3 inches of rainfall bares similar results to that of the ≥ 1 inch thresholding (Figure 205 and Figure 206). As expected, the event frequency is less, given the extreme nature of such a heavy rainfall day. Therefore, the change frequency is much more muted and mixed. Nevertheless, the Gulf Coast remains a region where the trend in the observed record shows an increase in these heavy rainfall days, while the West Coast features drying. Such a pattern across the Gulf Coast aligns with the heavier precipitation events such as the 2016 “Tax Day” floods and Hurricane Harvey in 2017.

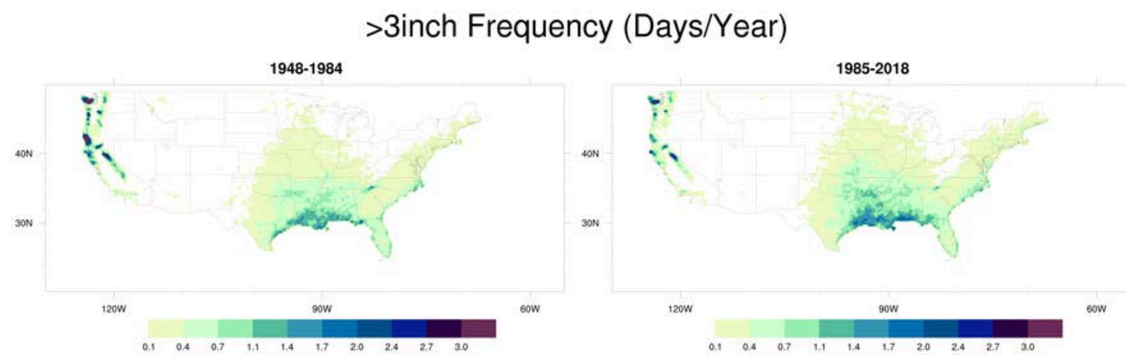

Figure 205. Comparison of average annual frequency of daily rainfall exceeding three inches (CPC data) for two periods: 1948-1984 and 1985-2018

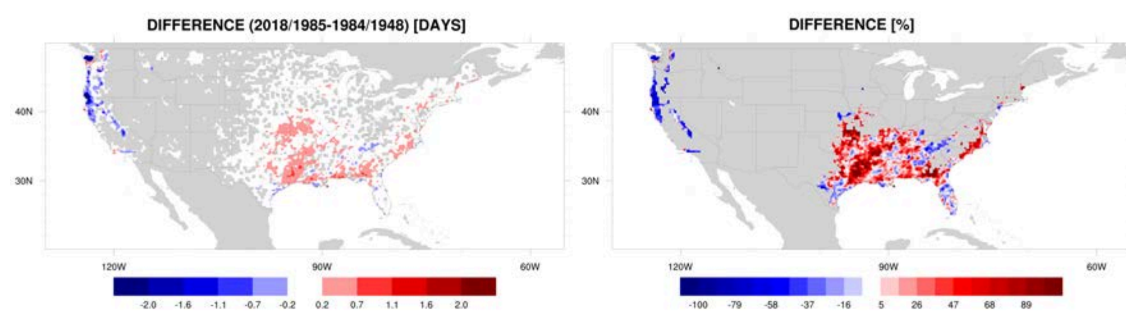

Figure 206. Absolute (left) and relative (right) differences in average annual frequency of greater than three inches daily precipitation for 1948-1984 compared to 1985-2018 (CPC data)

Despite the CPC’s long record from which the effect of climate change is obvious, it is a coarser dataset than PRISM. Given PRISM’s higher resolution (4 km), Verisk anticipated it would show even more pronounced interpolation effects when compared to gauging station data for the last 30 years. Figure 207 and Figure 208 clearly show that this is the case. While the discrepancy for PRISM is 7% to 10% (Figure 207) with the decrease of the recurrence interval, the discrepancy for CPC is 12% (Figure 208). Given these discrepancies, a reasonable approach to estimate where the Verisk model (i.e., the adjusted PRISM climatology) stands with respect to the current climate is a comparison with gauging station data with a long record.

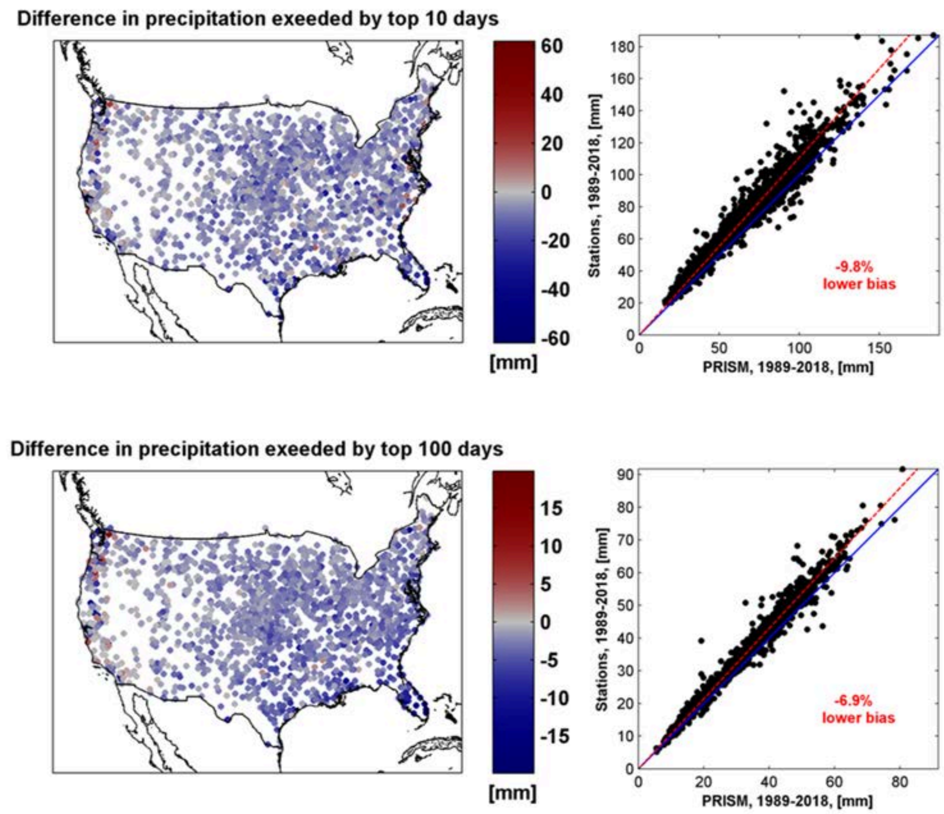

Figure 207. Comparison of PRISM extreme precipitation and gauging station data for the last 30 years
Precipitation is presented in terms of daily precipitation values exceeded by only 10 and 100 days.
Each dot represents a gauging station location. PRISM values have been interpolated for each station location.

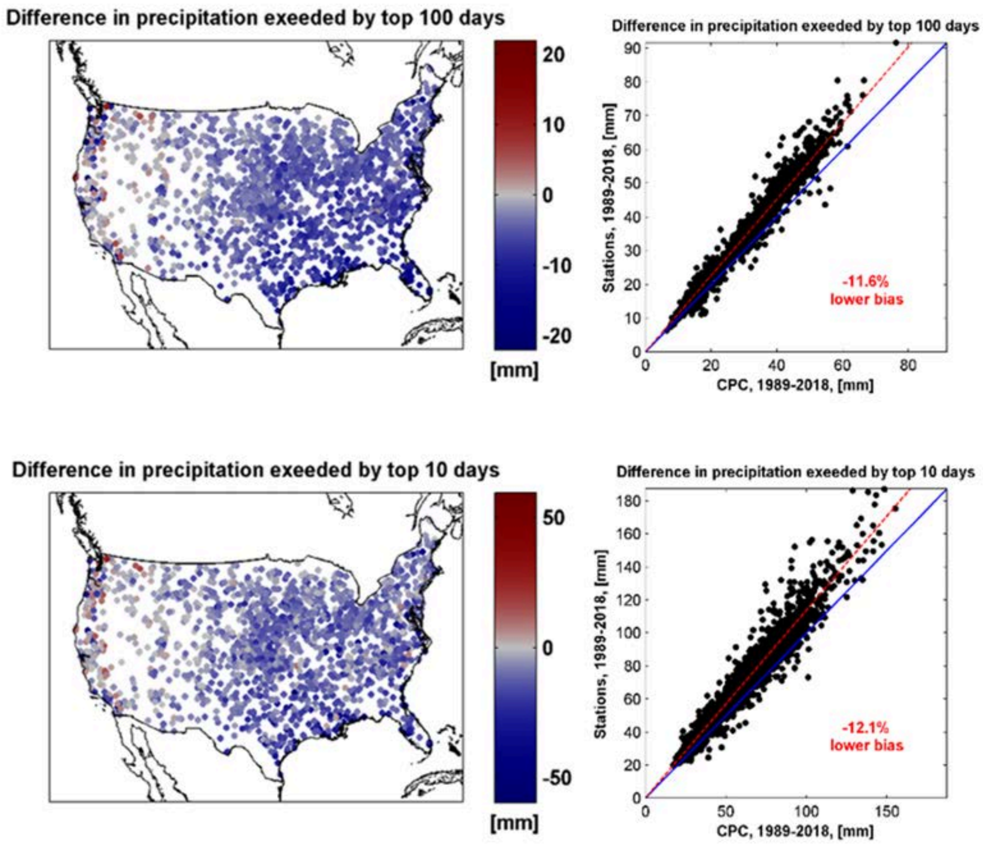

Figure 208. Comparison of CPC extreme precipitation and gauging station data for the last 30 years
Precipitation is presented in terms of daily precipitation values exceeded by only 10 and 100 days.
Each dot represents a gauging station location. CPC values have been interpolated for each station location.

Verisk repeated the test applied to the CPC data, using daily accumulations from over 1,700 gauging stations with at least 60 years of recorded data. For this, and all gauging station analysis, Verisk selected NOAA's Global Surface Summary of the Day (GSOD)[87] dataset of gauging station data, and compared extreme daily accumulations with different recurrence intervals for the two 30-years period 1959-1988 and 1989-2018. Figure 209 and Figure 210 clearly show an overall increase of extreme precipitation of about 4% to 5%. Similar to the CPC data trends, in the eastern United States there is a positive trend of increasing extreme precipitation, while in the western part of the country the trend is not so evident.

[87] GSOD is a meteorological summary dataset

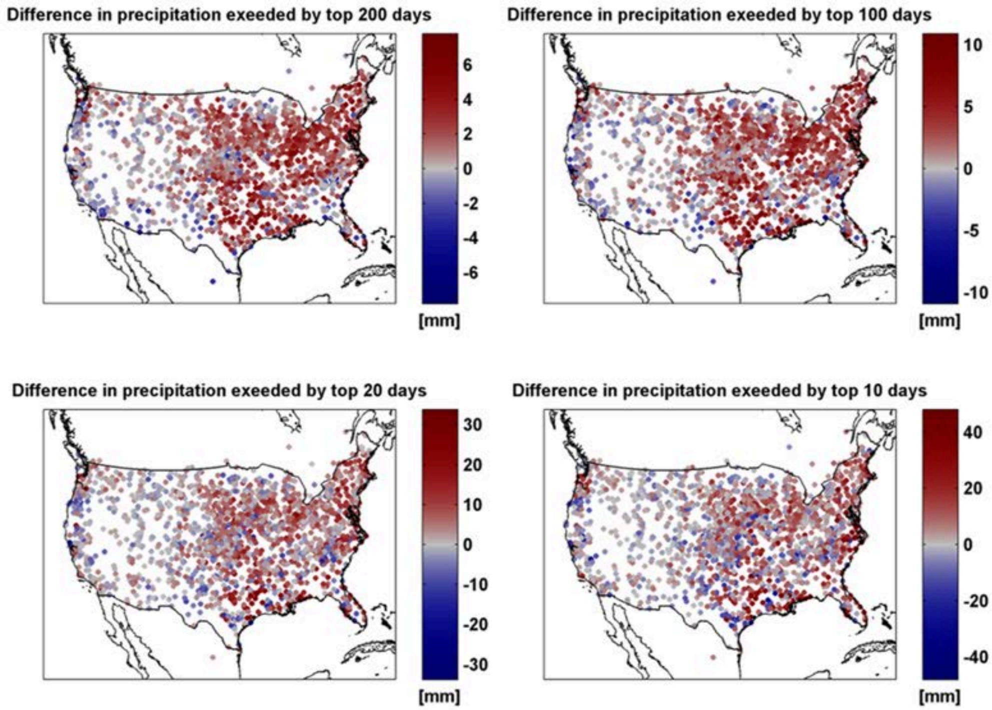

Figure 209. Difference in daily gauging station precipitation for extremes of different recurrence intervals for the two 30-year periods 1959-1988 and 1989-2018

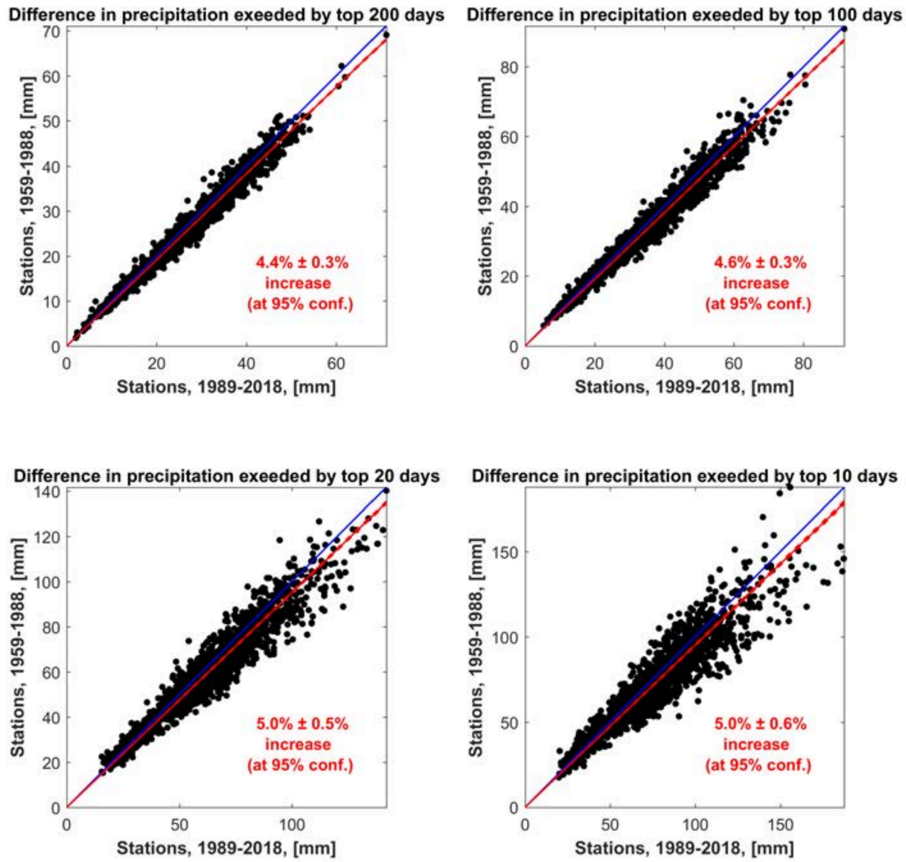

Figure 210. Daily gauging station precipitation for extremes of different recurrence for the periods 1959-1988 and 1989-2018.

As illustrated above, Verisk's research indicates an increase in extreme precipitation in the eastern United States in the past ~ 30 years, which is consistent with the literature.

7.2 Current Climate in the Verisk Model

The Verisk Inland Flood Model for the United States accounts for the recent climate in the precipitation catalog. Through a process of reanalysis and quantile mapping, Verisk has adjusted the simulated precipitation catalog to align with recent climate data.

The Verisk process consists of the following steps:

1. Selection of a target dataset

   Verisk selected the PRISM precipitation dataset (1981 to 2018) as a benchmark. This dataset serves as a good representation of the near-present climate.

2. Addressing the bias in the target dataset and building the climatology for each 8-km grid cell

   Verisk analysis indicated the PRISM dataset was 7% to 10% lower than the observed (gauging) data, increasing with the recurrence interval. To account for this bias, Verisk modified the PRISM daily precipitation distributions to agree with the NOAA Atlas' 2 to 1,000-year quantiles.
3. Quantile mapping to adjust the Verisk precipitation catalog to the target dataset (adjusted PRISM climatology)

Details of this process are included in the Precipitation Adjustment section of the Event Generation chapter.

See Also

Precipitation Adjustment

7.3 How the Model Climatology Compares with Near-present Activity

In an effort to analyze how well the modeled precipitation climatology (i.e., the adjusted PRISM dataset) represents the observed current climate, Verisk compared the modeled extreme precipitation at different recurrence levels to observed data from GSOD gauging stations for the last 30 years (1989-2018). Verisk estimated the probabilities corresponding to the precipitation values exceeded by the top 200, 100, 20, and 10 days,[88] and then extracted the values in the Verisk precipitation catalog that correspond to these probabilities and compared them to the gauging data. Figure 211 presents the differences between the modeled extreme and the corresponding extremes from the gauging station time series. Figure 212 provides scatter plots of the observed versus the modeled extremes. As illustrated, the model consistently exceeds the station data extremes by about 3% to 6%. Given the uncertainty in the procedures involved in the estimates of climatology in NOAA Atlas 14, this slight overestimation is solid evidence that the Verisk model is well positioned to represent the precipitation extremes for the next 10 years.

[88] $P_T = \{200, \quad 100, \quad 20, \quad 10\}$ days. These probabilities were estimated as $p = (L - P_T)/L$, where $L = 10957$ is the number of days in the period January 1, 1989 through December 31, 2018.

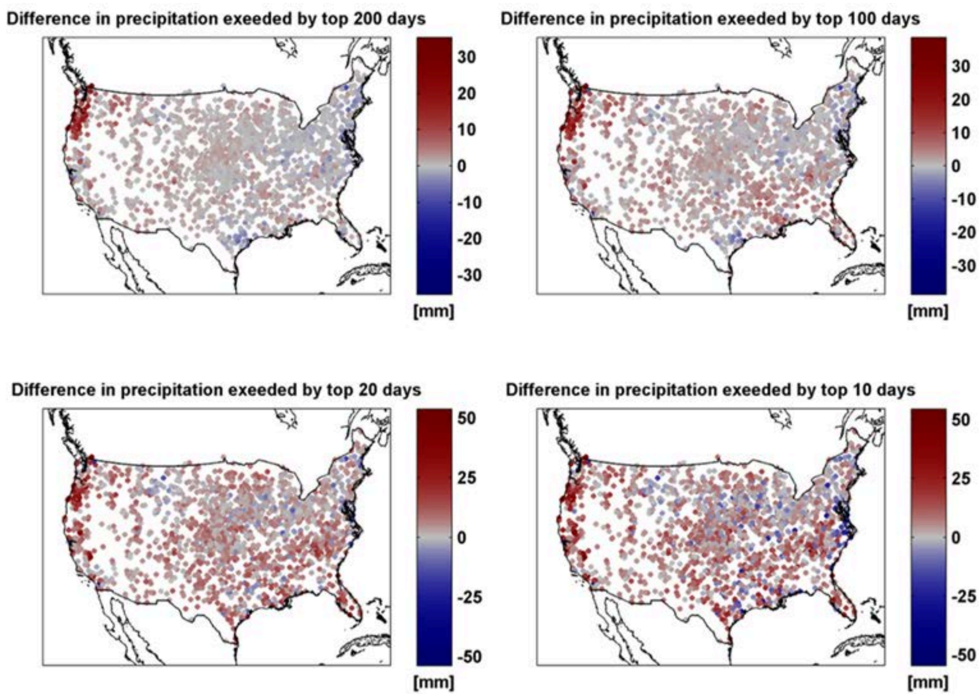

Figure 211. Difference in precipitation between the Verisk 10,000-year precipitation catalog and daily gauging station precipitation extremes from the period 1989-2018 for different recurrence intervals. Note that the slight bias is uniformly distributed across the country

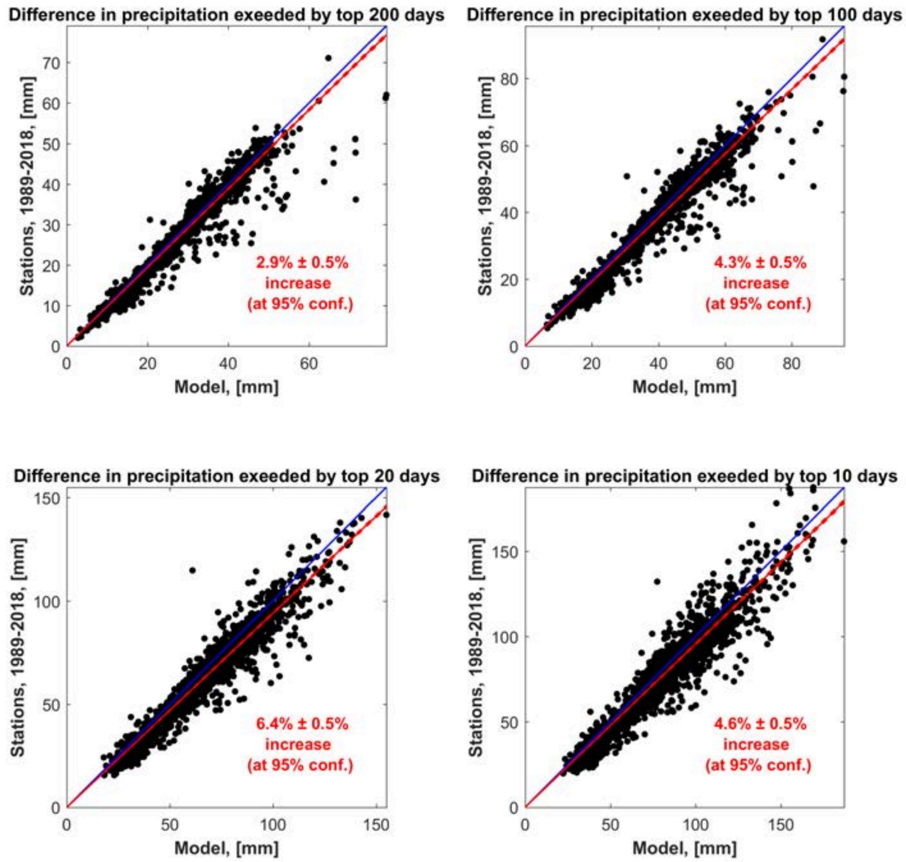

Figure 212. Verisk 10,000-year precipitation catalog extreme precipitation versus daily gauging station precipitation extremes from the period 1989-2018 for different recurrence intervals

Verisk researchers conclude with confidence that the Verisk precipitation catalog for the United States represents the near-present or recent climate and its possible extrema (i.e., the 100 to 1,000+ year return period values). Verisk has performed extensive validation in a wide range of metrics on scales from seasonality to extrema to historical event comparisons. All analyses compare favorably to the observed record over the past 30 years, including more recent events. For example, the Verisk precipitation catalog, contains both Harvey- and Florence-like hurricane precipitation events,[89] while also capturing other important hydrometeorological metrics such as the climatology of heavy rainfall days across the continental United States.

89 Precipitation-induced flooding from tropical cyclone events is addressed in the Verisk Hurricane Model for the United States.

8 AIR Inland Flood Model for the United States in Touchstone and Touchstone Re

8.1 Available Catalogs

Touchstone and Touchstone Re support a 10,000-year catalog and a historical event set for the Verisk Inland Flood Model for the United States.

Stochastic Catalog

Touchstone and Touchstone Re support a 10,000-year catalog.

See Also

Stochastic Catalog

Historical Event Set

Touchstone and Touchstone Re support a marquee event set, consisting of 20 historical events, listed below.

Table 23. Historical events available in the Verisk Inland Flood Model for the United States

Event ID	Year	Event Name
1	1993	Great Flood (Mississippi River)
2	1995	California Flood
3	1995	Gulf Coast Flood
4	1996-1997	Pacific Northwest Flood
5	1997	Red River Flood
6	1998	Texas Flood
7	2001	Tropical Storm Allison
8	2006	Northeast Flood
9	2008	Midwest Flood
10	2008	Tropical Storm Fay
11	2009	East Florida Storm
12	2010	Rhode Island Flood
13	2010	Tennessee Flood

Event ID	Year	Event Name
14	2011	Mississippi Flood
15	2011	Tropical Storm Lee
16	2013	Florida Panhandle Storm
17	2013	Colorado Flood
18	2015	South Carolina Flood
19	2016	Louisiana Flood
20	2017	California Flood

See Also

Modeled Losses for Historical Flood Events

8.2 AIR Inland Flood Model for the United States in Touchstone

Supported Geographic Resolutions

The following geographic resolutions are supported for the Verisk Inland Flood Model for the United States in Touchstone:

- County
- Zip code
- Address (city and state)
- Complete address (street, city, and state)
- User-specified latitude/longitude

Modeling Aggregate Data

Touchstone can be run with Disaggregation turned on or off. During analysis in Touchstone, if Disaggregation is on, the aggregate county, city, or Zip code exposures are automatically disaggregated to a 1-km grid, based on industry exposure weights, by line of business. County- and city-level data are disaggregated to the grid cells within a single Zip code that contains the centroid of the county or city.

Construction and Occupancy Classes, Year Built and Height Bands, and Relative Vulnerabilities

The vulnerability of a structure depends on its construction and occupancy class combination as well as its age and height. With the goal of enabling clients to code their exposure data as specifically as possible, the Verisk Inland Flood Model for the United States supports 84

Verisk

construction classes and 111 occupancy classes. Of the occupancy classes, 62 are classes for industrial facilities.[90]

Verisk has compiled the supported construction and occupancy information, along with relative vulnerabilities, in an Excel® spreadsheet available at the following link: *Verisk Inland Flood Model for the United States Supplement*.[91]

The workbook includes the following information:

- Complete lists of supported construction and occupancy classes
- Supported construction/occupancy class combinations
- Supported height and age bands
- Relative vulnerabilities (Coverage A) for construction classes, by height band and occupancy class
- Relative vulnerabilities (Coverage A) for construction classes, by age band and occupancy class
- Relative flood vulnerabilities for all supported construction and occupancy class combinations
- Supported secondary risk characteristics

Descriptions of the supported construction and occupancy classes are available in the *Touchstone Exposure Data Validation Reference*

Secondary Risk Characteristics

In addition to the primary determinants of vulnerability, the Verisk model supports secondary risk characteristics (SRCs). These individual risk modifiers are features of a building or its environment that affect resistance to damage. The use of SRCs can significantly impact losses sustained by residential, commercial, and industrial properties.

Verisk's SRC methodology is knowledge-based and relies on a combination[92] of simulations from the latest engineering models, observed performance data from historical events, and Verisk damage surveys. With the selection of SRCs in Touchstone, the model applies adjustment factors to the base damage function, resulting in a modified damage function reflecting the SRC impact. The model uses algorithms[93] to combine the effects of multiple features, which can be complex and not necessarily additive.

Verisk strongly encourages the collection of relevant exposure data, as the inclusion of SRCs in loss analysis can yield more accurate results and have a major impact on the view of risk.

The SRCs supported in this model are presented below.

- Base flood elevation

[90] The industrial facilities set of occupancy classes refers to the 400-series, which include structures that are very different from the 300-series as they represent large, complex facilities composed of many components and can be differentiated as facilities replacement value of with a replacement value of over USD 5 million. Small facilities (those with replacement values of USD 5 million or less) consist of mostly buildings and some machinery.

[91] The supplement is available on the Client Portal

[92] The type and specific combination of resources varies by peril and model.

[93] The specific algorithm varies by model.

- Basement finish
- Builders Risk (project completion, project phase code)
- Contents vulnerability
- Custom elevation
- Custom flood zone
- Custom standard of protection
- FIRM Compliance
- First floor height
- Floor of interest
- Foundation type
- Number of basement levels
- Service equipment protection
- Wet floodproofing

See Also

Secondary Risk Characteristics

Damage Functions for Unknown Characteristics

Often a characteristic of a building (e.g., its construction or occupancy class, height, etc.) is unknown. In these cases, Touchstone uses a composite damage function based on Verisk's Industry Exposure Database. For a given unknown characteristic, the unknown damage function represents a weighted average of the damage functions of the different classes that are in the Verisk Industry Exposure Database, with weights determined by the relative share of total insurable value of each class. The Verisk Inland Flood Model for the United States supports damage functions for risks with unknown characteristics at the state flood zone level.

See Also

Buildings with Unknown Characteristics

Supported Policy Conditions

The financial module in Touchstone allows for the application of a wide variety of location, policy, and reinsurance conditions. Location terms may be specified to include limits and deductibles by site or by coverage. Supported policy terms include blanket and excess layers, minimum and maximum deductibles, and sublimits. Reinsurance terms include facultative certificates and various types of risk-specific and aggregate treaties with occurrence and aggregate limits.

For more information about policy terms, see the Verisk publication *Industry Deductible Assumptions* for the appropriate year, available on the Client Portal.

Probabilistic Flood Hazard Maps

Licensed users can obtain an immediate visualization of the flood hazard in exposure summary views using the Verisk Probabilistic Flood Hazard Maps for the United States. The model-based hazard maps are available as flood depth layers for 20-, 50-, 100-, 200-, 250-, and 500-year return periods, or as Verisk Flood Zone layers for key return periods (100-, 250-, and 500-year). Verisk also offers the ability to visualize exposure using FEMA Flood Zones. Using Touchstone Geospatial Analytics, users can accumulate and apply damage ratios based on FEMA and Verisk Flood Zone categories, and they can select data sources and view results on the accumulations as tables and charts. The Touchstone Hazard Analytics module can be used to obtain site-level hazard information for underwriting, using these hazard maps.

See Also

Flood Hazard Maps

8.3 AIR Inland Flood Model for the United States in Touchstone Re

Resolution of Analysis Results

Modeled loss estimates for both on- and off-floodplain locations are calculated at a resolution of 10 m. Touchstone Re users may input risk at the county or state level; losses are reported at the county and state level.

Verisk Industry Exposure Database

The industry exposure database is an integral and highly valuable component of Touchstone Re. This database contains estimates of insured and insurable property exposures at a high degree of resolution, including the number of risks, their replacement values broken down by line of business (LOB), by coverage, by occupancy, and by construction type, building attributes, and information regarding standard policy terms and conditions. Verisk uses a variety of public and private sources to estimate industry exposures, including government data, commercially available demographic information, and other industry data. Verisk's industry exposure database is extensively validated via comparison against values obtained from various insurance industry and governmental sources.

The industry exposure database implemented in the Verisk Inland Flood Model for the United States is current through the end of 2019. For more details about the industry exposure database for this model, see the Verisk publication *Verisk Industry Exposure Database for the United States*, available through the Client Portal. This document provides further details, including:

- How Verisk developed the industry exposure database
- Data sources used in the database development
- Maps detailing the total exposure for the modeled region

- Share of industry exposure by LOB
- Construction splits by LOB
- Coverage splits by LOB
- Height band splits by LOB

Lines of Business for Reporting of Modeled Losses

Touchstone Re supports the following lines of business for reporting losses:

- Residential
- Mobile home
- Commercial/Industrial
- Auto

Supported Take-Up Rates and Policy Conditions

Touchstone Re event sets include the perspective of the private flood market in the United States. The private market insurable view provides flood losses for all lines of business and includes the application of private market deductibles and limits. To calculate the private market industry insured view for flood, users can enter the county-level private market U.S. flood take-up rates as user-specified market shares. Take-up rates are available in the Verisk publication *Industry Take-Up Rates* for the appropriate year, accessible through the Client Portal.

Verisk derived these private market deductibles, limits and take-up rates from several variables including the flood zone, market segment, and size of risk and occupancy, to reflect the current private flood market in the United States. Limits and deductibles are summarized below:

Limits:	Up to USD 5,000,000 for single family homes Up to USD 25,000 for renters and unit owners Range of up to USD 2,000,000 to USD 100,000,000 for apartments depending on the size of risk, market segment and flood zone Range of up to USD 2,000,000 to USD 100,000,000 for commercial depending on the size of risk, market segment and flood zone Range of up to USD 2,000,000 to USD 100,000,000 for industrial facilities depending on the size of risk, market segment and flood zone
Deductibles:	USD 2,000 for single family homes and mobile homes, applied separately to buildings and contents USD 1,000 for renters and unit owners, applied to contents

USD ranges from USD 2,500 to USD 75,000 for apartments, applied separately to buildings and contents based on size of risk, market segment and flood zone

USD ranges from USD 2,500 to USD 75,000 for commercial, applied separately to buildings and contents based on size of risk, market segment and flood zone

USD ranges from USD 2,500 to USD 75,000 for industrial facilities, applied separately to buildings and contents based on size of risk, market segment and flood zone

USD 250 for automobiles

A Analysis Settings

The following tables provide analysis settings used to produce modeled losses provided in this document. For information on take-up rate assumptions, see *The Verisk Industry Exposure Database for the United States* available on the Client Portal.

Table 24. Touchstone analysis settings for model runs

Setting	Selected Option(s)
Perils modeled	Inland flood
Catalog	10,000-year
Industry exposure vintage	2019 Flood private market insurable
Average Properties	Off
Demand surge	On
Disaggregation	Off

Table 25. Touchstone Re analysis settings for model runs

Setting	Selected Option(s)
Perils modeled	Inland flood
Catalogs	10,000-year
Industry exposure vintage	2019 Flood private market insurable
Take-up rates	2020 Take-up Rates[94]
Demand surge	On

[94] For take-up rates, see the Verisk publication *Industry Take-Up Rates* for the appropriate year, available through the Client Portal.

Selected References

General References

Center for Columbia River History (Washington State University at Vancouver, Washington, Portland State University, Portland, Oregon and Washington State Historical Society, Tacoma, Washington).

Environmental Protection Agency and U.S. Geological Survey, National Hydrography Dataset Plus (NHD Plus), Version 2.0

National Climatic Data Center, National; Oceanographic and Atmospheric Administration (NOAA)

National Weather Service, Climate Prediction Center

Tennessee State Library and Archives

Upper Mississippi River Basin Association

U.S. Geological Survey, National Hydrography Dataset, Digital Terrain Model, river gauge data, land use and land cover data, historical flood data

Precipitation Model

Conley, A.J., et al. (2012). Description of the NCAR Community Atmosphere Model (CAM 5.0). http://www.cesm.ucar.edu/models/cesm1.0/cam/docs/description/cam5_desc.pdf

Goff, J. A., and Jordan, T. H. (1988). Stochastic Modeling of Seafloor Morphology: Inversion of Sea Beam Data for Second-Order Statistics, *Journal of Geophysical Resources*, 93(B11), 13589–13608, doi:10.1029/JB093iB11p13589.

von Kármán, T. (1948). Progress in the Statistical Theory of Turbulence, Proceedings of the National Academy of Sciences of the United States of America, 34 (11), 530-539.

National Centers for Environmental Prediction at NOAA for the North American Regional Reanalysis (NARR), https://www.ncdc.noaa.gov/data-access/model-data/model-datasets/north-american-regional-reanalysis-narr

NOAA National Weather Service, Hydrometeorological Design Studies Center, Precipitation Frequency Data Server (PFDS), Atlas 2, Atlas 14, https://hdsc.nws.noaa.gov/hdsc/pfds/index.html

PRISM Climate Group, Oregon State University, http://prism.oregonstate.edu, Feb 2004.

Skamarock, W.C. (2005), A description of the Advanced Research WRF Version 2. NCAR.

Hydrological Model

Allcroft, D.J., and Lasbey, C.A. (2003). A Latent Gaussian Markov Random Field Model for Spatio-Temporal Rainfall Disaggregation. *Applied Statistics*, 52, 487-498.

Allen, R.G., Walter, I.A., Elliott, R.L., Howell, T.A., Itenfisu, D., Jensen, M.E., and Snyder, R.L. (2005). *The ASCE Standardized Reference Evapotranspiration Equation*, American Society of Civil Engineers (ASCE), Reston, Virginia.

Anderson, E. (2006). Snow Accumulation and Ablation Model – SNOW-17, National Oceanic and Atmospheric Administration (NOAA).

Arcement, G.J. and Schneider, V.R. (1989). Guide for Selecting Manning's Roughness Coefficients for Natural Channels and Flood Plains, U.S. Geological Survey Water-supply Paper 2339, https://pubs.usgs.gov/wsp/2339/report.pdf

Bárdossy, A. and Li, J. (2008). Geostatistical Interpolation using Copulas. *Water Resources Research*, 44, W07412, 15 pp.

Bontempi, G., Ben Taieb, S., Le Borgne, Y.A. (2013). Machine Learning Strategies for Time Series Forecasting, in: Aufaure, M.-A., Zimányi, E. (Eds.), Business Intelligence: Second European Summer School, EBISS 2012, Brussels, Belgium, July 15-21, 2012, Tutorial Lectures. Springer Berlin Heidelberg, Berlin, Heidelberg, 62–77. https://doi.org/10.1007/978-3-642-36318-4_3

Department for Environment, Food and Rural Affairs (DEFRA) (2001). National Appraisal of Assets at Risk from Flooding and Coastal Erosion, Including the Potential Impact of Climate Change, DEFRA.

Cleveland, T.G., Thompson, D.B., Fan, X., and He, X. (2008). Synthesis of Unit Hydrographs from a Digital Elevation Model, Journal of Irrigation and Drainage Engineering, ASCE March/April 2008. 212-221.

Dodov, B., and Foufoula-Georgiou, E. (2004). Generalized Hydraulic Geometry: Derivation Based on a Multiscaling Formalism. *Water Resources Research*, 40, W06302, 22 pp.

Dodov, B., and Foufoula-Georgiou, E. (2006). Floodplain Morphometry Extraction from a High-Resolution Digital Elevation Model: a Simple Algorithm for Regional Analysis Studies. *Geoscience and Remote Sensing Letters*, IEEE, 3, 410–413.

Ghosh, S., Kondapalli, S., Sawicz, K., Chinnayakanahalli, K., and Chowdhary, H. (2019). Derivation of Operational Rule Curves for Simulating Reservoir Regulation in Hydrological Models. ISH-HYDRO 2019, International, Osmania University, Hyderabad, India, 18-20 December 2019.

Hazus Flood Model. (n.d.). Retrieved February 28, 2018, available at https://www.fema.gov/hazus-mh-flood-model

Hirpa, Y.H. (2005). Regionalization of Parameters of a Conceptual Rainfall-Runoff Model. Institut für Wasserbau Universität Stuttgart, 94 pp.

HEC-HMS, Hydrologic Engineering Centers, Hydrological Modeling System. (2000). Technical Reference Manual, Hydrologic Engineering Center, U.S. Army Corps of Engineers (Davis, California), available at: http://www.hec.usace.army.mil/software/hec-hms

HEC-RAS. Hydrologic Engineering Centers River Analysis System. (2000). Hydraulic Reference Manual, Hydrologic Engineering Center, U.S. Army Corps of Engineers (Davis, California), available at: www.hec.usace.army.mil/software/hec-ras

International Commission on Large Dams (ICOLD), headquartered in Paris, France.

Kirchner, J.W. (2009). Catchments as simple dynamical systems: Catchment Characterization, rainfall-runoff modeling, and doing hydrology backward. *Water Resources Research*, 45, February.

Kjeldson, T.R. (2007). Flood Estimation Handbook, Supplementary Report No. 1, The Revitalised FSR/FEH Rainfall-Runoff Method. Centre for Ecology and Hydrology (Oxfordshire, United Kingdom).

Kolmogorov, A.N. (1941). Dissipation of Energy in a Locally Isotropic Turbulence. *American Mathematical Society Translations 1958*, Vol. 8 (Providence, Rhode Island).

Larson, L. W. (1997). The great USA flood of 1993. *IAHS Publications-Series of Proceedings and Reports-Intern Assoc Hydrological Sciences*, 239, 13-20.

Lehner, B., Reidy Liermann,C., Revenga, C., Vörösmarty, C., Fekete, B., Crouzet, P., Döll, P., Endejan, M., Frenken, K., Magome, J., Nilsson, C., Robertson, J.C., Rodel, R., Sindorf, N., and Wisser, D. (2011). Global Reservoir and Dam Database, Version 1 (GRanDv1): Dams, Revision 01. Palisades, NY: NASA Socioeconomic Data and Applications Center (SEDAC). https://doi.org/10.7927/H4N877QK. Accessed Day Month year.

Lehner, B., Reidy Liermann,C., Revenga, C., Vörösmarty, C., Fekete, B., Crouzet, P., Döll, P., Endejan, M., Frenken, K., Magome, J., Nilsson, C., Robertson, J.C., Rodel, R., Sindorf, N., and Wisser, D. (2011). High-Resolution Mapping of the World's Reservoirs and Dams for Sustainable River-Flow Management. *Frontiers in Ecology and the Environment* 9 (9): 494-502. http://dx.doi.org/10.1890/100125.

Mockus, V. (1949). Estimation of Total (and Peak Rates of) Surface Runoff for Individual Storms. Exhibit A in Appendix B, *Interim Survey Report, Grand (Neosho) River Watershed*, United States Department of Agriculture (Washington, D.C.)

Moore, R.J. (1985). The Probability-Distributed Principle and Runoff Production at Point and Basin Scales. *Hydrological Sciences Journal*, 30, 263–297.

Moore, R.J. (2007). The PDM rainfall-runoff model. *Hydrology and Earth System Sciences*, 11, 483—499.

Moore, R.J. and Bell, V.A (2002). Incorporation of groundwater losses and well level data in rainfall-runoff models illustrated using the PDM. Hydrology and Earth System Sciences Discussions, European Geosciences Union, 2002, 6 (1), pp.25-38. ffhal-00304647f

Müllner, Daniel (2013). Fastcluster: Fast Hierarchical, Agglomerative Clustering Routines for R and Python. Journal of Statistical Software, 53(9), 1-18. URL http://www.jstatsoft.org/v53/i09/.

Nadarajah, S. (2006). The Exponentiated Gumbel Distribution with Climate Application. *Environmetrics*, 17, 13–23.

National Aeronautics and Space Administration (NASA), Global Reservoir and Dam (GRanD), V1, Socioeconomic Data and Applications Center (SEDAC), hosted at Columbia University.

National Aeronautics and Space Administration (NASA), Shuttle Radar Topography Mission (SRTM), Jet Propulsion Laboratory, California Institute of Technology

National Oceanic and Atmospheric Administration (NOAA), National Weather Service (NWS)

Prechelt, L. (2012). Early Stopping — But When? *Neural Networks: Tricks of the Trade: Second Edition*, Lecture Notes in Computer Science, G. Montavon, G. B. Orr, and K.-R. Müller, eds., Springer Berlin Heidelberg, Berlin, Heidelberg, 53–67.

Reed, D.W., Faulkner, D., Robson, A., and Houghton-Carr, H. (2002). Flood Estimation Handbook. Natural Environment Research Council, Centre for Ecology and Hydrology (Wallingford, UK).

Reynolds, A.P., Richards, G., de la Iglesia, B. et al.(2006). Clustering Rules: A Comparison of Partitioning and Hierarchical Clustering Algorithms. *Journal of Mathematical Modelling and Algorithms*, 5, 475–504. https://doi.org/10.1007/s10852-005-9022-1

Riedmiller, M., and Braun, H. (1993). " direct adaptive method for faster backpropagation learning: the RPROP algorithm. *IEEE International Conference on Neural Networks*, 586–591 vol.1.

Rue, H. (2001). Fast Sampling of Gaussian Markov Random Fields. *Journal of the Royal Statistical Society*, Series B, 63, 325–338.

Sivapalan, M., and Blöschl, G. (1998). Transformation of Point Rainfall to Areal Rainfall: Intensity-Duration-Frequency Curves. *Journal of Hydrology*, 204, 150–167.

Tessier, Y., Lovejoy, S. , and Schertzer, D. (1993). Universal Multifractals: Theory and Observations for Rain and Clouds. *Journal of Applied Meteorology*, 32, 223–250.

Vincent, L., and Soille, P. (1991). Watersheds in Digital Spaces: An Efficient Algorithm Based on Immersion Simulations. *IEEE Transactions on Pattern Analysis and Machine Intelligence – PAMI*, 13, 583–598

Hydraulic Model

Aronica, G., Bates, P.D. , and Horritt, M.S. (2002). Assessing the uncertainty in distributed model predictions using observed binary pattern information within GLUE. *Hydrological Processes*, 16, 2001–2016.

Bates, P.D. and DeRoo, A.P.J. (2000). A simple raster-based model for flood inundation simulation. *Journal of Hydrology*, 236, 54–77.

Bates, P.D., Horritt, M.S., and Fewtrell, T.J. (2010). A simple inertial formulation of the shallow water equations for efficient two-dimensional flood inundation modelling. *Journal of Hydrology*, 387, 33–45.

Büchele, B., Kreibich, H., Kron, A., Thieken, A., Ihringer, J., Oberle, P., Merz, B., and Nestmann, F. (2006). Flood-risk mapping: contributions towards an enhanced assessment of extreme events and associated risks. *Natural Hazards and Earth System Sciences*, 6, 485–503.

Castellarin, A., Domeneghetti, A., and Brath, A., (2011). Identifying robust large-scale flood risk mitigation strategies: A quasi-2D hydraulic model as a tool for the Po river," *Physics and Chemistry of the Earth*, 36, 299–308.

Committee on FEMA Flood Maps; Board of Earth Sciences and Resources/Mapping Science Committee; National Research Council. (2009). *Mapping the Zone: Improving Flood Map Accuracy*. The National Academies Press, Washington, D.C.

Cunge, J.A. (1975). Two-dimensional modeling of flood plains. *Water Resources Publications*, 17, 705–762.

DeHaan, H., Stamper, J., and Walters, W. (2012). Mississippi River and Tributaries System 2011 Post-Flood Report, U.S. Army Corps of Engineers, Mississippi Valley Division.

Falter, D., Vorogushyn, S., Lhomme, J., Apel, H., Gouldby, B., and Nerz, B. (2013). Hydraulic model evaluation for large-scale flood risk assessments. *Hydrological Processes*, 27, 1331–1340.

Federal Emergency Management Agency (FEMA), Midterm Levee Database

Gouldby, B., Sayers, P., Mulet-Marti, J., Hassan, M., and Benwell, D. (2008). A methodology for regional-scale flood risk assessment. *Proceedings of the Institution of Civil Engineers – Water Management*, 161, 169–182.

Horritt, M.S. and Bates, P.D. (2002). Evaluation of 1D and 2D numerical models for predicting river flood inundation. *Journal of Hydrology*, 268, 87–99.

Hydrologic Engineering Centers River Analysis System (HEC-RAS). (2002). Hydraulic Reference Manual, Version 3.1. U.S. Army Corps of Engineers, HEC (Davis, California)

Krupka, M, Pender, G., Wallis, S., Sayers, P.B, and Mulet-Marti, J. (2007). A rapid flood inundation model. *Proceedings of the 32nd Congress of the International Association for Hydraulic Research*, pp 1–28.

Liu, Y and Pender, G. (2010). A new rapid flood inundation model. *Proceedings of the First IAHR European Congress*, ed. S. Arthur, Edinburgh, United Kingdom.

Moussa, R. and Bocquillon, C. (2009). On the use of the diffusive wave for modelling extreme flood events with overbank flow in the floodplain. *Journal of Hydrology*, 116–135.

Mujumdar, P.P. (2001). Flood wave propagation – The Saint Venant Equation. *Resonance*, 6, 66–73.

Ponce, V.M., Li, R.M., and Simons, D.B. (1978). Applicability of kinematic and diffusion-models. *Journal of the Hydraulics Division, American Society of Civil Engineers*, 104, 353–360.

Singh, V.P. and Aravamuthan, V. (1996). Errors of kinematic-wave and diffusion-wave approximations for steady-state overland flows. *Catena*, 27, 209–227.

United States Army Corps of Engineers (USACE), National Levee Database

Xu, H. (2006). Modification of normalized difference water index (NDWI) to enhance open water features in remotely sensed imagery. *International Journal of Remote Sensing*, 27, 3025–3033.

Flood Peril in the United States

Gochis, D., Schumacher, R., Friedrich, K. et al. (2015). The Great Colorado Flood of September 2013. *Bulletin of the American Meteorological Society*, 96, 1461-1487, http://dx.doi.org/10.1175/BAMS-D-13-00241.1

Damage Estimation

American Society of Civil Engineers (ASCE). 2017. Minimum Design Loads and Associated Criteria for Buildings and Other Structures. ASCE Standard 7-16.

Federal Emergency Management Agency (FEMA), Base Flood Elevation data, Flood Insurance Rate Maps (FIRMs), data and studies on historical flood damage

Florida Division of Emergency Management (division of FEMA). (2009). North Florida Flood Event, Spring, 2009, Post Disaster Assessment of Previously Mitigated Projects, FEMA-1831-DR-FL.

Hall, C., Hoff, W.D., and Nixon, M.R. (1984). Water Movement in Porous Building Materials-VI. Evaporation and Drying in Brick and Block Materials. *Building and Environment*, 19, 13–20.

Hazus Flood Model. (n.d.). Retrieved from https://www.fema.gov/hazus-mh-flood-model

Merz, B., Kreibich, H., Thieken, A., and Schmidtke, R. (2004). Estimation Uncertainty of Direct Monetary Flood Damage to Buildings. *Natural Hazards and Earth System Sciences*, 4, 153–163

U.S. Army Corps of Engineers (USACE). (1992). *Catalog of Residential Depth-Damage Functions used by Army Corps of Engineers in Flood Damage Estimations*, IWR Report 92-R-3, Army Engineer Institute for Water Resources (Fort Belvoir, Virginia)

Insured Loss Calculation

Federal Emergency Management Agency. (2015). *National Flood Insurance Program: Report to Congress on Reinsuring NFIP Insurance Risk and Options for Privatizing the NFIP.* U.S. Department of Homeland Security. https://fedweb.com/wp-content/uploads/2017/08/FEMA-Reinsuring_NFIP_Insurance_Risk_and_Options_for_Privatizing_the_NFIP_Report-Aug-13-2015.pdf

National Oceanic and Atmospheric Administration's National Center for Environmental Information's Storm Events Database. (n.d.). Storm Events Database. Retrieved from https://www.ncdc.noaa.gov/stormevents

U.S. Department of Homeland Security's Federal Emergency Management Agency. (2019, December 23). Significant Flood Events. Retrieved from https://www.fema.gov/significant-flood-events

U.S. Department of Homeland Security's Federal Emergency Management Agency. (2020, March 9). Statistics by Calendar Year. Retrieved from https://www.fema.gov/statistics-calendar-year

Accounting for Climate Change

Berg, P., Moseley, C. & Haerter, J. (2013). Strong increase in convective precipitation in response to higher temperatures. *Nature Geoscience*, 6, 181–185, https://doi.org/10.1038/ngeo1731

Fischer, E., Knutti, R. (2016). Observed heavy precipitation increase confirms theory and early models. *Nature Climate Change*, 6, 986–991, https://doi.org/10.1038/nclimate3110

Kharin, V.V., Zwiers, F.W., Zhang, X. et al. (2013). Changes in temperature and precipitation extremes in the CMIP5 ensemble. *Climatic Change*, 119, 345–357, https://doi.org/10.1007/s10584-013-0705-8

Myhre, G., Alterskjær, K., Stjern, C.W. et al., (2019). Frequency of extreme precipitation increases extensively with event rareness under global warming. *Scientific Reports*, 9, 16063, https://doi.org/10.1038/s41598-019-52277-4

Papalexiou, S., and Montanari, A. (2019). Global and regional increase of precipitation extremes under global warming. *Water Resources Research*, 55, 4901– 4914. https://doi.org/10.1029/2018WR024067

About Verisk

Verisk Analytics (Verisk) provides risk modeling solutions that make individuals, businesses, and society more resilient to extreme events. In 1987, a Verisk subsidiary founded the catastrophe modeling industry and today models the risk from natural catastrophes, terrorism, pandemics, casualty catastrophes, and cyber incidents. Insurance, reinsurance, financial, corporate, and government clients rely on Verisk's advanced science, software, and consulting services for catastrophe risk management, insurance-linked securities, longevity modeling, site-specific engineering analyses, and agricultural risk management. Verisk (Nasdaq:VRSK) is headquartered in Jersey City, New Jersey with many offices throughout the United States and around the world. For information on our office locations, visit https://www.verisk.com/about/locations/.

Contact Information

Verisk Analytics
Lafayette City Center, 2nd Floor
Two Avenue de Lafayette
Boston, MA 02111
USA

Tel: (617) 267-6645
Fax: (617) 267-8284

Verisk welcomes feedback on its documentation. If you need assistance in using the software or understanding the information in this document, please email us at DocumentationFeedback@verisk.com.